Post

GEORGIA INSTITUTE OF TECHNOLOGY
ENGINEERING EXPERIMENT STATION

PROJECT INITIATION

Date: May 13, 1975

Project Title: Applications of Submillimeter Wave Gigawatt Sources

Project No.: A-1717

Project Director: Mr. J. J. Gallagher

Sponsor: Office of Naval Research; Arlington, Va 22217

Agreement Period: From February 3, 1975 Until May 3, 1975 (work period)

Type Agreement: Contract N00014-75-C-1011

Amount: $27,827

Reports Required: Monthly Management Letters; Final Technical Report

Sponsor Contact Person:

Technical Matters
(Scientific Officer)
Dir., Physics Program
Physical Sciences Division
Office of Naval Research
Dept. of the Navy
800 North Quincy St.
Arlington, Va 22217

CONTRACTUAL MATTERS
(Thru GTRI)
Mr. R. J. Whitcomb (ACO)
ONR Resident Representative
Campus

DEFENSE PRIORITY RATING: DO-C9 under DMS Reg. 1

Assigned to: SPECIAL TECHNIQUES

COPIES TO:

Project Director
Director, EES
Director, ORA/GTRI
Assistant Director
Division Chief
EES Accounting
Patent Coordinator

EES Supply Services
Photographic Laboratory
Security—Reports—Property Office
General Office Services
Library, Technical Reports Section
Office of Computing Services
Project File
Other Sue Corbin; Bonnee Wettlaufer

RA-3 (3-75)

GEORGIA INSTITUTE OF TECHNOLOGY
ENGINEERING EXPERIMENT STATION

PROJECT TERMINATION

Date: March 9, 1976

Project Title: Applications of Submillimeter Wave Gigawatt Sources

Project No: A-1717

Project Director: J. J. Gallagher

Sponsor: Office of Naval Research

Effective Termination Date: 10/1/75 (Final Report Due)

Clearance of Accounting Charges: 10/31/75

Grant/Contract Closeout Actions Remaining:

Final Invoice & Closing Doc's.
Final Report of Inventions

Assigned to: Electromagnetics Laboratory

COPIES TO:
Project Director
Director, EES
Assistant Director
Division Chief
EES Accounting
Patent Coordinator
Research Services/Photo Lab
EES Supply Services
General Office Services
Library, Technical Reports Section
Office of Computing Services
Project File
Other Sue Corbin

EES 402 (R10-75)

SUBMILLIMETER APPLICATIONS

ARPA Order Number 2840
Contract Number N00014-75-C-1011
Program Code Number 5E20

Principal Investigator: James J. Gallagher
Phone Number: (404) 894-3500

Name of Contractor: Georgia Tech Research Institute

Scientific Officer: Director, Physics Program
Physical Sciences Division
Office of Naval Research
800 N. Quincy Street
Arlington, Virginia 22217

Effective Date of Contract: 3 February 1975

Contract Expiration Date: 3 May 1975

Amount of Contract: $27,827.00

Sponsored by: Advanced Research Projects Agency
ARPA Order No. 2840

ENGINEERING EXPERIMENT STATION
GEORGIA INSTITUTE OF TECHNOLOGY • ATLANTA, GEORGIA 30332

7 May 1975

Director
Advanced Research Projects Agency
1400 Wilson Boulevard
Arlington, Virginia 22209

Attention: Program Management, DODAAD Code/H x 1241

Subject: Submillimeter Applications

1. Research Program Plan

The research performed under this program involves the analysis of physical phenomena associated with the employment of intense submillimeter radiation in various tactical and strategic scenarios. The program is being performed in accordance with the Contractor's proposal entitled "Applications of Submillimeter Wave Gigawatt Sources," dated 22 January 1975. Researchers with expertise in particular areas have been assigned to analyze the subjects discussed in the original proposal. From the original list of applications, priorities have been assigned to each item. The analysis has proceeded through the items with major attention being given to the high priority items.

2. Major Accomplishments

The areas of highest priority are atmospheric and propagation characteristics in the submillimeter region, antenna properties, countermeasure techniques, radar-type applications and radiative effects from the source. The submillimeter propagation characteristics which are being analyzed are molecular attenuation, particulate scattering (rain, fog, aerosol, etc.), and refractive effects. Thermal blooming and atmospheric breakdown have

been reviewed for the submillimeter spectral region. Antenna parameters which are being studied include, in addition to the submillimeter antenna characteristics, minimizing of side- and back-lobes of the radiated energy and the capability of handling more than one frequency from the one antenna.

The countermeasures studies have been concerned mainly with unconventional techniques, since we have to a major degree avoided efforts which might only duplicate what NRL has treated.

A large list of radar problems has been established, and investigations have addressed this list.

Preliminary progress reports have been prepared on several topics. Further treatment is necessary for most of these areas before completion of the project. The preliminary reports treat

(1) Countermeasures,
(2) Potential Radiation Hazard,
(3) Antenna Techniques,
(4) Atmospheric Breakdown and Thermal Blooming Effects,
(5) Competitive Submillimeter Sources, and
(6) Atmospheric Topics.

Further work on radar applications and covert communications is necessary.

3. Problems Encountered: None

4. Fiscal Status

i. Amount currently provided in contract: $27,827.00

ii. Expenditures and Commitments to Date:

Personal Services	$9,510.96
Retirement	565.54
Overhead	6,182.12
Travel	572.94
Materials and Supplies	30.34
TOTAL	$17,108.22

iii. Estimated Funds Required to Complete Work: $10,000

iv. Estimated Date of Completion of Work: July 1, 1975

5. Action Required by ARPA or ONR: None

6. Future Plans

During the remaining period of the program, the individual topics will be investigated as completely as time permits. A briefing has been arranged for May 28 at ARPA. The program results will be presented in a final report to be distributed by 3 July 1975.

SUBMILLIMETER APPLICATIONS - Monthly Management Report
for Period 7 May 1975 - 12 August 1975

ARPA Order Number 2840

Contract Number N00014-75-C-1011

Program Code Number 5E20

Principal Investigator: James J. Gallagher

Phone Number: (404) 894-3500

Name of Contractor: Georgia Tech Research Institute

Scientific Officer: Director, Physics Program
Physical Sciences Division
Office of Naval Research
800 N. Quincy Street
Arlington, Virginia 22217

Effective Date of Contract: 3 February 1975

Contract Expiration Date: 1 September 1975

Amount of Contract: $27,827.00

Sponsored by: Advanced Research Projects Agency
ARPA Order No. 2840

ENGINEERING EXPERIMENT STATION
GEORGIA INSTITUTE OF TECHNOLOGY • ATLANTA, GEORGIA 30332

12 August 1975

Director
Advanced Research Projects Agency
1400 Wilson Boulevard
Arlington, Virginia 22209

Attention: Program Management, DODAAD Code/H x 1241

Subject: Submillimeter Applications

1. Research Program Plan

The research performed under this program involves the analysis of physical phenomena associated with the employment of intense submillimeter radiation in various tactical and strategic scenarios. The program is being performed in accordance with the Contractor's proposal entitled "Applications of Submillimeter Wave Gigawatt Sources," dated 22 January 1975. Researchers with expertise in particular areas have been assigned to analyze the subjects discussed in the original proposal. From the original list of applications, priorities have been assigned to each item. The analysis has proceeded through the items with major attention being given to the high priority items.

2. Major Accomplishments

During the past reporting period, a presentation was given at DARPA on 29 May 1975, and this was followed by a more detailed quantitative briefing on 15 July 1975. The latter briefing was given by J. J. Gallagher and H. A. Ecker and covered applications in radar, ECM, Communications, plasma penetration and tunability in the infrared wavelength region.

Currently, the final report is being prepared and will include discussions of the above subjects. This report will be submitted on 1 September 1975.

3. Problems Encountered

None

4. Fiscal Status

(i) Amount currently provided in contract: $27,827.00

(ii) Expenditures and Commitments to Date:

Personal Services	$15,828.01
Overhead & Retirement	11,549.53
Travel	1,082.61
Materials & Supplies	177.19
TOTAL	$28,637.34

(iii) Estimated Funds Required to Complete Work: None

(iv) Estimated Date of Completion of Work: September 1, 1975

5. Action Required by DARPA or ONR

None

6. Future Plans

The program results will be presented in the Final Report.

A-1717

GT/EES Project No. A-1717 Contract N00014-75-C-1011

Applications of Submillimeter Wave Gigawatt Sources

by

J. J. Gallagher, H. A. Ecker,
M. D. Blue and R. G. Shackelford

Prepared for
Defense Advanced Research Projects Agency

ENGINEERING EXPERIMENT STATION
GEORGIA INSTITUTE OF TECHNOLOGY
Atlanta, Georgia 30332

FINAL REPORT

ARPA Order Number 2840

Program Code Number 5E20

Scientific Officer:
Director, Physics Program
Physical Sciences Division
Office of Naval Research
800 N. Quincy Street
Arlington, Virginia 22217

GT/EES Project No. A-1717 Contract N00014-75-C-1011

Applications of Submillimeter Wave Gigawatt Sources

by

J. J. Gallagher, H. A. Ecker,
M. D. Blue and R. G. Shackelford

Prepared for
Defense Advanced Research Projects Agency

ENGINEERING EXPERIMENT STATION
GEORGIA INSTITUTE OF TECHNOLOGY
Atlanta, Georgia 30332

FINAL REPORT

ARPA Order Number 2840

Program Code Number 5E20

Scientific Officer:
Director, Physics Program
Physical Sciences Division
Office of Naval Research
800 N. Quincy Street
Arlington, Virginia 22217

SUBMILLIMETER APPLICATIONS

ARPA Order Number 2840

Contract Number N00014-75-C-1011

Program Code Number 5E20

Principal Investigator: James J. Gallagher

Phone Number: (404) 894-3503

Name of Contractor: Georgia Institute of Technology
Engineering Experiment Station
Atlanta, Georgia 30332

Scientific Officer: Director, Physics Program
Physical Sciences Division
Office of Naval Research
800 N. Quincy Street
Arlington, Virginia 22217

Effective Date of Contract: 3 February 1975

Contract Expiration Date: 3 September 1975

Amount of Contract: $27,827.00

Sponsored by: Defense Advanced Research Projects Agency

TECHNICAL REPORT SUMMARY

Recent advances in the technology of relativistic electron beam devices have indicated their potential capability in military applications. This report has briefly considered the applications of a gigawatt source mainly in the areas of radar, ECM and communications. While the majority of the applications has been at millimeter-submillimeter wavelengths, no restricts have been placed on investigations in the microwave region.

The attractiveness of this high power source for millimeter wavelength radar has been studied, and, while several such applications are evident, attention in this report has been mainly given to the important areas of low angle tracking and limited vulnerability radars. It is shown in Chapter 2 that the use of a gigawatt millimeter wave low angle tracking radar system provides a better performance for lower targets, results in reduced multipath effects and improved target-to-clutter ratio, while performing well in all but worst weather conditions and rendering low targets visible at the horizon. The low vulnerability radar, on the other hand, is shown to give reduced vulnerability by its tunability from 60 to 70 GHz and a detection radar range that is not significantly reduced. Among the advantages of this system, are its high resolution at high frequency for reasonably sized antennas and the frequency tuning capability of gigawatt sources which provides the ability to respond to changing weather, range requirements and vulnerability constraints.

In the area of ECM applications of the gigawatt source, calculations have been performed to show that the source can be utilized for range denial at greater distances than conventional source, both in-beam and in sidelobes, has a crystal burnout capability at 22 nmi, can provide significant confusion of victim radar at low PRF and can render a threat radar ineffective by continuous TR tube activation or front-end saturation if very high PRF's are possible for the source.

The area of communications with high power sources presents several interesting potential applications in millimeter wave communications.

Calculations are performed in Chapter 3 related to scenarios requiring low probability of detection, high data rate communications, transmissions through plasma sheaths and plumes, RPV communications and troposcatter techniques. The calculations indicate that the flexibility of the gigawatt source can serve a large number of requirements, not previously satisifed by other technologies. It is determined that system operation is feasible with the gigawatt source under extremely severe weather conditions. The availability of a high power CW relativistic electron beam device, which is not included in the discussions of this report, can contribute further to the applications of this apparatus.

In other applications treated in the report, the production of a tunable IR source by nonlinear optical mixing, submillimeter active imaging schemes, and weather radar applications are discussed. Table 43 on page 144 summarizes the conclusions reached on some of the applications.

In support of the material in the main text of the report, appendices on radiation hazards, antenna considerations, competitive submillimeter sources and atmospheric phenomena are presented. When the relativistic electron beam source is developed, no sources currently being considered for the short millimeter/submillimeter wavelength range will be competitive with these devices.

TABLE OF CONTENTS

LIST OF FIGURES

List of Figures (Cont'd) Page

APPENDIX FIGURES

Appendix Figures (Cont'd) Page

LIST OF TABLES

List of Tables (Cont'd)

List of Tables (Cont'd.) Page

Appendix Tables

CHAPTER 1

INTRODUCTION

Recent developments in the field of linear beam devices have resulted in a new class of relativistic electron beam sources, which offer dramatic increases in pulsed microwave power. These devices can potentially improve the effective operating range of many military electronic systems. In addition, the cyclotron mode of operation, rich in powerful harmonics up to the near infrared wavelength region, could ultimately provide a millimeter or submillimeter wave generator far superior in performance to conventional tubes or projected quantum sources for this spectral region. These new sources can be made tunable over a wide range of frequencies, while the bandwidth of the radiation is less than a few percent. The submillimeter wavelength region has long been considered a fruitful region for applications, yet its critics have properly pointed out that the lack of a suitable source has limited the use of the spectral region to research investigations in the laboratory. The availability of tunable high power sources which can result from the development of the beam devices offers the potential of opening up the short wavelength region for important military applications. No other source, optically pumped lasers or nonlinear optical mixing schemes included, appears to offer the advantages for applications which the beam systems do.

The investigations performed in this program have been the identification and analysis of potential applications of a gigawatt source. While the study is concerned with submillimeter wave applications, no limit has been placed on the region of interest for a particular application. Thus, one of the most promising applications is the use of the source for countermeasures in the X-band wavelength region. In addition, the submillimeter wave radiation was not limited to power less than a gigawatt, even though at present, power levels on the order of gigawatts do not appear to be possible in the near future. In order to perform the study, it was assumed that the source was capable of emitting a gigawatt of power, that PRFs of 1 kHz or greater are possible, and that the source could be considered coherent or incoherent depending upon the application need. These assumptions were made independent of the operating wavelength.

In the discussions of this report, comparisons are made, in several instances, of the gigawatt source with a conventional lower power generator. Despite the fact that the greater power may not be an advantage in all applications considered, it must be emphasized that in the shorter millimeter wavelength region or in the submillimeter wavelength region, the linear beam sources potentially are the only sources available with the peak power, efficiency or flexibility of tuning required for various applications. Thus, while a gigawatt of power may not be necessary for some applications, a smaller version of such sources can be the most appropriate for lower power requirements.

A variety of possible military uses are discussed below. While the length of the program did not allow investigations in great depth, applications were chosen for which the gigawatt source would be most effective. In Chapter 2 of the report, two radar applications, low angle tracking and limited vulnerability radar, and electronic countermeasures have been treated as possibly the most important applications of the high energy sources. In Chapter 3, a large number of communications applications have been discussed. Chapter 4 presents some interactions of the source radiation with plasma phenomena, while Chapter 5 proposes an extension of the tunable source to the infrared and visible region by nonlinear optical mixing schemes. During the course of the study, several topics were considered as possible uses of a gigawatt source. However, the limitations of time have permitted little beyond the tabulation of these subjects. This is presented in Chapter 6 with brief comments on each. In all uses which have been considered, the effects of inclement weather have been included in the calculations. It is under these adverse conditions that the gigawatt source is most valuable, since scenarios do exist for which a conventional lower power source is rendered inadequate. In turn, one might expect that an enemy attack would be launched under cover of inclement weather.In the European theater, the anticipated inclement weather can result in approximately 10% down time for low power sources and infrared systems. The gigawatt source is an appropriate device to consider for this application. Appendix IV briefly summarizes the atmospheric parameters which must be included in any calculations and presents several curves from the literature which are convenient for the determinations. Several papers which contain important infor-

mation are referenced in the appendices. A summary of the applications which have been treated and concluding statements are presented in Chapter 7.

In the applications which have been studied, it has been assumed only that the source exists. The techniques of generating the power, safety precautions, and methods of launching the signal have not been included in the discussions. Some information, however, including the nature of competitive sources, is given in the appendices. The open literature has discussed the developments of the relativistic electron beam devices, and review articles have discussed the current state of the sources [1]. In several applications which can be considered for the sources, the gigawatt source would be used in an airborne system. With currently available power supplies, it can be projected that the beam devices can be packaged for airborne applications [2].

Throughout the report, the high power source is interchangeably referred to as the gigawatt (GW) source, relativistic electron beam (REB) and linear beam device. As indicated previously, assumptions have been made on the nature of the source, and, in order to emphasize the characteristics which have been employed in the calculations, the following parameters are assumed for the gigawatt source:

Output power = 1 Gigawatt
Pulse Repetition Rate = 1 kHz
Pulse Width = 15 - 500 nanoseconds
Pulse Rise Time = 2 - 3 nanoseconds
Source efficiency = 20 - 30 %

It is assumed further that the GW source is either coherent or incoherent as the application requires. For the electronic countermeasure application of range denial, it is also assumed that future developments will result in higher pulse repetition rates. Of the applications which have been studied in this program, the radar applications for low flying vehicles, the low vulnerability radar and the electronic countermeasures are considered the most important applications. Because of the high attenuation and the lack of high power sources in the millimeter wavelength region, the source, on the other hand, has very high potential for short wavelength applications. The difficulties of the use of the visible

and near infrared wavelength regions for imaging and target designation in adverse weather have resulted in the consideration of longer wavelengths in the submillimeter region for these applications. The linear beam devices may prove to be the radiation sources required for the success of such military systems.

The authors wish to acknowledge the contributions and support of several individuals during the course of the study. The contributions of S. Piper, F. Cain, W. Sears, G. Riley, J. Schuchardt and C. Ryan, all of the Georgia Tech Engineering Experiment Station are appreciated. We wish to thank Colonel R. Sullivan of DARPA for his support of the project, and Dr. Victor Granatstein of NRL and Mr. Steve Johnston of MICOM for discussions related to the device and its applications. We wish to acknowledge the support which was provided by the Engineering Experiment Station because of the potential importance of this technology to national needs.

CHAPTER 2

APPLICATIONS OF GIGAWATT SOURCE TO RADAR AND ECM

The possibility of generating RF power at gigawatt levels suggests that radar and countermeasures applications with transmitters at this high level should be investigated. Undoubtedly, many technical problems associated with this high power such as transmission, antenna characteristics, and personnel safety must be solved before a practical implementation can be achieved. However, the basic question that must be answered first is the following: "If all the practical problems are solved, what new capability would be possible for radar and ECM with a gigawatt source that is not possible with current sources?". The approach taken in this report is to consider the above question without specifying the details of practical implementation.

In modern radar, limitations on achieving high angular resolution in real time remain as significant constraints on performance. Antenna aperture size and wavelength are the primary factors that control angular resolution. Because of practical limitations on the physical size of an aperture that is manageable in operational situations, the only alternative to improve angular resolution, other than synthetic aperture radar (SAR), is to operate at shorter wavelengths. For most radar applications, wavelengths shorter than those found in the microwave band have not been practical because of high atmospheric attenuation and limitations on transmitter power.

If an RF power source can be developed to generate a gigawatt of peak power at millimeter wave frequencies, then the advantages of increased antenna gain and angular resolution at millimeter wave frequencies coupled with the availability of a gigawatt of peak power could offset the disadvantages of atmospheric attenuation. Preliminary analyses of a variety of radar applications for a gigawatt source in the millimeter wave region were made. From this group of potential applications, the two uses of a gigawatt source in radar that appeared to have significant capabilities not currently available are (1) low angle tracking over sea clutter, and

(2) a quasi-covert system with limited vulnerability to anti-radiation missiles (ARM) threat. Analyses of these two radar systems are given in the following sub-sections.

Threat radars do not exist operationally in the millimeter wave region. Therefore, for ECM applications the gigawatt source must be considered in the microwave region and below. Conventional ECM applications such as range denial, confusion, and deception were investigated. In addition, non-conventional applications that might be possible with the significantly increased transmitter power such as TR tube activation, front-end saturation, stray path voltage transients, and crystal burnout were analyzed.

The increase in power of course significantly increases the capability of an ECM system for conventional applications. Range denial using a gigawatt source appears to be the most promising of the conventional techniques. An estimate of range denial capability with a gigawatt source at a frequency of 10 GHz is given in the following sub-sections.

Of the unconventional ECM techniques suggested, the capability to produce crystal burnouts in radar receivers offers the greatest promise. This capability does not exist currently; however, a gigawatt source with a 2 nano-second rise time could produce crystal burnouts at useful ranges. A discussion of this technique also is presented later.

2.1 Low Angle Tracking Radar System

A serious problem facing the Navy today is the defense of ships against very low flying aircraft and missiles. The high speed and low altitude over the sea of these attacking vehicles makes radar detection and tracking an extremely difficult problem. Although MTI techniques can be employed they are degraded significantly by multipath effects and high return from sea clutter. If frequencies in the millimeter wave region can be used, the multipath effect would be reduced and narrower antenna beamwidths can be achieved to reduce the amount of sea clutter return in a given angular resolution cell. (Both elevation and azimuth cells).

The use of millimeter waves for the low angle tracking problem has not been practical previously because with the power levels available sufficient

detection range could not be achieved. The availability of a gigawatt source in the millimeter wave region could produce the necessary detection ranges under both good and bad weather conditions with antenna apertures of reasonable size.

Consider as a typical scenario a low flying vehicle approximately 50 feet above the sea, and the radar antenna in the most optimum position at the top of the mast of a ship, such as the new patrol frigate. This situation would be illustrated in Figure 1 for an antenna height of 110 feet above the surface. If the refraction of the radar signal is assumed to be approximately that which would occur with a 4/3 earth radius model, the line-of-sight distance from the antenna to the vehicle 50 feet above the sea surface would be

$$R_{50} = 17.3 \text{ nautical miles.}$$

The distance from the radar antenna to a tangential point on the earth surface would be

$$R_{tan} = 12.9 \text{ nautical miles.}$$

Thus, a low angle tracking radar should have system characteristics that would produce adequate detection in the range from 12.9 to 17.3 nautical miles. Except under unpredictable, anomalous propagation conditions, detection beyond 17.3 nautical miles would be impossible regardless of power level or method of signal processing.

Low Angle Performance

One factor affecting the ability to track radar targets at low angles is the elevation beamwidth of the antenna on the tracking radar. If a rule of thumb [3] is used that it is desirable for tracking to have less than one-fourth of a 3 dB beamwidth in elevation intercept the surface of the sea at the tangential point, then a comparison can be made between X-band frequencies centered at 9.375 GHz and millimeter wave frequencies centered at 94 GHz for low angle tracking.

If an antenna with aperture diameter of 2 meters is assumed for the tracking radar, then at 9.375 GHz a 3 dB beamwidth in elevation of 1.1 degrees

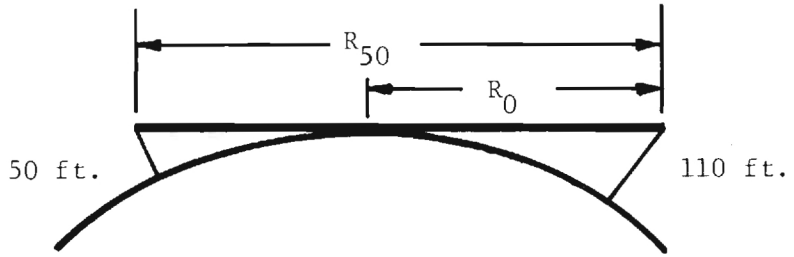

4/3 Radius Refraction Conditions
Radar Height 110 ft.
Aircraft Height 50 ft.

R_0 = 12.9 nmi

R_{50} = 17.3 nmi

Figure 1. 4/3's Earth Radar Horizon

would be possible whereas at 94 GHz a 3 dB elevation beamwidth of 0.11 degrees would be achievable. For the same scenario described previously with an antenna height of 110 feet and a range to a tangental point on the surface of the earth of 12.9 nautical miles, the height of the target above the surface along the boresight line of the antenna when one-fourth of the 3 dB beamwidth intercepts the surface of the sea would be as follows.

Frequency	3 dB Beamwidth	Minimum Height
9.375 GHz	1.1 degrees	382 feet
94 GHz	0.11 degrees	38 feet

Thus, as expected a 10 to 1 increase in frequency (a 10 to 1 decrease in wavelength) will produce a 10 to 1 improvement in minimum height at which a target can be tracked for the same size antenna aperture. At 9.375 GHz, almost one-half of the 3 dB beamwidth would intercept the surface of the sea if the boresight were at a height of 38 feet at the tangential point.

Target-to-Clutter Ratio

In addition to the improved tracking performance that would be possible in the millimeter wave region because of a smaller elevation beamwidth, a smaller azimuth beamwidth would reduce the size of each resolution cell containing clutter and therefore the target-to-clutter ratio. If the following set of parameters are assumed for the low angle tracking radar

(1) pulsewidth - 15 nanoseconds
(2) antenna aperture diameter - 2 meters
(3) range resolution - 2.25 meters
(4) range to clutter cell - 12.9 nautical miles

then the size of the resolution cell can be estimated at both 9.375 GHz and at 94 GHz.

For near grazing and narrow beamwidth, the resolution cell area can be approximated as

$$A = (d)\ (R\theta)$$

where d is the range resolution and Rθ is the azimuth resolution. The calculated resolution cell area at 9.375 GHz is approximately 1,000 square meters, and the resolution cell area for the same antenna diameter is only approximately 100 square meters at 94 GHz. Expressed in dB relative to one square meter (dBsm) the resolution cell area is 30.2 dBsm for 9.375 GHz and 20.2 dBsm for 94 GHz.

If the average radar cross section (RCS) of the target is assumed to be approximately one square meter, then the target-to-clutter ratio for three different values of clutter reflectivity σ_0 will be as given below in Table 1.

Thus, we see from Table 1 that the target-to-clutter ratio is 10 dB higher at 94 GHz than at 9.375 GHz for the same reflectivity of the target and the same clutter reflectivity. Radar cross section measurements on other vehicles have indicated that the radar cross section at 94 GHz will be somewhat higher than that at 9.375 GHz. Therefore, it is possible that even greater improvement could be achieved by going to an operating frequency of 94 GHz.

Comparison of Attenuation Effects

The major disadvantage of operating a radar at 94 GHz is atmospheric attenuation. The question to be answered is "What is the maximum attenuation that can be tolerated and still achieve detection at acceptable ranges?" The same radar characteristics for the 94 GHz radar that were used in previous calculations were used to calculate the maximum tolerable attenuation. These parameters are summarized in Table 2.

With the gigawatt source operating at 94 GHz, an attenuation of 1.8 dB per kilometer can be tolerated for detection at 12.9 nautical miles (the tangential point in the described scenario). At this frequency, fog which reduces visibility to about 300 feet or rain at approximately 2 millimeters per hour will produce an attenuation of approximately 1.8 dB per kilometer. To achieve detection at the maximum line-of-sight range of 17.3 nautical miles, the maximum tolerable attenuation is 1.26 dB per kilometer. This attenuation factor corresponds to fog which reduces visibility to 600 feet or to rain at 1 millimeter per hour.

TABLE 1

TARGET-TO-CLUTTER RATIO FOR TARGET RCS = 0 dBsm AND INDICATED VALUES OF σ_0

Frequency	(σ_0 = -10 dB)	(σ_0 = -20 dB)	(σ_0 = -30 dB)
9.375 GHz	-20.2 dB	-10.2 dB	-0.2 dB
94 GHz	-10.2 dB	-0.2 dB	+9.8 dB

TABLE 2

RADAR CHARACTERISTICS OF 94 GHZ RADAR FOR LOW ANGLE TRACKING

Peak Power	10^9 W	Antenna Diameter	2 m
Frequency	94 GHz	3 dB Beamwidth	0.11^o
Sensitivity	-90 dBm	Gain	64 dB
RCS	1 m^2		

TABLE 3

RADAR CHARACTERISTICS OF 9.4 GHZ RADAR FOR LOW ANGLE TRACKING

Peak Power	10^9 W	Antenna Diameter	2 m
Frequency	9.375 GHz	3 dB Beamwidth	1.1°
Sensitivity	-100 dBm	Gain	44 dB
RCS	1 m^2		

If the same size antenna (2 meter aperture diameter) is used at 9.375 GHz with a gigawatt source and typical radar parameters as indicated in Table 3, the line-of-sight detection range of 17.3 nautical miles can be achieved with an attenuation of 1.01 dB per kilometer. This value of attenuation is greater than any reported for atmospheric attenuation at a frequency of 9.375 GHz. Thus, line-of-sight detection range is easily achievable at 9.375 GHz under all weather conditions with a gigawatt source.

It should be pointed out that although the 94 GHz radar would be detection range limited under adverse weather conditions, the current close-in weapon system (CIWS) under development by the Navy, claims a detection range of only 3 nautical miles. At that range, an attenuation of 9.5 dB per kilometer could be tolerated with a gigawatt source at 94 GHz. This attenuation factor corresponds to a heavy rain of 16 millimeters per hour or a fog corresponding to 100 feet visibility. Thus, even under very severe weather conditions, the 94 GHz low angle tracking system operating with a gigawatt source would be superior to the CIWS.

Multipath Effects

One of the serious problems that can affect radars operating in the microwave region over the sea is that of multipath lobing. Under many conditions of low incidence angle and sea state, the direct radiation from the radar and forward scattered multipath from the sea can produce an interference pattern of peaks and deep nulls. Figure 2 shows a typical multipath lobe plot for a radar operating at 9.375 GHz from an antenna 110 feet above the sea with a mean wave height of 3 feet; coverages shown are for a curved earth as a function of target height elevation angle and range in nautical miles. The free space coverage contour is also shown for comparison. A target flying at a constant altitude above the sea and approaching the radar would have numerous fades as it passed through nulls in the multipath pattern.

At 94 GHz, the surface of the sea appears much rougher than at 9.375 GHz because of the much shorter wavelength of the operating frequency. Figure 3 shows that for the same antenna height and average wave height

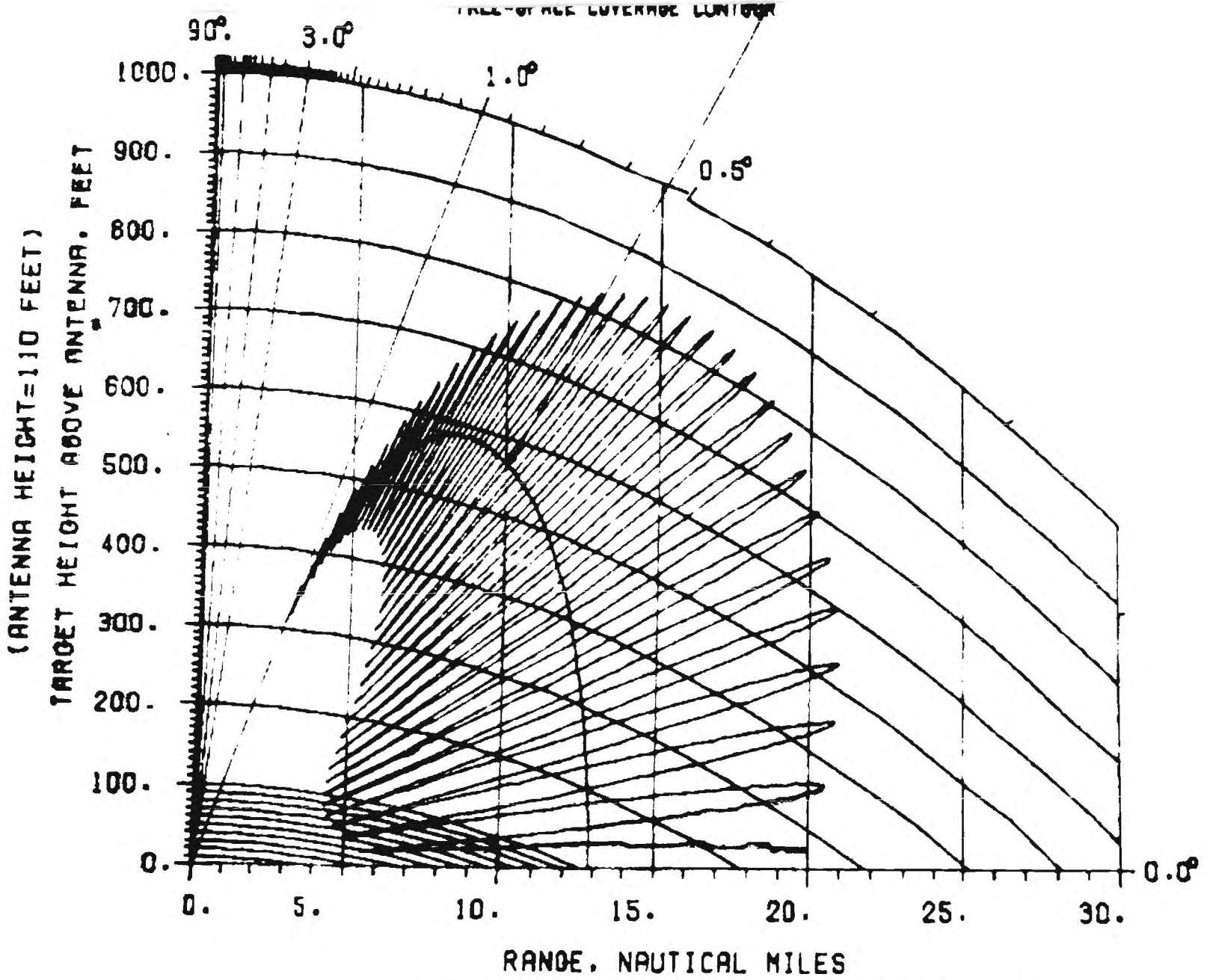

Figure 2. Multipath Lobe Plot, Wave Height 3 ft., Frequency 9.375 GHz.

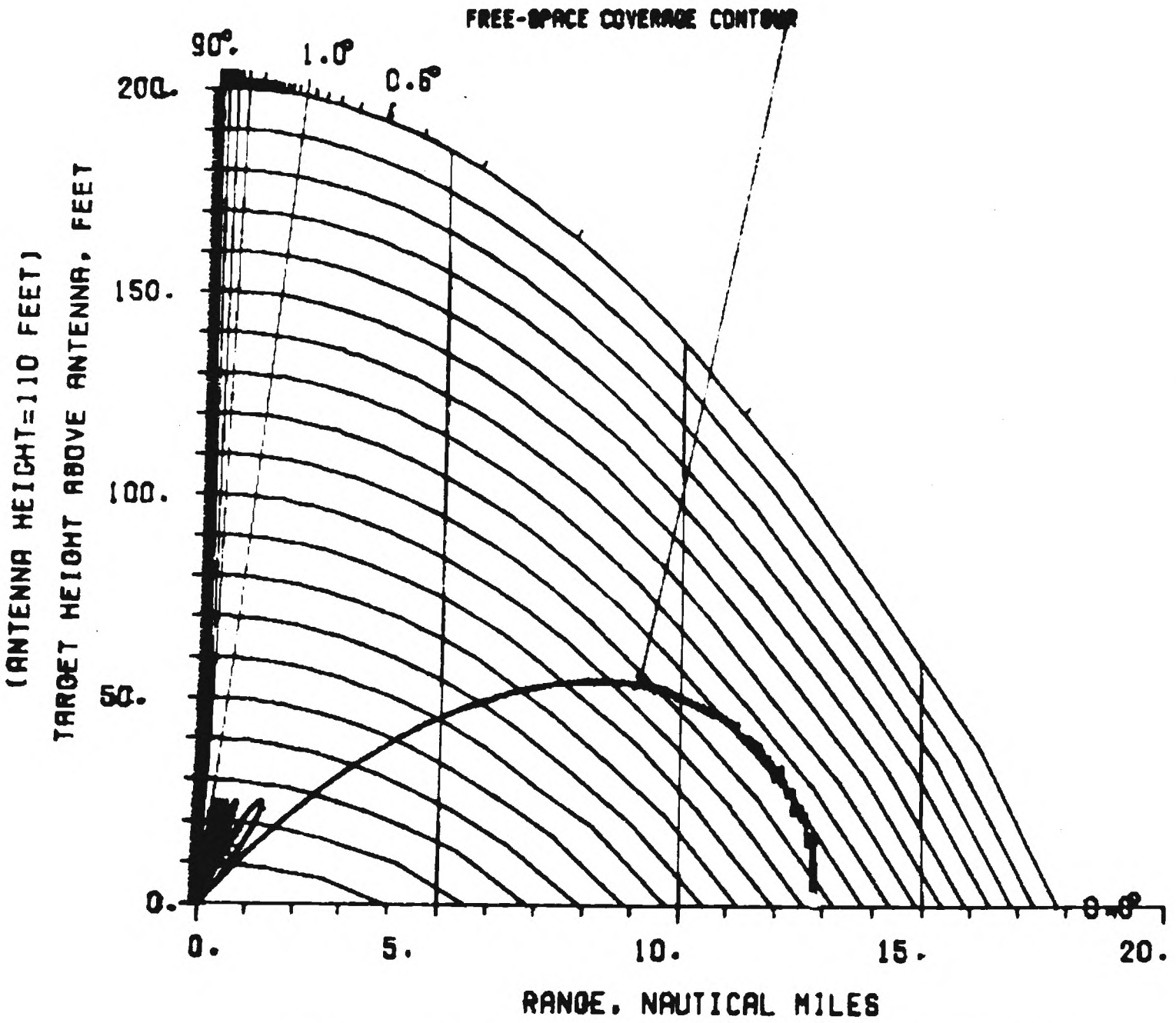

Figure 3. Multipath Lobe Plot, Wave Height 3 ft., Frequency 94 GHz.

that were used in Figure 2 for a 9.375 GHz radar that little multipath lobing would occur at a frequency of 94 GHz. The multipath plot is essentially an overlay of the free space coverage contour. A similar plot was calculated for a mean wave height of 1 foot, and still very little multipath lobing was observed. Thus, it can be anticipated that operating at 94 GHz would provide a significant advantage over operating in the microwave region for multipath problems.

Summary of Low Angle Tracking Radar Performance

The ability to achieve a 10 to 1 reduction in both elevation and azimuth beamwidths by operating at 94 GHz rather than at 9.4 GHz yields improved low angle tracking because less sea clutter would be illuminated in both azimuth and elevation at low tracking angles. Operation at the much shorter wavelength corresponding to 94 GHz significantly reduces the effect of multipath lobing. The availability of a gigawatt source would make operation at 94 GHz practical because the improved angular resolution and reduction of multipath would be possible with acceptable detection ranges. Table 4 summarizes these conclusions.

2.2 Limited Vulnerability Radar System

The availability of a tunable gigawatt source operating at frequencies of 60 GHz and above would permit the use of the attenuation versus frequency characteristics of the oxygen absorption line to control detectability of a radar signal by antiradiation missile (ARM) threats and D-F equipment. For example, moving up in frequency from 64 GHz to 70 GHz will produce a change in atmospheric attenuation from 3 dB per kilometer to 0.7 dB per kilometer. A further increase to 94 GHz will reduce the atmospheric attenuation to 0.4 dB per kilometer under clear weather conditions. Figure 4 shows the power that would be available at a threat system from a gigawatt source operating at three different frequencies and under two different weather conditions. Also indicated by X's are the detection ranges against a one square meter target for the radar operating at the indicated frequency. This figure demonstrates dramatically the difference in the attenuation rate at 10 GHz and at 64 GHz for either clear or rain conditions and for 94 GHz

TABLE 4

LOW ANGLE TRACKING RADAR SYSTEMS

Conclusions For Gigawatt Millimeter Wave Systems:

- Low Targets Visible At The Horizon
- Improved Target-To-Clutter Ratio - Better Tracking
- Reduced Multipath Effects
- Better Performance For Lower Targets
- System Performs Well In All But Worst Weather Conditions

Upper 10 GHz curves are for typical X-band radar. Lower 10 GHz curve is for same target detection range as 64 GHz, rain curve.

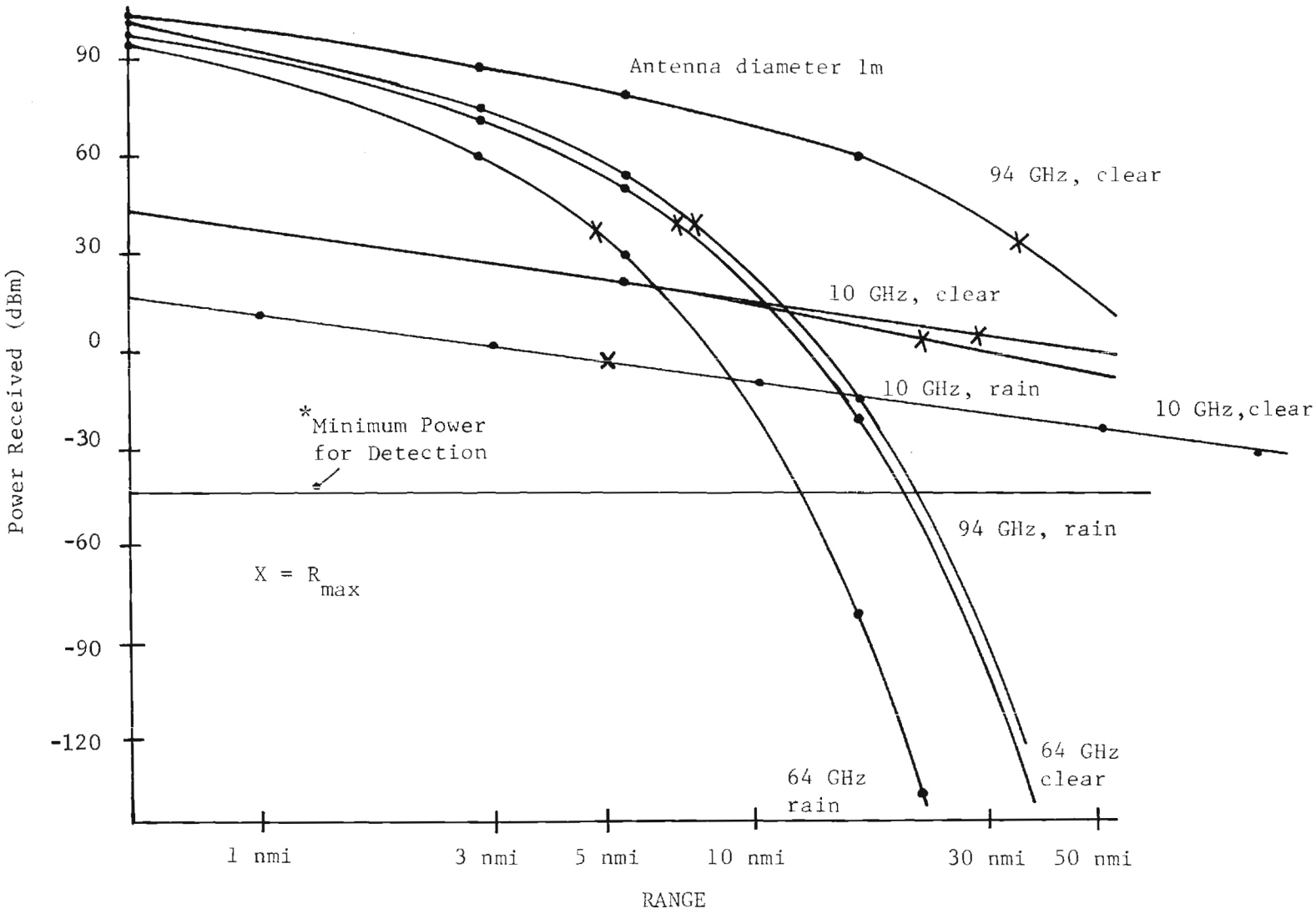

Figure 4. Power Received at Threat Detection System.

with rain. For these calculations, it was assumed that both the radar antenna and the antenna on the threat detection system had diameters of one meter. Under these conditions, the radar can detect targets in the region from 5 to 10 nautical miles and could not be detected by a threat system at ranges greater than 25 to 30 nautical miles. If 10 GHz were used as the operating frequency, even though detection out to 30 nautical miles by the radar would be possible, detection by the threat systems could easily be achieved at ranges greater than 150 to 200 nautical miles.

It is impractical to assume that the antenna size on an ARM could be as large as that used to generate the data in Figure 4. If a more practical antenna diameter of 1/2 meter were assumed for the ARM, then the power received at the threat would be as shown in Figure 5. For this situation, of course, the detection ranges for the radar system operating in the millimeter band would be unaffected and still would be in the 5 to 10 nautical mile region. However, the detectability of the radar signal by the ARM would be reduced because of the smaller ARM antenna. Typically, some ARMs achieve a sensitivity of -45 dBm. With that sensitivity, the detection range by the ARM would be less than 15 nautical miles.

Variation of Radar Detection with Frequency

To illustrate how the limited vulnerability system would operate in different weather conditions, the detection range against a one square meter target has been calculated for four different frequencies and three different weather conditions. The results of these calculations are summarized in Table 5. Also indicated for comparison are the ranges at which the radar signals would be detectable by an ARM with a -45 dBm receiver sensitivity and a 1/2 meter diameter antenna. Note that approximately a 7 nautical mile detection range would be possible under clear conditions at 64 GHz but would be reduced to a 4.4 nautical mile detection range with moderate rain. Under moderate rain conditions, it would be desirable to tune the frequency to approximately 70 GHz to achieve the same approximately 7 nautical mile detection range and to maintain limited vulnerability. Under conditions of fog, as indicated in the Table, approximately 66 GHz would be the desired frequency.

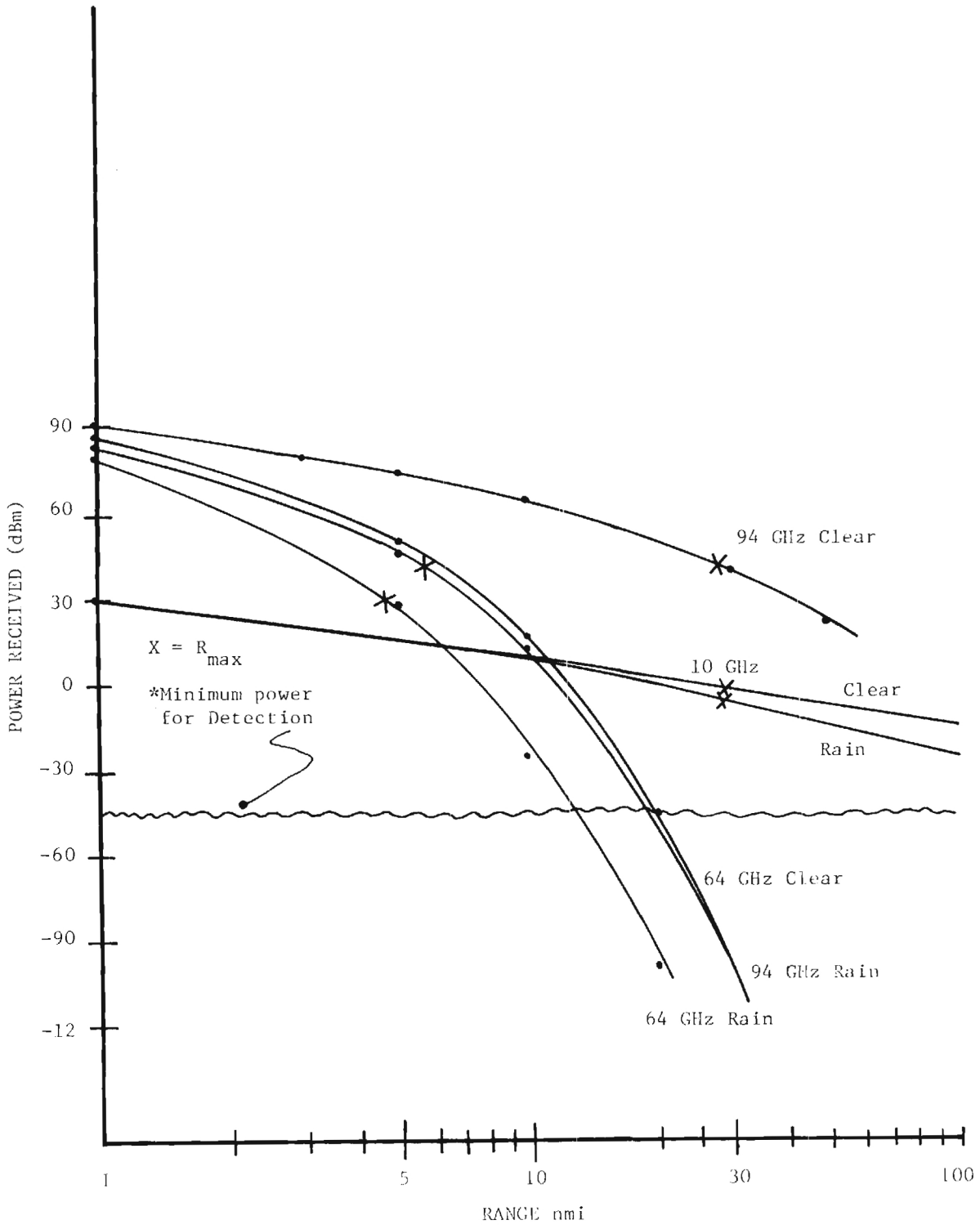

Figure 5. Power Received at Anti-Radiation Missile with 1/2 Meter Diameter Antenna.

TABLE 5

GIGAWATT RADAR SYSTEM

Peak Power = 10^9 Watts
Sensitivity = -90 dBm

Antenna Diameter = 1m
Radar Cross Section = $1m^2$

FREQUENCY	64 GHz	66 GHz	70 GHz	94 GHz
Wavelength	4.7 mm	4.5 mm	4.3 mm	3.2 mm
ANTENNA				
3 dB BW	0.33°	0.32°	0.30°	0.22°
Gain	54.6 dB	54.9 dB	55.4 dB	58.0 dB

CONDITION	64 GHz			66 GHz			70 GHz			94 GHz		
	L dB/km	R_{max} (nmi)	ARM Detection Range	L dB/km	R_{max} (nmi)	ARM Detection Range	L dB/km	R_{max} (nmi)	ARM Detection Range	L dB/km	R_{max} (nmi)	ARM Detection Range
Clear	3	6.8	19 nmi	2	9.5	28 nmi	0.7	21.6	75 nmi	0.4	34.4	129 nmi
Fog ($0.32 g/m^3$)	3.5	6	17 nmi	2.5	7.9	23 nmi	1.3	13.4	43 nmi	1.4	13.1	40 nmi
Rain (4 mm/hr)	5.1	4.4	12 nmi	4.1	5.3	15 nmi	2.9	7.1	20 nmi	3	7.1	20 nmi

Data for an operating frequency of 94 GHz are shown to reference the results in the table to the window at that operating frequency. For the objective of limited vulnerability under a variety of weather conditions, it can be seen that little is gained by going from 70 GHz to 94 GHz. Thus, with a tuning range only from 64 to 70 GHz the necessary control over detection range and detectability can be achieved. Of course, the gigawatt source is necessary to obtain useful detection ranges.

If a comparison is made with a typical X-Band radar with the parameters indicated in Table 6, it can be seen that detection ranges greater than 20 nautical miles are possible under all three weather conditions used previously for the millimeter wave radar. These data are summarized in Table 7 along with the detectability of an ARM with -45 dBm sensitivity and a 1/2 meter diameter antenna. Subject to ARM propulsion limitation, the very long detection ranges by the ARM threat render this system considerably more vulnerable than the tunable millimeter wave radar system.

Summary of Performance for Limited Vulnerability Gigawatt Radar

In this subsection it has been shown that a gigawatt signal source tunable from 60 to 70 GHz will enable the radar designer to exploit the reduced vulnerability which results from the high atmospheric attenuation in this region without reducing the detection range of the radar. In addition to this advantage, operation at such high frequencies makes possible high angular resolution with reasonably sized antennas. By tuning the frequency of the gigawatt signal source, the radar operator is able to respond to changing weather conditions, range requirements, and vulnerability constraints. Table 8 indicates the conclusions on the limited vulnerability radar.

2.3 Electronic Countermeasures Applications

The availability of a gigawatt source will make conventional electronic countermeasures (ECM) techniques such as range denial, confusion, and de-

TABLE 6

10 GHz RADAR PARAMETERS

Peak Power = 5.0×10^4 W	Antenna Diameter = 1 m
Wavelength = 3 cm	3-dB Beamwidth = 2.1°
Sensitivity = -100 dBm	Antenna Gain = 38.5 dB
Radar Cross Section = 1 m^2	

TABLE 7

WEATHER CONDITION

	Clear	Fog ($0.32 g/m^3$)	Rain (4 mm/hr)
Attenuation	0.02 dB/km	0.04 dB/km	0.08 dB/km
Maximum Range	27.8 nmi	25.3 nmi	21.6 nmi
Arm Detection Range	550 nmi	330 nmi	200 nmi

TABLE 8

LIMITED VULNERABILITY GIGAWATT RADAR

CONCLUSIONS

- Tunability from 60 to 70 GHz gives reduced vulnerability
- Detection range of radar not significantly reduced
- High angular resolution at high frequency for reasonably sized antennas
- Frequency tuning of GW source provides capability to respond to changing weather, range requirements and vulnerability constraints

ception useful at greater ranges and more devastating at close ranges than is possible with present day signal sources. In addition to these applications, the unique characteristics and tremendous power available with the gigawatt source also enable exploitation of other unconventional ECM techniques such as crystal burnout and front-end saturation.

An example of a conventional ECM application is utilization of the gigawatt source to generate signals which will deny range information to the victim radar operator. For this technique the gigawatt jammer transmits pulses which are out of synchronism with the victim radar. This results in a multitude of target blips at various ranges on the victim radar display so that the range information for a given target is confused.

For sufficiently close ranges, the gigawatt source will have sufficient power to enter the sidelobes of the victim radar antenna and generate these confusing target blips at all azimuths. With a high enough jamming prf it is possible to saturate the entire display of the victim radar. A sample calculation will demonstrate the potential of this technique. It is assumed that the victim radar display has 500 range cells and 30 azimuth cells for a total of 15,000 resolution cells and that the display phosphor has a 1 second memory. The victim radar antenna is assumed to have a 0.5 meter diameter with sidelobes 24 dB down and the receiver saturates at -10 dBm of received power. In order to saturate this display fully, each resolution cell must be saturated at least once during the phosphor memory time, therefore a prf of at least 15 kHz is required for a jammer. Because the jammer and radar are not synchronized, the signals will be dispersed and fill the display. For operation at 10 GHz, a conventional 200 kW jammer will have only enough power to saturate the victim radar system through its antenna sidelobes at 1.1 nmi while the gigawatt jammer would be effective out to 79 nmi. This demonstrates the tremendous improvements in ECM capability which a gigawatt source would make possible. A prf of 15 kHz is high; however, even if the jammer is only capable of a fraction of this prf, it would still result in a thoroughly confusing display of the victim radar. Table 9 summarizes the range denial case.

An interesting electronic countermeasure capability which the gigawatt signal source makes possible is crystal burnout. This technique takes advantage

TABLE 9

RANGE DENIAL

Objective: Saturate Display In All Resolution Cells

Assumptions: Radar Display - 15,000 Display Resolution Cells, -10 dBm Received Power Required, 1 Second Phosphor Memory.

Radar Antenna - 0.5 Meter Diameter, -24 dB Sidelobes

Source Requirement - PRF: 15,000 pps

Results For 10 GHz Sources:

		Max Jamming Range (nmi) 3 dB Beamwidth	Sidelobe
Conventional Mag.	-200 kW	17.7	1.1
REB Source - 1 GW		1,252	79

of the fast rise time of the gigawatt source to apply sufficient energy to the diode before the radar TR tube activates so that the diode junction overheats and destroys itself before it can dissipate the energy thermally.

For a gigawatt signal source which achieves peak power in 2 nanoseconds and a threat radar system with TR tube response of 5 nanoseconds, it is possible to apply a 3 nanosecond high power pulse to the receiver diode. This is a much shorter period than that required by the diode to thermally dissipate the applied energy. Therefore, by applying the 10^{-7} joules of energy required to burn out a typical diode in 3 nanoseconds, the crystal can be destroyed. This requirement corresponds to +45 dBm (30W) received power. At a frequency of 10 GHz and a transmitting antenna gain of 38 dB, the gigawatt signal source is effective for crystal burnout out to 22 nmi with a 32 dB receiving antenna gain. It is important to note that this technique is not possible with conventional microwave sources because their rise times are not fast enough. Table 10 presents the case of crystal burnout by the gigawatt source.

With a high prf on the order of several thousand pps, it is possible to achieve range denial at long ranges with the gigawatt source. For a lower prf of say several hundred, it is still possible to achieve significant confusion of the victim radar display. By employing the gigawatt source as a very high power amplifier, it is possible to do deception jamming at long ranges.

By taking advantage of both the fast rise time and high power of the gigawatt signal source, it is possible to burn out the crystal of a threat radar system. With very high prf's on the order of several hundred thousand pps, the threat radar can be rendered ineffectual by continuous TR tube activation or front-end saturation. Table 11 presents the conclusions of the study of ECM applications of a GW source.

TABLE 10

CRYSTAL BURNOUT

Objective: Threat Denial By Thermal Destruction Of Mixer Crystal

Assumptions: Crystal Is TR Tube Protected

TR Tube Response is 5 ns

REB Source Achieves Peak Power in 2 ns Results in 3 ns High Power Pulse

Ballistic Heating (Short Time Compared to Diode Thermal Time Constant)

10^{-7} Joule Required Absorbed Energy

$$\text{Required Received Peak Power} = \frac{10^{-7}\ \text{J}}{3 \times 10^{-9}\ \text{s}}$$

= 33.3 Watts = +45 dBm

Transmitter: G_t = 38 dB, $P_t = 10^9$ W, $F_t = 10^{10}$ Hz

Receiver: G_r = 32 dB, F_r = In Band

RESULTS

Conventional Magnetron: Impossible At Any Range Due To Slow Rise Time Of Pulse

REB Source: Burnout Range: 22 nmi

TABLE 11

ECM APPLICATIONS OF A GIGAWATT SOURCE

Conclusions:

- Range Denial At Greater Distances Than Conventional Sources, Both In Beam And In Side-Lobes
- Crystal Burnout Capability at 22 nmi
- Significant Confusion Of Victim Radar At Low PRF
- Threat Radar Ineffective By Continuous TR Tube Activation Or Front-End Saturation If Very High PRF Possible For GW Source

CHAPTER 3

COMMUNICATIONS APPLICATIONS

The frequency spectrum above 10 GHz is becoming an important frequency region further transmission of very wideband data such as high speed digital data. Communication system parameters must be adjusted to maximize the use of this spectral region because of the propagation characteristics of the region. The frequency range below 10 GHz, which is almost ideal for communication facilities because of propagation conditions, is becoming crowded. The increased demand for data transmission channels and the demand for channels which can accommodate data rates in excess of 100 Mbps are for any future communication systems to use the frequency region above 10 GHz.

The availability of gigawatt sources can provide the transmitter power necessary for many successful communications systems under several propagation conditions. The availability of transmission windows in the millimeter and submillimeter region provides the means of communicating over large distances at several frequencies under diverse military requirements. The gigawatt source in turn allows these communications to occur in severe rain, snow and fog conditions, a considerable advantage over transmission of high data rates under similar conditions at optical frequencies. The molecular absorption regions can also be used for secure communications for a variety of military scenarios. While several covert communications systems have been postulated for the millimeter wavelength region with low power sources, the gigawatt source yields the capability for secure operation under the most inclement atmospheric conditions. The tunability and multiple frequency characteristics of such sources as the REB can be used for a large number of broad frequency coverage techniques and frequency diversity schemes. In some covert applications, the range limiting effects of the atmosphere in the millimeter and submillimeter regions indicate that a gigawatt of power is not necessary. However, it must be emphasized that sources such as the REB may be the only sources capable of providing adequate power in the short wavelength regions.

Digital bit streams having bit rates in the hundreds of megabits per second provide a communication capability useful for the transmission of many forms of information. Table 12 shows a comparison of several carrier modulation techniques with respect to bandwidth and relative energy per bit to noise power spectral density. The quadriphase modulation QPSK provides bandwidth efficiency as well as good power efficiency. With the projected gigawatt sources, bandwidths on the order of 600 MHz should be possible so that the bit rates given in the last column of Table 12 would apply to each modulation method. Which of these modulation methods can be employed with a REB source must be determined; however, consideration can be given to using the gigawatt source as an amplifier of a modulated input signal.

TABLE 12

POWER AND BANDWIDTH COMPARISON IN DIGITAL COMMUNICATIONS

Digital Modulation Methods	Normalized Average Energy per Bit (BER = 10^{-5})	Bits Per Cycle of Bandwidth	Resulting BIT-RATE (Mbps)
16-ary PSK	18 dB	4 bits/Hz	2400
16-ary MFSK	31 dB	4 bits/Hz	2400
Quadriphase	10 dB	2 bits/Hz	1200
Coherent PSK	10 dB	1 bit/Hz	600
Amplitude (DSB)	10 dB	1 bit/Hz	600

To be useful as a communication device, the relativistic electron beam (REB) source must be capable of being modulated by some means or it must be capable of amplifying a modulated signal without producing too much distortion to render the modulated signal useless. If the source is coherent, the possibility of angle modulation exists. This would probably be accomplished at a low level and the REB device used as an amplifier to produce the high power output signal, thus eliminating the necessity of high level modulation. The

phase characteristics of the device would be important in determining distortion effects such as intersymbol interference for digital modulation or distortion of analog signals. Amplitude modulation is also a possible technique which may be used with the REB. If the modulation is produced at a low level and the REB used as an amplifying device, its amplitude linearity must be considered.

Since the pulse of the device is so short (∿15 nanoseconds), any modulation technique such as digital angle modulation or amplitude modulation of the device must operate at a very high rate. If a bit time were 15 nanoseconds and the REB operated at the 15 nanosecond pulse length, then, of course, the transmission of one bit per pulse is possible, unless some multiphase or multiple amplitude system is used (m-ary system).

There is also a limitation in the transmission of real time data with the pulse rate (or sampling rate of 1 kHz) since a signal must be sampled at a very minimum of twice the highest frequency in the signal. This, when practical considerations enter, would limit the transmission of real time data to signals having a maximum frequency of several hundred cycles per second. For voice communications, sampling rates of the order of 8 kHz would be required for real time operation, and digitizing into 7 bits per sample would probably be required.

For lasers, pulse position modulation (PPM) which includes on-off modulation for Q-switched lasers represents a modern modulation technique, with PPM requiring a bandwidth at least twice the bit rate. [4] This is the most likely modulation method for application with the gigawatt source as a transmitter so that bit rates on the order of 300 Mbps should be possible.

For communication in the millimeter and submillimeter wavelength region, the higher frequency increases the number of frequency bands which can be used as communication channels. In the spectral region from 300-1300 μm, there are six atmospheric windows of intermediate transmission, shown in Appendix IV, and these can be used for communication applications of the gigawatt source. In these spectral regions, the reduced antenna dimensions, because of the shorter wavelength, is an advantage for receiver systems in aircraft, satellites and mobile vehicles.

3.1 Millimeter Wave Covert Communications

Improved surveillance techniques have necessitated consideration of several covert communications systems with the millimeter and submillimeter spectral regions providing advantages for this type of application. Several covert systems, operating in the spectral region of the O_2 absorption lines (50-60 GHz), have been proposed and investigated. The oxygen band is composed of 43 known lines between 48.9 GHz and 70.5 GHz. The studies of covert systems have all mainly been concerned with low power sources for very short range applications. In addition, operation during the most severe weather conditions has not been included in these low power systems. In adverse weather applications, low power systems are limited to ranges much less than is adequate for the covert application.

The availability of a tunable gigawatt source in the millimeter or submillimeter wavelength region provides considerable flexibility in choosing the mode of operation. The source can be operated in clear weather at reduced power and at its maximum power in inclement weather to achieve the same transmission distance, or for a longer overt distance operated at maximum power on an O_2 line and, with the same power output, moved onto the wing of the line as the inclement weather worsens. The large frequency band of the millimeter/submillimeter region in itself affords a degree of covertness since predetermined frequency agility schemes or multi-frequency transmissions could render the system inaccesible to an enemy surveillance system.

Several advantages are obtained from operation of a covert communications system in the millimeter or submillimeter wavelength region. The regions of high attenuation in this spectral region, discussed in Appendix IV, provide secure operation over limited range with a rapid exponential decay for detection much beyond the intended receiving range. In addition, the narrow beamwidths that are obtainable with reasonably sized antennas contribute further to the covertness. Because of the availability of strong absorptions throughout the millimeter/submillimeter region, the communication system has an anti-jamming capability, unless, as shown later, a gigawatt jammer is available for use against the covert system. In any event, the short range required for jamming

a ground system causes enemy jamming aircraft to be vulnerable to surface-to-air guided missiles. On the other hand, the atmospheric attenuation of the short wavelength region does result in a reduced threat imposed by radiation-seeking missiles. In addition to these advantages, covert communications will enjoy those advantages which apply to conventional short wavelength communications, i.e. a high data rate capability and narrow beamwidths, while the tunability of a device such as the REB affords all weather capability.

Two disadvantages are caused by the atmospheric attenuation of the millimeter/submillimeter region. For a covert horizontal air-to-air communication link operating on an O_2 line, the channel capacity is limited to approximately 80 MHz at 20 km altitude. This limitation is imposed by the narrow breadth of the oxygen absorption lines when transmission is performed either horizontally or vertically through the atmosphere. Figure IV-2 shows this effect, as transmission on any one absorption line is limited to a narrow bandwidth around the line peak. For greater bandwidth requirements in a surface-to-air covert communication application, transmission at a higher frequency on a broader H_2O absorption peak can be employed. In the short millimeter or submillimeter wavelength region where water lines limit the range, atmospheric transmissivity is variable due to changes of relative humidity and air temperature so that adjustments of the power level or operating frequency are required as a function of the meteorological parameters. Table 13 summarizes the advantages and disadvantages of the millimeter and submillimeter regions for covert communications.

In order to demonstrate the applicability of the gigawatt source to the problem of covert communications, the subsections that follow present examples utilizing frequencies in the millimeter and submillimeter wavelength regions.

TABLE 13

COVERT COMMUNICATIONS

Advantages Of Operation In MM Or Submm Wavelength Region:

- High Attenuation Provides Secure Operation Over Limited Range-Rapid Exponential Decay
- Anti-Jamming Capability
- High Data Rate Capability
- Narrow Beamwidths
- Short Range Causes Enemy Jamming Aircraft To Be Vulnerable To Surface-To-Air Guided Missiles
- Tunability Affords All Weather Capability
- Reduced Threat Imposed By Radiation-Seeking Missiles

Disadvantages Of Operation In MM Or Submm Wavelength Region:

- In Shorter MM or Submm Wavelength Region - Atmospheric Transmissivity Is Variable Due To Changes Of Relative Humidity And Air Temperature
- For O_2, Channel Capacity of Surface-To-Air Is Limited To Approximately 80 MHz

3.1.1 Covert Ground-to-Ground Communications

Several important military applications require ground-to-ground communications for a limited range. Such is the case in battlefield command and control situations or in amphibious operations in ship-to-shore communications. Consider the case of communications on the 5 mm O_2 line complex where advantage can be taken of the high molecular absorption and where the range can be varied by tuning on the wings of the lines. If one considers the molecular attenuation at two near-lying frequencies for clear weather conditions, it is seen from Figure IV-1 of Appendix IV that the attenuation at 60 GHz is approximately 14 dB/km while at 56 GHz, the attenuation has dropped to approximately 7 dB/km. Figure IV-18 in Appendix IV shows the attenuation in the millimeter wavelength region for various rainfall rates. From this, it is assumed that the attenuation α_R for 22 mm/hr rainfall rate is 7 dB/km. Thus, the total attenuation during such a rainfall is

$$\alpha = 21 \text{ dB/km at 60 GHz}$$

$$\text{or} \quad \alpha = 14 \text{ dB/km at 56 GHz}$$

By operating at 60 GHz in clear weather and 56 GHz during a 22 mm/hr rainfall, the communication range is held practically constant at 10.89 km. Table 14 summarizes the results for this operation. It is seen that, even during heavy rain, the propagation range at 60 GHz is on the order of 8 km.

The following serves as an example of the range calculation and is, in addition, typical of the cases which follow:

Consider the range equation

$$R^2 e^{\alpha R} = \frac{P_o \lambda^2 G_1 G_2}{(4\pi)^2 \text{ FkTB (S/N)}} .$$

If we assume

$A = 1 \text{ m}^2$, antenna area

F = 10 dB, Noise Figure

$k = 1.38 \times 10^{-23}$ joules/degree, K

TABLE 14

COVERT GROUND-TO-GROUND COMMUNICATION

Battlefield Command and Control

Amphibious Operations: Ship-to-Shore

Communication on 5 mm O_2 Lines

For Clear Weather -

α = 14 dB/km at 60 GHz

α = 7 dB/km at 56 GHz

For Inclement Weather (Rain) -

Assume α_R = 7 dB/km for 22 mm/hr rainfall rate

α = 21 dB/km at 60 GHz

α = 14 dB/km at 56 GHz

Tunability of GW source provides constant range

GHz	Attenuation dB/km	Range, km
60	14	10.89
60	21	7.96
56	7	21.06
56	14	10.93

$T = 300^{o}K$

$B = 2 \times 10^{8}$ Hz, receiver bandwidth

$S/N = 10$ dB

$$G_1 = \frac{4\pi\eta A}{\lambda^2} \text{ where } \eta = 0.75$$

$= 55$ dB gain at 60 GHz

and $G_2 = 55$ dB (receiver antenna same as transmitter antenna). Then, with $P_o = 10^9$ watts, under clear weather conditions, $\alpha = 14$ dB/km at 60 GHz so that R = 10.89 km. In a rainfall of 22 mm/hr, tuning to 56 GHz yields approximately the same propagation range.

For acquisition by a 60 GHz intercept receiver, assume that the intercept receiver has the same characteristics as the communications receiver, but that S/N = 3 dB is required for detection instead of 10 dB as assumed for communications. Consider that the intercept receiver is in the side-lobe of the transmitter antenna pattern. Then, $G_1 = 0$ dB for this case and the detection range is calculated to be 7.69 km for clear weather and 5.28 km in the rainfall assumed above. Table 15 summarizes the intercept conditions. It is seen that, unless the intercept receiver is in the direct beam of the transmitter, it must be at a distance from the transmitter which is less than the distance of the communication receiver from the transmitter. The assumption that the intercept receiver is as sensitive as the operational receiver concedes greater capability to the interceptor than a field unit would have in reality. The requirement for a smaller portable or airborne unit including a smaller antenna will result in less sensitive detection of the radiation. On the other hand, if the intercept receiver were directly in the transmitter antenna beam, was of the same sensitivity as the communication receiver and required only S/N = 3 dB, the detection range at 60 GHz in clear weather for $B = 2 \times 10^8$ Hz would be R = 11.23 km, only 0.25 km beyond the intended receiver.

Table 16 gives a comparison of covert communications for the GW source with lower power sources. The calculations have been made for receiver bandwidths of 2×10^8 Hz and 0.5×10^6 Hz. The range limited

TABLE 15

COVERT GROUND-TO-GROUND COMMUNICATIONS

Acquisition by 60 GHz Intercept Receiver

Assume Same Characteristics for Intercept Receiver
With S/N = 3 dB for Detection

Intercept Receiver is in Side-Lobe of Transmitter

Then G_1 = 0 dB for This Case

Detection Range = 7.69 km in Clear Weather
= 5.28 km in Rain

TABLE 16

COMPARISON OF COVERT COMMUNICATIONS (GROUND-TO-GROUND)
WITH DIFFERENT TRANSMITTER POWERS

a) Bandwidth = 2×10^8 Hz

Operating Frequency (GHz)	Rainfall Rate (mm/hr)	Total Attenuation (dB/km)	RANGE (km) $P_T = 10^9$W	$P_T = 10^4$W	$P_T = 10^3$W	$P_T = 10$W
60	0	14	10.89	7.53	6.87	5.57
	22	21	7.42	5.17	4.73	3.87
56	0	7	21.06	14.35	13.04	10.45
	22	14	10.93	7.57	6.91	5.61

b) Bandwidth = 0.5×10^6 Hz

60	0	14	12.64	9.26	8.59	7.27
	22	21	8.59	6.33	5.88	5.00
56	0	7	24.56	17.81	16.47	13.83
	22	14	12.68	9.30	8.63	7.31

operation involved in all covert communications results in a small range advantage with a GW source. The real advantages of the source, however, are its reliability in the most severe rainfall conditions and the tunability which it affords. Thus for rainfall rates very much in excess of the example used here, for instance, in the region of 50 mm/hr, the lower power sources will not be capable of covert communications for ranges in excess of 8 km at any operating frequencies above 50 GHz. By the flexibility offered by its tuning capability, the GW sources in addition can be employed in both covert and long range overt communications. The effect of the exponential term in the range equation is dramatically shown in this section. For the 48 dB difference in detection assumed for the communications receiver and the acquisition receiver, the ratio of the ranges for the two cases would be 256 without the exponential term whereas it is only 1.43 with the term included.

3.1.2 Short Range Ship-to-Ship Communications

Limitation of fleet communications to ranges within the fleet is an important requirement for maintenance of normal communications during EMission CONtrol conditions. Small hand-held millimeter wave systems have been demonstrated for covert communications between individual ships; however, these devices have been shown to be inadequate during inclement weather. On the other hand, the necessity of communication from the fleet command ship to the other vessels of the fleet places further limitations on the command ship antenna.

Consider a covert system employing a gigawatt source as the command ship transmitter, and assume that a low gain transmitting antenna with a small vertical beamwidth and 360^{o} horizontal beamwidth for transmission to the fleet is employed. The communication system is operated at a wavelength of 5 mm. The command ship antenna is assumed to have G = 13 dB with a beamwidth = 360^{o}H, 3^{o}V. For antennas with G = 55 dB on the individual vessels, the range has been calculated for clear weather and heavy rain (22 mm/hr and 100 mm/hr). Table 17 states the conditions, and Table 18 gives the results for the three cases at 60 GHz. It is seen from Table 18 that the intercept range for a low-flying airborne receiver places the enemy aircraft within range of the fleet anti-aircraft weapons. Operation at 56 GHz allows the communication range under 22 mm/hr rainfall to be equal to that under clear conditions. For the very heavy rainfall rate of 100 mm/hr, frequency tuning to 52 GHz lowers the attenuation to approximately 27 dB/km so that the range is then 4.43 km for communications and 4.08 km for interception.

A comparison has been made with lower power sources for the various weather conditions. As in the previous case (ground-to-ground communications), the ranges are considerably less than for the GW source and covert communications at 8 km range would not be possible with sources of less power for inclement weather conditions. Table 19 shows the comparison. The calculations were performed for $B = 2 \times 10^{8}$ Hz.

TABLE 17

SHORT RANGE SHIP-TO-SHIP COMMUNICATIONS

Fleet Command Ship -

Low gain transmitting antenna;
Small vertical beamwidth;
360^{o} horizontal beamwidth for transmission to fleet.

Operation at 60 GHz: $\lambda = 5$ mm

Antenna for Command Ship -

$G \simeq 13$ dB
Beamwidth = 360^{o}H, 3^{o}V

Calculate for Clear Weather and Heavy Rain -

$\alpha = 14$ dB/km (clear)
$= 21$ dB/km (22 mm/hr)
$= 42$ dB/km (100 mm/hr)

Determine Intercept Range

System Parameters for Calculation -

$B = 2 \times 10^{8}$ Hz
S/N = 10 dB
F = 10 dB
G = 55 dB, for individual vessels
T = 300° K

TABLE 18

SHORT RANGE SHIP-TO-SHIP COMMUNICATIONS

f = 60 GHz

ATTENUATION	COMMUNICATION RANGE (km)	INTERCEPT RANGE (km)*	RAINFALL RATE
14 dB/km	8.114	6.939	Clear
21 dB/km	5.565	4.780	22 mm/hr
42 dB/km	2.916	2.522	100 mm/hr

*Acquisition by airborne intercept receiver with 1/2 m^2 antenna in side-lobe of transmitter.

TABLE 19

COMPARISON OF SHIP-TO-SHIP COVERT COMMUNICATIONS

FOR DIFFERENT POWER LEVELS

Frequency (GHz)	Rainfall Rate (mm/hr)	Total Attenuation (dB/km)	RANGE $P_T = 10^9W$	$P_T = 10^4W$	$P_T = 10^3W$	$P_T = 10W$
60	0	14	8.11	4.81	4.18	2.97
	22	21	5.57	3.36	2.94	2.12
	100	42	2.92	1.81	1.60	1.18
52	100	27	4.43	2.73	2.60	1.76

3.1.3 Covert Air-to-Air Communication

The capability for covert communications in the region of 60 GHz provides the means for secure operation in air-to-air systems with complete shielding from the ground. This technology is demonstrated by considering two aircraft at an altitude of 11 km communicating at 60.435 GHz which corresponds to the 7^+ line of O_2. The attenuation at 11 km is 3 dB/km horizontally so that the horizontal range is R = 42.57 km with a 1 gigawatt source as the transmitter. This range is for the receiver and antennas assumed in Section 3.1.1.

At this altitude, it is not possible to detect or jam the receiver under any conditions since the zenith attenuation from ground to 11 km is 400 dB. The altitude at which an aircraft transmitter can be detected on the ground is 2.2 km. The attenuation for the first 2.2 kilometers of the atmosphere (at 60.435 GHz) is 120 dB. This intercept range is for an aircraft antenna gain of 57 dB, and the intercept receiver in the sidelobe of the transmitter antenna (G = 0 dB). Table 20 summarizes the results described above for the 1 GW source. The ranges for lower powers are given at the bottom of Table 20. Approximately 9.6 km difference in range exists between the GW source and the 10^4 W source.

TABLE 20

COVERT AIR-TO-AIR COMMUNICATIONS

Consider - 2 Aircraft at 11 km Altitude Comunicating at 60.435 GHz corresponding to the $7^{+}0_2$ line

Attenuation: = 3 dB/km at 11 km

Horizontal Range: R = 42.57 km

Intercept of Airborne Receiver:

- Attenuation From Ground to 11 km = 400 dB
- Not Possible to Detect Receiver Under Any Conditions

Altitude at Which Aircraft Signal Can Be Seen From Ground With G_2 = 57 dB, G_1 = 0 dB -

R $\sim$ 2.2 km, where α = 120 dB

Lower Power Sources at Same Frequency:

P_T(W)	Range (km)
10	24.8
10^3	30.8
10^4	33.9

3.1.4 Covert Communication at Frequencies Above 60 GHz

It has been indicated previously that secure or non-interfering communication techniques can be employed at the shorter millimeter or submillimeter wavelengths if suitable sources exist. The gigawatt source can provide the necessary transmitter capability for the short wavelength systems in which wide frequency diversity, very narrow beams, atmospheric windows and high attenuation regions can be employed. Table 21 shows some of the absorption parameters of the short wavelength region which are significant for the covert communications applications. Included in these data are the absorption coefficients in the five submillimeter windows in which the attenuation ranges from 6 dB/km to 45 dB/km. In addition, the absorption coefficient on the water vapor lines at 1.63 mm and 0.92 mm are listed. It can also be seen from Table 21 that attenuation changes of 10 dB/km can be achieved on the water lines so that tunability, similar to that shown with the O_2 lines, can be employed to maintain a constant range under adverse weather conditions.

Table 22 demonstrates three modes of operation in the submillimeter wave region with the assumed system parameters given in the table. For communication in the windows, it is seen that, at λ = 0.85 mm, a large transmission range is possible for applications not requiring a limited secure range, while the shortest range of transmission in the windows listed occurs at 0.36 mm. For the all weather covert operation, the frequency diversity or agility schemes shown in the table can be employed. The H_2O line at 1.64 mm can be utilized by tuning to longer or shorter wavelengths from the absorption peak during rain to maintain the constant range of 5.54 km, or operation can consist of tuning on the wing of the 0.762 mm H_2O line to restrict propagation to 8.20 km.

A technique using the high attenuation of the submillimeter lines and a frequency division or hopping scheme is demonstrated in the table. This technique consists of utilizing two frequencies with nearly identical high absorption coefficients. The water absorption spectrum, Figure V-1, shows such regions. The frequencies 183.3 GHz and 321 GHz both have 30 dB/km, or 500 GHz and 666 GHz with 35 dB/km and 37 dB/km respectively could be used.

TABLE 21

COVERT COMMUNICATION AT f > 60 GHz

1. Absorption coefficient in submillimeter windows

$T = 300^{o}K$, P = 760 mm Hg, $\rho = 7.5\ g/m^3$

λ	0.85	0.72	0.6	0.46	0.36	mm
α	6	14	35	37	45	dB/km

2. Absorption coefficient in H_2O lines

λ	1.63	0.92	mm
α	30	40	dB/km

3. Attenuation changes

on 1.63 mm H_2O line:
30 dB/km (183 GHz)
20 dB/km (181 GHz)
20 dB/km (185 GHz)

in 0.72 mm window:
15 dB/km (408.2 GHz)
20 dB/km (397.4 GHz)
25 dB/km (393.7 GHz)

TABLE 22

SUBMILLIMETER COMMUNICATIONS

Assume: $P_T = 10^9 W$, $\frac{S}{N} = 10$, F = 10 dB

$A = 1\ m^2$, $\eta = 0.5$, $B = 2 \times 10^8$ Hz

1. Communications in Windows:

λ(mm)	0.85	0.72	0.60	0.46	0.36
α(dB/km)	6	14	35	37	45
R(km)	26.35	11.89	5.02	4.82	4.05

2. Frequency Diversity, All Weather System:

λ(mm)	1.62	1.64	1.657	0.735	0.755	0.762
α(dB/km)	20	30	20	15	20	25
R(km)	8.14	5.54	8.13	11.13	8.45	8.20

3. Two Frequency Communication System:

f(GHz)	183.3	321	500	666
α(dB/km)	30	30	35	37
R(km)	5.54	5.69	5.02	4.83
Fundamental (GHz)	42.825		83.3	

The frequencies 183.3 GHz and 321 GHz are harmonically related to 45.825 GHz while the same applies to 500 and 666 GHz relevant to 83.3 GHz. For a gigawatt source producing harmonics at these frequencies, a covert system, using one source, could operate at high attenuation (limiting the range) and on two frequencies (limiting the access). Such a system at high frequencies with narrow beams, frequency hopping and limited range can provide one of the most secure means of communicating.

The use of lower power sources results in shorter ranges under all conditions and less satisfactory operation during inclement weather, as shown for previous examples.

3.1.5 Ground-to-Satellite Communications

Ground-to-satellite communications in the millimeter and submillimeter wavelength regions affords not only the opportunity for broad-band communications but also a degree of security by its high frequency, narrow beam and diversity of frequencies available.

For operation at the zenith angle, communication on the water lines at 183 GHz and 325 GHz is shown to be possible, providing additional security of interception of the ground transmitter at ground level.

In considering the use of short millimeter wavelengths for the transmission from the ground, it is interesting to consider the power transferred at various frequencies under the idealized conditions that antenna tolerances can be achieved and the necessary stabilization and pointing of the antenna is possible. For a gigawatt source with a pulse width of 500 ns and PRF of 10^3, the average power is 0.5×10^6 W. The power transferred is given by

$$\frac{P_R}{P_T} = \frac{f^2 A_R A_T \eta^2}{c^2 R^2} \text{ (ATTEN)}$$

where f is the operating frequency, $A_T = 10\ m^2$, the transmitter antenna area and $A_R = 1\ m^2$, the satellite receiver antenna area. For a satellite altitude of 185.3 km, Table 23 shows the power transferred at four frequencies. It is seen that the f^2 dependence favors the higher frequencies until the attenuation becomes the predominant factor. The frequency 222 GHz is the highest frequency before the power transfer begins to decrease due to the attenuation. Of course, under rain conditions, the signal at the higher frequencies will rapidly deteriorate.

For the ground-to-satellite communication system, an example calculation has been performed to show the signal-to-noise and the maximum range which can be expected for some significant submillimeter wavelengths. It is assumed that the gigawatt source is employed, both antenna areas are $1\ m^2$, the receiver bandwidth is 2×10^8 Hz and receiver noise figure is 10 dB. The calculation was performed for angles of 0° and 60° with respect to zenith in the transmission windows at 222

TABLE 23

POWER TRANSFER TO SATELLITES FROM GROUND

Frequency (GHz)	Zenith Attenuation (dB)	Power Transferred* (W)
10	0	0.04
90	1	2.60
140	3	3.95
222	5	6.3

Power Transfer: $\frac{P_R}{P_T} = \frac{f^2 A_R A_T \eta^2 (ATTEN)}{c^2 R^2}$

Calculated For Satellite Altitude = 185.3 km, $A_T = 10\ m^2$, $A_R = 1\ m^2$
$\eta = 0.5$

*$P_{T_{AVER}} = 0.5 \times 10^6 W$ For Pulse Width = 500×10^{-9} sec. PRF = 10^3,
$P_o = 10^9 W$

GHz and 333 GHz and on the H_2O absorption lines at 183 GHz and 325 GHz. Table 24 shows the results. In the windows, it is seen that considerably less power could be employed during the clear weather conditions assumed while on the absorption lines insufficient power is available for propagation at an angle of 60° with the zenith. Adequate S/N is possible at the absorption frequencies for transmission along the zenith.

For security from detection of the ground transmitter by a ground intercept receiver, it is seen that communication on the 183 GHz and 325 GHz absorption lines offers the maximum protection. Calculation of the S/N and maximum range has been performed for a transmitter power of 10^4W, and the results for this determination are given in Table 25. It is seen that, for clear weather operation, the signal-to-noise ratio is very large. However, for a rainfall of 50 mm/hour or greater for the lower 5 km of the atmosphere, an additional 100 dB loss is imposed so that the communication to an orbiting or data relay satellite is not possible for 10^4W.

The same type of calculation (identical system parameters) has been performed for a synchronous satellite at 37,063 km for the same frequencies and angles. The GW source is used only for transmission from the ground unless a means for employing high power sources in satellites is used. Table 26 demonstrates the S/N achievable under clear weather conditions for $P_T = 10^9$W. Transmissions at 325 GHz and 183 GHz for 60° from the zenith are not feasible means for communicating to a synchronous satellite. From a security viewpoint, surveillance satellites observing at an angle of 60° to the nadir will not detect signals at 183 GHz and 325 GHz which are transmitted along the zenith. Choice of other frequencies throughout the millimeter and submillimeter wavelength regions can result in high zenith attenuation so that the operating parameters can be optimally adjusted to permit effectual communications only through a narrow range of nadir or zenith angles. For computing transmission path losses as a function of angle from zenith, the zenith attenuation is modified by the secant of the angle so that $L(dB) = Z_o(dB) \sec\Theta$ where $L(dB)$ is the transmission path loss in dB, $Z_o(dB)$ is the value of the zenith attenuation in dB and $\sec\Theta$ = secant of the angle. Receiving stations outside this range of angles will suffer severe attenuating

TABLE 24

GROUND-TO-SATELLITE COMMUNICATIONS
DETERMINE S/N AND MAXIMUM RANGE
IN SUBMILLIMETER REGION

1. S/N For Ground-to-Satellite

$P_T = 10^9$W, F = 10 dB

A = 1 m^2, B = 2 x 10^8 Hz

Angle from zenith = 0°, 60°

f(GHz)	Angle from Zenith (Degrees)	R(km)	S/N (dB)
222	0	185.3	137
222	60	370.6	127
333	0	185.3	115
333	60	370.6	83
183	0	185.3	50
183	60	370.6	-46
325	0	185.3	35
325	60	370.6	-66

2. Maximum Range in Submillimeter Region

f (GHz)	Angle from Zenith(Degrees)	R(km)
222	0	4.03 x 10^8
333		3.41 x 10^7
183		1.87 x 10^4
325		3.33 x 10^3

TABLE 24 (Cont.)

f(GHz)	Angle from Zenith (Degrees)	R(km)
222	60	2.54×10^{8}
333	60	1.71×10^{6}
183	60	-
325	60	-

3. Horizontal Range - Intercept Receiver in Side-Lobe

f (GHz)	α (m^{-1})	R (km)
222	2.87×10^{-4}	65.99
333	1.26×10^{-3}	17.14
183	6.89×10^{-3}	3.59
325	9.20×10^{-3}	2.75

TABLE 25

SUMMARY
GROUND-TO-SATELLITE FOR $P_T = 10^4$W

f (GHz)	S/N(dB) Zenith	60°
183	+8.7	-87.4
222	+95.4	+85.3
333	+73.9	+41.8
325	-6.3	-107.3

f (GHz)	Maximum Range (km) Zenith	60° from Zenith
183	160	5.03×10^{-3}
222	3.43×10^{6}	2.17×10^{6}
333	2.90×10^{5}	1.45×10^{4}
325	28.3	5.04×10^{-4}

TABLE 26

GROUND-TO-SYNCHRONOUS SATELLITE
FOR SATELLITE AT 37,063 km
$P_T = 10^9 W$

f(GHz)	Angle from Zenith (Degrees)	Range (km)	S/N (dB)
222	0	37063	91
222	60	74126	81
333	0	37063	69
333	60	74126	37
183	0	37063	4
183	60	74126	-92
325	0	37063	-11
325	60	74126	-112

TABLE 27

GROUND-TO-SYNCHRONOUS SATELLITE
FOR SATELLITE AT 37,063 km
$P_T = 10^4 W$

f(GHz)	S/N (0°) dB	S/N (60°) dB
183	-37.4	-133.4
222	49.3	39.3
333	27.9	1.8
325	-52.3	-153.3

effects of the atmosphere so that interception by covert monitors and interference or jamming of the satellite or ground station receivers are highly unlikely.

Communication with lower power ($P_T = 10^4$W) has also been calculated for the ground-to-synchronous satellite case with the results given in Table 27 for the signal-to-noise ratio. Sufficiently large S/N is achieved with the lower power source in clear weather, but a rainfall of 22 mm/hr confined to the lower 5 km of the atmosphere reduces the S/N by a factor of 50 dB. This would prevent use of the lower power source during rains exceeding 22 mm/hr. The same type of determinations could be made in the region of O_2 lines.

The large power margin which exists in the use of a gigawatt source for the satellite applications considered here can be a great advantage in maintaining continuous communication for military operations during inclement weather and periods of severe fading. While spatial diversity has been shown to be effective for satellite-to-ground transmission during adverse conditions, a military scenario may not allow the use of more than one transmitter for ground-to-satellite communications so the large available S/N is desirable.

A related important application is the transmission of data from an aircraft to a synchronous satellite serving as a data relay satellite. Because of the strong absorptions throughout the millimeter/submillimeter regions, the transmission from aircraft to satellite could be chosen at any one of several frequencies. From Figure IV-4 of Appendix IV, the attenuation from an aircraft to the satellite can be obtained for a frequency of 60,465 MHz. At an aircraft altitude of 12.5 km, α = 80 dB and for an altitude of approximately 7 km, the attenuation $\alpha \simeq 240$ dB. The aircraft signal is, on the other hand, shielded from detection from the ground where a covert monitor would be in the side or backlobes. Communication from the altitude of 12.5 km to the satellite is possible for the following parameters:

$P_T = 10^9$W, transmitter power

G_1 = 57 dB, satellite antenna gain

G_2 = 60 dB, aircraft antenna gain

F = 6 dB, noise figure

$\lambda \sim 5$ mm

$T = 300°K$

$B = 2 \times 10^8$ Hz

For these conditions, $S/N \sim 45$ or 16.5 dB. Communication for $P_T < 10^9$W would not be possible. Satellite command and control information for the aircraft, on the other hand, could be transmitted at other millimeter wavelengths where attenuation is less.

3.2 Communication to RPVs

The interest in recent years in RPVs has stimulated the need for improving communication to the RPVs, which could be full size aircraft or mini-RPVs. The gigawatt source can serve as a long range transmitter to provide command data directly to the RPV, rather than to the RPV by way of a relay aircraft, or it could be mounted in the delivery aircraft for increased stand-off control to the RPV or increased distance for relay of data to ground control. The gigawatt source could provide the means for operating RPVs in or through inclement weather.

Consider the following cases of communications involving RPVs:

1.) Control and command communications from ground directly to mini-RPV. The antenna of a mini-RPV would be omni-directional (G = 0 dB), and the ground antenna would have an area of 1 m^2. For covertness and narrow beam systems, operation would be at either 56 GHz or 94 GHz. For operation in inclement weather, transmission in rainfalls of 50 mm/hr ($\sim$18 dB/km) and 12.5 mm/hr (6 dB/km) are determined. Table 28a presents the results for transmitter power $P_T = 10^9$W and 10^4W for parameters:

$\eta = 0.75$

F = 10 dB

S/N = 10

B = 2×10^8 Hz

2.) The same situation for an RPV which is a full-size aircraft with an antenna having an area of 1/2 m^2. Table 28b shows the results for the conditions of Table 28a.

3) Transmission, from relay aircraft, of commands to the RPV and of RPV data to ground control. This is particularly important in deep penetration operations in which the RPV can be carried aloft and deployed from either a ground-launched ballistic missile or an aircraft. Calculations show that, for $P_T = 10^9$W or 10^4W, clear weather transmission is possible at 56 GHz and 94 GHz for ranges of 20 km and 10 km, but, for average path losses of 10 dB/km due to rain, transmission for $P_T = 10^4$W is not possible for the above ranges

TABLE 28

SUMMARY OF RPV CALCULATIONS

a.) Mini RPV's $G = 1$, $A_2 = 1\ m^2$

Calculated Range (km)

	$P_T = 10^4 W$		$P_T = 10^9 W$	
	f =56 GHz	f =94 GHz	f =56 GHz	f =94 GHz
Clear	7.33	78.6	13.71	187.2
Rain (50 mm/hr)	2.43	3.19	4.25	5.65
Rain (12 mm/hr)	4.04	7.00	7.25	13.04

b.) Full Sized RPV's $A_1 = 0.5\ m^2$, $A_2 = 1\ m^2$

Calculate Range (km)

	$P_T = 10^4 W$		$P_T = 10^9 W$	
	f =56 GHz	f =94 GHz	f =56 GHz	f =94 GHz
Clear	14.15	205.5	20.8	323
Rain (50 mm/hr)	4.37	6.05	6.25	8.6
Rain (12 mm/hr)	7.46	14.03	10.8	20.4

while an average rainfall loss of 7.5 dB/km (∿13 mm/hr) yields S/N = 10.5 dB for $P_T = 10^9$W at 94 GHz over a range of 20 km. For the 10 km range, rainfall rates on the order of 40 mm/hr corresponding to 13.4 dB at 56 GHz and to 15.6 dB/km at 94 GHz can be tolerated for $P_T = 10^9$W. In summary, long range RPV data relay from aircraft to ground is possible under a variety of weather conditions or the range can be greatly extended when a GW source is employed. The GW source can also be employed to transmit to the RPV in a long range stand-off mode of operation.

4.) Because of its potential wide bandwidth, the GW source can transmit coded signals to two (or more) RPVs, both of which would be in the sidelobes of the transmitter antenna. One RPV would, for instance, fill the function of target location and target designation for the second carrying a high-explosive warhead. Initial control of the second RPV would be by the GW source. It is seen from Table 29 that, for the frequencies chosen, the range can be quite large for the GW source case so that secure stand-off control is possible.

TABLE 29

GW SOURCE APPLICATION: TRANSMISSION OF CODED SIGNALS FROM AN AIRBORNE GW SOURCE

Assume:

G_1 = 0 dB, RPV Antenna Gains

G_2 = 15 dB, Sidelobe Antenna Gain for GW Source

RPVs and Aircraft at 4 km

Calculations performed for

f = 30 GHz, = 0.015 dB/km

f = 94 GHz, = 0.1 dB/km

at powers of $P_T = 10^9$ W and 10^4 W

Receiver Characteristics used:

F = 10 dB, Noise Figure

S/N = 10

B = 2×10^8 Hz

Range of Transmission to Two RPVs

	$P = 10^4$ W	$P = 10^9$ W
f = 30 GHz	59 km	1517 km
f = 94 GHz	18 km	280 km

3.3 Tropospheric Scatter Communications

During the past twenty years, the development of tropospheric scatter communications has provided the means for radio communications between two points on the earth's surface separated by distances of several hundred miles. Such a span may be augmented by other spans in tandem to permit end-to-end or through circuits up to many thousand miles. This method of communication allows operation with excellent reliability and good information capacity. While satellite communications can be employed to perform the long distance transmission in several cases, military applications, in which access to a satellite link is not possible, can profit from tropo-scatter systems. In polar regions, where synchronous satellite coverage is more difficult, tropo-scatter can provide means for long range communications. The ability of tropo techniques to span hundreds of miles of inhospitable terrain with circuits of relatively high traffic density is of importance to military operations.

The tropospheric propagation mechanism has been the subject of several investigations [5,6,7]. The average amplitude of the field propagated beyond the horizon is greatly attenuated with respect to the transmitted field. In addition, the amplitude of the received field varies substantially with time over a given path. For convenience, these amplitude variations are separated into short-term (periods shorter than a few minutes) and long-term distributions, which are variations of hourly median levels over a longer period of time (month, season of year).

A third propagation effect is signal distortion due to multipath effects when wide frequency bands are used for transmission of intelligence. This distortion places an upper limit on the bandwidth that can be transmitted successfully.

For a high-quality, long distance, multichannel communications system, the tropo system must satisfy two requirements, i.e. reliability and delivery of a favorable signal-to-noise ratio. To achieve reliability, the two types of signal fading (short and long-term) must be counteracted. This is achieved by diversity techniques, which utilize more than one independent and uncorrelated transmission path over a single span to afford greater reliability than that provided by a single transmitter and receiver at each end. Both space

diversity, in which two antennas, separated by 100 wavelengths or more, are used to receive the signals, and frequency diversity, in which two or more frequencies are transmitted, can be employed. The use of both space and frequency diversity simultaneously will provide quadruple diversity.

In order to maintain high S/N or to extend the range of tropo-scatter communication, high power sources are important elements of the system. Klystron amplifiers provide maximum power on the order of 10^5 watts. A tunable gigawatt source will yield high power, and, by use of more than one frequency output from a source like the REB, frequency diversity can be obtained. Thus, one source could be used with two or more receivers to provide quadruple diversity. Multiple frequencies from a REB device could be employed for a secure spread spectrum scheme. The ability to transmit over greater distances would lessen the number of tropo-spans necessary in a tandem long distance system. Lengthening of the tropo-link in a military scenario would lessen the probability of jamming of the receivers.

The path propagation loss can be determined by using any one of several prediction methods [5] together with available empirical data for various geographic locations. The method of NBS [6] can be used to demonstrate a typical prediction formula for the total path loss:

$$L = 30 \log f - 20 \log d + F(\theta_d) + L_c - V(d_e) - F_o + H_o + A_a$$

where f is the operating frequency in MHz, d_e is the mean sea level arc distance in kilometers, $F(\theta_d)$ is an attenuation function, F_o a scattering-efficiency term, H_o the frequency-gain function, $V(d_e)$ a climate-variation factor, L_c the aperture-medium coupling loss coefficient and A_a the atmospheric absorption.

For our purposes, a technique prepared by Collins Radio Company [7] will allow estimates to be made. This technique employs a basic propagation loss for 1 GHz, a frequency correction curve (actually the graph of 30 log f), a loss due to elevated horizontal angles and a nomogram determination of the aperture-to-medium coupling loss. Calculations can then be made to compare the GW source with a 10^5W klystron amplifier, operating at 2.5 GHz and 5 GHz with an

antenna of 20 feet diameter (G = 41 dB at 2.5 GHz and G = 47 dB at 56 GHz). The distances for each tropo-span are taken to be 300 statute miles and 800 statute miles. The calculations do not include intermodulation effects, weighting considerations, nor detailed consideration of the paths.

The received power level for a tropo-scatter system is given by [5]

$$P_r(dBW) = P_t(dBW) + G_p - L_{fs}(dB) - L_s(dB) - L_t(dB)$$

where

P_r = received power level, dBW

P_t = transmitter power, dBW

$G_p = G_t + G_r$ = net tropo-scatter path antenna gain, dB (L_c, coupling loss is included in L_s)

L_{fs} = free-space loss, dB

L_t = terminal losses for both transmitting and receiving stations, dB

The total path losses have been estimated and are given in Table 30. The terminal losses L_t were assumed to be 5 dB.

The received power is compared with the receiver thermal noise power, $P_n = kT_oFB$, to give the carrier-to-noise ratio (CNR).

The receiver thermal noise level, P_n, can be given as

$$P_n(dBW) = -204 \text{ dBW} + F + 10 \log B$$

where $-10 \log k T_o = -204$ dBW

for k = Boltzmann's constant and $T_o = 288°K$

for F = 2 dB and B = 1 MHz, $P_n = -142$ dBW

The carrier-to-noise ratio (CNR) is

$$CNR(dB) = P_r(dBW) - P_n(dBW)$$

Table 30 gives the results of the calculations. For 300 miles at both 2.5 GHz and 5 GHz, the GW source produces a 40 dB improvement in CNR over conventional sources and therefore a far greater reliability. For the 800 mile link, both 2.5 GHz and 5.0 GHz provide CNRs in excess of 10 dB while the 10^5W source results in CNRs < -10 dB. The latter would be inadequate for transmissions on the order of 800 miles. Further improvements of the tropo performance can result from channel considerations. It is shown [5] that, by bandwidth reduction ($\sim$3.2 kHz) and the use of proper pre-emphasis networks, the resulting unweighted S/N can be improved by 26 dB over the calculated CNR. This further improves the reliability in the 800 mile link for the GW source while the performance for the conventional sources will exceed the noise by only 2 dB for the 2.5 GHz system and 13 dB for the 5.0 GHz system.

From this discussion, it is seen that the gigawatt source can increase both the reliability and range of a tropo-scatter communication system over currently employed sources.

TABLE 30

TROPO-SCATTER COMMUNICATION WITH GW SOURCE
AND CONVENTIONAL SOURCE

	GW SOURCE				10^5W Amplifier			
Frequency (GHz)	2.5		5		2.5		5	
Distance (mi)	300	800	300	800	300	800	300	800
Path Loss, L (dB)	235.5	293	236	294	235.5	293	236	294
Total Antenna Gain (dB)	82	82	94	94	82	82	94	94
Bandwidth (MHz)	1	1	1	1	1	1	1	1
Receiver Noise Level (dBW)	-142	-142	-142	-142	-142	-142	-142	-142
Received Carrier Level (dBW)	-68.5	-126	-57	-115	-108.5	-166	-97	-155
Carrier-to-Noise Ratio (dB)	73.5	16	85	27	+33.5	-24	45	-13
*Signal-to-Noise (dB) (unweighed)	+98.5	+42	+111	+53	+59.5	+2	+71	+13

*For Bandwidth Reduction Factor of +22 dB and Pre-Emphasis Improvement of +4 dB.

3.4 Deep Space Communication Links

During deep space missions, the signal-to-noise ratio in a given bandwidth must be maintained above a minimum value in order to provide effective performance. It is necessary to use maximum gain antennas for the earth stations and to employ earth-based high-power transmitters. The link must provide the three functions of tracking, telecommand and telemetry over interplanetary distances. The tracking function provides information for determination of position and velocity of the spacecraft, for critical maneuvers, and angular pointing, pointing for highly directional earth-station receiving and transmitting antennas. The telecommand function permits earth stations to guide and control the space station, while the telemetry function provides for transmission of data back to the earth station. Since transmitter power aboard the vehicle is low compared to the earth-based system, it is necessary to use as much antenna gain as possible in the earth-based antenna.

For interplanetary distances, a minimum of 10^3 GW eirp (equivalent radiated power relative to an isotropic antenna) will be required to communicate at distances equal to the orbits of the three outer planets (e.g. Pluto, average range = 6×10^9 kilometers; Neptune, average range = 5×10^9 kilometers).

At 2.1 GHz with earth station antenna diameters of (a) 64 meters and (b) 26 meters, and the spacecraft with an isotropic antenna, the ranges of a gigawatt source and a megawatt source are compared. The conditions of transmitting bandwidths of 1 MHz and 20 Hz are considered. Table 31 gives the results of the calculations. The greater range with the GW source is evident for each determination. The calculations were for a 10 dB signal-to-noise ratio in each case. At 2.1 GHz, the MW source range is sufficient for a spacecraft at Pluto's range only for the low data rate with the large 64 meter antenna. The advantages of the higher frequencies in extending the range can be seen from the determinations for 10 GHz and 37 GHz. The calculations are based on a 2 meter antenna earth-based and a 1 meter antenna in the spacecraft with a receiver noise figure of 5.0 dB. For both 10^6 Hz and 20 Hz bandwidths, the GW source at 37 GHz has sufficient range to exceed the distance to the outer planets. Smaller antennas at the higher frequencies can result in cost reduction. At 37 GHz, inclement earth weather conditions can cause fading difficulties at

TABLE 31

DEEP SPACE COMMUNICATIONS
(EARTH-TO-SPACECRAFT)

Frequency (GHz)	Antenna Gain (dB)	Antenna Diameter (m)	Receiver Noise Figure (dB)	Bandwidth (Hz)	GW Source Range (km)	MW Source Range (km)
2.1	63	64	2.5	10^6	1.05×10^9	3.32×10^7
2.1	63	64	2.5	20	2.35×10^{11}	7.41×10^9
2.1	55	26	2.5	10^6	4.27×10^8	1.35×10^7
2.1	55	26	2.5	20	9.56×10^{10}	3.03×10^9
10	46.4	2	5.0	10^6	2.57×10^9	8.16×10^7
	40.4*	1				
10	46.4	2	5.0	20	5.74×10^{11}	1.82×10^{10}
	40.4*	1				
37	58	2	5.0	10^6	8.61×10^9	2.72×10^8
	51.9*	1	5.0	20	1.92×10^{12}	6.08×10^{10}

* Spacecraft Antenna.

the receiver, but the use of a CW source can provide a wide S/N margin at the spacecraft receiver.

It has been shown that a CW source provides a larger range, or greater S/N and reliability than lower power sources used in deep space missions.

CHAPTER 4

APPLICATION OF GIGAWATT SOURCES TO PLASMA INTERACTIONS

The propagation characteristics of millimeter and submillimeter waves in plasma media are relevant to fusion devices, rocket exhausts, ionized flow fields of projectiles and similar ionized media. The interaction can be described in terms of the bulk parameters of the plasma which depend upon basic particle interactions. The degree of ionization or mixture of gases comprising the plasma determines the electron density within the plasma. The interaction of these electrons with neutral atoms, ions and each other determines the collision frequency ν_c of the plasma constituents, a measure of the average number of collisions an electron undergoes per unit time. Further complications exist within the plasma. The electron density, collision frequency and external forces determine the conductivity of a plasma.

The plasma frequency (ω_p) for electrons in a plasma (ions regarded as stationary points) is given by

$$\omega_p = (\omega_e e^2/\varepsilon_o m)^{1/2}$$

where n_e = electron number density

e = charge on electron

m = mass of electron

ε_o = permittivity of free space

The plasma frequency is

$$\frac{\omega_p}{2\pi} = 8.98 \times 10^{-6} \sqrt{n_e} \text{ GHz.}$$

Table 32 lists the plasma frequency vs. the electron density.

The plasma may be considered a dielectric gas of complex dielectric constant different from the value measured in free space. The relative dielectric constant at frequency ω is expressed as

TABLE 32

PLASMA FREQUENCY VS. ELECTRON DENSITY

n_e Electrons/cm^3	Plasma Frequency
10^8	90 MHz
10^9	285
10^{10}	900
10^{11}	2,850
10^{12}	9 GHz
10^{13}	28.5
10^{14}	90
10^{15}	285
10^{16}	900
10^{17}	2,850
10^{18}	9,040

$$K = K_r - i K_i = 1 - \left(\frac{\omega_p}{\omega}\right) \frac{1}{\left(1 + \frac{\nu_c}{\omega}\right)^2} - i\left(\frac{\omega_p}{\omega}\right)^2 \frac{\nu_c}{1 + \left(\frac{\nu_c}{\omega}\right)^2}$$

The electromagnetic properties of a plasma depend upon whether the frequency of the electromagnetic field is greater than or less than ω_p, the plasma frequency. For the signal frequency ω greater than ω_p, the plasma behaves like a dielectric with the lossiness determined by ν_c, the collision frequency. For $\nu_c << \omega$ and $\omega_p < \omega$, K_r is positive, and electromagnetic propagation is possible. For $\omega < \omega_p$, the plasma acts like a very good conductor, while, for $\omega \sim \omega_p$, K_r goes to zero (for $\nu_c << \omega$), and the plasma is cutoff and very highly attenuated and reflective so that the wave cannot penetrate to any great depth into the plasma. Thus, for a given frequency, a sufficiently large value of n_e will cause the plasma to become opaque. For plasma with large values of n_e, it is necessary to use extremely high frequencies in order to penetrate them. These effects are shown in Figure 6, where the power transmission coefficient at the air-plasma interface is shown as a function of $(\omega_p/\omega)^2$ for particular normalized collision frequencies and in Figures 7 and 8, where the attenuation is given for small and large collision frequencies respectively. It is seen from Figure 6 that, for the higher frequencies $(\omega/\omega_p) > 1$, the transmission coefficient at the interface is on the order of 1; in addition, for high collision frequency, the transmission is high for $\omega_p/\omega > 1$. Figures 7 and 8 show the lowering of the attenuation as ω_p/ω decreases. The optimum frequencies for both transmission through the interface and propagation in the plasma occur at the higher frequencies, characteristically the millimeter and submillimeter regions attainable by the tunable gigawatt source.

The electron density and its distribution, and the collision frequency of the plasma can be determined by measuring the transmission and reflection of an electromagnetic signal. Submillimeter waves are useful for plasmas with densities greater than can be measured with lower frequencies. Because of the improved spatial resolution, the region of the plasma being measured can be better defined. Measurement of the phase shift and attenuation of a signal passing through a plasma allows determination of K_r and K_i to compute n_e and ν_c.

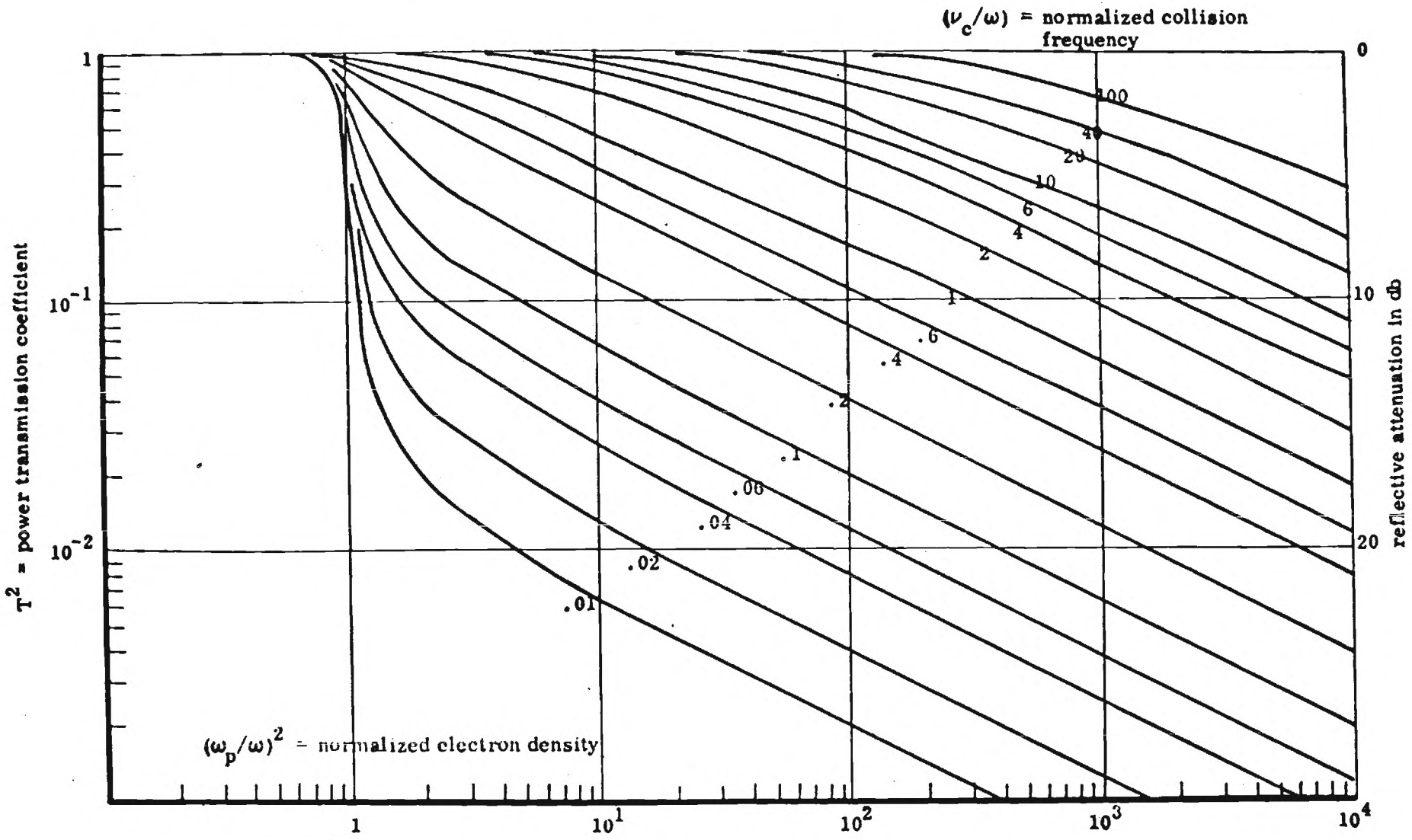

Figure 6. Power Transmission Coefficient For Electromagnetic Waves at Air-Plasma Interface.

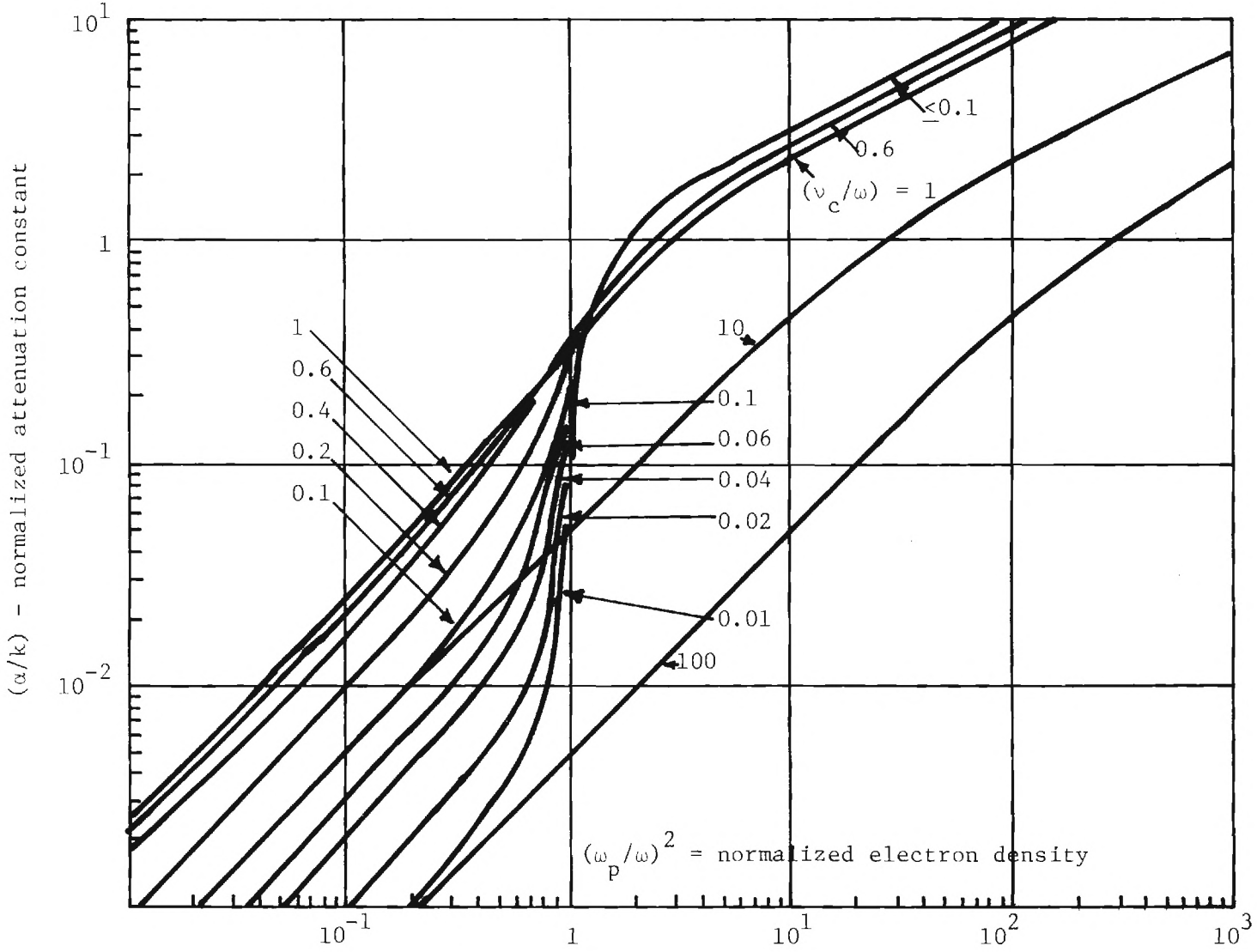

Figure 7. Attenuation of Electromagnetic Waves in Plasma (Small Collision Frequency).

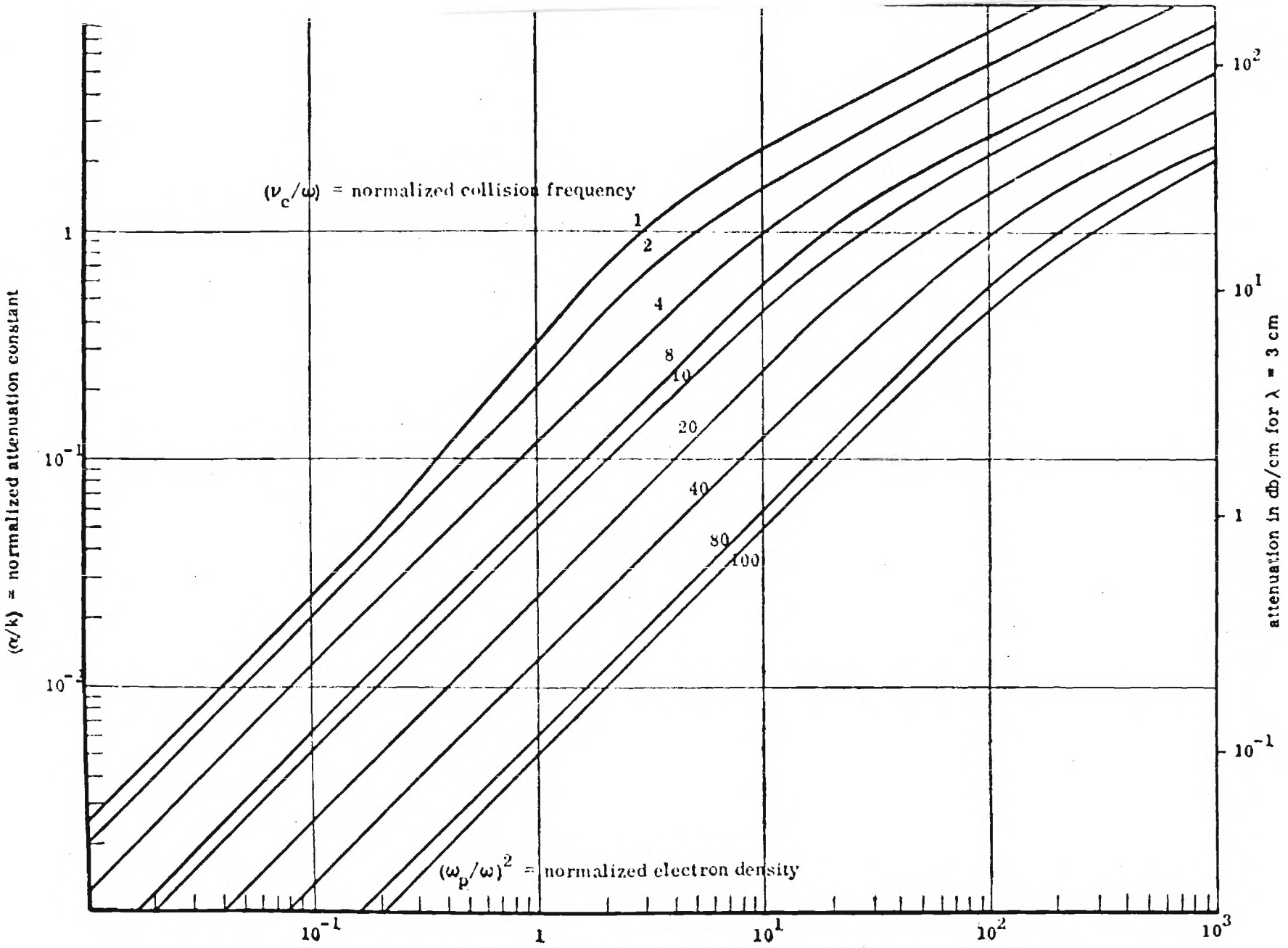

Figure 8. Attenuation of Electromagnetic Waves In Plasma (Large Collision Frequency).

The use of high frequencies permits transmission of signals for phase measurements.

As a result of the effects discussed above, it is evident that the submillimeter wavelength region is optimum for diagnostics of Tokamak plasmas which have electron densities in the range from 10^{13} to 10^{14} cm^{-3} and electron temperatures of several keV.

4.1 Plasma Diagnostics

The availability of tunable gigawatt sources in the millimeter and submillimeter wavelength regions will provide means for investigation of plasma phenomena. Recently, with the development of Tokamak plasmas, interest has been generated in the interaction of intense submillimeter radiation with plasma. Lax and Cohn [8] have reviewed several effects which can be investigated in the Tokamak machines. Currently, power levels on the order of 10^4 W in 200-μs pulses can be achieved [9] with 496 μm CH_3F lasers pumped by high power pulsed CO_2 lasers. The optically pumped lasers are discussed in Appendix V.

The gigawatt sources can be employed for the following area of investigation, discussed by Lax and Cohn [8]:

1.) Plasma breakdown and heating;

2.) Excitation of parametric decay instability at the plasma frequency;

3.) Tokamak diagnostics.

For the plasma breakdown and heating, the availability of high power submillimeter sources in conjunction with the high magnetic fields will permit the use of cyclotron resonance effects. This reduces the breakdown threshold by orders of magnitude at low pressures and results in the heating of plasma electrons very efficiently to relatively high temperatures. The theory of radiation-induced gas breakdown in a magnetic field has been worked out [10], and, in the "short-pulse limit," the ratio of breakdown threshold power at resonance to breakdown threshold power at zero magnetic field is

$$\frac{W_{th}(\omega_c = \omega)}{W_{th}(\omega_c = o)} \sim \frac{\nu_c}{\omega}$$

when $\nu^2 >> \nu_c^2$ and ω_c is the cyclotron resonance frequency.

The resonance absorption thus significantly decreases the breakdown threshold power.

Lax and Cohn [10] have assumed that, for the resonant heating of a plasma, all of the source energy is utilized in heating the plasma.

Then, $$E_L \sim (3n_e/2)\, k_B(T_e + T_i)\, AL$$

where E_L = source pulse energy

n_e = plasma density

T_e = electron temperature

T_i = ion temperature

A = cross-sectional area of plasma

L = plasma length = $V_T \tau_e$ where V_T is the ion velocity and τ_e the source pulse length.

If the electron temperature is assumed to be three times the ion temperature,

$$L = (k\, T_e/3M)^{1/2}\, \tau_L$$

so that

$$(k\, T_e)^{3/2} = \frac{E_L\, (3M)^{1/2}}{2\, n_e\, A\, \tau_L}$$

For a submillimeter GW source with $\tau_e = 20 \times 10^{-9}$s, E_L = 20J, A = 0.1 cm^2 and $n_e = 10^{15}$ cm^{-3}, a hydrogen plasma can be heated to temperatures on the order of 1.46×10^5 electron volts, compared to 1.46×10^3eV for a MW pulse and approximately 10^2ev for a 10^4W pulse.

It has been shown by Jassby [11] that the excitation of the parametric decay instabilities may be studied by irradiating dense arc plasmas with intense submillimeter radiation. The arc plasmas have density gradients, dimensions and excitation characteristics that are appropriate for submillimeter diagnostics. The parametric decay instability takes energy from the radiation field (ω) and converts it into the energy of a Langmuir wave (ω_ℓ) and an ion acoustic wave (ω_i). The instability is excited only near the cutoff density n_c, where $\omega \sim \omega_\ell$. For 500 μm, n_e is equal to 5×10^{15} cm^{-3}.

It is shown [8] that the threshold intensity of the pump for excitation of the parametric decay instability is given by

$$I_c = \frac{1}{G} \frac{4n_e(T_e + T_i)\,\gamma_L\,\gamma_i}{\omega_e\,\omega_i\,c}$$

where G is the "linear swelling factor" and γ_L and γ_i are the damping rates of the Langmuir and ion acoustic waves.

For a helium arc, it has been shown [8] that the threshold intensity $I_c \sim 4 \times 10^4$ W/cm^2 corresponding to a critical power of 5800 W for focussing to a radius of 2 mm. The tunable GW source can provide sufficient power to excite this parametric effect.

The ion temperature of a Tokamak plasma can be measured by a tunable GW submillimeter signal. The linewidth of Thomson scattered radiation is determined by the ion temperature. The scattering angle Θ for λ = 500 μm, $n_e = 5 \times 10^{13}$ and T_e = 2 keV, is 30°. The advantage over using a 10.6 μm CO_2 laser for measurements of ion temperatures is seen from the fact that at 10.6 μm it is necessary to work at $\Theta \leq 1°$ where scattering experiments are very difficult.

The power scattered from a thermal plasma, detected at an angle Θ, is

$$P_s(\Theta) = P_o\, n_e\, \sigma \ell d\Omega$$

where P_o = incident power

P_s = scattered power

σ = Thomson-scatter cross section per solid angle = 4×10^{-26} cm^2

ℓ = length of scattering region in detector FOV

$d\Omega$ = solid angle subtended by the detector

For $P_o = 10^9$W, $n_e = 5 \times 10^{13}$ cm^{-3}, ℓ = 5 cm and $d\Omega = 10^{-3}$, the P_s = 1×10^{-5}W, which can be detected by an incoherent submillimeter detector with sufficiently short response time.

The ion temperature is determined from the width of the central peak of

the scattered spectrum, which is about 500 MHz for $\theta = 30°$ and ion temperature $T_i = 2$ keV. This is detectable with the GW source with a 20 ns pulse width or a line width on the order of 50 MHz. It has been shown [8] that 1 MW of incident power will also provide sufficient scattered intensity to measure the ion temperature, possibly requiring a heterodyne detection system.

The high power sources with tunability similar to that of the sources considered in this report have also been shown [8] to contribute to Tokamak diagnostics for measurements of the transverse thermal conductivity [12] and for coherent scattering from plasma fluctuations. The scattered intensity in the latter case is expected to be at least 100 times greater than the intensity of ordinary Thomson-scattered radiation. An advantage of the tunable GW sources in the measurement of transverse thermal conductivity is the capability of working at $\lambda = 1$ mm where no high power sources currently exist. This allows the possibility of performing the required absorption of the second harmonic of the cyclotron resonance at magnetic fields that are reasonably accessible for several Tokamak machines.

The case of collective scattering from thermonuclear plasma has been discussed by Gehre [13], who has shown the advantage of the high power submillimeter sources. For coherent scattering from overthermal density fluctuations, the scattered radiation is given by [13]

$$P_s = \lambda_L^2 \, \tilde{n}^2 \, \sigma \, \ell^2 \, P_L$$

where P_s = scattered power, P_L = incident laser power, λ_L = laser wavelength, $\tilde{n}$ is the density fluctuation amplitude, σ the Thomson cross-section and ℓ, the length of the scattering volume. The value $\tilde{n} = 10^9$ cm^{-3} has been measured for the turbulent density-fluctuation level, so that, for a GW source at $\lambda \sim 0.5$ mm, with $\ell = 1$ cm and $\sigma = 10^{-26}$ cm^2, the scattered power $P_s \sim 25$ mW far exceeds current or projected values. Video detection with the calculated power levels will simplify experimental investigations. Scattering from much lower density fluctuations will be possible at the gigawatt power levels without resorting to heterodyne detection.

Recent investigations have shown the importance of plasma impurities on

the interpretation of magnetically confined plasmas of the Tokamak type. Laser radiation scattering has been proposed [14] as a means for measuring these impurity densities. The GW source would provide the best means for performing these experiments and could conceivably be used to measure the effective charge $\bar{Z}$ of the plasma directly [14].

As indicated previously, the measurement of the plasma parameters, electron densities and collision frequencies, is important for an understanding of the plasma. A technique employing a millimeter or submillimeter Fabry-Perot interferometer is appropriate for measurements of these parameters in dense plasma [15]. The open structure of the Fabry-Perot interferometer makes it possible to apply the resonator to plasma diagnostics in plasma machines where the plasma cannot be confined in a closed measuring cavity. In addition, it can avoid measuring phase shift in the plasma which would be difficult for the high power sources in dense plasma. On the other hand, the measurement of frequency shift and resonator Q changes required in the Fabry-Perot technique will require stability and frequency reproducibility of the high power signal. The technique must be compared with the technique using a Mach-Zender interferometer and a low power HCN laser [16].

In the Fabry-Perot interferometer, the introduction of a lossy plasma region into the resonator results in a frequency shift and Q change given by [15]

$$2\left(\frac{\omega_1 - \omega_o}{\omega_o}\right) = P\,\frac{\omega_p^2}{\omega_o^2}$$

and

$$\frac{Q_o - Q_p}{Q_o\,Q_p} = P\,\frac{\omega_p^2\,\nu}{\omega_o^3}$$

where ω_o and ω_1 are the frequencies, and Q_o and Q_p the resonator Q's before and after the introduction of the plasma. The relation $\omega_p^2 << \omega^2$ must hold, and P

is an effective filling factor. The minimum detectable frequency shift depends on the linewidth and the stability of the high power source. For a width limitation of 100 MHz on the frequency shift at $\frac{\omega}{2\pi}$ = 890 GHz, the minimum measurable electron density is $2 \times 10^{11}\ cm^{-3}$ for a filling factor P = 1/4, compared with $2 \times 10^{12}\ cm^{-3}$ detectable with the Mach-Zender interferometer. The thermonuclear plasmas with densities in the range $10^{13} - 10^{15}\ cm^{-3}$ can readily be measured with the Fabry-Perot scheme. The collision frequency is calculated from the Q-shift with n_e determined from the frequency shift.

4.2 Interaction with Re-entry Plasma and Rocket Exhausts

Transmission of electromagnetic radiation through plasma plays a significant role in the areas of radar detection, tracking and communication associated with re-entry vehicles and missiles, or in communicating guidance commands to missiles through their own plumes. In addition, the dense plasma which occur during nuclear explosions also cause blackout for communications and radar. The communications scenarios which might be envisioned include ground to vehicle, high flying aircraft to re-entry vehicle, or transmission through ionized rocket exhausts between two high altitude hypersonic vehicles. In the case of a manned re-entry vehicle which descends slowly in altitude, the plasma sheath ionization can persist over a large part of its flight path, thus making guidance and control difficult from ground stations. From the radar viewpoint, the characteristics of the plasma are important because the ionized wake of a re-entry vehicle provides a significant target from which radar signals can be reflected. To obtain meaningful information about the vehicle for discrimination purposes, it is necessary to understand the scattering properties of the plasma sheath so that the vehicle and plasma returns can be separated. Operation with a GW source at high frequencies will permit penetration of the sheath and will provide the necessary data on the vehicle cross-section.

For both the radar and communications applications, the interaction of the electromagnetic wave with the plasma sheath is complicated by a large number of parameters [17]. For the cases which can be considered here, the simplifying assumption that the signal interacts with a slab of plasma in which the plasma properties are constant must be made. The penetration of the stagnation point at the nose of a blunt re-entry body will be the most difficult transmission with the electron density decreasing but spreading along and beyond the body. Figure 9 shows the variations with velocity and altitude of the electron density and plasma frequency at the stagnation point of a blunt body.

Consider first the case of radar detection of a body which is re-entering the earth's atmosphere. As indicated previously, the penetration, absorption and reflection of the signal interacting with the plasma is a function of the

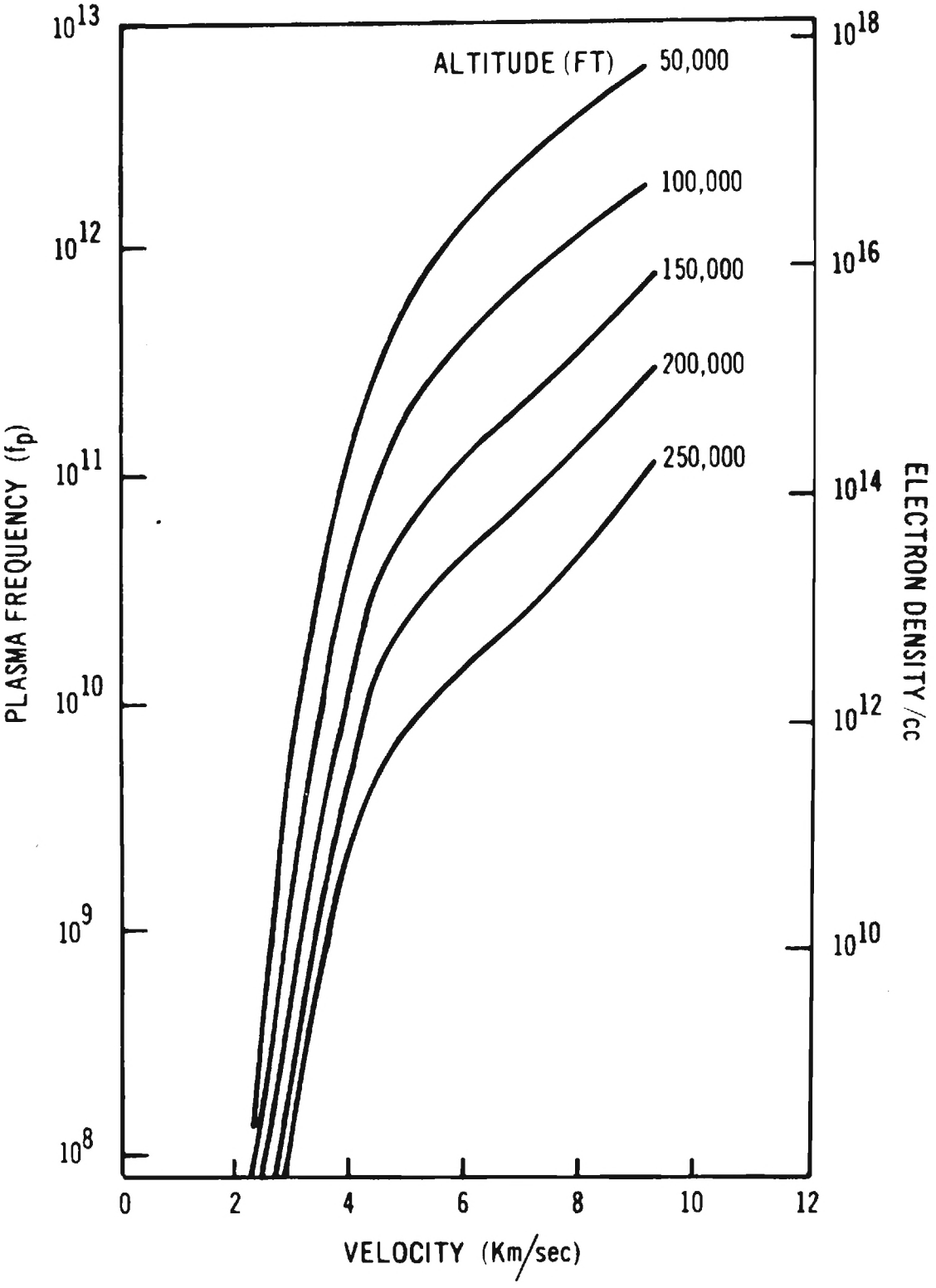

Figure 9. Variations With Velocity and Altitude, of The Electron Density and Plasma Frequency at The Stagnation Point of a Blunt Body [17].

operating frequency relative to the plasma frequency and collision frequency. Figure 10 shows a re-entry diagram [18] in which contours of constant plasma frequency ($f_p = \omega_p/2\pi$ = 5 GHz, 35 GHz, 300 GHz) are shown. For a fixed radar frequency, $f = \omega/2\pi$, maximum absorption will occur near one of the contours, i.e. for $f \sim f_p$.

A typical ballistic trajectory is also shown on the diagram. Maximum absorption at the frequency f, due to the stagnation region, can only occur in the region near where the ballistic trajectory intersects the contour $f = f_p$ [18]. It is shown that two such intersections take place, one at high altitude and the other at low altitude. For the very high frequency (f_p = 3000 GHz), minimum absorption occurs. In turn, for the high frequency curves which are intercepted by the typical ballistic curve, the initial intercept altitude, where high absorption takes place, occurs at lower altitudes than in the case of lower frequencies. Thus, at high altitudes which are critical for ICBM defense, strong absorption at high altitudes would not be experienced for high frequency radars.

The radar detection of a re-entering ICBM can be calculated in the following manner:

From the typical ballistic trajectory of Figure 10, the values for f_p and n_e from Figure 9, and the values for ν_c from Figure 11, the parameters for various altitudes are given in Table 33. If we define the frequency ratios as [17]

$$N = \left(\frac{\omega_p}{\omega}\right)^2 = \text{normalized electron density}$$

and

$$S = \frac{\nu_c}{\omega} = \text{normalized collision frequency,}$$

then for α/k and β/k defined as the normalized attenuation and normalized phase constants with $k = \frac{2\pi}{\lambda}$, it is shown [19] that

$$\frac{\alpha}{k} = \left[\frac{1}{2}\sqrt{\frac{S^2 + (1 - N)^2}{1 + S^2}} - \frac{1}{2}\,\frac{S^2 + (1 - N)}{1 + S^2}\right]^{1/2}$$

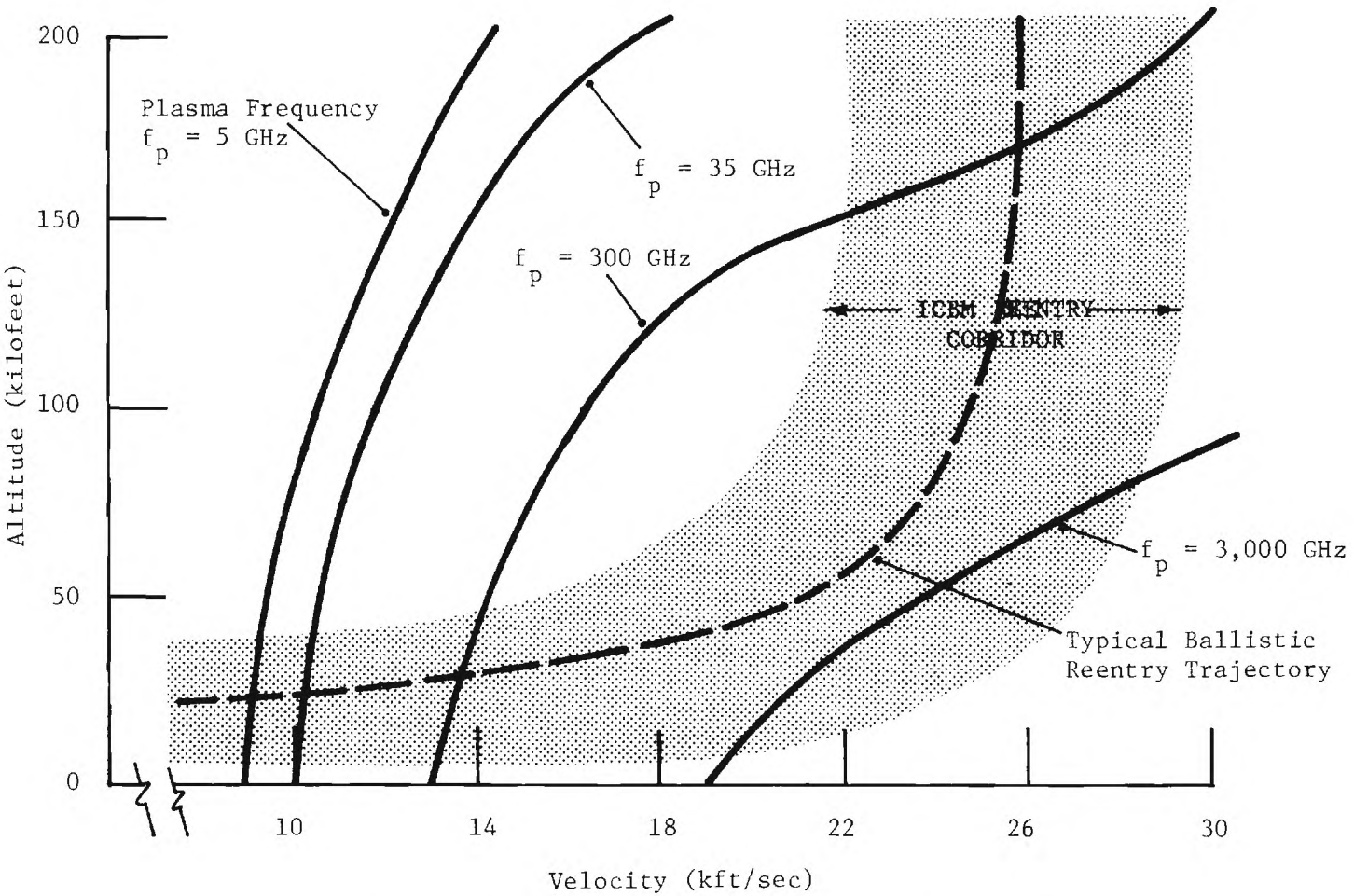

Figure 10. Radar Absorption Reentry Chart [18].

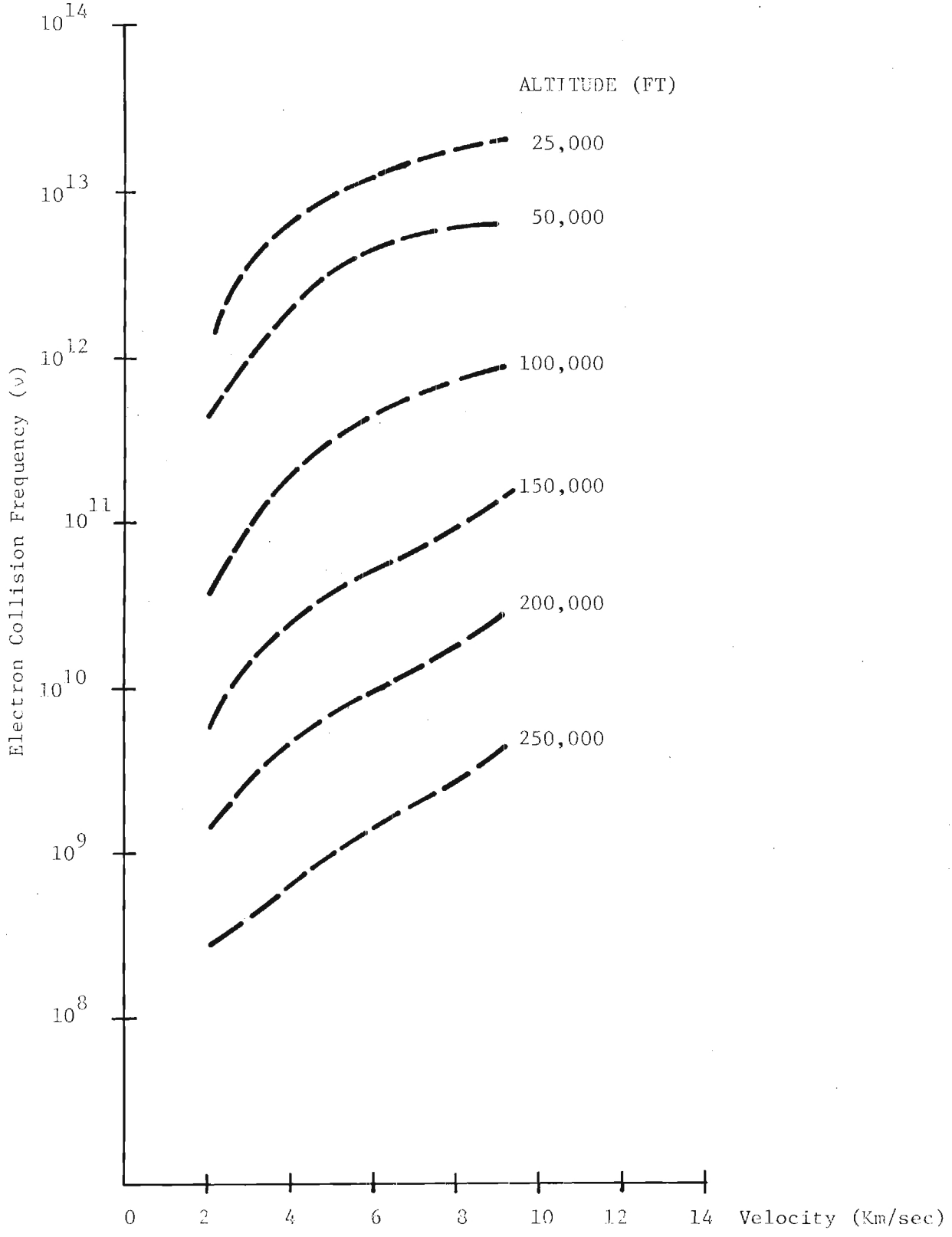

Figure 11. Electron Collision Frequency (ν) at the Stagnation Point of a Hypersonic Vehicle with Velocity at Various Altitudes Above the Earth [17].

TABLE 33

PLASMA FREQUENCY AND COLLISION FREQUENCY
AS A FUNCTION OF ALTITUDE AND VELOCITY

Altitude (KFT)	Velocity (KM/SEC)	f_p (GHz)	ν_c (GHz)
250	8.00	60	4
200	7.93	150	25
150	7.86	500	90
100	7.71	1,000	750
50	6.52	2,500	7,500
25	3.96	450	8,000

and

$$\frac{\beta}{k} = \left[\frac{1}{2} \sqrt{\frac{S^2 + (1 - N)^2}{1 + S^2}} + \frac{1}{2} \frac{S^2 + (1 - N)}{1 + S^2} \right]^{1/2}$$

From these relations, the plasma attenuation and air-plasma power transmission coefficients at the stagnation point have been calculated for the re-entry vehicle with the results given in Table 34. The calculations have been performed for 222 GHz, 340 GHz, 400 GHz, 660 GHz, 890 GHz and 3088 GHz. Because of the high atmospheric attenuation at the higher frequencies, the detection of a re-entry vehicle would have to be made from an aircraft with the exception of observation at 222 GHz. The coefficient, α, is the voltage attenuation coefficient, so that, for power attenuation, the factor 2α must be used.

To calculate the capabilities of radars operating at the frequencies given in Table 34, the total attenuation through the atmosphere must be employed. If the atmospheric attenuation occurs in the lower 30 km of the atmosphere, then from the curves of Appendix IV, it is evident that the one way total attenuation for observations at an angle of 60° with the zenith is given by the following:

Frequency (GHz)	One Way Attenuation (dB)
222	9
340	25
400	∿ 45
660	∿ 110
890	∿ 170
3088	∿ 3000

Of the frequencies listed, only at 222 GHz can radar detection be performed, and this is only in the vicinity of and greater than 250,000 feet. It can be shown that, for a radar operating from an aircraft at approximately 30,000 feet, the re-entry vehicle (RV) can be detected through the sheath at

TABLE 34

PLASMA ATTENUATION AND AIR-PLASMA TRANSMISSION COEFFICIENTS FOR A RE-ENTRY VEHICLE

Altitude (KFT)	Frequency, f (GHz)	$N = \left(\frac{f_p}{f}\right)^2$	$S = \frac{\nu_c}{f}$	T^2	$\frac{\alpha}{k}$	$\left(\frac{\alpha}{k}\right)\left(\frac{54.5}{\lambda}\right)$ (dB/cm)
250	222	0.07305	0.01802	1.0	6.833×10^{-4}	0.276
200		0.4565	0.1126	1.0	3.421×10^{-2}	13.810
150		5.0726	0.4054	0.38	0.1117	45.094
100		20.291	3.3784	0.65	1.2420	501.40
50		126.816	33.7838	0.85	1.1716	472.979
25		2.0270	36.0360	1.0	3.7416×10^{-4}	0.1510
250	340	0.03204	0.0119	1.0	1.936×10^{-4}	0.120
200		0.2007	0.0746	1.0	8.321×10^{-3}	5.147
150		2.229	0.269	0.37	2.607×10^{-2}	16.127
100		8.9102	2.239	0.80	0.7757	480
50		55.6963	22.39	0.90	0.8747	541
25		1.8036	23.88	1.0	4.106×10^{-3}	2.540

TABLE 34 (Cont.)

Altitude (KFT)	Frequency, f (GHz)	$N = \left(\frac{f_p}{f}\right)^2$	$S = \frac{\nu_c}{f}$	T^2	$\frac{\alpha}{k}$	$\left(\frac{\alpha}{k}\right)\left(\frac{54.5}{\lambda}\right)$ (dB/cm)
250	400	0.0225	0.010	1.0	1.136×10^{-4}	0.0825
200		0.1406	0.0625	1.0	47.20×10^{-4}	0.343
150		1.5625	0.225	0.54	0.06113	44.421
100		6.250	1.875	0.8	0.5841	424
50		39.0625	18.75	0.95	0.7598	552
25		1.2656	20.00	1.0	0.0183	13.298
250	660	8.263×10^{-3}	6.06×10^{-3}	1.0	2.828×10^{-5}	0.0339
200		0.05153	3.79×10^{-2}	1.0	1.001×10^{-3}	1.201
150		0.5746	0.758	1.0	0.05789	69.458
100		1.3271	1.136	0.95	0.1935	232
50		14.3489	11.36	0.95	0.4702	564
25		0.4651	12.12	1.0	0.0191	22.917
250	890	4.542×10^{-3}	4.49×10^{-3}	1.0	6.4807×10^{-5}	.105

TABLE 34 (Cont.)

Altitude (KFT)	Frequency, f (GHz)	$N = \left(\frac{f_p}{f}\right)^2$	$S = \frac{\nu_c}{f}$	T^2	$\frac{\alpha}{k}$	$\left(\frac{\alpha}{k}\right)\left(\frac{54.5}{\lambda}\right)$ (dB/cm)
200		2.839×10^{-2}	2.81×10^{-2}	1.0	4.0435×10^{-4}	0.654
150		0.3156	0.1011	1.0	1.904×10^{-2}	30.81
100		1.2625	0.8427	0.9	0.2304	373
50		7.8905	8.4270	0.94	0.3170	513
25		0.2556	8.8989	1.0	1.4205×10^{-2}	22.98
250	3088	3.7752×10^{-4}	1.295×10^{-3}	1.0	0	0
200		2.36×10^{-3}	8.096×10^{-3}	1.0	0	0
150		2.621×10^{-2}	2.915×10^{-2}	1.0	3.8704×10^{-4}	2.173
100		0.1049	0.2429	1.0	1.2667×10^{-2}	71.11
50		0.6555	2.4288	1.0	0.1203	675
25		0.02123	2.5907	1.0	3.5706×10^{-3}	20.05

higher altitudes. As higher frequencies are employed, detection further into the atmosphere is possible.

The calculation of the radar application is performed as follows:

It is assumed that the vehicle is observed at 60° to the zenith and that the radar cross-section is $\sigma = 0.1\ m^2$.

It is further assumed that

$F = 15$ dB, receiver noise figure

$A = 1\ m^2$, antenna area

$\eta = 0.75$

$T = 300°$ K

$R_1 = 4$ cm, typical thickness of radar sheath [17]

Pulse widths of 10 ns and 50 ns were compared so that

$B = 2 \times 10^8$ Hz in one case and

$B = 4 \times 10^7$ Hz in the other.

Table 35 gives the results of the radar detection of an RV through its sheath. The table presents results for the two pulse widths for $P_T = 10^9$W and 10^7W. The observations from aircraft shows very large S/N for both power levels. The S/N increases as higher frequencies are used, and, in addition, observation further into the atmosphere is possible at the higher frequencies. In this calculation, it has been assumed that the entire signal passes through a plasma characteristic of the stagnation region. Actually, the attenuation is considerably lower as the electron density drops in regions back from the RV nose.

While the calculations, which have been made, are rough estimates, it is indicated that the use of high power sources as high frequency radar transmitters can provide supplementary data for discrimination of RVs from decoys, chaff and confusion devices.

For the case of communication through the plasma sheath to a re-entry vehicle, it is assumed that the receiver antenna is located on the side of the vehicle where the electron density and the collision frequency are lower than the values at the nose of the vehicle. Typical values [17] for n_e and ν_c in this case are 4×10^{13} cm^{-3} and 1.2×10^{10} Hz. Calculations have been

TABLE 35

RADAR DETECTION OF AN RV THROUGH ITS PLASMA SHEATH

a.) Observation From Ground (60° to Zenith)

Frequency	Range (km)	Atmospheric Attenuation (dB)	S/N (dB) ($B = 4 \times 10^7$ Hz)	S/N (dB) ($B = 2 \times 10^8$ Hz)	P_T (W)
222 GHz	152.44	18	9.2	2.2	10^9

b.) Observation From Aircraft (60° to Zenith)

			$P_T = 10^9$W		$P_T = 10^7$W	
Frequency (GHz)	Altitude (km)	Range (km)	S/N (dB) ($B=4\times10^7$ Hz)	S/N (dB) ($B=2\times10^8$ Hz)	S/N (dB) ($B=4\times10^7$ Hz)	S/N (dB) ($B=2\times10^8$ Hz)
222	76.220	134.146	29	22	9.4	2.4
340	76.220	134.146	34	27	14	7
400	76.220	134.146	35	29	15	9
	60.976	103.659	38	31	18	11
666	76.220	134.146	41	34	21	14
	60.976	103.659	36	29	16	9
890	76.220	134.146	43.4	36.4	23.4	16.4
	60.976	103.659	42.9	35.9	22.9	15.9
3088	76.220	134.146	54	47	34	27
	60.976	103.659	49	42	29	22
	45.732	73.171	47.6	40.6	27.6	20.6

performed for communicating from ground to a vehicle at 250,000 feet at an angle of 60° with the zenith and for frequencies of 94 GHz and 222 GHz. A two meter dish on the ground and a six inch dish on the vehicle were assumed. The following parameters and results serve as examples of these calculations:

At 94 GHz,

$G_1 \simeq 61$ dB for a 2 meter dish

$G_2 \simeq 40.5$ dB for a 6 inch dish

$\eta = 0.5$ assumed for all cases

$B = 2 \times 10^8$ Hz

$F = 7$ dB

$T = 300°K$

$\frac{\alpha}{k} = 0.004341$

$\frac{f_p}{f} = 0.60415$

$\frac{\nu_c}{f} = 1.8963 \times 10^{-2}$

Total atmospheric attenuation = 3 dB.

Assume a 1 meter path through the plasma.

Vehicle altitude = 250,000 feet.

For clear air propagation, the power received is
$P = 7.20 \times 10^{-7}$ W for transmitter power of 10^9 W, and
$P = 7.20 \times 10^{-12}$ W for transmitter power of 10^4 W

The result for $P_T = 10^4$ W does not yield a S/N = 3 dB for the parameters given above while the GW source provides $S/N = 1.7 \times 10^5$. In addition, the GW source yields S/N in excess of 10 dB for average rainfall rates of 7 dB/km for the lower 3 km of atmosphere.

At 222 GHz,

$G_1 \simeq 68.4$ dB

$G_2 \simeq 48$ dB

$\eta = 0.5$

$B = 2 \times 10^8$ Hz

$F = 13$ dB

$T = 300°K$

$\frac{\alpha}{k} = 2.718 \times 10^{-4}$

$\frac{f_p}{f} = 0.25583$

$\frac{\nu_c}{f} = 8.0298 \times 10^{-3}$

Total atmospheric attenuation = 9 dB.

Assume a 1 meter path through the plasma.

Vehicle altitude = 250,000 feet.

Under these conditions, the received power is

$P = 2.145$ W for $P_T = 10^9$W and

$P = 2.145 \times 10^{-5}$W for $P_T = 10^4$W

At both power levels, communication is possible. In rain, however, operation at the lower power level is limited to rainfall rates less than 20 mm/hr (9.5 dB/km), while the GW source can communicate through rainfalls up to 50 mm/hr corresponding to 17.5 dB/km.

Propagation through ionized rocket exhaust plumes presents problems similar to those encountered in propagation through the plasma associated with re-entry vehicles. When an electromagnetic propagation path is intercepted by the ionized exhaust of a missile, severe degradation of the performance capability of guidance, telemetry, and tracking can occur [20]. The complexity of the transmission phenomena is not treated in this report, but the possible application of a high power source, capable of operation at high frequencies, is indicated. The characteristics of the rocket exhaust are such that within the exhaust jet, spatial variations of the electron concentration and collision frequency exist, particularly at low altitudes. At low altitudes, the exhaust jet is confined to a relatively small volume by the pressure of the atmosphere. As the missile ascends, the exhaust jet expands and the internal shocks become displaced further down stream in regions where the surrounding electron concentration is relatively low. Because of the increased exhaust size, propagation paths are more readily intercepted at the higher altitudes, but interference is

not usually as severe because of the accompanying reduction in the plasma density.

Interception of electromagnetic waves by the ionized exhaust can lead to absorption, reflection, refraction and diffraction of the waves. In addition, because the properties of the ionized exhaust can fluctuate rapidly with time, amplitude and phase modulation of the intercepted waves can occur. When these effects take place, they lead to signal attenuation, multipath effects, beam distortion and other forms of interference. In extreme cases, attenuation of electromagnetic waves by absorption or reflection can be large enough to result in complete loss of signal. Other manifestations of the interaction of electromagnetic waves with the ionized exhaust are inaccuracies in data transfer, and errors in range and angle determinations obtained by both pulsed and cw radar systems during powered flight.

Attenuation through the plume can be calculated by estimating the electron concentration and collision frequency for slabs of plasma and considering the plume to consist of a series of these slabs with characteristic parameters for each. To provide a simple example of the role that a GW source might play in this application, we will only consider a plume of average n_e and ν_c and assume that this plume is approximately 5 meters in length. Table 36 gives representative values of the plasma parameters and attenuation near the nozzle and exit of rocket engines [20]. If we consider the plume to have the characteristics of one set of parameters of Table 36, it can be shown that for the values chosen ($n_e = 4 \times 10^{10}$ cm^{-3}, $\nu = 4 \times 10^{11}/2\pi$ Hz and $\alpha = 4.4$ dB/m), communication through the plume is possible with relatively low power at X-band, but radar tracking is not possible at this frequency even with a GW source. When the system is operated at 94 GHz, calculations indicate that the radar detection of a 1 meter^2 target is possible at 10 km through the 5 meter long plume with a S/N of 60, only if a gigawatt source is used. A shorter range or lower S/N will result under the more realistic condition of a smaller cross-section.

The effects on radar and communication of plasma produced by nuclear detonation in the atmosphere at both high and low altitudes should be investigated in the light of the GW source capabilities at high frequencies. The

TABLE 36

REPRESENTATIVE VALUES OF THE PLASMA PARAMETERS AND ATTENUATION NEAR THE NOZZLE AND EXIT OF ROCKET ENGINES [20]

n_e (10^{10} cm^{-3})	ν (10^{11} s^{-1})	f_p (GHz)	Attenuation (dB/m at 10 GHz)
30	3	4.9	39.5
4	4	1.8	4.4
1.5	5	1.1	1.4
0.3	0.08	0.5	0.3
0.08	1.5	2.5	0.2

importance of propagation for communications, radar tracking, damage assessment, etc. as a function of time after the detonation and of the distance from the center of the explosion must be considered. With the high reflectivities encountered during nuclear explosions, reflective communications similar to that employed in troposcatter communications could be a significant application for a gigawatt source at relatively high frequencies.

CHAPTER 5

TUNABLE INFRARED TECHNIQUES

This chapter briefly discusses potential techniques for using the tunable millimeter or submillimeter high power sources to generate a tunable infrared signal useful at frequencies where tunable laser sources do not currently exist. The tunable IR scheme can be applicable to many military problems. It is conceivable that a nonlinear optical element and a laser can be switched into the beam of a submillimeter GW source to provide a countermeasure at wavelengths which are unaccessible by conventional laser techniques.

The tunable source, achieved by nonlinear optical mixing of a laser and gigawatt source, can be considered for several other applications:

a. With an output in the 12 μm – 16 μm spectral range, as a source for isotope separation.

b. With the mixed signal output in the visible region, for interrogation of enemy optical systems and for countermeasures.

c. As a spoofer or jammer for 1.06 μm target designator receivers.

d. As a spoofer/jammer for a 4–5 μm seekers.

e. As a jammer at 10.6 μm, 5 μm, 3.8 μm and 1.06 μm against potential communications or radar receivers.

f. As a tunable (covert) radar in the 8–12 μm region (CO_2 + REB).

The techniques which could make these applications possible involve the nonlinear optical mixing of an IR or visible wavelength laser with a GW source such as the REB device. Mixing schemes such as that required have been demonstrated some time ago [21] by using a nonlinear crystal GaAs to mix a CO_2 laser with a millimeter wavelength klystron. Figure 12 demonstrates this mixing configuration in which a second CO_2 laser was employed as a local oscillator in a superheterodyne receiver. More recently, the techniques have been used to provide chirped 10 μm signals [22]. To handle power levels on the order of gigawatts, nonlinear elements capable of operating free of damage are required.

Techniques have been employed to take advantage of the nonlinear effects of gases in order to generate third harmonics and to mix signals [23]. Inert

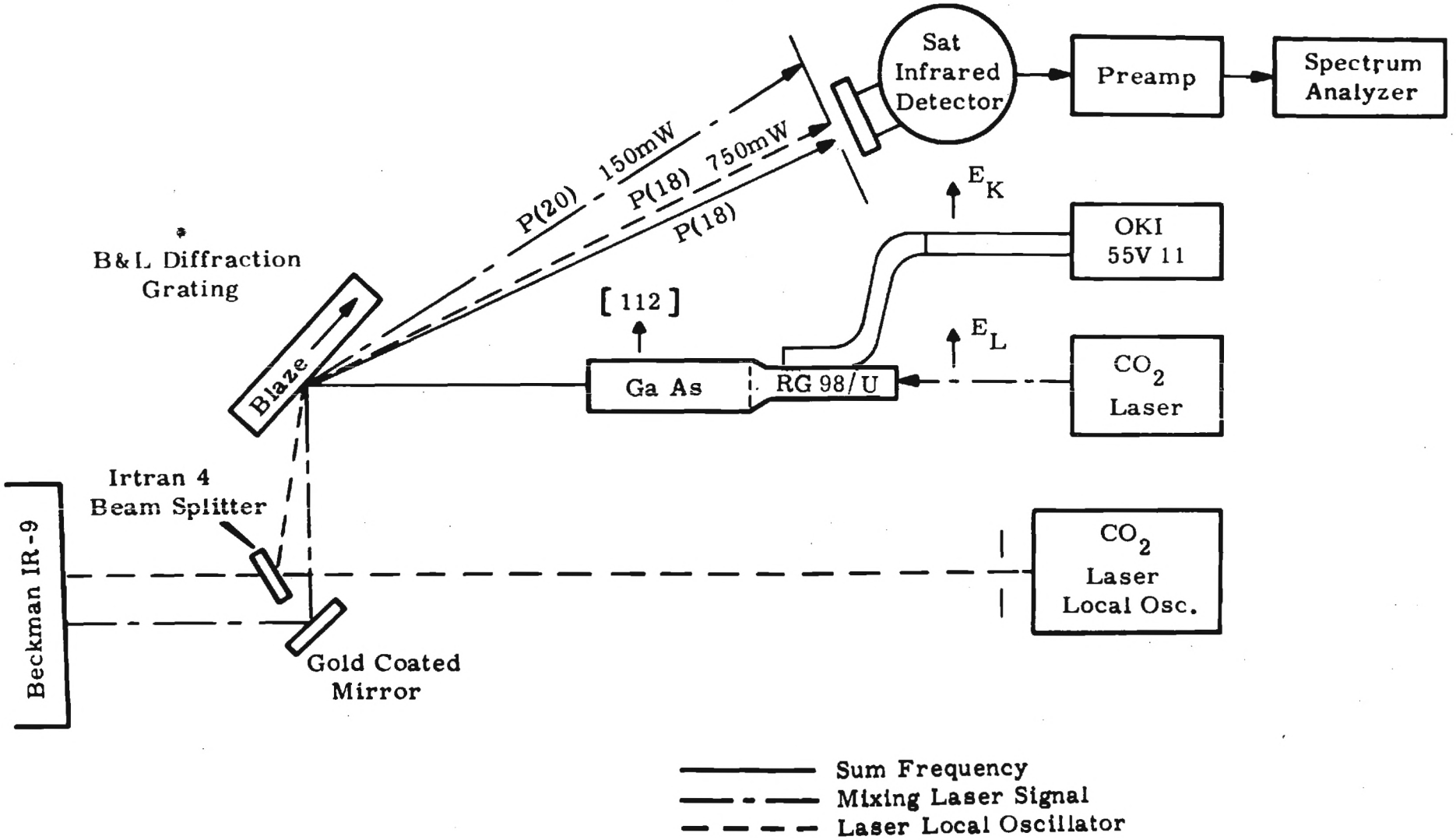

Figure 12. Experiment Diagram to Generate Sum and Difference Frequencies of a Laser and a Klystron - Sum of P(20) and 53,548 MHz Illustrated.

gases and alkali metal vapors have been shown to exhibit nonlinear effects with the capability for phase matching. The majority of the applications which have been made of this technique has been in the generation of tunable ultraviolet signals. Efficient conversion of high power pulses has been possible because of the existing resonant nonlinear susceptibility of these vapors, the capability for phase matching and the transparency in the spectral regions of interest. To employ the techniques of mixing in vapors in the infrared, investigations will have to be made to provide the appropriate vapor. The vapor elements have a number of significant advantages over nonlinear crystals [23]. Nonlinear crystal transparency usually is more limited than that of gases. The isotropic nature of gas mixtures eliminates Poynting vector walkoff which is characteristic of birefringent phase matching in crystals. Breakdown power and energy densities are higher in gases, and breakdown does not destroy the medium. Gas cells may be ultimately made with very large apertures to handle incident optical energies.

To use the gigawatt source for generation of visible or ultraviolet radiation, techniques can be used similar to those which have been employed for efficient up-conversion of IR radiation to the near ultraviolet [24]. The process has used a resonantly enhanced third order nonlinear susceptibility. Several schemes can be considered which include two-photon pumping of non-allowed transitions of metal vapors such as sodium.

To employ the two photon resonantly enhanced technique in the IR, energy level schemes must be investigated. Figure 13a shows a diagram of the mixing scheme. A pump laser at frequency ω_p is tuned so that the sum of two photons is equal to an unallowed transition ω_{02}. The GW source at frequency ω_t mixes with the pump signal to produce the sum or difference frequency $\omega_p \pm \omega_t$. It has been shown that the process is particularly efficient if the generated frequency lies near an allowed transition ω_{03}.

Harris and Bloom [25] have given the expressions for mixing of two signals to produce sum or difference power. It is assumed that the pump power density is limited by two-photon absorption of an intermediate non-allowed transition. The power density generated in a single coherence length at the sum (or difference) frequency ω_s is given by

$$\frac{P}{A}(\omega_s) = \left(\frac{1}{2\pi^2}\right) \eta\, \omega_s^2\, |P(\omega_s)|^2\, L_c^2, \text{ where}$$

$P(\omega_s)$ is the generated dipole moment, L_c = coherence length, and $\eta = (\mu/\varepsilon_o)^{1/2}$. For the energy level system such as that in Figure 13b, the dipole moment and coherence length are approximated by

$$P(\omega_s) = \frac{N\mu_{01}\,\mu_{12}\,\mu_{23}\,\mu_{30}\,E_p^2\,E_t}{4\hbar^3\,(\Delta\omega_1)(\Delta\omega_2 + \frac{1}{2}\,j\delta\omega_2)\,\Delta\omega_3}$$

and

$$L_c = \frac{2\pi\,\hbar}{N\,\eta}\,\frac{1}{\omega_s}\,\frac{\Delta\omega_3}{\mu_{03}^2}$$

where N = atomic (or molecular) density

μ_{ij} = various dipole matrix elements

$\Delta\omega_1 = \omega_p - \omega_{01}$

$\Delta\omega_2 = 2\,\omega_p - \omega_{02}$

$\Delta\omega_3 = 2\,\omega_p \pm \omega_t - \omega_{03}$

$\delta\omega_2$ = half-power linewidth of ω_{02} transition

E_p, E_t = electric field strengths of pump and tunable GW source

To use this scheme, an energy level configuration appropriate for IR mixing must be determined. The output power is proportional to the square of the pump power and to the GW source power.

To overcome the problem of having appropriate energy levels for IR mixing, it has recently been proposed to use molecular media if resonance enhancement is to be used [26]. For molecular systems, the energy levels are complex, and transition probabilities often unknown. To eliminate the problem of small nonlinear interactions which could result from the vibrational level dipole moment being smaller than atomic electronic state moments, it is proposed that virtual vibronic (vibration-electronic) transitions with much larger

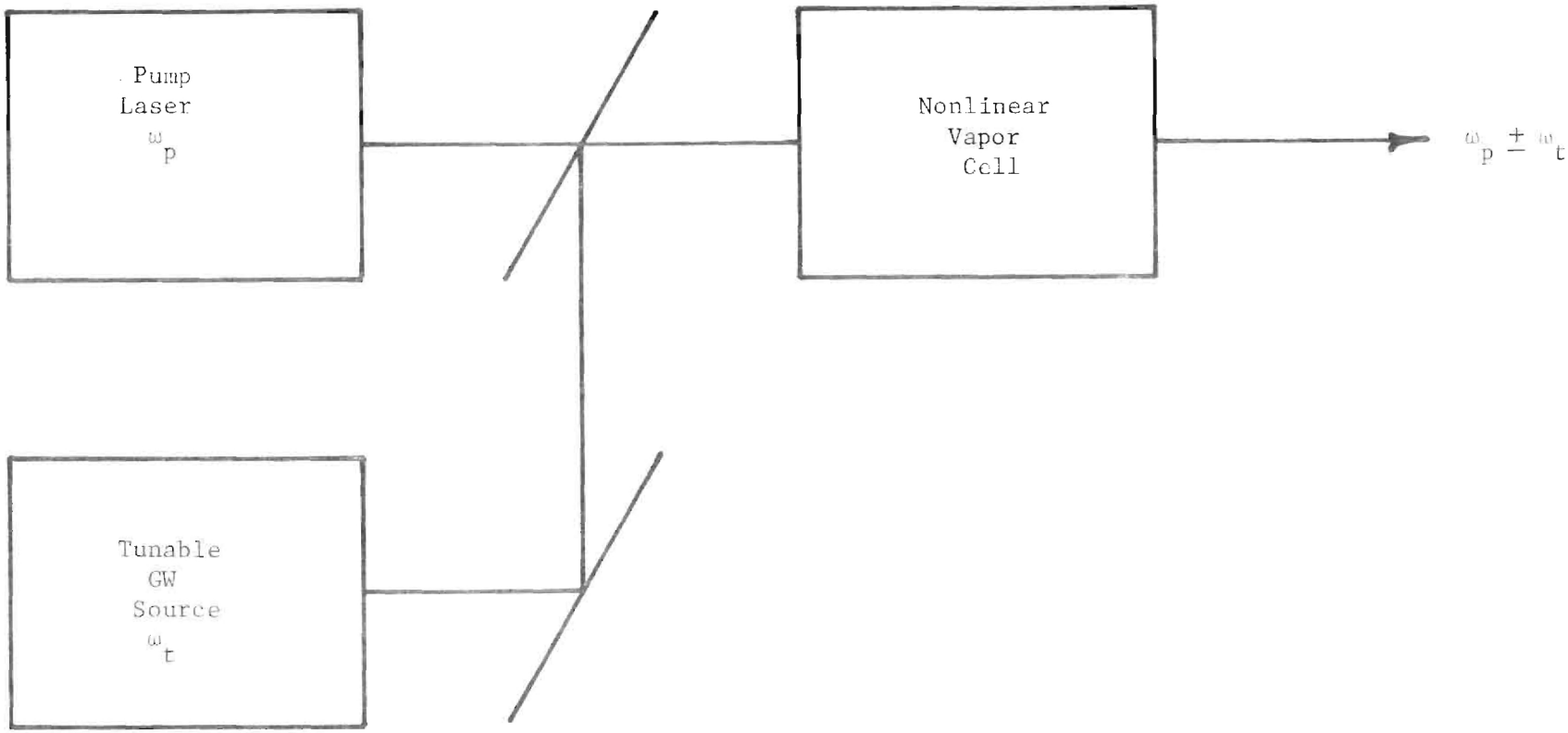

Figure 13a. Mixing of Tunable GW Source (ω_t) with Pump Laser (ω_p).

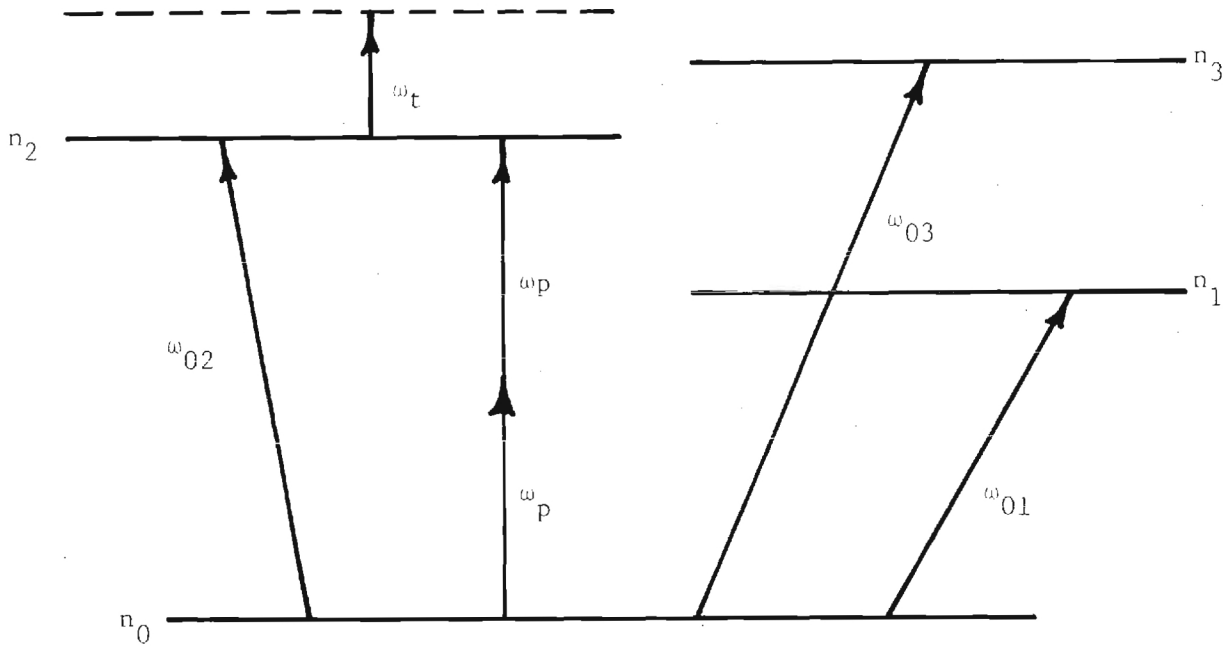

Figure 13b. Energy Level Configuration for Resonantly Enhanced Two-photon Optical Mixing.

transition moments be employed.

To employ the techniques discussed here, it is necessary that detailed investigations be performed on energy levels appropriate for generating an IR signal at a particular frequency. The GW source, with suitable mixing schemes, can provide sum or difference signals for applications similar to those listed at the beginning of this chapter.

CHAPTER 6

ADDITIONAL POTENTIAL APPLICATIONS OF GIGAWATT SOURCES

The applications discussed thus far are those which the authors of this report have considered the most appropriate for a gigawatt source. The potential of the devices is such that a large number of possible applications can be proposed. Because of the limited time for this program, it has not been possible to consider all the subjects which may find solutions in the gigawatt sources. During the course of the program, however, various applications have been discussed and notes made on several of these potential uses. Because of the need for sources in the millimeter and submillimeter wavelength regions, a large number of interesting applications, which, prior to the possibility of the existence of the sources of interest to this report, have not been considered in detail, appear as potential uses. Several of these applications do not necessarily require a gigawatt of power, but, as it has been emphasized throughout this report, the success of the application may require power of a level which can be attained only by the availability of sources based on the principle of operation of the GW sources in parts of the spectrum where it is not evident that other sources will fill the role.

In this chapter, a number of potential applications are treated. Further investigation of several of these schemes should be performed in a more detailed fashion. Following the discussion of some of these topics, brief statements are given on several other applications which could not at this time be treated in detail.

6.1 Submillimeter Imaging

A strong case for submillimeter inclement weather viewing systems has been made by several people including Paul W. Kruse of the Army Scientific Advisory Panel [27]. Establishing the need for such a system is not the objective of this discussion. However, pointing out some inherent problems and limitations of such a system is necessary to establish the need for a REB submm source. If these viewer systems are developed to operate at wavelengths longer than 10.6 μm, a scaled down REB has greater promise for meeting the requirements of this application than conventional sources such as klystrons, carcinotrons, etc.

One of the principal long range military objectives is to be able to operate during all environmental conditions at an efficiency comparable to clear weather daylight operations. An important first step has been made in development of FLIR systems. These systems provide thermal images under "no light" conditions and limited inclement weather performance. There are several needs for short range inclement weather viewing systems such as: naval operations, airport ground operations, army battlefield surveillance, etc. As an example, Figure 14 shows that during midwinter in central Europe, the probability of visual range limitations of 1 km or less can be as high as 10%, and 5 km or less up to 50%. Figure 15, from another source, claims an even higher probability, up to 20% for 1 km or less range in midwinter. Rain and fog are also a problem along the US eastern seaboard creating problems with naval operations and taxying aircraft.

An inclement weather viewing system should allow operations during fog, rain and snow. The viewers should be transportable and provide images of object sizes equivalent to military surface vehicles at 1 to 5 km ranges. The Army operations require detection and recognition of surface vehicles with 2.2 m minimum dimensions. If these requirements can be met the airport ground traffic problems and naval operations problems would also be solved since they are often less stringent.

A very large part of the rationale for submm wavelengths is their relatively good adverse weather performance. Practical constraints on size and angular resolution cause the operating wavelengths to lie between 10 μm and 1 mm. Atmospheric transmission properties even in clear weather further limit the allowable wavelength to six bands: 8 to 13 μm, 15 to 25 μm, 350 μm, 750 μm, 850 μm, and 1.3 mm. The ability of an active system to penetrate fog increases with increasing wavelength, whereas that to penetrate rain and snow is nearly independent of wavelength in these bands. For a given aperture, the angular resolution and therefore the range at which an object can be recognized improves with decreasing wavelength due to diffraction limits. For the active systems being considered, fog penetration increases with increasing wavelength. Therefore, there should exist an optimum condition for power limited and diffraction

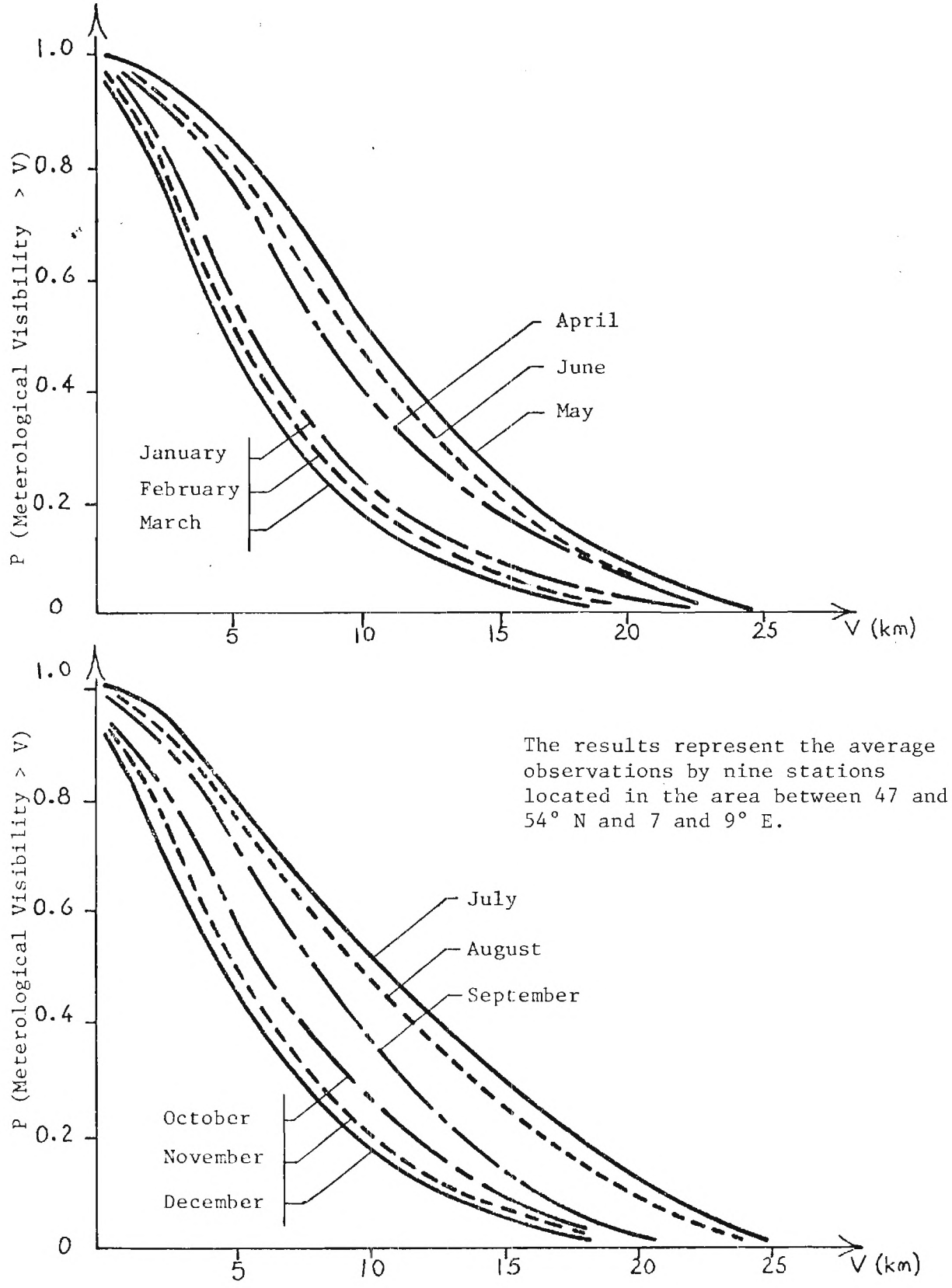

Figure 14. Possibility of Horizontal Meteorological [27]. Visibility at Least Equal to a Given Value

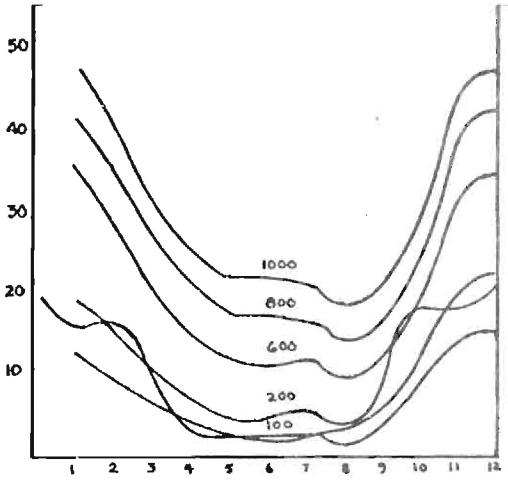

- Time With Cloud Coverage $\leq$ 4/8 in percent (Parameter: Altitude in M)

- Time With Visual Range 1 km (log) in percent.

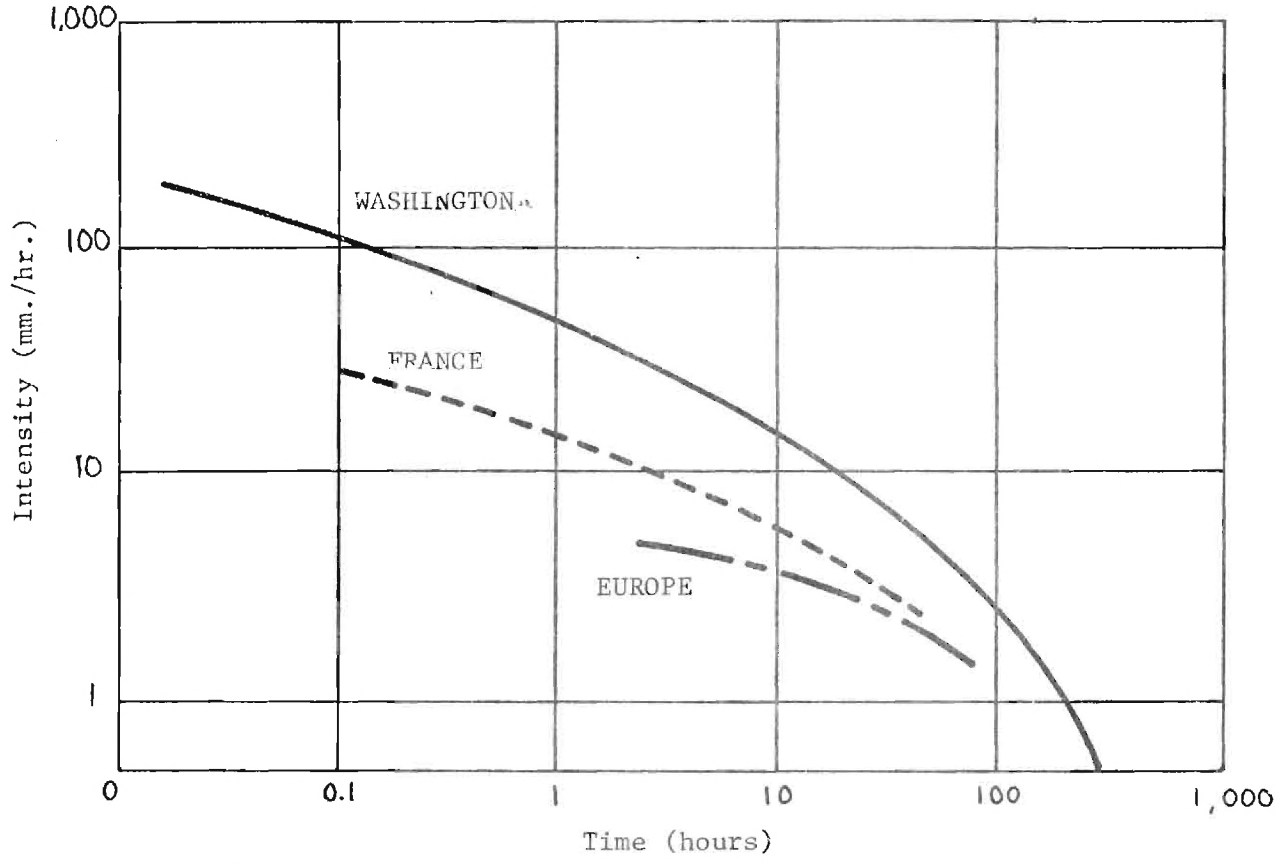

Figure 15. Number of Hours Per Annum When Rain Intensity Is Greater Than or Equal to a Given Value [27].

limited detection and recognition performance. Table 37 and Figures 16 through 21 are taken directly from a report by Paul W. Kruse entitled "A System Enabling the Army to See Through Inclement Weather." [27] This discussion will neither vouch for their accuracy or attempt to defend conclusions drawn from these curves. However, these curves do establish a comparative evaluation for a fixed set of conditions. Table 37 gives values of attenuation coefficients used in calculating the power limit curves shown in Figures 16 through 21. The power limited range is the range in clear and inclement weather at which adequate signal-to-noise ratio can be achieved in terms of transmitted power; the basic received parameters such as detector sensitivity, receiver bandwidth, etc; and atmospheric attenuation. Diffraction limit is the ability to detect and recognize a target in terms of target size and system spatial resolution. Figures 16 through 21 are calculated assuming diffraction limit with a 1 meter aperture. Detection and recognition criteria are given as 0.75 line pairs per minimum dimension for detection and 3.5 line pairs per minimum dimension for recognition.

Any suitable inclement weather viewer should be capable of detecting an M-48 tank size target in excess of 3 km and recognizing it at ranges in excess of 1 km under all conditions of weather. Using these hypothesized parameters and referring to Figure 16 through 21, it is readily apparent that for $\lambda > 337$ μm the diffraction limit recognition range for an M-48 tank is less than 1 km. Wavelengths < 337 μm have a detection power limit range less than 1 km. Thus it appears as though a combination of wavelengths would be used for the separate functions of detection and recognition. Using the conditions relating to the calculations of Figures 16 through 21 and assuming a source power of 10^9 W, any wavelength > 337 μm would give the 1 km recognition range and a wavelength around 750 μm would give approximately 3 km detection range. All wavelengths longer than 750 μm may be discounted for imaging systems because of diffraction resolution limits. If the REB source is tunable from 100 microns to X-band, and an optical heterodyne receiver is used, the multiband system problem would be solved. Under these conditions, the wavelength could be increased above 750 μm and used with an MTI processing scheme to improve performance. A brief discussion for each of the six bands considered is given below.

TABLE 37

Values Of Attenuation Coefficients Used In Calculating The Performance Of An Inclement Weather Viewing System [27]

Wavelength (μm)	γ_{CLEAR} (dB/km)	γ_{FOG} (dB/km)	γ_{RAIN} (dB/km)
10.6	0.5	48	6.5
20	7.4	45	7
337	50	4	15
750	10	2	15
850	10	2	15
1300	2	1	15

Fog - 0.1 g/m^3

Rain - 25 mm/hr

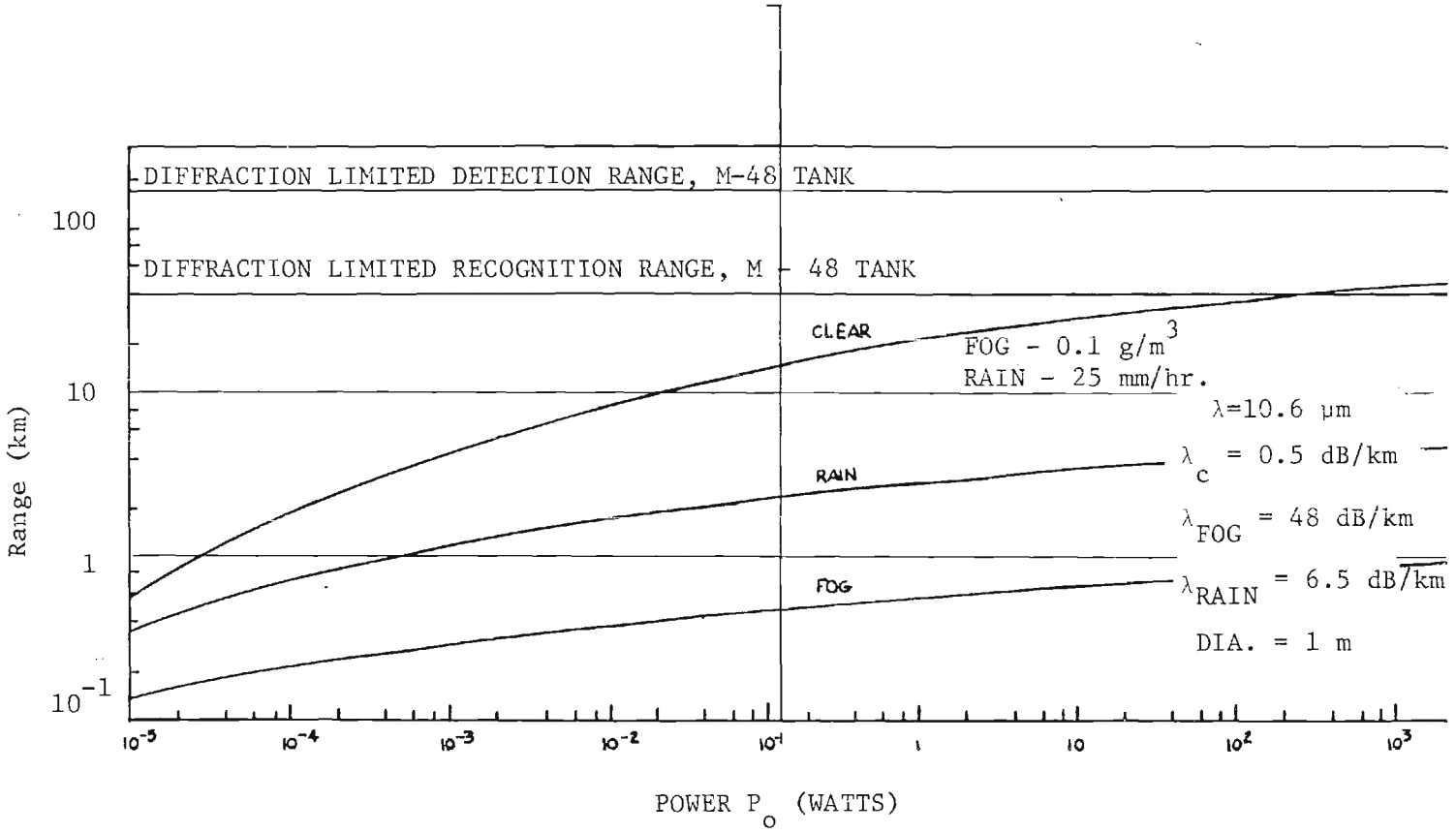

Figure 16. Range of an Inclement Weather Viewing System Operating at 10.6 μm [27].

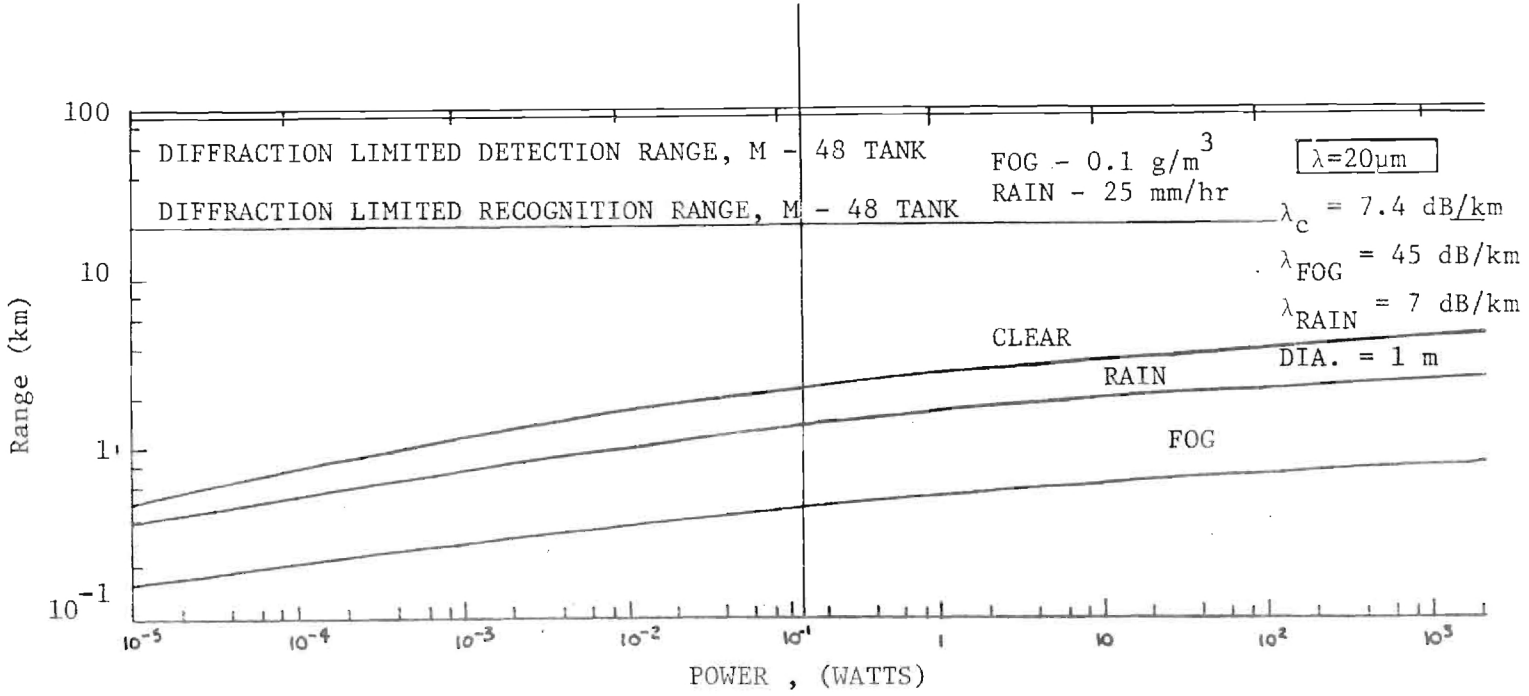

Figure 17. Range of an Inclement Weather Viewing System Operating at 20 μm [27].

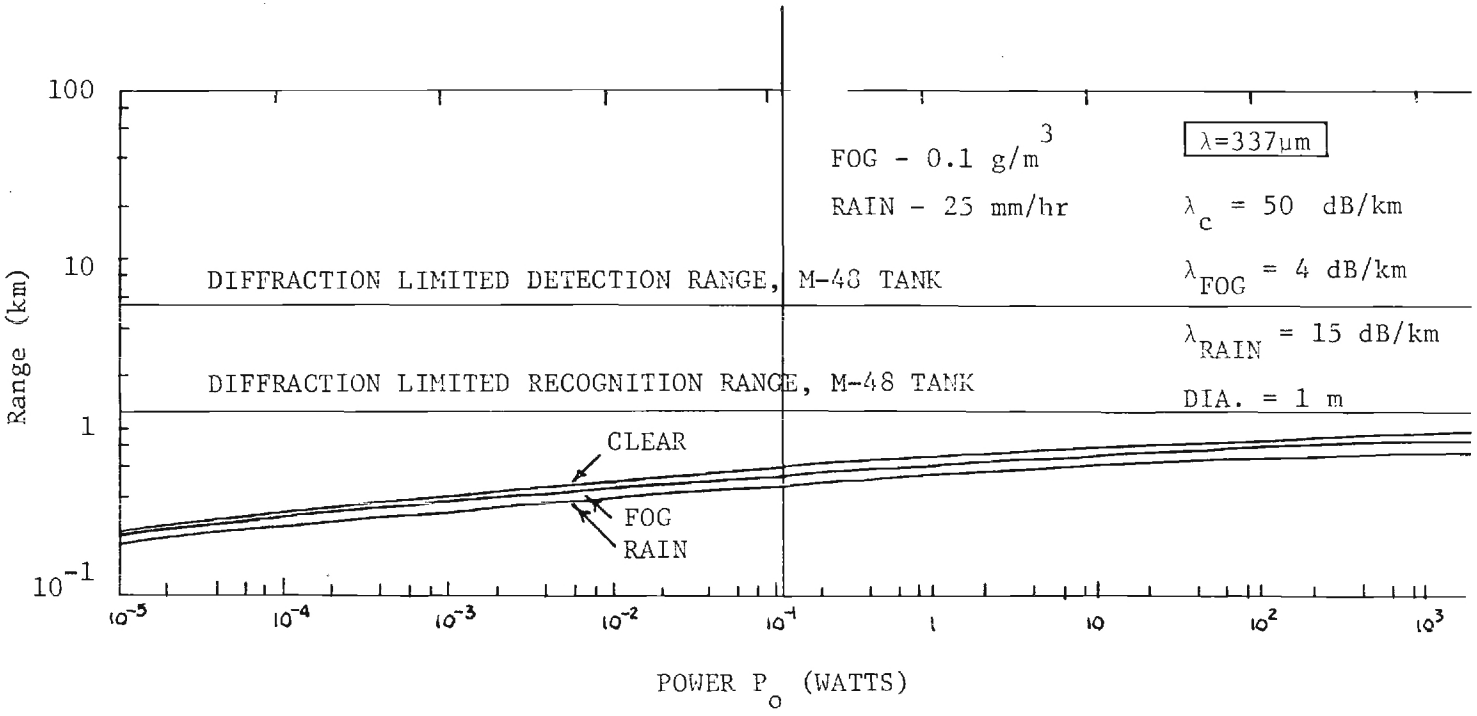

Figure 18. Range of an Inclement Weather Viewing System Operating at 337 μm [27].

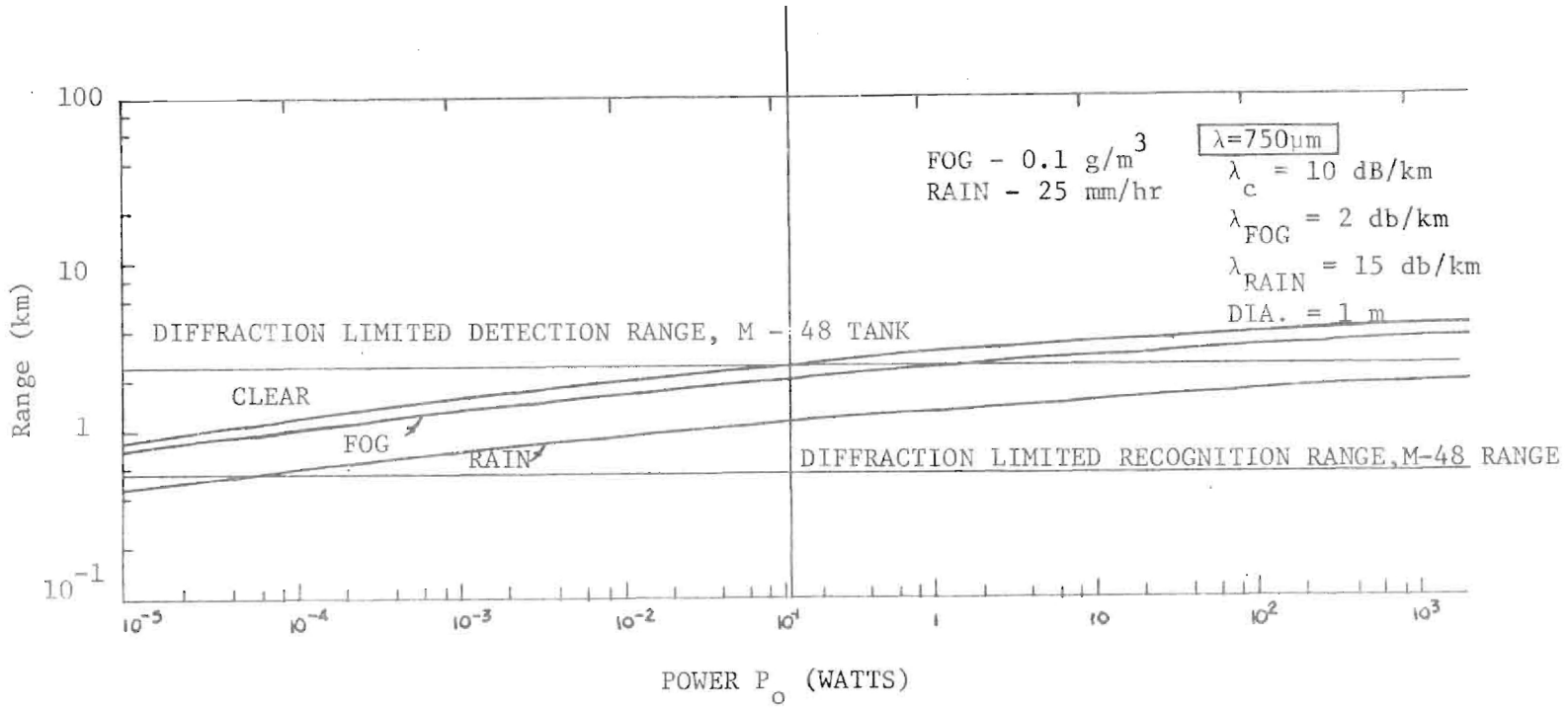

Figure 19. Range of an Inclement Weather Viewing System Operating at 750 μm [27].

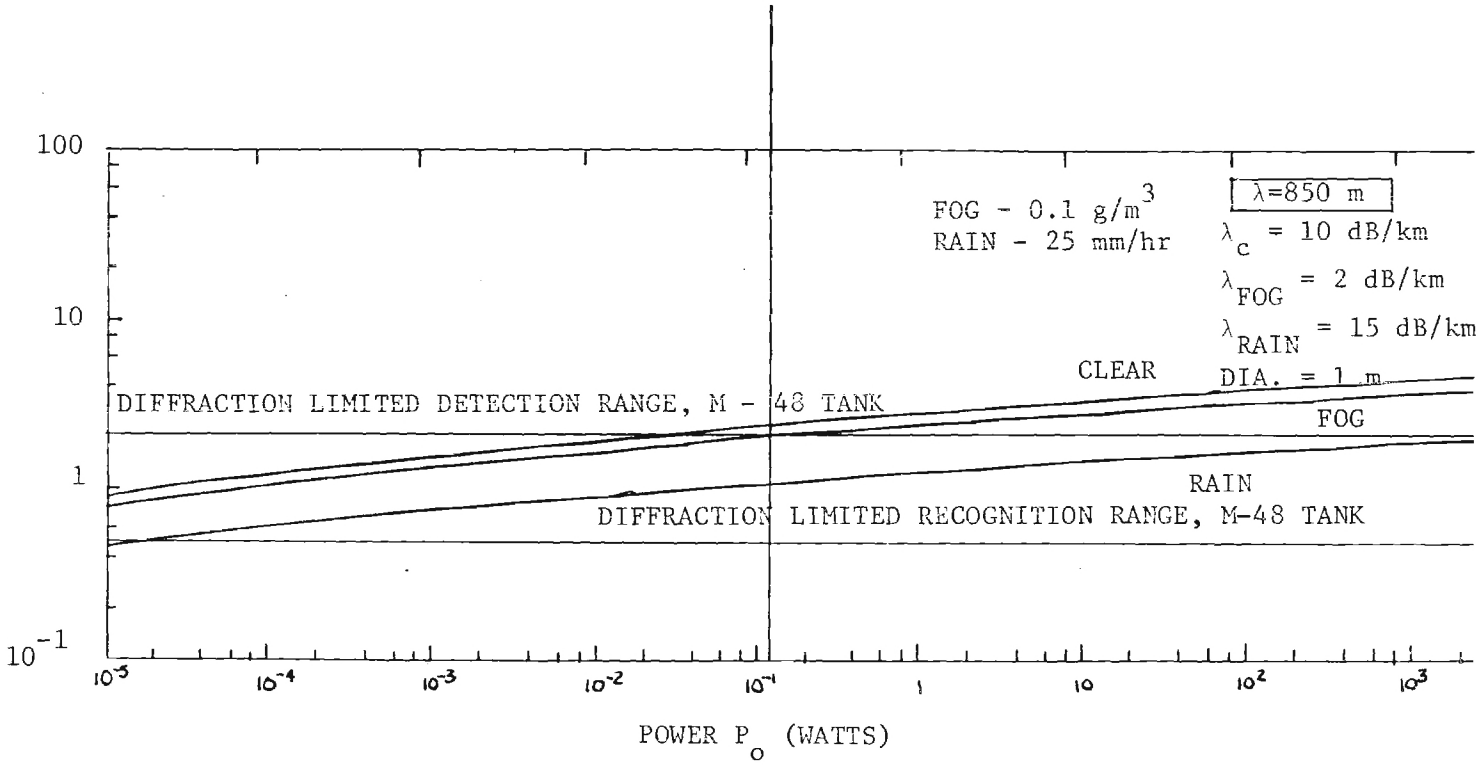

Figure 20. Range of an Inclement Weather Viewing System Operating at 850 μm [27].

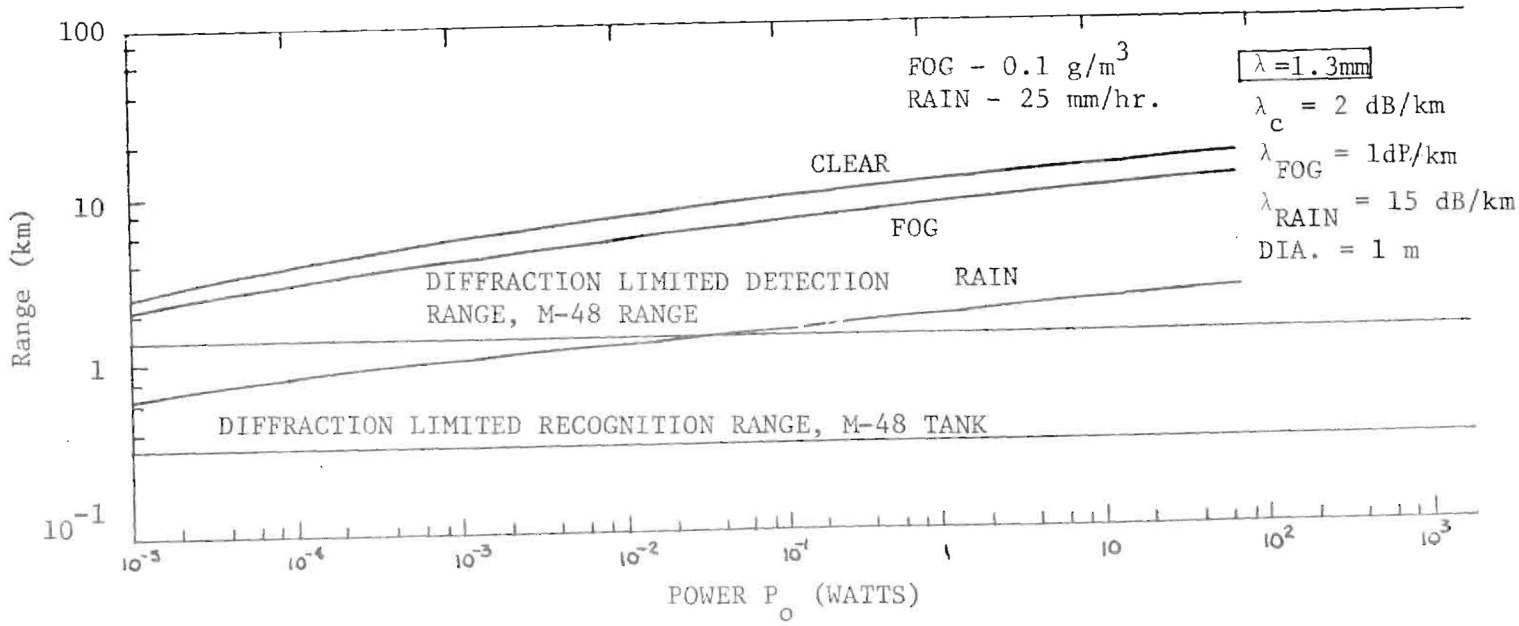

Figure 21. Range of an Inclement Weather Viewing System Operating at 1.3 mm [27].

1) 10.6 μm - The diffraction limit for practical size apertures considerably below the assumed 1 meter will meet all detection and recognition range criteria. Both clear weather and rain ranges are sufficient, but fog penetration performance is poor. The maximum fog penetration range is approximately 1 km with power in excess of 10 kW. Performance at this band is of little interest here since the REB will not operate in the 10.6 μm band.

2) 20 μm - Performance is similar to 10.6 μm except for an improvement of 3 dB/km fog penetration and approximately 2:1 decrease in diffraction limit. Again it is of little interest since the REB will not operate in the 20 μm band.

3) 337 μm - This system appears to offer the optimum diffraction limited 1 km recognition range performance and power limit fog penetration. If this wavelength is used for recognition, it becomes desirable to operate at longer wavelengths for detection performance. The 337 μm detection range is approximately equal to recognition range due to poor fog and rain penetration.

4) 750 μm - Transmission in clear weather and fog improves dramatically over that of 337 μm while the rain transmission remains constant. This is the longest acceptable wavelength since detection range for diffraction limit and power limit approaches 3 km.

5) 850 μm - Penetration through clear weather, fog and rain improves slightly over that of 750 μm. The diffraction limit range for detection and recognition decreases and becomes impractical for an imaging system.

6) 1.3 μm - Transmission through clear weather and fog is much improved over the shorter wavelengths. There is also a slight improvement in transmission through rain. However, the diffraction limit for detection and recognition are below 1 km.

It is not entirely evident from Figures 16 through 21 that the submillimeter wavelength region above 10 micrometers offers any advantage over the active 10.6 μm CO_2 system. Although the 10.6 μm system is limited to approximately 1 km recognition performance in fog, it offers other advantages such as good clear weather and rain penetration. Another advantage is the combination of two well developed technology areas of FLIR and CO_2 technology. In addition to these two well known technology areas, a limited amount of active FLIR imagery

work has already been completed [27]. However, if 10.6 μm active FLIRs are used then some alternative detection scheme must be used for ranges beyond 1 km. This is not a desirable situation since two active imaging systems would be required.

A single system operating at different wavelengths and constant power output would serve both detection and recognition functions. For a system of this type, a significant development program is required for both transmitter and receiver. This development program would certainly be profitable to generate an entire new radar family. A single system development program would yield technology useful for imaging, target discrimination, and target recognition.

The heterodyne system could be used at a number of wavelengths depending on the exact application. The system would be tuned to shorter wavelengths (350 μm) for imaging and longer wavelengths (750 μm and above) for detection. If detection is required for ranges beyond 3 km, the wavelength could be increased above 750 μm. At these wavelengths MTI and frequency agile techniques would be used for target discrimination. After target discrimination is performed, potential targets would be supplied to an electronic target recognizer for decision.

Several problems must be solved to implement such a system but only two of these problems are directly associated with the REB. These problems are transients and backscatter. For Figures 16 through 21, backscatter power was considered as a noise component which added incoherently to the receiver noise. To minimize this effect, the transmitter was assumed to be operating in a pulsed mode. In a pulsed mode, only the backscatter arising from a volume of the beam whose length is $c\tau_p/2$ (τ_p = pulse length) located at the target contributes to the noise. Pulsed operation will also allow transients to be blanked from the image display. Pulsing then creates the problems of range ambiguity and minimum range established by receiver blanking. Both these problems are solved for present radar systems.

An alternate scheme for actually imaging a potential target is electronically processing return signals to achieve recognition. This method is capable of using time gates to achieve spatial resolution at longer wavelengths which cannot be achieved by direct imaging.

One general pulsed operational problem with frequency agile target discrimination and handoff to a target recognizer is the required short pulses. For this operation pulse durations of 15 nanoseconds or less are required for a 10 kW peak power source. Present technology is extremely limited for systems operating above K_u-band. The REB would solve these problems and make target discrimination and recognition techniques compatible.

These problems are closely related to the imaging problems and do not require significant additional development. The target discrimination/recognition system is one of many areas that may benefit from a frequency agile short duration pulsed system such as the REB. A qualitative description of the discrimination/recognition problem is given below.

Radar clutter is perhaps the most pressing problem which must be overcome in order to perform target discrimination, recognition and acquisition tasks satisfactorily. This is particularly true when a target of interest is stationary such that Doppler characteristics cannot be exploited. For that case, target-to-clutter ratio becomes extremely important in conventional radar systems because spectral components of the target return and clutter return occupy the same regions in the frequency spectrum, and spectral discrimination is therefore precluded. Simply amplitude thresholding within the radar processor is not a satisfactory solution even for detecting large target returns in the presence of weaker clutter return, primarily because clutter is not homogeneous in the real world; for example, the optimum detection threshold is both angle and range dependent. Thus, a target discrimination algorithm is needed that provides designation of all potential threat targets and at the same time suppression of unwanted clutter targets. In addition, a target recognition algorithm is needed to scrutinize the return from each potential threat target and to recognize and designate the returns from those that are actual threats.

Target discrimination algorithms that provide dramatic performance in detecting stationary tactical targets while at the same time suppressing unwanted clutter have been developed and evaluated. The algorithms are designed to exploit characteristics in the radar returns that are forced

through the use of either frequency agility or polarization agility. They operate in real-time at video bandwidths and have been tested successfully with polarization agile and frequency agile radars operating in X-band and K_u-band, respectively.

A target recognizer algorithm has been implemented, tested and shown to have the ability to recognize various tactical targets including tanks and trucks. The current configuration of the target recognizer precludes processing of the return from all resolution cells due to the immense amount of data involved. Thus, from a practical viewpoint the target recognizer algorithm is best suited for processing a limited number of radar returns from cells that have been deemed to contain potential threat targets.

At this point, one can see obvious potential advantages of combining target discrimination techniques with target recognition techniques in an airborne air-to-ground targeting and missile system or battle field surveillance system. For example, the target discrimination algorithm in effect would serve as a prefilter to reduce the number of potential threat returns to be examined by the target recognizer algorithm. The spatial coordinates of targets recognized as actual threats would then be supplied to the weapons system or observer.

A Target Discrimination and Recognition Concept

Typical area search requirements and parameters for a helicopter-borne radar targeting system might include the following.

- o Azimuth scan sector: $\pm$ 45°
- o Azimuth resolution: 1° or less
- o Detection range: up to 10 km
- o Range resolution: 3 to 15 meters
- o Antenna scan rate: 180° per second

For a system with parameters as described above, there are up to 73,800 1 degree by 15 nanosecond cells interrogated by the radar during each 90 degree antenna scan. In its present configuration, the target recognizer system described previously can process the return from only one 15 nanosecond

range interval per 26 radar transmissions. The target recognizer divides the return from a given 15 nanosecond radar interval into several samples and then those data are correlated sequentially with up to 10 hyperplanes on a sample-by-sample basis.

As stated before, the target recognizer requires a time interval corresponding to 26 radar interpulse periods in order to process a single 15 nanosecond range interval. Obviously, the target recognizer in its present form could not accommodate a continuous stream of video data to which it would be subjected in a real-time nonscan situation. The process would be further complicated for a scanning antenna case because of the enormous amount of video data to be processed. Thus, it becomes apparent that the target recognizer is not suitable for processing real-time raw video data. However, a target recognizer of the type described previously could be configured to process the return from a limited number of 1 degree by 15 nanosecond radar cells provided a priori information on angle and range coordinates is provided to the target recognizer.

The target discrimination processors operate in real-time at video bandwidths. They designate potential threat target video signals and at the same time suppress unwanted vegetation clutter signals. Hence, the number of target signals at the output of the target discrimination processor is reduced drastically relative to the number of target signals at the input to the processor. Target signals at the output of the target discrimination processors correspond to potential threat targets, and since the target discriminators operate in real-time, both angle and range information for each threat target are preserved in the output. Thus, a priori information on the spatial location of stationary threat targets is available at that point. There are obvious advantages in combining target discrimination techniques with target recognition techniques for application in a helicopter-borne targeting system or battle field surveillance system. A target discriminator would process real-time video data such that potential threat targets are designated along with spatial coordinates for each. That information would be employed to range and angle gate the corresponding video signals for each threat target to the target

recognizer for detailed examination and target recognition. Thus, the target discriminator would serve as a prefilter to the target recognizer such that a practical number of potential threat targets could be designated for scrutiny by the target recognizer.

From this discussion, it is seen that a REB device can provide advantages for active imaging in inclement weather. The tunability of the source offers the possibility of a combination of wavelengths for detection and recognition. Wavelengths of $\lambda \geqq 750$ μm are appropriate for detection while $\lambda \geqq 337$ μm can be employed for recognition. The short pulse capability of the REB sources is compatible with the target discrimination/recognition techniques which have been discussed here. Table 38 shows the parameters of active imaging systems at wavelengths from 10.6 μm to 1.3 mm. Table 39 presents the advantages and disadvantages of the systems, for which a REB device would serve as the source in the case of the submillimeter systems.

TABLE 38

Active Submm Imaging

Fog 0.1 g/m^3 Rain 25 mm/hr

Wavelength	Diffraction Limit Range Performance		Power Limit Range Performance		Desired Range	
	Recognition	Detection	Recognition	Detection	Recognition	Detection
10 μm	> 3 km	> 3 km	1 km	1 km	≥ 1 km	≥ 3 km
20 μm	> 3 km	> 3 km	1 km	1 km		
337 μm	1.5 km	5 km	1 km	1 km		
750 μm	.8 km	2.5 km	Diff Limit	3 km		
850 μm	.5 km	2.0 km	Diff Limit	Diff Limit		
1.3 mm	.35 km	1.5 km	Diff Limit	Diff Limit		

TABLE 39

Active Imaging Systems

	ADVANTAGES	DISADVANTAGES
10.6 μm	- Existing Technology - Active FLIR Imagery Systems Tested	- 1 km Maximum Range for Detection and Recognition - Multiple Systems Required for Ranges > 1 km Rain Ranges OK but Fog Penetration is Poor
Sub mm	- Multi Wavelength Performance - Compatible with Target Discrimination/Recognition Techniques - Existing Signal Processing Techniques Applicable	- 1 km Maximum Range for Recognition - 3 km Maximum Detection Range - Requires Multiple Wavelength Systems for Range Recognition and Detection - Technology Required For Military Applications

6.2 Weather Radar Systems as an Application Area For Gigawatt Signal Sources

Weather radar systems seek to locate, track, and make measurements on various weather formations. Ground based weather radars are limited in range by the curvature of the earth. Therefore high power alone is of little additional value for weather radar applications because it would merely increase the detectability of very small targets. Under average atmospheric conditions, the height of the antenna beam axis when directed at 0° elevation angle will be 9.4 km at a range of 400 km. Thus unless storms extend above this height, it will be impossible to detect them beyond 400 km and even then only that portion of the storm extending above 9.4 km would be visible. Ordinary weather radars employ frequencies up to 10 GHz partly because of the strong atmospheric attenuation at higher frequencies. However with a gigawatt signal source, the attenuation can be overcome. Thus, a weather radar system can operate at frequencies in the millimeter band realizing better angular resolution, greater precipitation reflectivity, and increased Doppler sensitivity.

Employment of higher frequencies will mean narrower antenna beamwidth for the same antenna size, which results in higher angular resolution and improved low-angle performance. Because these wavelengths are approximately equal to the dimensions of rain drops, the radar reflectivity of the precipitation at these frequencies is highest. This effect helps to decrease the effect of ground clutter and other non-precipitation targets. Another benefit of this higher transmission frequency is greater Doppler sensitivity, that is, a certain relative velocity will result in increased Doppler frequency shift with increased radar frequency. However, this improvement is somewhat offset by a decrease in the maximum unambiguous velocity, an effect which results from increasing the radar frequency while the pulse repetition frequency (PRF) is held fixed. If the PRF is also increased, then this effect can be overcome but the maximum unambiguous range is decreased. Obviously this latter effect conflicts with the original intent of maintaining maximum range while increasing frequency. PRF compromises and/or more sophisticated signal processing can result in satisfactory performance; however, this is an area which demands attention in designing a high frequency gigawatt weather radar system.

The increased atmospheric attenuation at these frequencies has two major components. One component is the absorption of microwave energy by water vapor and other gases in the atmosphere. This effect depends on both frequency and the gaseous composition of the air, especially the humidity. The other component of atmospheric attenuation results from the reflectivity of precipitation. This effect depends on rain drop size and rainfall rate and also on frequency [28]. The rainfall rate is highly variable over the radar sector, therefore it is much more difficult to accurately determine than the gaseous composition of the air. For this reason relating radar signal levels to rainfall rates is not accurate. While the signal from a given range can be measured, it is not possible to determine the precipitation through which the signal propagated. Therefore, a high frequency radar system cannot be used for quantitative rain measurements and its usage is limited to Doppler frequency measurements. This measurement of relative velocities within a storm is a very important function of a weather radar and a high frequency system with its high resolution will be better able to distinguish positive and negative velocity areas within a vortex area than an ordinary radar which might only distinguish a cell in which the relative velocity averaged to zero. The permanent nature of most weather radar installations makes possible fencing and other measures to deny access to unsafe areas. This factor and the fact that the main beam of the antenna will always be directed upward indicates that the hazards of a high frequency gigawatt weather radar can be overcome.

In the discussion which follows, the maximum range for detection of rain is computed under the assumption of uniform rainfall rate throughout the propagation path. This assumption is not realistic; however, it will be useful for relative comparisons of performance. Currie, Dyer, and Hayes reported rainfall backscatter data at 9.375 GHz, 35 GHz, 70 GHz, and 95 GHz [29]. Smith, Hardy, and Glover have reported approximate attenuation factors for propagation in rain [28]. With these data, it is possible to determine the maximum range of the gigawatt weather radar at these four frequencies and at rainfall rates of 1 mm/hr and 10 mm/hr. Also, in order to reflect the affect of frequency on antenna beamwidth, the computations will be done for fixed antenna gain of 40 dB

and for a fixed antenna aperture of 1 m^2.

Smith, Hardy, and Glover give the following weather radar equation [28]

$$\overline{P}_r = (4.28 \times 10^4 \frac{m}{s}) P_t \tau \lambda^2 G^2 \frac{\Theta\phi\eta k}{R^2}$$

where $\overline{P}_r$ = average received power, watts

P_t = peak transmitted power, watts

λ = radar wavelength, meters

τ = pulse duration, seconds

G = antenna gain

Θ = 3-dB beamwidth of the antenna in the horizontal direction, radians.

ϕ = 3-dB beamwidth of the antenna in the vertical direction, radians.

η = radar reflectivity (backscattering cross section per unit volume, m^{-1})

R = range to target, meters

k = attenuation factor.

We know that

$$P_r = \frac{1}{\tau \ (PRF)} \ \overline{P}_r$$

where P_r = peak received power, watts.

PRF = radar pulse repetition frequency, Hz.

Our hypothetical weather radar has a pencil beam antenna so that $\Theta = \phi$. Substituting in these conversions and rearranging the expression, we have:

$$P_r = \frac{1}{\tau \ (PRF)} (4.28 \times 10^4 \frac{m}{s}) P_t \tau \left(\frac{c}{f}\right)^2 G^2 \Theta^2 \eta k R^{-2}$$

$$R^2 k^{-1} = \frac{(4.28 \times 10^4 \frac{m}{s}) P_t G^2 \Theta^2 c^2 \eta}{(PRF) P_r f^2}$$

Antenna gain G and 3-dB antenna beamwidth δ in degrees are assumed to be related by

$$G = \frac{3.0 \times 10^4}{\delta^2}$$

We know $\delta = (57.3)\ \Theta$, and

substituting gives $G = \frac{9.14}{\Theta^2}$.

Substituting this expression into the weather radar equation for one of the G's gives

$$R^2\ k^{-1} = \frac{(3.91 \times 10^5\ \frac{m}{s})\ P_t\ G\ c^2\ \eta}{(PRF)\ P_r\ f^2}$$

We will use this expression to compute the maximum range for the fixed antenna gain expression.

In order to compute the maximum range for the fixed antenna aperture expression, we substitute for the other G giving

$$R^2\ k^{-1} = \frac{(3.57 \times 10^6\ \frac{m}{s})\ P_t\ d^2\ \eta}{(PRF)\ P_r}$$

We will use this expression to compute the maximum range for the fixed antenna aperture expression. Note that the radar frequency does not enter into this expression directly.

Our hypothetical weather radar system has the following parameters

$P_t = 1.0 \times 10^9$ W

$P_r = 10^{-11}$ W = -80 dBm

PRF = 5×10^3 Hz

$k = 10^{2R\ (\alpha \times 10^{-4})}$, where α is the attenuation in dB/km.

Substituting these parameters into the first radar equation with $G = 10^4$

$$R^2\ 10^{2R(\alpha \times 10^{-4})} = (7.04 \times 10^{42}\ \frac{m^3}{s^2})\ \frac{\eta}{f^2} \qquad (1)$$

And substituting these parameters into the second radar equation with $d = 1\ m^2$ gives,

$$R^2\ 10^{2R(\alpha \times 10^{-4})} = (7.14 \times 10^{22}\ m^3)\ \eta \qquad (2)$$

Table 40 gives values for the attenuation factors as given in reference 28. These factors are approximated, but they do reflect the attenuation dependence on frequency and radar frequency.

Table 41 gives radar reflectivity values as given in reference 28. We will use the vertical polarization values in this effort.

The maximum ranges are tabulated in Table 42 along with antenna beamwidths for each case. These values apply for a peak transmitted power of 1 gigawatt, sensitivity of -80 dBm and a pulse repetition frequency of 5×10^3 GHz.

The values in this table demonstrate that even though the radar relectivity of precipitation is greater at higher frequencies and for higher rainfall rates, the increased atmospheric attenuation under these conditions dominates the radar performance. However it is still possible to take advantage of the increased angular resolution if one is willing to give up maximum range. This is evident from the values given for the 1 m antenna diameter, which show the range possible with this reasonably sized antenna and the antenna beamwidth.

The gigawatt weather radar is also a very important instrument in the investigation of fog formation, presently under study at NELC. Richter and Squire [30] have proposed a high frequency ($f \geqq 35$ GHz) radar system for investigations of Pacific fog formation. The system should contribute not only to cloud and fog research but to military scenarios requiring knowledge of formation of adverse weather conditions.

TABLE 40

ATTENUATION COEFFICIENT, α

RAINFALL RATE	Radar Frequency (GHz) 9.375	35	70	95	UNIT
1 mm/hr	0.02	0.2	0.4	0.5	dB/km
10 mm/hr	0.2	2.0	4.0	5.0	dB/km

TABLE 41

RADAR REFLECTIVITY, η

RAINFALL RATE	Radar Frequency (GHz) 9.375	35	70	95	UNITS
1 mm/hr.	3.0×10^{-8}	1.0×10^{-6}	4.0×10^{-5}	2.5×10^{-5}	m^{-1}
10 mm/hr.	7.0×10^{-7}	6.0×10^{-6}	4.0×10^{-4}	2.0×10^{-4}	m^{-1}

TABLE 42

MAXIMUM WEATHER RADAR RANGE

a.) Maximum Weather Radar Range For System With 40 dB Antenna Gain

Rainfall Rate	Radar Frequency (GHz) 9.375	35	70	95	
1 mm/hr	472	74	46.5	35	nmi
10 mm/hr	86	12	6.5	5	nmi
Antenna Beamwidth	1.7	1.7	1.7	1.7	degrees

b.) Maximum Weather Radar Range For System With 1 m Antenna Diameter

Rainfall Rate	Radar Frequency (GHz) 9.375	35	70	95	
1 mm/hr	467	87	57	44	nmi
10 mm/hr	85	13	7.5	6	nmi
Antenna Beamwidth	1.8	0.5	0.25	0.2	degrees

6.3 Countering Low Angle Missile Threats as an Application for a Gigawatt Signal Source

In Chapter 2, consideration was given to the use of a GW source for low-angle tracking and electronic countermeasures. With the continued improvement of millimeter wave technology, the possibility of a missile threat having a millimeter radar exists. Assume that the missile radar has an effective aperture A_e of 10^{-3} m^2. In addition, assume that the peak received power of one watt is sufficient to render the missile radar ineffective. Consider the conditions which result in sufficient power from a ship's gigawatt radar to produce one watt at the missile. The power received at the missile, P_r, is given by

$$P_r = P_d A_e$$

where P_d is the power density and is required to be

$$P_d = P_r/A_e = \frac{1 \text{ watt}}{10^{-3} m^2} = 10^3 W/m^2$$

Thus, a peak power density of $10^3 W/m^2$ is sufficient to negate the radar's effectiveness. The peak power density radiated by the GW radar with 58 dB antenna gain is

$$P_d = \frac{G_t P_t (\text{atten})}{4\pi R^2}$$

$$= \frac{10^{5.8} 10^9 W(\text{atten})}{4\pi R^2}$$

where (atten) is the atmospheric attenuation.

At a range of 15 km, the power density is

$$P_d = 2.23 \times 10^5 (\text{atten})$$

If we substitute for the power density required to engage the missile, it is possible to find the maximum tolerable attenuation at the operating wavelength. The result is that the attenuation which can be tolerated and still allow sufficient power to negate the missile radar at 15 km is 1.57 dB/km. The performance of a GW jammer at 9.375 GHz, 35 GHz, 70 GHz and 95 GHz has been calculated under this condition. The rainfall rates given below correspond to the maximum rainfall which can be tolerated and still result in 1 watt received power for a missile radar with an antenna effective aperture of 10^{-3} m^2 at a range of 15 km. It is assumed that the jammer antenna has 58 dB gain and that the rainfall rate is uniform over the propagation path.

Frequency (GHz)	= 9.375	35	70	95
Approximate $\frac{dB/km}{mm/hr}$ Atten. Coeff	= 0.02	0.2	0.4	0.5
Max. Tolerated Rainfall Rate (mm/hr)	= 78.5	7.85	3.9	3.1

If we would be satisfied to negate the missile radar at 10 km rather than the 15 km as above, then the maximum attenuation which can be tolerated for this situation is 2.7 dB/km. The maximum rainfall rates which can be tolerated at 10 km are given by the following:

Frequency (GHz)	= 9.375	35	70	95
Approximate $\frac{dB/km}{mm/hr}$ Atten. Coeff	= 0.02	0.2	0.4	0.5
Max. Tolerated Rainfall Rate (mm/hr)	= 135	13.5	6.75	5.4

It is seen that over 70% higher rainfall rates can be tolerated if it is satisfactory to jam at 10 km rather than 15 km.

As a result of these calculations, it has been shown that a gigawatt source can provide jamming protection against low flying missiles at various frequencies at rainfall rates given above.

6.4 Miscellaneous Gigawatt Source Applications

The limitations imposed by a short study of the nature performed during this program did not permit the treatment of all possible applications. However, several subjects can be listed as warranting further consideration:

1) Fire control and ordnance delivery. Because of the high infrared attenuation in fog, accurate weapon delivery is not possible. A submillimeter GW source can provide the accurate guidance required in fog. This is particularly important in the European theatre during winter where delivery through overcast is of benefit for a large fraction of the time. As an example, during December and January in Berlin, the ceiling is less than 3000 feet and/or the visibility is less than 3 miles thus precluding electo-optical target acquisition about 2/3 of the time.

The use of the gigawatt source as a target illuminator in a semiactive designator system should be analyzed. The high power source can serve in the dual role of a short wavelength radar for acquisition and tracking followed by use as a target designator. Missile guidance systems can profit from the availability of a short wavelength gigawatt source. This might occur in command links from ship in off-shore activities in which battle debris and fog can negate electro-optic systems. The guidance and launching of defensive missiles for land-based systems might also employ the GW source. Beam-riding techniques at short wavelengths through cloud and inclement weather require a high power source.

Various tracking applications have not been analyzed in this report, but should be investigated. These include:

2) Initial tracking for hand-over to a passive system;

3) Auxiliary millimeter or submillimeter tracking for laser weapons. HELW systems require much greater tracking precision than low frequency microwave systems can provide;

4) Ground-based tracker for exoatmospheric vehicles;

5) Covert tracking at high altitudes for use with mm wavelength seekers;

6) Dual frequency tracking with outputs at both frequencies originating from same source

Other applications requiring investigation include:

7) High resolution mapping for airborne cases through cloud coverage;

8) Use as a decoy for microwave seekers by sea surface reflection for microwave seekers;

9) Station keeping functions such as long range accountability of aircraft in military scenarios, fleet accountability in fog and covert situations and airport surveillance in fog and rain of all aircraft on the ground and in the air;

10) Beacons for air traffic and navigation. Short wavelength radars for docking, harbor navigation in fog and automatic carrier landing systems for heavy fog can employ a REB source.

Many of the applications, particularly at short wavelengths, do not require a source operating at a gigawatt output, but the electron beam devices provide the only means of generating sufficient power to perform the mission. This could be the case for a docking radar system or for the carrier landing system.

Doppler techniques for high frequency applications, e.g. damage assessment systems, and the use of pulse compression techniques can possibly be exploited for use with the REBs. The pulse compression techniques might be particularly applicable when the REB is used as an amplifier with a master oscillator which can be chirped.

A few remarks, involving Figure 22 can be made concerning the application to covert radar systems. The broad tunability of the REB sources can provide a system which is adaptable to changes in the operational covertness (range) requirements. Figure 22 shows the radar range of a 1 GW source as a function of frequency and atmospheric attenuation in clear weather conditions where the range is calculated from the radar relation:

$$R^4 = \frac{PG^2\lambda^2\sigma \exp(-2\alpha R)}{(4\Pi)^3 k\, TBF(SNR)L}$$

where

$G = 60$ dB, antenna gain

$P = 10^9$ W

$\sigma = 1\ m^2$, target cross-section

$T = 300°K$

$B = 10^6$ Hz, receiver bandwidth

F = 10 dB, noise figure

SNR = 10 dB

L = 10 dB, system losses

It is seen from Figure 22 that a clear weather radar range R > 1 km can be selected by operation at any chosen frequency up to 400 GHz.

In this chapter, several topics not treated in the previous chapter have been briefly discussed. The list of applications of high power beam sources extends to a greater length than given here. Only a few subjects have been mentioned which should have further attention.

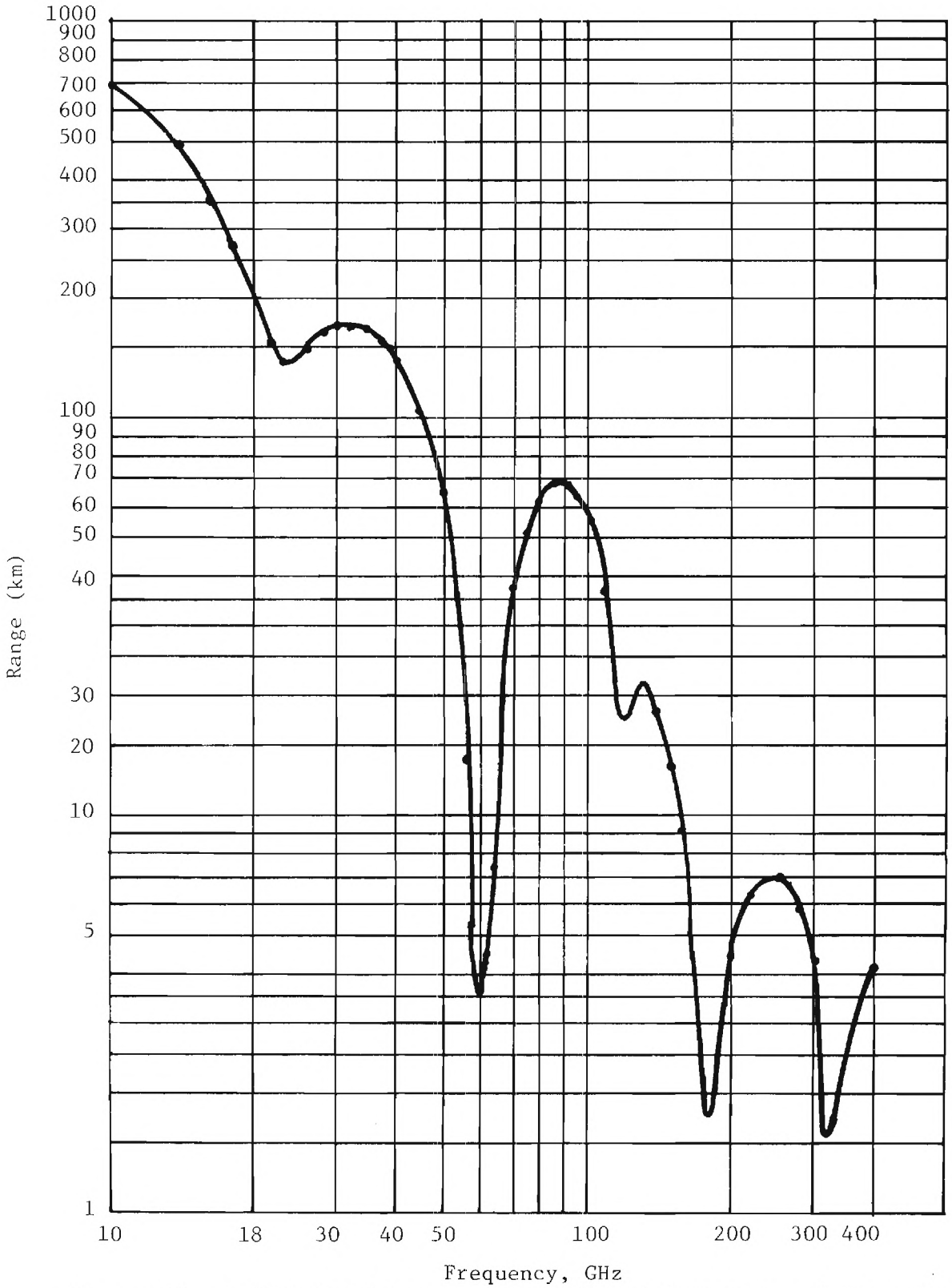

Figure 22. 1 GW Radar Range as a Function of Frequency and Atmospheric Attenuation

CHAPTER 7

CONCLUSIONS AND RECOMMENDATIONS

During this program, a large number of applications of gigawatt sources has been investigated. The utility of the apparatus has been demonstrated for radar, electronic countermeasures, communications applications, plasma diagnostics, plasma penetration, nonlinear optical applications, and several applications which have been listed in Chapter 6. The investigations which have been studied have been concerned with pulsed gigawatt sources. In summary, it has been shown that the following potential applications exist for such sources when they are developed to have the characteristics which have been assumed:

1. Low angle tracking radar at millimeter wavelengths can profit from the availability of the GW sources. Comparisons made in Chapter 2 for the GW radar with X-band systems demonstrate the advantages of the millimeter wave system. Table 4 summarizes the low angle tracking radar systems.

2. The gigawatt source has been studied as a limited vulnerability radar by covert operation in the millimeter region. Table 8 summarizes the advantages of this system.

3. The GW source offers considerable advantages for electronic countermeasures. Tables 9, 10, and 11 of Chapter 2 list the effects of using such a source for ECM applications.

4. Chapter 3 showed several communications applications of the GW source. Many of these uses involved the covert application in the millimeter and submillimeter wavelength regions where the advantage of strong atmospheric absorption exists for limiting the transmission distance. The fast exponential roll-off with range affords protection against detection by enemy monitoring systems. The GW sources prove particularly advantageous in adverse weather conditions where systems operating with lower power conventional sources cannot provide adequate transmission.

5. In addition to the covert communication applications, the GW signal source can produce greater range for tropospheric communication systems, allow greater standoff and versatility for RPV systems, and can be used for deep space applications.

6. The difficulty in penetrating dense plasma can be overcome with the use of high frequency sources with sufficiently high power outputs. The role of the linear beam sources in this important application has been considered in Chapter 4. Both plasma diagnostics and the tracking or communicating with reentry vehicles have been shown to be potential uses of the devices.

7. The potential of tunable sources in the infrared and visible wavelength regions has been briefly discussed in Chapter 5, where the nonlinear optical mixing of a REB with optical lasers has been treated.

8. Chapter 6 has listed several possible uses of the source, which are important and promising future applications. The importance of developing submillimeter imaging or target designator systems as an alternate approach to infrared systems for adverse weather requirements may prove to be one of the most important uses of the REB devices.

Throughout the discussions given in this report, it has been emphasized that the tunability and capability for operation during adverse weather make the beam sources potentially superior to any conventional sources for millimeter and submillimeter applications. Appendix V discusses submillimeter sources which are achieved by optical pumping or mixing schemes. These sources do not appear to be capable of providing power or tunability competitive with the REB sources, and by the theoretical limitations imposed by the Manley-Rowe relations cannot operate with efficiencies possible with the beam sources.

The gigawatt sources have been assumed throughout the study to be short-pulse devices. Recent developments in Russia of a gyrotron [31], which is actually a relativistic electron beam device, have demonstrated the capability of the apparatus as a cw source of high efficiency operating at 3 mm and shorter wavelengths. This source, employing superconducting magnets, must be studied in detail as a potentially small device for field applications such as submillimeter imaging, low angle tracker at mm wavelengths, and adverse weather submillimeter weapon support devices. The communications applications which have been discussed have been for pulsed sources which can create difficulties for modulation. The CW system could simplify the communication apparatus and be used with more flexible

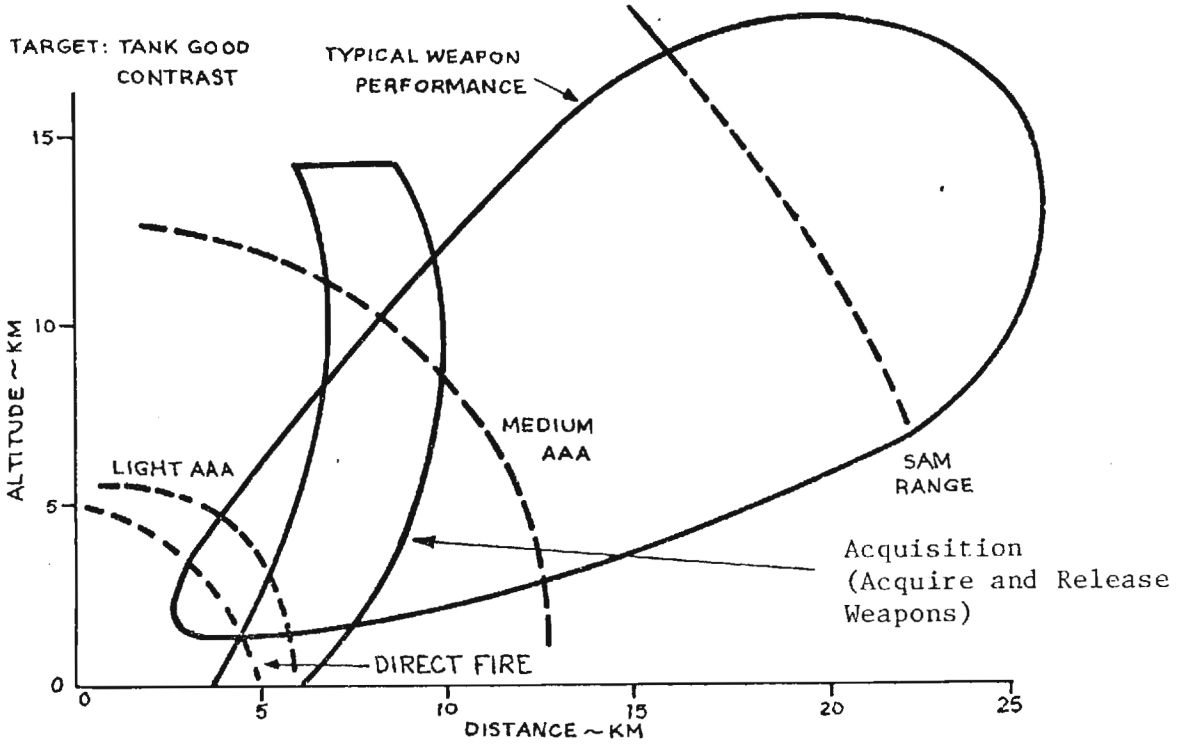

Figure 23. Weapon Capability Versus Sensor Capability

modulation formats. In turn, the possibility of a high frequency CW source, mixed with a chirping source at a lower frequency, offers the advantages of a radar pulse compression system as shown for CO_2 lasers [22].

The advantages of the high power sources exceed those which it has been possible to discuss in this report. With the long range capability of weapons systems as they exist today, it is extremely important that radar or communication systems be capable of long range transmission or stand-off operation. Figure 23 shows the range for various weapons systems which are in the field. It is important that military sensor systems be capable of operating at least outside the direct fire weapons range. Many of the sources which are in existence or which are predicted for future systems are not capable of sufficient range. This is particularly the case for the millimeter and submillimeter wavelength region. The REB devices appear to be the only means in several cases for achieving the required range.

The study which has been performed during this program has only scratched the surface of the potential uses of the sources of interest, and it is recommended that further, more detailed studies be performed on those uses which are viewed as critical needs. Table 43 summarizes the applications which have been given the most attention in this investigation.

TABLE 43

SUMMARY

GIGAWATT SOURCES

1. RADAR -
   - OPERATION AT HIGHER FREQUENCIES
   - GREATER RANGE AT MM WAVES
   - HIGHER RESOLUTION
   - MAKES MORE APPLICATIONS FEASIBLE

2. ECM -
   - PROVIDES SAURATION JAMMING IN-BAND
   - PROVIDES BURN-OUT CAPABILITY

3. COMMUNICATIONS -
   - ALLOWS GREATER RANGE
   - MM OPERATION PROVIDES COVERTNESS AND WIDE FREQUENCY COVERAGE
   - HIGH DATA RATES
   - APPLICABLE TO VARIETY OF SCHEMES

4. PLASMA PENETRATION -
   - OPERATION ABOVE PLASMA FREQUENCY
   - REENTRY COMMUNICATIONS AND RADAR
   - COMMUNICATION THROUGH PLUMES

5. TUNABLE OPTICAL APPLICATIONS

REFERENCES

1. Y. Carmel and J. Nation, "High Power M/W Generation," The Microwave Journal, June, 1975, p. 50.

2. V. Granatstein (private communication).

3. D. K. Barton, "Low Angle Radar Tracking," Proc. IEEE, Vol. 62, June 1974,

4. C. Cuccia and J. J. Spilker, Jr., "Wideband Spectrum Utilization Above 10 GHz for Communications and Monitoring the Ecology," The Microwave Journal, November 1971, pp. 24-30.

5. P. F. Panter, "Communication Systems Design," Chapter 13, McGraw-Hill Book Company, New York, New York, 1972.

6. P. L. Rice, A. C. Langley, K. A. Norton, and A. P. Barsis, "Transmission Loss Predictions for Tropospheric Communication Circuits," NBS Technical Note 101, May 7, 1965, revised January 1, 1967.

7. "Instruction Manual for Tropospheric Scatter-Principles and Applications," USAEPG-SIG 960-67, U.S. Army Electronic Proving Ground, Fort Huachuca, Arizona, March 1960.

8. B. Lax and D. R. Cohn, "Interaction of Intense Submillimeter Radiation with Plasma," IEEE Transactions, Microwave Theory and Techniques, MTT-22, 1049, December 1974.

9. F. Brown, S. R. Harman, A. Palevsky, and K. J. Button, "Characteristics of a 30 kW-peak, 496 μm Methyl Fluoride Laser," Optical Communications 9, 28, 1973.

10. B. Lax and D. R. Cohn, "Cyclotron Resonance Breakdown with Submillimeter Lasers," Applied Physics Lett. 23, 363, October 1973.

11. D. L. Jassby, "Parametric Heating of a Dense Arc Plasma with 0.337 mm Laser Radiation," Journal of Applied Physics 44, 919, February 1973.

12. D. L. Jassby, D. R. Cohn, B. Lax, and W. Halverson, "Tokamak Diagnostics with the 496-Micron CH_3F Laser," Princeton Plasma Physics Laboratory, Princeton, New Jersey, Report MATT 1020.

13. O. Gehre, "A Heterodyne-Detection System for Measurements in Collective HCN-Laser Scattering from Thermonuclear Plasmas," IEEE Trans. Microwave Theory and Techniques, MTT-22, 1061, December 1974.

14. D. E. Evans and M. L. Yeoman, "Spatially Resolved Measurement of Impurities and the Effective Charge $\bar{Z}$ in a Tokamak Plasma," Physical Review 33, 76, July 1974.

15. R. J. Chaffin and J. B. Beyer, "Plasma Diagnostics with a Microwave Fabry-Perot Resonator," IEEE Transactions Microwave Theory and Techniques, MTT-16, 37, 1968.

16. P. Brossier and R. A. Balnken, "Interferometry at 337 μm on a Tokamak Plasma," IEEE Trans. Microwave Theory and Techniques, MTT-22, 1053, December 1973.

17. I. P. French and M. P. Bachynski, "The Radio Spectrum from 10 GHz to 300 GHz in Aerospace Communications," Vol. V-Plasma Effects in Aerospace Communications, RCA (Montreal, Canada) Technical Report ASD-TR-61-589, March, 1962.

18. H. M. Musal, Jr., "Plasma Frequency and Electron Collisian Frequency Charts for Hypersonic Vehicle Equilibrium Flow Fields in Air," GM Defense Research Laboratories TR 62-209C, Santa Barbara, California, December 1962.

19. P. J. Keenan, "A Review of Electromagnetic Propagation in Plasmas," The Microwave Journal, pp. 56-60, September 1964.

20. A Boornard, "Interaction of Electromagnetic Waves with Ionized Rocket Exhausts," RCA Collection of Technical Papers on Plasma Physics Research and Engineering, 1966.

21. V. J. Corcoran, J. J. Gallagher, and R. E. Cupp, "Nonlinear Optical Effects Using a CO_2 Laser and a Klystron," Applied Physics Lett. 16, #8, 316, 15 April 1970.

22. W. E. Bicknell, L. R. Tomasetta, and R. H. Kingston, "10.6 μm FM-Chirp Radar Using Narrow-Band Correlation Detection," IEEE Journal Quant. Elect. QE-11, 308, 1975.

23. J. F. Young, G. C. Bjorklund, A. H. Kung, R. B. Miles, and S. E. Harris, "Third Harmonic Generation in Phase-Matched Rb Vapor," Physical Review Lett. 27, 1551, 1971; J. F. Ward and G. H. C. New, "Optical Third Harmonic Generation in Gases by a Focused Laser Beam," Physical Review 185, 57, 1969; R. B. Miles and S. E. Harris, "Optical Third Harmonic Generation in Alkali Metal Vapors," IEEE Journal Quant. Elect. QE-9, 470, 1973.

24. D. M. Bloom, J. T. Yardley, J. F. Young, and S. E. Harris, "Infrared Up-Conversion with Resonantly Two-photon Pumped Metal Vapors," Applied Physics Lett. 24, 427, 1974.

25. S. E. Harris and D. M. Bloom, "Resonantly Two-photon Pumped Frequency Converter," Applied Physics Lett. 24, 229, 1974.

26. C. Y. She and K. W. Billman,"Infrared-pumped Third Harmonic and Sum-frequency Generation in Diatomic Molecules," Applied Physics Lett. 27, 76, 1975.

27. P. W. Kruse, unpublished report, Army Scientific Advisory Panel.

28. P. L. Smith, Jr., K. R. Hardy, and K. M. Glover, "Applications of Radar to Meteorological Operations and Research,"Proceedings of IEEE, Vol. 62, pp. 724-745, June 1974.

29. N. C. Currie, F. B. Dyer and R. D. Hayes, "Some Properties of Radar Returns from Rain at 9.375, 35, 70, and 90 GHz," IEEE International Radar Conference, pp. 215-220.

30. P. Squire and J. Richter (private communication).

APPENDIX I

CONVENTIONAL MILLIMETER AND SUBMILLIMETER WAVE SOURCES

The sources which are available to be used in place of the GW source in the potential applications of this report do not approach the GW sources in power or tunability. Few sources with suitable power exist above 90 GHz and, in many cases, the efficiency of the sources does not exceed that of the gigawatt linear beam devices. Table I-1 presents a list of conventional sources taken from the open literature. This list includes several tubes which have been constructed or which are currently under development. The list does not include all sources which exist in the millimeter-submillimeter wavelength region. Low power klystrons are available from Varian (Canada) for frequencies up to 220 GHz. CSF (France) has produced a line of carcinotrons (BWO's) which oscillate as high as 630 GHz with power outputs on the order of fractions of watts. Russian carcinotrons cover a frequency range from 37.5 GHz to 375 GHz with no break in the spectrum. Six tubes cover this range with output power in the 2-200 mW range. Recent reports in the Russian literature indicate that a gyratron tube with superconducting magnet gives 10 kW at 2.78 mm and 1 kW at 0.92 mm. This is a significant advance over sources currently available at these wavelengths.

From the information presented in Table I-1, it is evident that no sources currently exist which are competitive with the linear beam devices in power output, tunability, narrow pulse widths and simplicity of their physical structure.

TABLE I-1

CONVENTIONAL MM AND SUBMM SOURCES

SOURCE	TYPE	f(GHz)	Power Output (W)	Efficiency (%)	REMARKS
1. WJ-282	Klystron	35.5	10^3	14	Watkins-Johnson CW, Fixed Frequency; Oscillator
2. WJ-266	Klystron	35	10^3	10	Watkins-Johnson CW, Amplifier (10-13 dB)
3. 196H	Klystron	92-95.5	$3x10^3$	--	Hughes 0.0003 duty cycle; oscillator
4. 197H	Klystron	93-95	10^4	--	Hughes; Oscillator; 0.0003 duty cycle
5. QKH-1663	Magnetron	32-35	$65x10^3$ Peak	24	Raytheon; 0.1-1 μs pulse width duty cycle=0.001
6. BLM-076A	Magnetron	34-36	10^3	9	Varian; 0.25 μs pulse width; duty cycle = 0.0005
7. SFD-319	Magnetron	34.5-35.2	10^5	17	Varian; 0.05 μs pulse width; duty cycle = 0.0005
8. BL-246	Magnetron	68.0-71.5	$8x10^3$	6.3	Varian; pulse width = 0.25 μs duty cycle = 0.00055
9. BL-246A	Magnetron	68.0-71.5	10^4	7.9	Varian pulse width = 0.25 μs duty cycle = 0.00055
10. BL-221	Magnetron	69-70.5	10^4	7.9	Varian pulse width = 0.3 μs duty cycle = 0.001
11. BL-234C	Magnetron	69.5-71.5	$0.4x10^3$	6.1	Varian pulse width = 0.25 μs duty cycle = 0.001
12. DX-423	Magnetron	95.53	$8x10^3$	4.5	Amperex pulse width = 0.05 μs duty cycle = 0.002
13. VMS-1043	Magnetron	34-35	$45x10^3$	20	Varian frequency-agile; pulse width = 1.0 μs duty cycle = 0.001

TABLE I-1 (Continued)

	SOURCE	TYPE	f(GHz)	Power Output (W)	Efficiency (%)	REMARKS
14.	841 H	TWT Amplifier	31.4-31.8	10^3	--	Hughes Max duty cycle = cW Gain = 50 dB
15.	VKQ-2416A	Extended Interaction Oscillator	35	10^3	10	Varian duty cycle = 0.001 pulse duration = 0.5 μs
16.	VKE-2412A	Extended Interaction Oscillator	50-75	10^4	10	Varian duty cycle = 0.001 pulse duration = 1 μs max
17.		Extended Interaction Oscillator	94.0	$8x10^3$	7.9	Varian proposed tube duty cycle = 0.001 pulse duration = 1.0 μs
18.	VKT-2411A1	Extended Interaction Oscillator	140	1	0.21	Varian proposed tube
19.	819H	TWT Amplifier	54.5-55.5	$7x10^3$	--	Hughes Max duty - CW Gain = 20 dB
20.	826HG	TWT Amplifier	93-95	10^3	--	Hughes max duty = 0.001 gain = 30 dB
21.	VRY 2432E1	Extended Interaction Oscillator	280 $\pm$ 15	1	--	Varian proposed tube; CW
22.	VRY 2430E1	Extended Interaction Oscillator	280 $\pm$ 15	10	--	Varian proposed tube; duty cycle = 0.1 max pulse length = 1 ms
23.	CO10.1	BWO	275-310	1	--	CSF;CW mode
24.	Ubitron	Undulating Beam Interaction	55	$150x10^3$	~6	GE 250 W average
25.	50M10	Magnetron	50	$20x10^3$	13	OKI duty cycle = 0.00025 pulse width = 0.25 μsec

TABLE I-1 (Continued)

SOURCE	TYPE	f(GHz)	Power Output (W)	Efficiency (%)	REMARKS
26. 184H	BWO	135-150	2	--	Hughes CW Oscillator
27. 815H	TWT	135-150	30	--	Hughes Amplifier 12 dB gain

APPENDIX II

POTENTIAL RADIATION HAZARDS OF RELATIVISTIC ELECTRON BEAM MICROWAVE SOURCES

OBJECTIVE

Due to recent advances in technology, it has become possible to generate radiation from intense relativistic beams at submillimeter wavelengths. Typical values of radiated power have been on the order of 100 kW and power levels as high as 1 gigawatt have been reported at longer wavelengths. The objective of this phase of the study was to survey the literature and summarize the type of work that has been accomplished with respect to characterizing potential radiation hazards to personnel. For the same reason that the gigawatt source is a potential EW instrument, it is also capable of affecting both the user's equipment and personnel. In addition, atmospheric scattering can be a source of hazard to personnel. At the end of this appendix, recommendations and conclusions are given for future consideration in the use of these sources.

APPROACH

Due to limited time available and the broad scope of the problem, the research in this area was limited to a review of published articles related to the types of radiation hazards associated with high power microwave sources. The initial point of the literature search focused around a compiled bibliography of papers devoted to radiation hazards problems entitled "Bibliography of Reported Biological Phenomena and Clinical Manifestations Attributed to Microwave and Radio-Frequency Radiation," compiled by Z. R. Glaser of the Naval Medical Research Institute at Bethesda, Maryland. Articles for review were chosen from the bibliography on the basis of the biological effect described, frequency, and the date of the paper, with preference being given to the most recent articles. Approximately forty articles were selected for review. Of these, twenty-seven papers have been located and reviewed. Also, articles from other sources, such as the "BRH Bulletin" from January to March 1975, have been reviewed for possible useful information on the current developments in the field of radiation hazards. In addition, the experience

gained by Georgia Tech personnel from various research has been utilized. For example, familiarity with radiation safety standards with respect to personnel was utilized.

RESULTS

Three types of potential health hazards relating to the generation and exposure to electromagnetic radiation have been identified. The first of these is the X-ray emission by high voltage power sources [1]. Due to extremely high voltage present in the power supply (Marx generator), the vacuum tubes can produce large quantities of X-radiation. The radiation poses the same threat to those exposed as any other source of ionizing radiation. Proper lead shielding of the X-ray sources is a possible means for minimizing the problem.

A second potential health hazard arises from the fact that significant quantities of ozone can be produced by high voltage power supplies in the microwave generator. Although Soviet scientists have ascribed the symptoms of fatigability, headaches, sleepiness, irritability, loss of appetite, and memory difficulties to exposure to microwave radiation, some evidence indicates that these symptoms may be caused by the inhalation of ozone [2]. As a result, methods for protecting the workers from exposure to ozone should be considered. A potential method for prevention of ozone inhalation could be accomplished by locating the power source in an airtight enclosure. A forced air system could be used both to cool the power source and to carry the ozone out of the working area with the exhaust air.

In addition to the personnel hazards from exposure to ozone and X-rays, non-ionizing radiation ranges downward from the ultra violet band. In general, the non-ionizing frequency spectrum is often divided into two frequency regions for analysis purposes. The first region extends from approximately 1 MHz to 300 GHz. In this region, very little EM scattering occurs, and most of the waveguide and transmission line concepts are applicable. In the far infrared through ultra violet region of the spectrum, however, significant wave scattering and molecular absorption occur, which require that different theoretical and analytical approaches be used. The effects of exposure to non-ionizing microwave

fields are generally classified as thermal effects and non-thermal effects.

Thermal Effects

For frequencies up to 300 MHz, heating in biological tissue generally arises from ionic conduction and from vibration of dipole molecules of water and proteins. Heating from ionic conduction occurs due to ions oscillating to and fro as the polarity of the field changes. Heating from dipole molecules occurs due to the molecular friction as the polar molecules attempt to align themselves to direction of the incident EM field. The field patterns producing the heating are complex functions of the frequency, source configuration, tissue geometry, and dielectric properties of tissues. The temperature rise further depends on the cooling mechanisms within the body.

The majority of the microwave irradiation studies in the United States has centered around the thermal effects due to exposure to microwaves. Whole body irradiation at high power densities leads to general hyperthermia and, in extreme cases, to death [3]. Non-lethal, whole-body irradiation in fields with power densities greater than 100 mW/cm^2 at 2.45 GHz, for example, can produce residual bradycardia (i.e. reduced pulse rate), while a power density of 40-50 mW/cm^2 at 2.45 GHz has in certain cases reversibly increased the latent period (i.e. period between stimulation and conduction) in central nervous system ganglia [4].

In tissues with high blood circulation, the blood acts as a coolant to remove heat from the region of microwave exposure. However, poorly vascularized tissues, such as those in the eye or testes, are especially susceptible to damage because their capacity to dissipate heat is very poor. Cataracts, for example, can be produced in the eyes of rabbits irradiated with a power density of 120 mW/cm^2 at 2.45 GHz for 230 hours over a period of 2 months [5].

Predicting personnel hazards based on extrapolation of experimental results obtained at lower microwave frequencies to frequencies well above 100 GHz is risky. There is no guarantee that the predicted results would be accurate, and furthermore, there is no accepted U.S. safety standard for frequencies above 100 GHz. However, it is possible to draw some conclusions based upon available data. For example, it is well known that as the frequency

increases, the depth of penetration of EM energy into tissue decreases [6]. Therefore, it appears that at a frequency of 200-300 GHz the penetration depth for skin and muscle tissue is approximately 1 mm and increases to 2 mm for bone and fat tissue. Based on the effects produced at lower microwave frequencies, it would appear that tissue damage at 300 GHz would be limited primarily to surface burns. This conjecture is partially corroborated by experiments at 70 GHz where 30-minute exposures to power densities of 610 mW produced dense, milky-white opacity (lenkoma) and invasion of the cornea by blood vessels (pannus) as opposed to lenticular opacities (cataracts) at lower frequencies.

Non-Thermal Effects

Non-thermal effects relate to those effects not associated with a temperature rise. The pearl-chain effect (which has only been observed in the 1 MHz to 100 MHz frequency range), dielectric saturation effects, behavioral effects, and central nervous system effects are examples of non-thermal types of effects. Thus, these effects have been limited to observation at the cellular and chemical levels.

Recently, several new non-thermal effects at microwave frequencies have been observed. One example is the germination patterns of spores of the Fusarium solani f. phaseoli exposed to microwave radiation as opposed to conventional heating techniques [7]. Conventional heating of spores yields percent growth curves which increase with time to a maximum level determined by the temperature to which the spores were heated, while microwave irradiation of spores yields growth curves which indicate that the spores either germinate on the first day or not at all. This step-function growth curve indicates that microwave irradiation possibly may destroy whole enzyme pathways.

Recent studies in the USSR concerning non-thermal effects have indicated that resonance effects are exhibited in cell division when exposed to low level millimeter wavelength radiation [8]. Cells of Phodotorula ruloa were exposed to very low-level radiation at frequencies of 41.89, 41.84, 41.78, and 41.72 GHz for a period of 15 hours. Ten experiments were performed at each frequency with resultant stimulation (factor of 1.5 increase) of cell

division at the three other frequencies. An explanation of the mechanism of the resonant effect of irradiation and some of its other properties presently does not exist. There have been a few attempts to explain the resonance effect, but no verification has been made. Further experimental and theoretical investigations are required.

Other work performed by USSR scientists to determine the effects of 42 GHz microwave irradiation on the bone marrow of mice has resulted in counts of bone marrow cells that remained undamaged by X-irradiation after prior irradiation with a microwave field in which the exposure time to the microwave field, the power density of the field, and frequency were varied [9]. Counts of undamaged bone marrow cells exposed to power densities from 1 to 75 mW/cm^2 for a 60 minute period before X-irradiation indicated that the number of undamaged cells increased nearly instantaneously to 0.85 of the control value when the incident power density exceeded 9 mW/cm^2. These results indicate that a certain power density threshold may exist below which microwave irradiation has no effect. Survival of cells pre-treated with 42 GHz irradiation had a 85-90% survival as opposed to a 50% survival for cells treated with X-radiation alone. Other non-thermal effects have been noted, but as in the above cases, studies until now indicate that these effects seem to have limited applicability when dealing with personnel hazards.

Current Safety Standards for Non-Ionizing Radiation

The safety levels established with respect of personnel to non-ionizing EM radiation vary widely between the countries of the free-world and the countries of the Soviet block. This variance is typically illustrated by the U.S. and USSR safety standards in which the U.S. safety level for continuous exposure is 1000 times greater than that of the USSR.

The most widely accepted safety standard with respect to exposure to non-ionizing electromagnetic radiation is that promulgated by the American National Standards Institute (ANSI) C-95 Subcommittee IV, "Safety Levels and/or Tolerances With Respect to Personnel." This safety standard (identified as ANSI C95.1-1973) sets a safety level guide of 10 mW/cm^2 for continuous exposure over the frequency range of 10 MHz to 100 GHz for whole body and partial body irradiation.

It should be noted that this level is only a guide and that under certain conditions and circumstances it should probably be reduced. It is the present consensus that thermal effects, which are considered to be the most harmful, were used as the basis for establishing the guide level of 10 mW/cm^2 for moderate environments. Obviously, for people with poor blood circulation or who are under severe heat stress, the guide number should be appropriately reduced.

The guide level of 10 mW/cm^2 in the ANSI standard was based on an evaluation of available literature up to 1973. Sufficient information was not available to substantiate adjustment of the radiation protection guide to account for peak power effects, modulation effects, field intensity effects, and frequency dependencies. Our survey has not uncovered any additional information that has been generated since 1973 that provides a basis for justifying a change. However, it is generally agreed that radiation levels which are tenfold larger than recommended are certainly dangerous. Based on available information, no quantitative evaluation of personnel safety to EM radiation for frequencies above the ANSI limit of 100 GHz can safely be projected. However, it is known that the details of the anatomy, the frequency of radiation and its penetration depth affect the percentage of absorbed radiation. Therefore, the establishment of safe power levels will be related in a complicated way to power levels at which damage occurs.

CONCLUSIONS

Based on the studies conducted to date, the following conclusions are projected:

1.) A potential health hazard exists due to the generation of ionizing radiation (X-rays) by the high voltage tubes in the power supplies;
2.) A potential health hazard exists due to generation of ozone by the high voltage power supplies; and
3.) A potential health hazard exists due to personnel exposure to non-ionizing radiation.

It appears that safety precautions could probably be easily implemented to prevent the first and second above health hazards, respectively, by lead

shielding the appropriate components of the power supply and by enclosing the power supply in an airtight enclosure with proper ventilation. However, the precise determination and control of the third hazard above is much more difficult.

Currently, there is insufficient information available to accurately and precisely determine the magnitude of the potential personnel hazard with respect to exposure to non-ionizing electromagnetic radiation, due either to thermal effects or to non-thermal effects. This conclusion is particularly true for frequencies above 100 GHz where there is no safety standard at all that can be used as a guide and where very little research has been conducted. However, based on common sense, several obvious potential danger areas with respect to personnel could exist due to generation and propagation of gigawatt power levels. These areas include (1) sidelobe radiation levels which easily could be on the order of 100 kW, (2) reflections of the main beam of the antenna from nearby structures, (3) backscatter from precipitation such as rain, and (4) near-field effects such as broadening of the main beam in the near field.

REFERENCES

1. Fetner, R. H.,"X-Radiation Effects in Euploid Human Cell Cultures," Final Technical Report, Project B-258, P.H.S. Grant No. RH 00035-03, November 1965.

2. Fetner, R. H.,"Research and Reports on Ozone-Induced Effects on Living Cells," Final Technical Report, Project A-430, Contract No. AF-41(657)-263, April 1961.

3. Johnson, C. C. and Guy, A. W.,"Nonionizing Electromagnetic Wave Effects in Biological Materials and Systems," Proceedings of the IEEE, Vol. 60, No. 6, June 1972, pp.692-718.

4. Lambert, P. D., Nealeigh, R. C., and Wilson, M.,"Effects of Microwave Exposures on the Central Nervous System of Beagles," Journal of Microwave Power, Vol. 7, No. 4, 1972, pp. 367-380.

5. Haidt, S. J. and McTighe, A. H.,"The Effect of Chronic, Low-Level Microwave Radiation on the Testicles of Mice," IEEE International Symposium on Microwave Theory and Techniques Digest, University of Colorado, Boulder, Colorado, June 1973, pp. 324-5.

6. Schwan, H. P.,"Survey of Microwave Absorption Characteristics of Body Tissues," Proceedings of the 2nd Tri-Service Conference on Biological Effects of Microwave Energy, 1958, pp. 126-145.

7. Olsen, C. M., Drake, C. L., and Bunch, S. L.,"Some Biological Effects of Microwave Energy," Symposium on Microwave Power, University of Alberta, March 1966.

8. Devyatkov, N. D.,"Influence of Millimeter-Band Electromagnetic Radiation on Biological Objects," Sov. Phys.-Usp., Vol. 16, No. 4, January-February 1974, pp. 568-9.

9. Sevast'yanova, L. A. and Vilenskaya, R. L.,"A Study of the Effects of Millimeter-Band Microwaves on the Bone Marrow of Mice," Sov. Phys.-Usp., Vol. 16, No. 4, January-February 1974, pp.570-1.

APPENDIX III

ANTENNA CONSIDERATIONS

GAIN, BEAMWIDTH AND POINTING

Controlling the spatial radiation of a REB device is a challenging antenna problem involving combinations of technologies - many of them at their limits. Effective antenna designs must consider additional factors involving: (a) high intensity fields and radiation hazards, (b) high gain-narrow beam antennas requiring precision surfaces and (c) ultra precise pointing with probably new quasi-optical techniques for controlling and positioning the radiated (and received) energy.

A range of the antenna gain, beamwidth and pointing precision for the 10 to 250 GHz region is shown in Figures III-1 and III-2. These Figures show that antenna gain in the range of 30 to 60 dB is achievable with moderate size antenna apertures. These same size antennas produce beams with half-power widths of 6° to 0.1° requiring antenna pointing precision as precise as $\pm$ 0.03° ($\pm$0.5 milliradian). Thus while high gain is achievable it is accompanied with a possible penalty of high pointing precision.

Reflector surfaces must be precisely fabricated and, once made, they must be structurally supported to maintain this precision in a variety of environments. Figure III-3 shows the range of tolerances needed for low gain loss. To maintain a gain loss of 0.1 dB or less, the required rms tolerance varies from $\pm$ 0.04 inches at 10 GHz to $\pm$ 0.0006 inches at 250 GHz.

ANTENNA SIDELOBE AND BACKLOBES

The ever present side and backlobes associated with antenna patterns of the antennas used in the subject ultra-high-power systems present further problems. This is especially the case for potential radiation hazards to operating personnel as well as potential electromagnetic interference and ECM and ECCM aspects.

Very low sidelobes (and backlobes) are achievable-but require careful (and costly) antenna design. Attention must be paid to several factors including: aperture illumination shaping, aperture blockage, aperture surface tolerances, structure edge illumination and scattering and feed moding and purity. Both parallel and cross polarization aspects for the above factors must be considered.

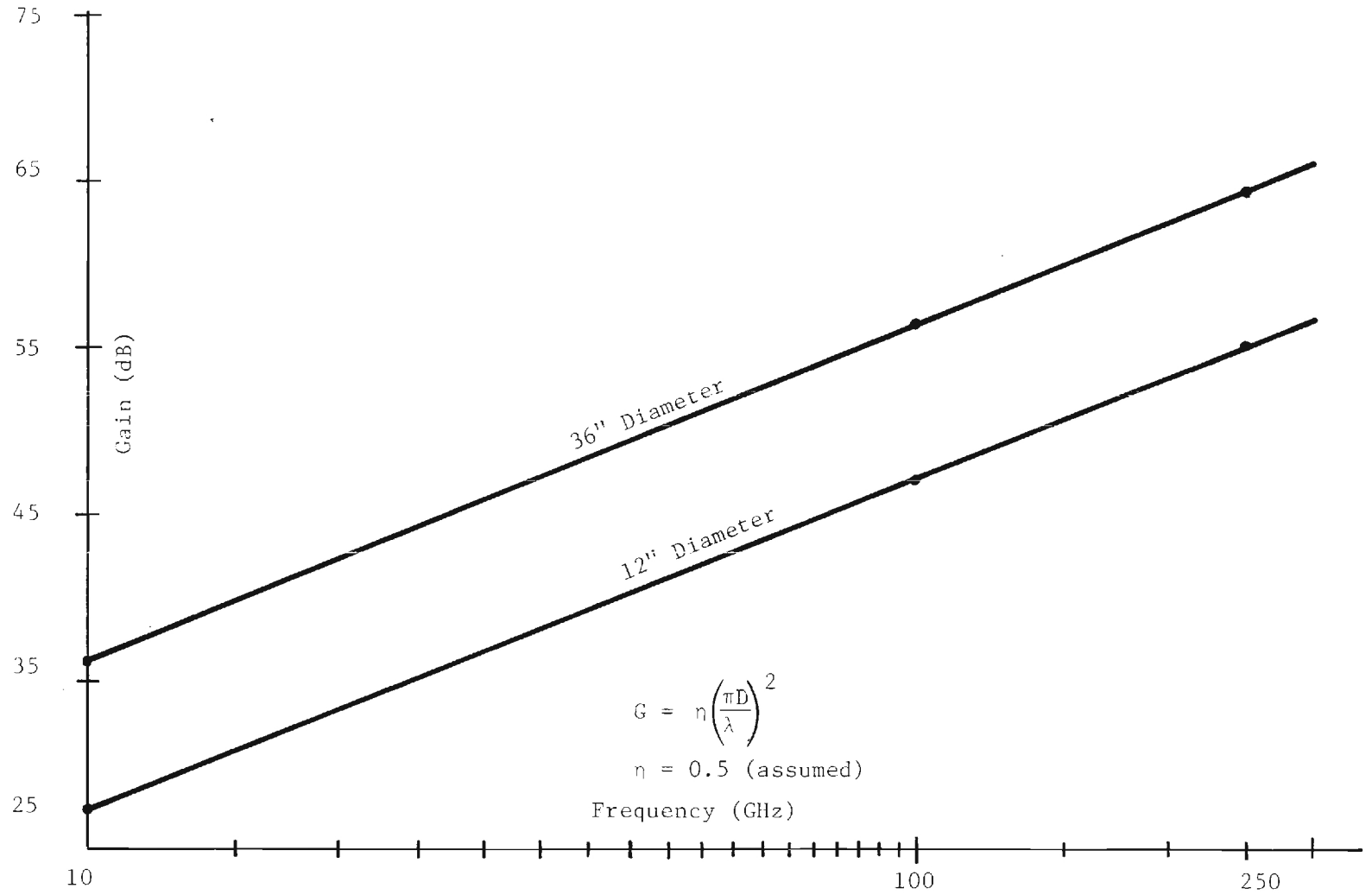

Figure III-1. Antenna Gain (12 and 36 inch diameters) Versus Frequency.

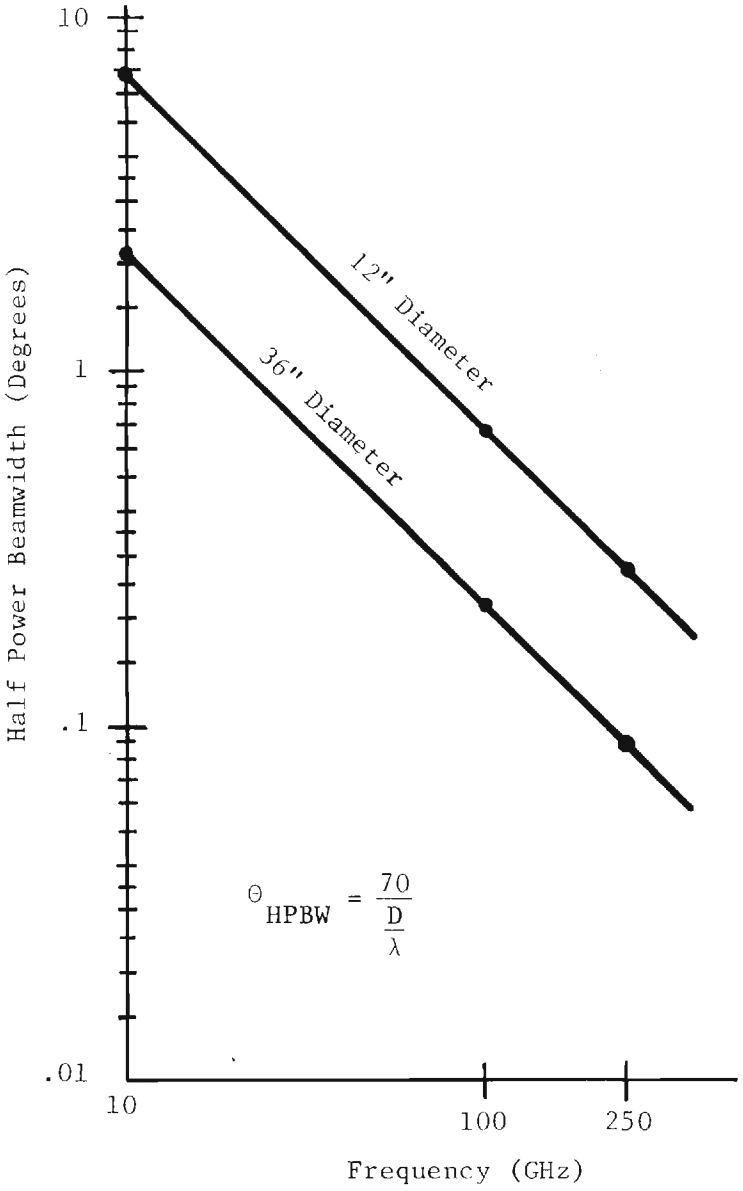

Figure III-2. Antenna Half-Power Beamwidth (12 and 36 inch diameters) versus Frequency.

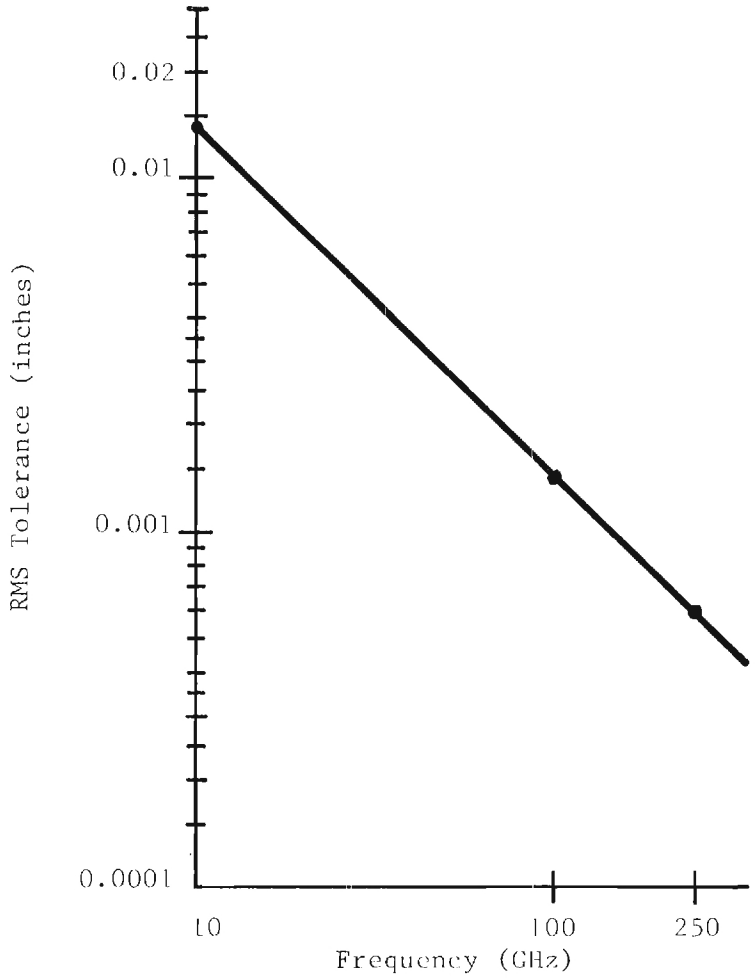

Figure III-3. RMS Surface Tolerance (for 0.1 dB Gain Loss) Versus Frequency.

While these aspects are in general complex and a practical solution is not always readily achieved, some of the considerations have been investigated in detail for horn type antennas. These are discussed below.

SIDELOBE AND BACKLOBES IN HORN ANTENNAS

Because horn antennas are used as primary antennas and as feed antennas for reflector antenna systems, an investigation of their radiation characteristics has wide applicability. Horn antennas, as well as all antenna systems, radiat energy into the side and back regions as shown in Figure III-4. The sidelobe and backlobes are usually not considered to be a radiation hazard for low and moderate power microwave systems. However, for high power microwave systems these lobes can create radiation hazards. Also the energy transmitted in the side/backlobe regions can create interference with other external electronic equipment (EMI) and, in receiving mode, the incoming side/backlobe energy can cause electromagnetic interference in the system. This property is often exploited in ECM systems.

The present state-of-the-art with respect to the radiation pattern side/back lobe levels of horn-type antennas are discussed below by comparison of results for both "standard" pyramidal horn antennas and for horn antennas which have been modified to achieve low side/back lobe levels.

Choke flanges located around the horn rim can reduce the side and backlobe patterns of a horn antenna[1]. Figure III-5 shows experimental results. The unmodified antenna has a backlobe level of -23 dB which is reduced to approximately -40 dB by using a choke flange. The choke flange also tends to make the E and H plane identical, although the E and H plane sidelobes remain different. The E-plane sidelobe envelope is approximately a straight line (when plotted in dB), and as for all horn antennas the E-plane sidelobes are greater than the H-plane sidelobes.

Note that a -40 dB backlobe level may not be considered adequate for a very high power system. However, better performance has been achieved as will be discussed later.

Analyses have been performed for both the E-plane [2] and H-plane [3] patterns of horn antennas and the primary radiation mechanisms of these antennas have been identified. Based upon this understanding of the radiation mechanisms which contribute to the sidelobe/backlobe regions, modifications have been

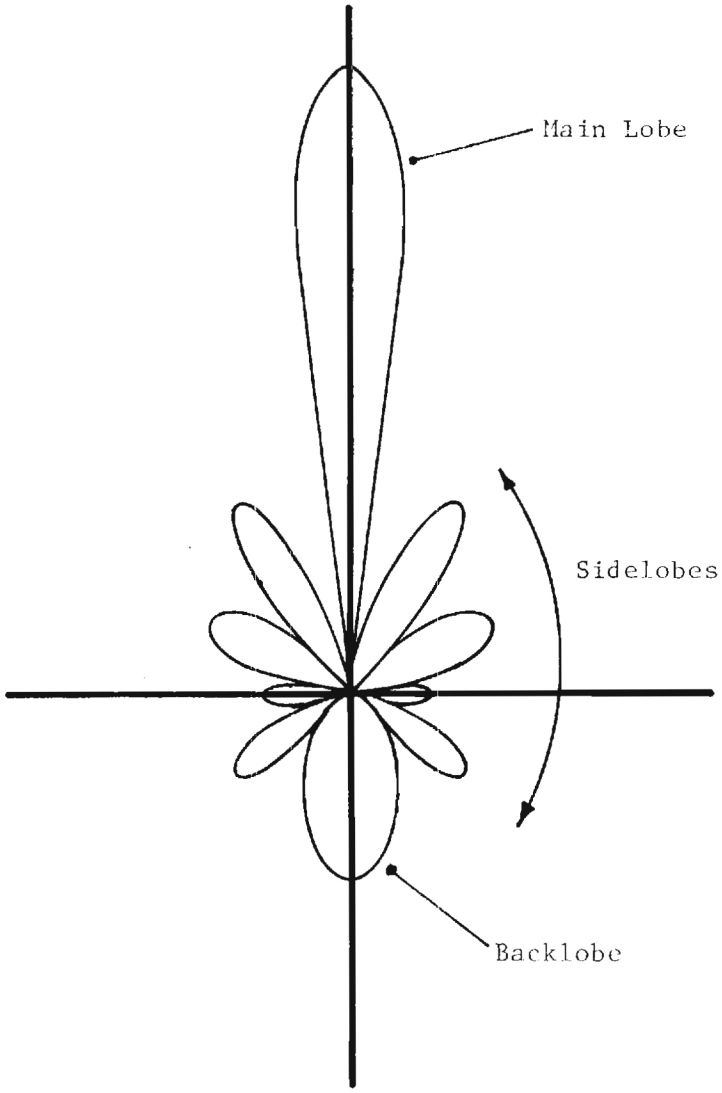

Figure III-4. Typical Horn Antenna Pattern.

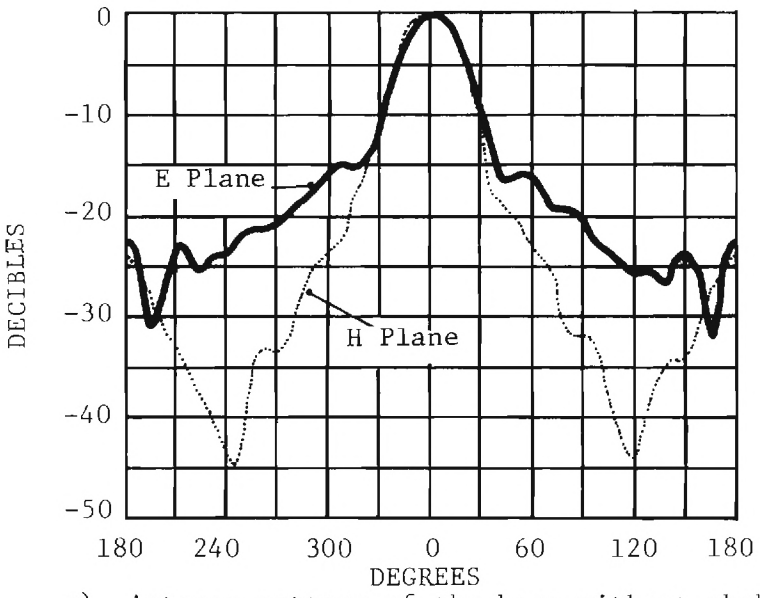

a) Antenna pattern of the horn without chokes.

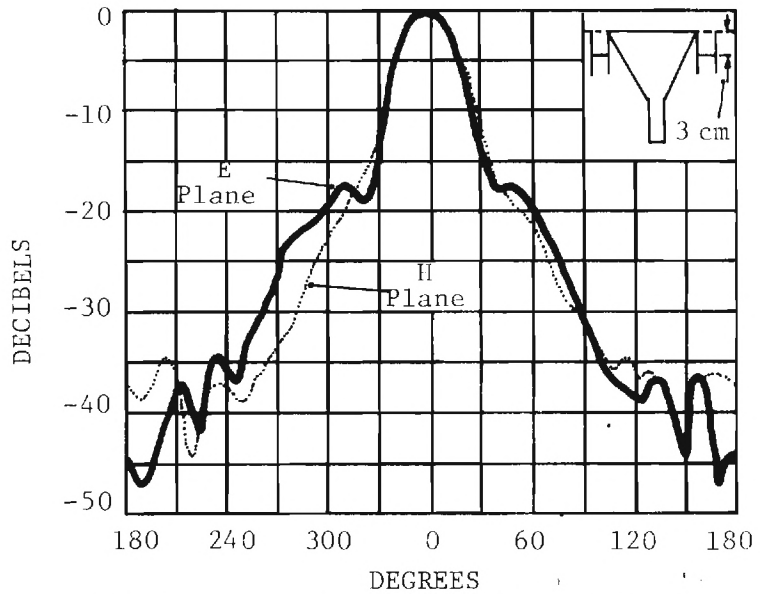

b) Antenna pattern with 3-cm choke depth.

Figure III-5. Horn Antenna Patterns with and without Choke Flange.

designed to attain lower side/back lobe levels. These modifications are discussed in Reference 3. Several modifications were tested including a choke system similar to that described in Reference 1. This choked horn, when operating at the design frequency of 6.6 GHz produced a backlobe level in excess of -35 dB. However, the antenna performance deteriorated when the frequency was increased to 12.0 GHz even though the choked horn still exhibited lower sidelobe levels than the unmodified control horn.

A second type of horn, known as the corrugated horn, is also described in Reference 3. This antenna incorporates a series of slots (corrugations) located on the inside of the horn wall normal to the electric field vector. The slot geometry is designed to "cut-off" propagation of the electric field on the horn wall to reduce the excitation of the horn edge and minimize the edge diffracted energy which contributes to the side/backlobe region. Two corrugated horns were tested. A small corrugated horn (3.5 in. square aperture, 50° total flare angle) with a 3 dB beamwidth of approximately 24° exhibited backlobes lower than -40 dB over a frequency range of 8 to 14 GHz. A large corrugated horn (9.7" square aperture 15.85" slant length, 34° flare angle) was tested which exhibited a backlobe level lower than -57 dB and a gain of 22.3 dB. This horn has been operated at 20 kW of peak power at 10 GHz with no evidence of any corona or breakdown phenomena. However, the high power limit of this design does not appear to have been determined.

Georgia Tech has recently demonstrated on NASA Grant NSG-5012 that corrugated horns can be successfully fabricated at frequencies operating above 100 GHz. Figure III-6 shows a corrugated conical horn that has yielded excellent antenna patterns at 180 GHz.

Note that the use of corrugations produces a frequency sensitive antenna and thus has an effect upon the VSWR as a function of frequency. Acceptable VSWR's have been attained over octave bandwidths [3]. These corrugations can also cause higher order mode excitation [4] which can produce frequency sensitive patterns which can in some cases possess exceptionally low sidelobes. An S-band horn described in Reference 4 achieved sidelobe levels more than 55 dB below the main beam maximum at all angles removed more than 40° from boresight. This appears to represent the present state-of-the-art with respect to horn antenna sidelobes. Other moding considerations are discussed later for other situations including beam shaping and broadband incoherent radiation.

The corrugated horn antenna appears to offer the best front-to-backlobe ratios currently available. However, other backlobe reduction procedures such

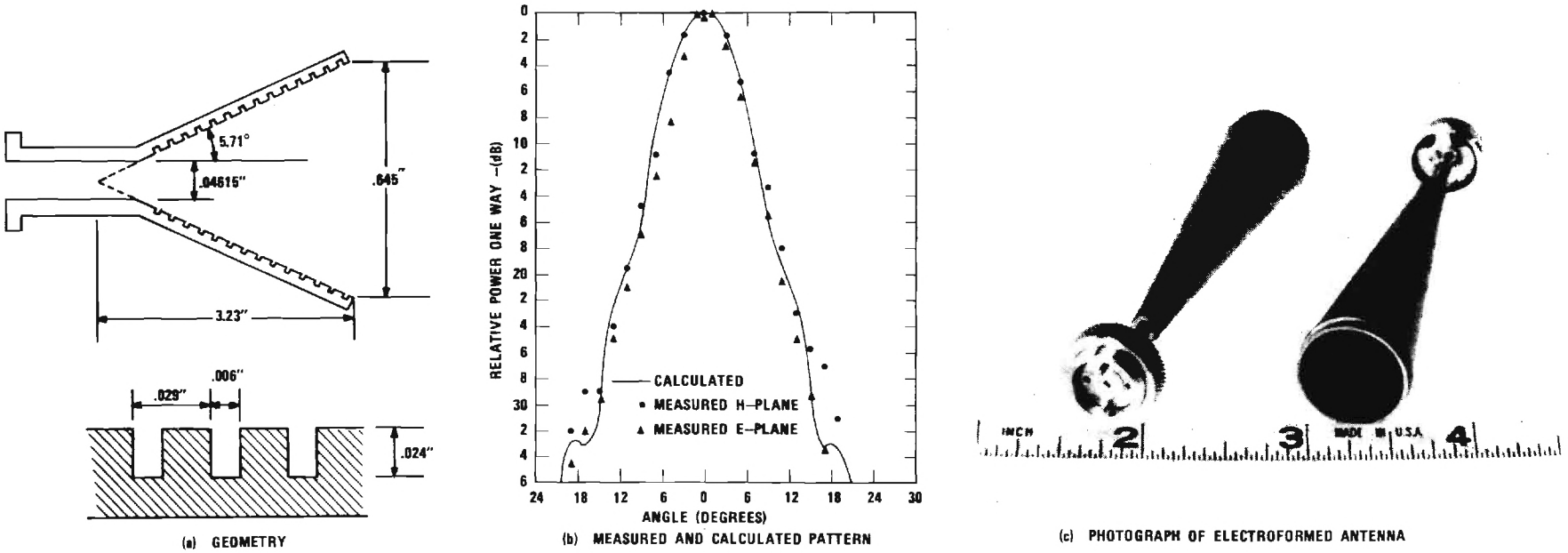

Figure III-6. Data on 180 GHz Feed Horn Developed on NASA Grant NSG-5012.

as the use of microwave absorbing materials might be employed in addition to the corrugations in order to obtain a lower backlobe level. Based upon the above results it may be feasible to obtain a relative front to back ratio of approximately 70 dB through the use of such a combination. See Table III-1.

As previously noted the use of corrugations to reduce the side/backlobe level is sensitive to the operating frequency. A property of the corrugated surface is that it possesses contiguous, alternating stop and pass bands as in the case of filters. This limits the bandwidth of the corrugated horn.

Reference 7 presents some results on a special antenna designed for multi-octave frequency band operation. However, this type of antenna has application primarily as a receiver. An application of this design to a high-power system may be feasible but this has not been demonstrated. Due to the ridge type excitation mechanism this antenna may encounter high-voltage breakdown (arcing) at high power levels. However, redesign for high power may be feasible.

ANTENNA EFFECTS WITH BROADBAND NONCOHERENT SIGNALS

Beamwidth/Gain

Consider that the half-power beamwidth of an antenna with coherent illumination is given by

$$\text{HPBW (degrees)} = \frac{70}{\frac{D}{\lambda}}$$

where D is the aperture diameter of the antenna - be it a horn or reflector. The gain of the antenna for the same coherent illumination is

$$\text{GAIN} = \eta\left(\frac{\pi D}{\lambda}\right)^2$$

where η is the antenna efficiency. When illuminated by a band of (either continuous or discrete) frequencies, the net antenna emission is going to be spatially weighted by the antenna pattern, and frequency weighted by: (a) the varying HPBW and (b) the varying gain of the antenna. As a result, the net beam will tend to smear out and probably assume a Gaussian spatial shape for moderate bandwidth signals.

TABLE III-1

SIDE- AND BACK- LOBE LEVELS FOR HORN ANTENNAS

HORN TYPE	SIDELOBES	BACKLOBE
Unmodified	-15 dB to -30 dB	-23 dB to -30 dB
Choke Flange	-17 dB to -35 dB	-35 dB to -40 dB
Corrugated	-20 dB to -40 dB	-40 dB to -57 dB
Corrugated/Absorber (estimated)	-20 dB to -40 dB	-50 dB to -70 dB

For a modulated signal, it should be noted that the modulation envelope can become distorted due to the various frequency components undergoing amplitude and phase changes. These occur by the varying antenna gain and the related problem of varying phase and group velocities of such wideband signals due to not only the antenna transmission structures but the atmospheric medium as well.

For rough estimating purposes, the net HPBW for a wideband signal should be approximately that obtained from the above equation at midband (assuming a band here is no more than a typical waveguide band).

Modes

The above discussion applied primarily to those cases where a single dominant mode is propagated. In situations where this is not the case, the problem is more complicated. Two situations need to be considered:

(1) There are circumstances (extreme symmetry for example) where even though a higher order mode(s) can exist, it actually does not. In that event, the beamwidth/gain discussion above should apply.

(2) In other circumstances, high order modes are generated at the higher frequencies, perhaps even intentionally. Three factors affect the net antenna performance:
   (a) The mode(s) excitation amplitude and phase relative to each other or the fundamental mode,
   (b) The varying phase velocity of each mode in the transmission structure, and
   (c) The spatial distribution of the mode(s) and their resultant antenna pattern.

When a very wide frequency band is used, it is likely that the horn antenna will not maintain a good radiation pattern due to excitation of higher-order waveguide modes. These effects have been observed in near-field measurements of horn-fed-parabolic reflector antennas [8]. However, the specific mixture of modes which are excited at a given frequency is sensitive to many parameters, such as bands used in the waveguide feed system and irregularities in the waveguide antenna system. These higher-order effects manifest themselves in shifts and splitting of the antenna main beam and as changes in the side and back lobe structure.

A statistical approach has been derived to determine the effects of higher-order mode excitation of a phased array composed of rectangular waveguide [9]. This analysis included the effects of statistically mixed higher order modes in the array elements and examined the effects of such modes upon the radiation pattern of the array. This analysis could be extended to examine the statistical nature of the pattern of a horn exciter for out-of-band frequencies and for large frequency bandwidths. In general it is likely that such an over-moded horn antenna will exhibit several "main beams" which can be canted off the horn axis and relatively high side and back lobe levels. However, this question would have to be examined in more detail in order to arrive at an accurate statistical description of the pattern.

While multimode operation, in general, appears undesirable in antenna applications, there are a few examples where higher order and multimode operation was found desirable in the past.

(1) Use of a combination of TE and TM modes produced an excellent equal E and H plane beam and very low sidelobes over narrow RF bandwidths [10].

(2) Use of higher order modes permitted monopulse operation for angle tracking [11,12].

(3) Use of the TM°_{01} mode can achieve an omnidirectional (in azimuth) beam useful in communication applications [13].

(4) Use of the TE°_{01} mode waveguides permits very low loss propagation in waveguides over km paths [14].

Polarization

It is not precisely known at this time just how pure the REB emission polarization is. Optical techniques can be used to linearize the polarization (e.g., Brewster Angle plates or grids or other waveguide structures) if necessary. Totally random polarization is not necessarily undesirable, it more or less means certain components or techniques suitable for (linearly) polarized sources are not usable. Most circular waveguide transmission systems appear suitable for even randomly polarized energy.

Antenna Concepts

Since specific antenna configurations are highly dependent on the application, no detailed antenna designs are presented. Rather, some general techniques useful in several broad applications are described for consideration. These antennas take into consideration the high power density available and generally are quasi-optical configurations where the REB radiation is controlled but higher field intensities than are inherent in the beam are avoided.

Pencil beams can be controlled by two methods outlined below. A simple beam scanning antenna is shown in Figure III-7. Here the REB output is made to impinge on a planar (or curved as needed) mirror for beam pointing. Mirror motion scans the beam over a relatively narrow angular sector.

Wider azimuth coverage can be achieved by utilizing confocal paraboloids in an arrangement shown in Figure III-8. Here the REB is fixed and beam scanning is achieved by rotating the reflector assembly as a unit.

It may be desirable to provide omnidirectional azimuth coverage in certain communications applications. Figure III-9 is a sketch of an antenna utilizing the TM_{01}° mode to generate an omnidirectional azimuth pattern. This concept has been considered in the past for certain hardened antenna applications - hence the debris pit.

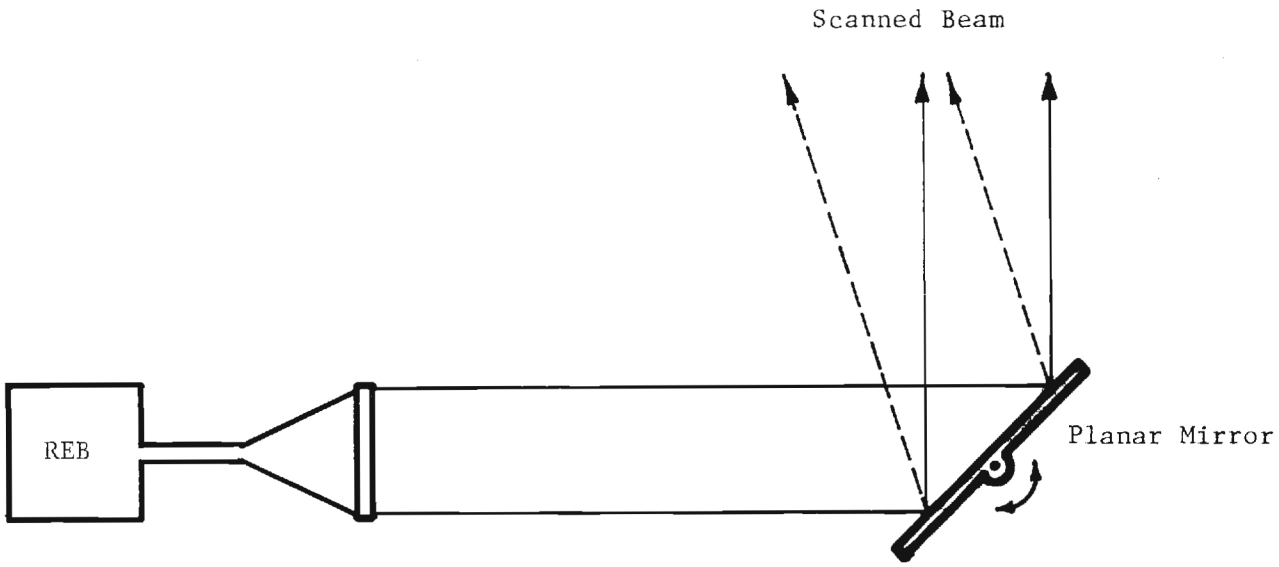

Note: Angle Sector Covered is Small

Figure III-7. Planar Mirror Antenna Scanner for Pencil Beams.

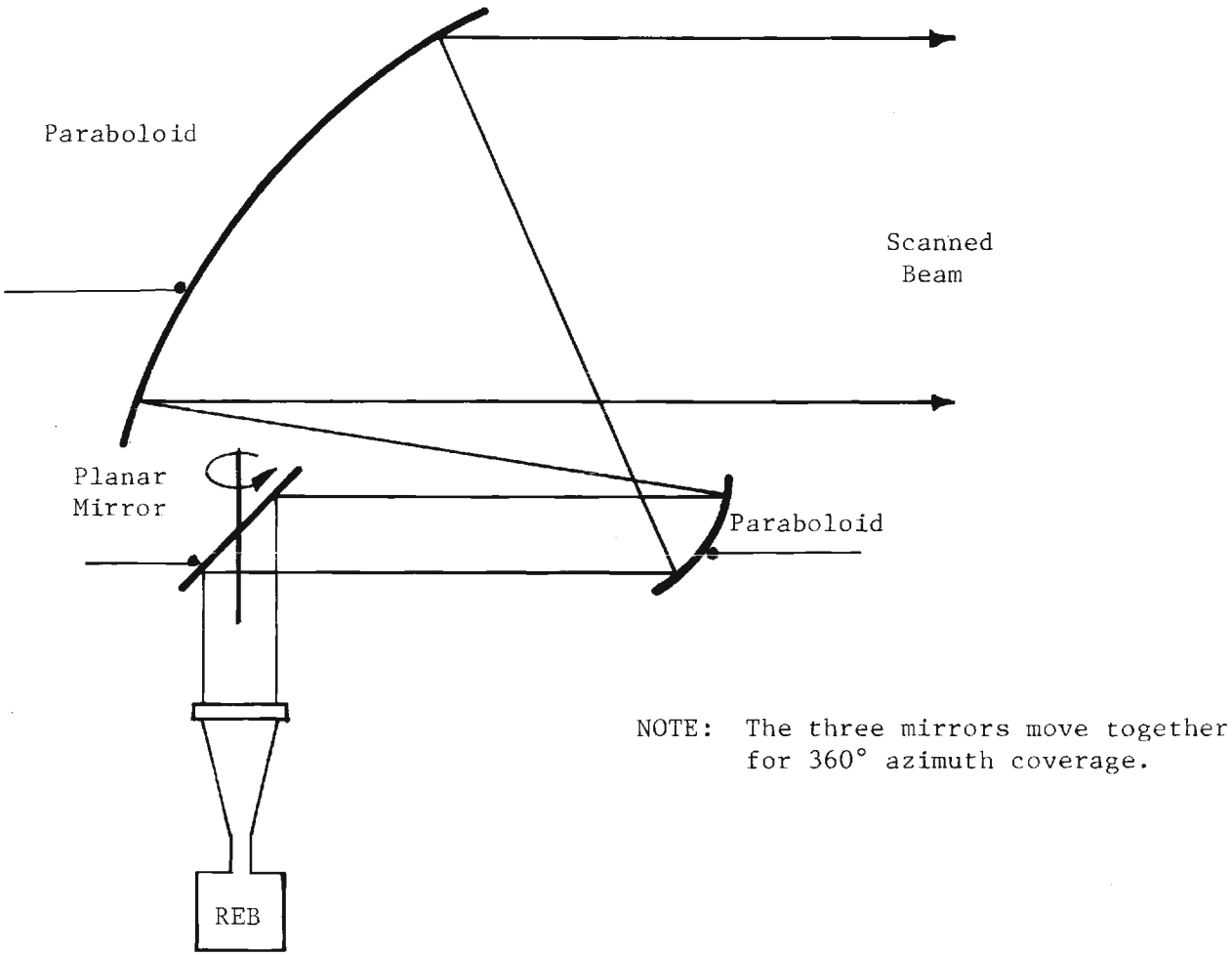

Figure III-8. Confocal Paraboloid Azimuth Scanner for Pencil Beams.

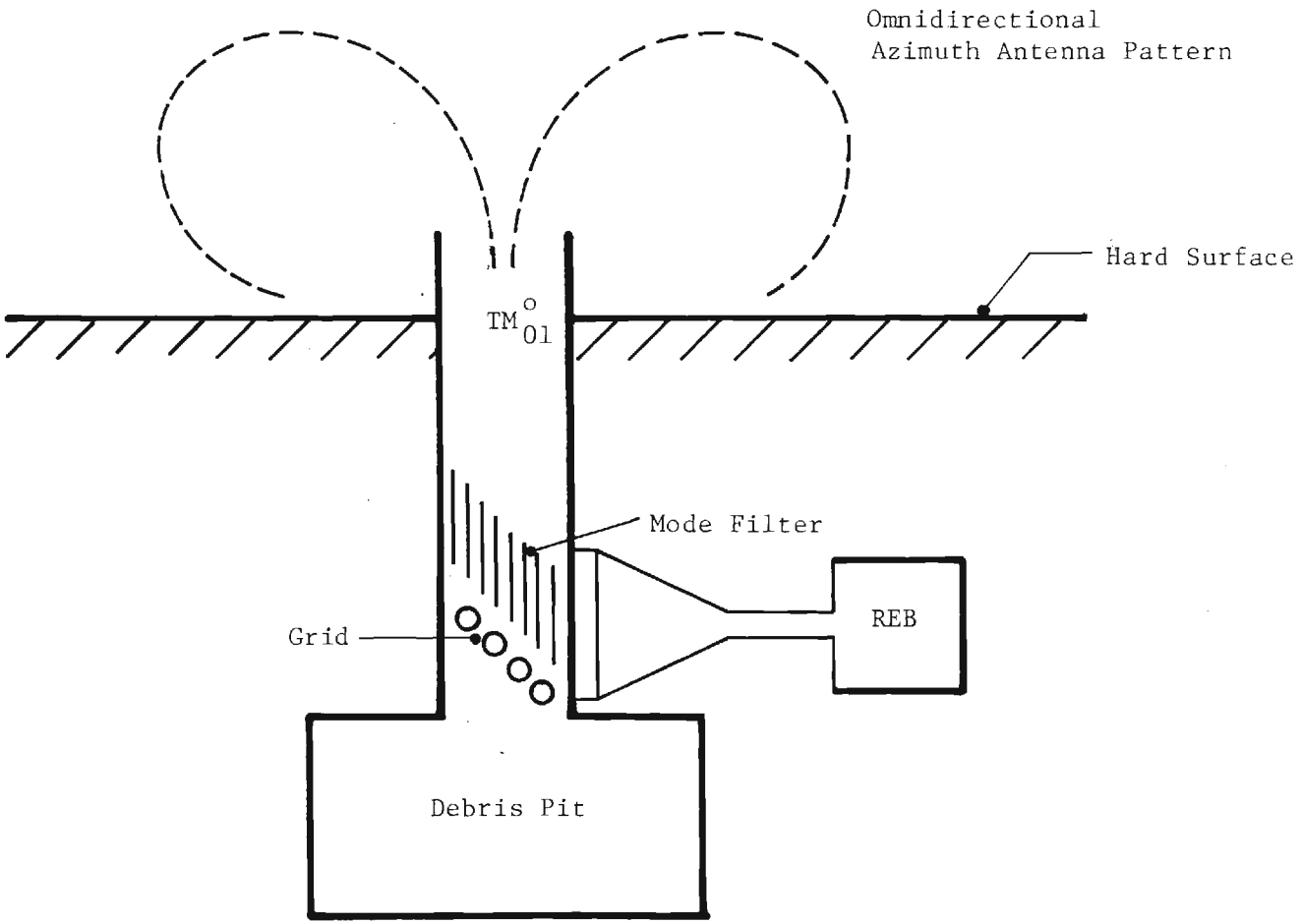

Figure III-9. Higher Order Mode Antenna for an Omnidirectional Azimuth Beam.

REFERENCES

1. LaGrone, A.H. and Roberts, G.F., "Minor Lobe Suppression in a Rectangular Horn Antenna through the Utilization of a High Impedance Choke Flange," IEEE Transactions on Antennas and Propagations, Vol AP-14, No. 1, Jan. 1966 pp. 102-104.

2. Yu, J.S., Rudduck, R.C., and Peters, L.,"Comprehensive Analysis for E-Plane of Horn Antennas by Edge Diffraction Theory," IEEE Transactions on Antennas and Propagation, Vol. AP-14, No. 2, March 1966, pp. 138-149.

3. Lawrie, R.E., and Peters, L.,"Modifications of Horn Antennas for Low Sidelobe Levels," IEEE Transactions on Antennas and Propagation, Vol. AP-14 No. 5, Sept. 1966, pp. 605-610.

4. Bahret, William F., Peters, L, "Small-Aperture Small-Flare-Angle Corrugated Horns," IEEE Transactions on Antennas and Propagation, July 1968, pp.494-5.

5. Nair, K.G., Srivastava, G.P., Hariharan, S., "Sharpening of E-Plane Radiation Patterns of E-Plane Sectoral Horns by Metallic Grills," IEEE Transactions on Antennas and Propagation, Jan. 1969, pp. 91-93.

6. Yu, J.S., Rudduck, R.C., "H-Plane Pattern of a Pyramidal Horn," IEEE Transactions on Antennas and Propagation, Sept. 1969, pp. 651-652.

7. Kerr, J.L., "Short Axial Length Broad-Band Horns," IEEE Transactions on Antennas and Propagation, Sept. 1973, pp. 710-714.

8. Cain, F.L., Weaver, E.E., and Ryan, C.E., "Determination of Out-of-Band Antenna Performance Using Near-Field Measurements," IEEE Antenna and Propagation Society-International Symposium, 10-12 June 1974, Atlanta, Ga. pp. 169-173.

9. Cain, F.L., Cown, B.J., Weaver, E.E., and Ryan, C.E.,"Far-Field Antenna Performance Investigations Concerning In-band Effects of Near-Field Structures and Out-of-Band Phased Arrays," A-1613 Final Engineering Report, Contract No. N00024-74-C-1215, 31 Jan. 1975, Naval Ship Engineering Center, Code 6175D, Naval Sea Systems Command 0341, Washington, D.C. 20360.

10. Potter, P. D., "A New Horn Antenna with Suppressed Sidelobes and Equal Beamwidths," Microwave Journal, June, 1963, pp. 71-78.

11. Howard, D. D., "Single Aperture Monopulse Radar Multi-Mode Antenna Feed and Homing Device," 1964 IEEE Conv. on Mil Elec., Sept. 14-16 1964, pp. 259-63.

12. Das, A., "Multi-mode Excitation of Large Aperture Horns to Produce Electronic Deflection of Directional Pattern," The Radio and Electronic Engineer, Vol. 38, No. 3, September 1969, pp. 181-183.

13. Stephens, M. A., "Testing a Hardened VHF Antenna," Vol. 2, Martin-Marietta and Bunker Ramo Antenna Symposium, August 21-22, 1967.

14. Ramo, S., Whinnery, J. R. and Van Duzer, T., "Fields and Waves in Communications Electronics," John Wiley and Sons, New York, 1965, pp. 434-439.

APPENDIX IV

ATMOSPHERIC PROPERTIES

The application of gigawatt sources is heavily dependent upon atmospheric properties as a function of wavelength. The transmission characteristics of the atmosphere have been treated in several investigations. In order to utilize the existing data for the investigation of the gigawatt sources, this Appendix briefly surveys the currently available information and presents data which are considered significant for the applications of gigawatt sources. In addition to the importance of attenuation in applications of the gigawatt sources, atmospheric breakdown, thermal blooming and turbulence must be considered for high power systems. Backscatter from rain and refractive effects are also important considerations for the high power sources. For the applications which can be considered, the spectral range of interest lies in the wavelength region from approximately 100 μm to 10 cm.

In the sections of this Appendix which follow, the atmospheric properties of attenuation, atmospheric breakdown, thermal blooming and turbulence are discussed. Comparisons are made of the long wavelength characteristics of the atmosphere with the optical region characteristics since several applications of the gigawatt sources are significant when trade-offs are made against equivalent optical systems.

IV-1 Atmospheric Attenuation

The transmission qualities of the atmosphere are a function of several parameters of the atmosphere. Of particular interest are the characteristics during inclement weather, i.e., rain, fog, haze and clouds. The water vapor absorption in the atmosphere is the major attenuator in the wavelength region from approximately 15 μm into the microwave region. In Appendix V on optically pumped lasers, the water vapor spectrum from the microwave region to 10 μm is presented with optically pumped laser outputs superimposed at the appropriate wavelength. The water vapor spectrum presented in Appendix V is a reproduction of the work of Zhevakin and Naumov [1]. Two spectra are given in this work; the one (solid trace marked 1) is the result obtained with line shapes of Zhevakin and Naumov while the other (dashed curve marked 2) is the calculated curve using the Van Vleck line shape. The line shape of Zhevakin and Naumov provides the best fit to experimental data at short wavelengths. The curves have been prepared by using H_2O rotational lines for rotational states to J = 12. More recent data and calculations [2] provide improved accuracy for lines through J = 40, which can be populated by a light molecule like H_2O, and the millimeter/submillimeter curves should be recalculated.

At longer wavelengths, the oxygen molecule plays a prominent role in determining the position of transmission windows. In the region of 60 GHz, the attenuation, shown in Figure IV-1, is very strong and provides a spectral region applicable for covert communications as discussed in Chapter 3. The zenith attenuation, shown in Figure IV-2, is extremely high with peaks of several of the O_2 lines at high altitudes affording additional attenuation. Because of these relatively narrow peak attenuations, communication from aircraft to satellites is limited in bandwidth to less that 80 MHz. It is seen from Figure IV-2 that the magnitude of the O_2 zenith attenuation is such that detection on the ground of 60 GHz communications between aircraft is virtually impossible. As a function of altitude, shown in Figure IV-3, the attenuation decreases significantly so that, at very high altitudes, propagation at frequencies between the individual lines of the O_2 complex suffers very little attenuation. To calculate the total attenuation from a particular

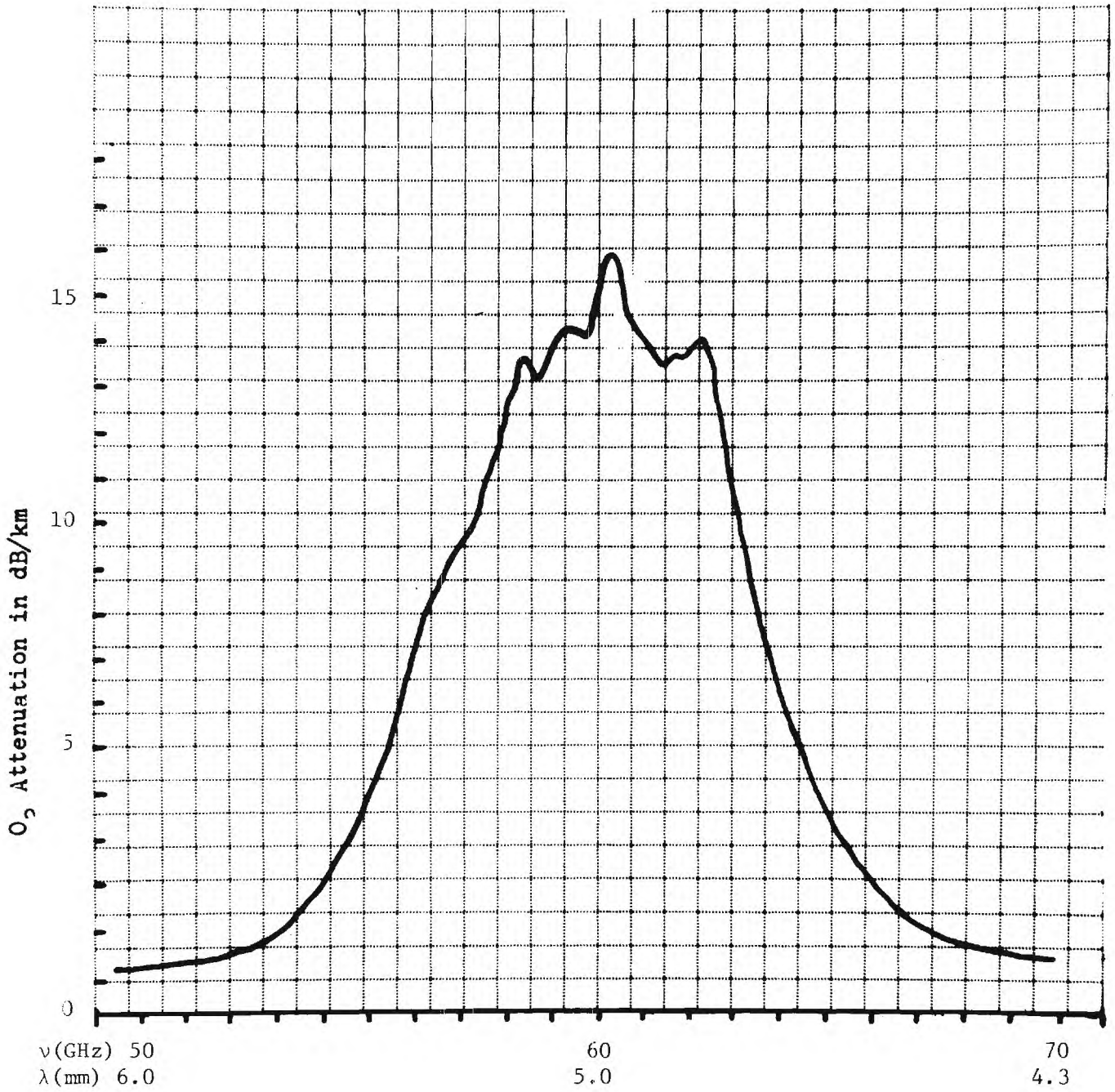

Figure IV-1. Attenuation Due to O_2 at Sea Level (f = 60 GHz)

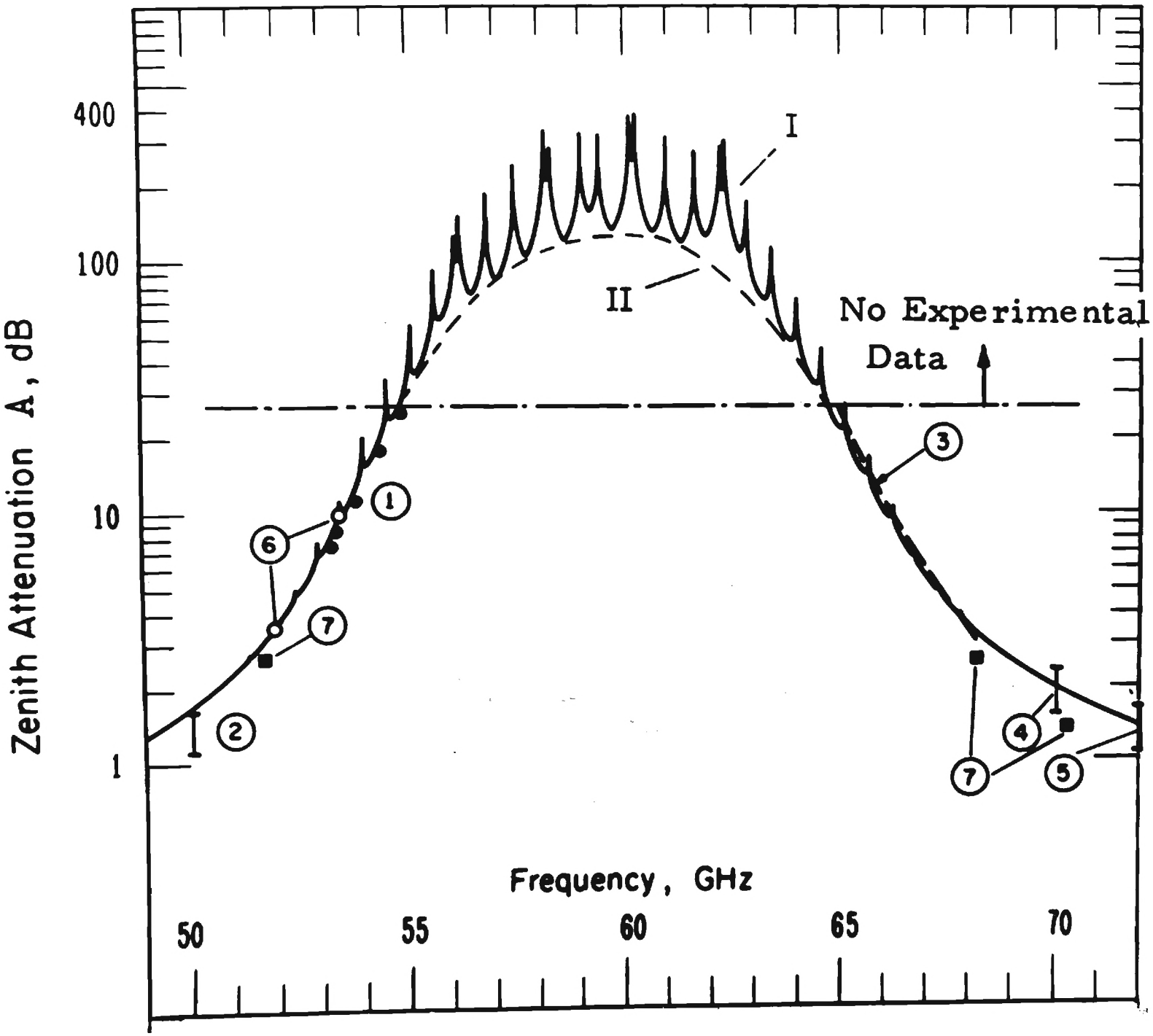
400
100
10
1
Zenith Attenuation A, dB
I
II
No Experimental
Data
1
2
3
4
5
6
7
7
Frequency, GHz
50
55
60
65
70

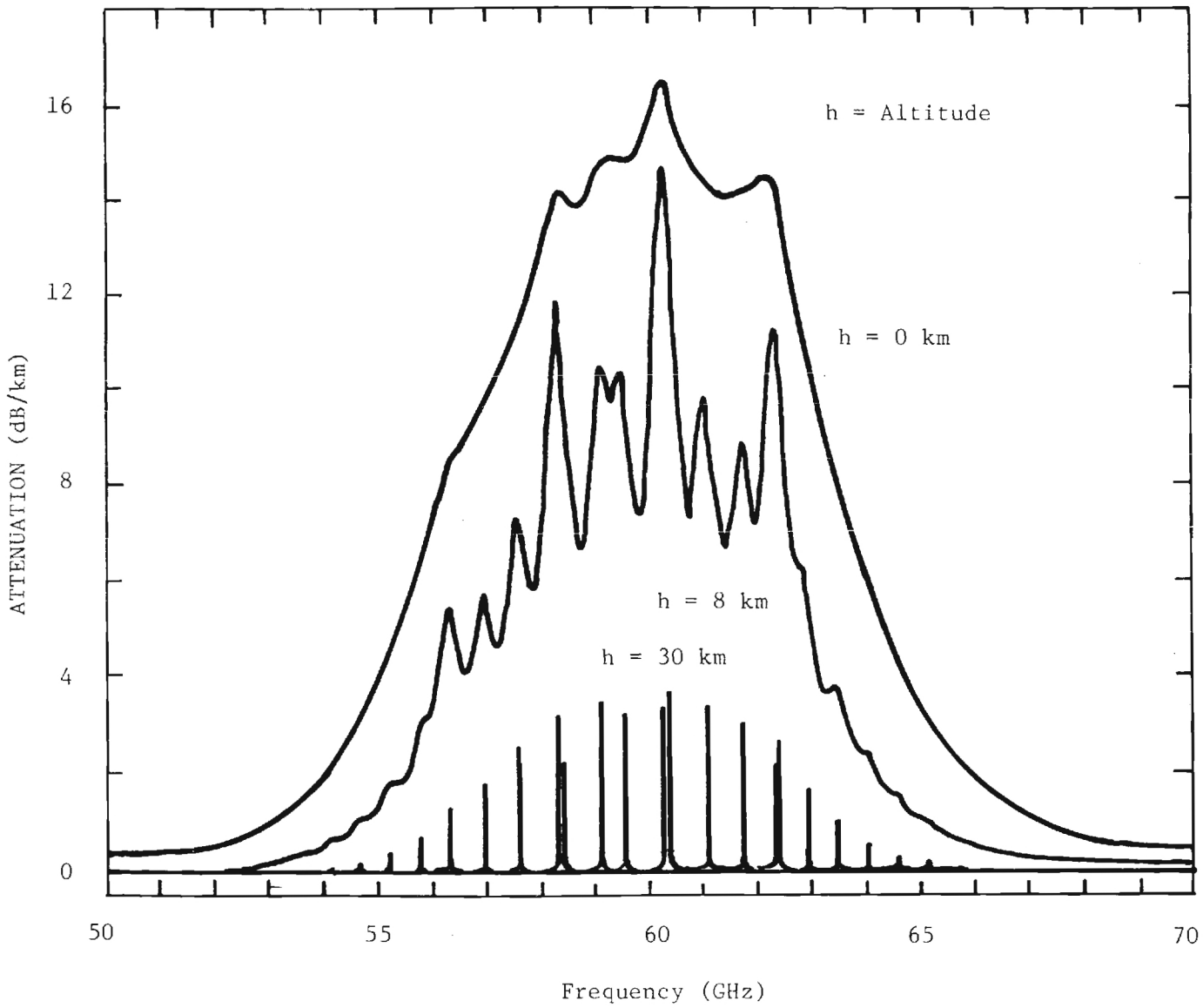

Figure IV-3. Attenuation Due to Oxygen as a Function of Altitude

altitude to a satellite, use can be made of curves such as that given in Figure IV-4 in which the abscissa is the lower altitude and the ordinate is the attenuation from this lower altitude up through the remaining atmosphere. In turn, the attenuation from ground to a given altitude can be determined for these O_2 curves by taking the difference of the attenuations for the altitude h and that for h = 0. Excellent treatment of atmospheric O_2 has been performed by Liebe [3] who has presented detailed data important for propagation applications.

In addition to its complex of lines at 60 GHz, O_2 has a strong individual transition at 118 GHz. In the atmosphere, these lines are superimposed on the water vapor lines with the resulting millimeter wave absorption shown in Figure IV-5. This figure presents the average atmospheric absorption of the millimeter wavelength in dB/km for sea level and 4 km altitude. Curve A at sea level is the long wavelength end, with O_2 included, of the absorption curves for the atmospheric H_2O given in Appendix V.

For computational purposes, the clear weather atmospheric attenuation has been presented in several forms, which in general are consistent but, for need of further experimental data, in detail variations can be noted. Some data are presented in Figures IV-6 through Figure IV-9 for use in calculating applications of a GW source, and for future use in determining the effects on millimeter/submillimeter propagation of high power signals. Figure IV-6 shows the zenith opacity of H_2O vapor as a function of the water density or mean zonal value. The total attenuation for one way transmission through the atmosphere is given in Figure IV-7. At the lower frequency end of the graph, the attenuation as a function of the angle from zenith is given. The total H_2O attenuation through the atmosphere without O_2 effects is given in Figure IV-8 for several frequencies as a function of elevation angle. With O_2 included, the total absorption at various millimeter region frequencies is given in Figure IV-9.

As wavelength decreases in the submillimeter region, the absorption increases drastically to values as high as 10^6 dB/km and not until wavelengths on the order of 20 μm are reached does the attenuation decrease so that horizontal transmission at sea level is possible (See the figure of Appendix V.) At the long wavelength end of the submillimeter region, six

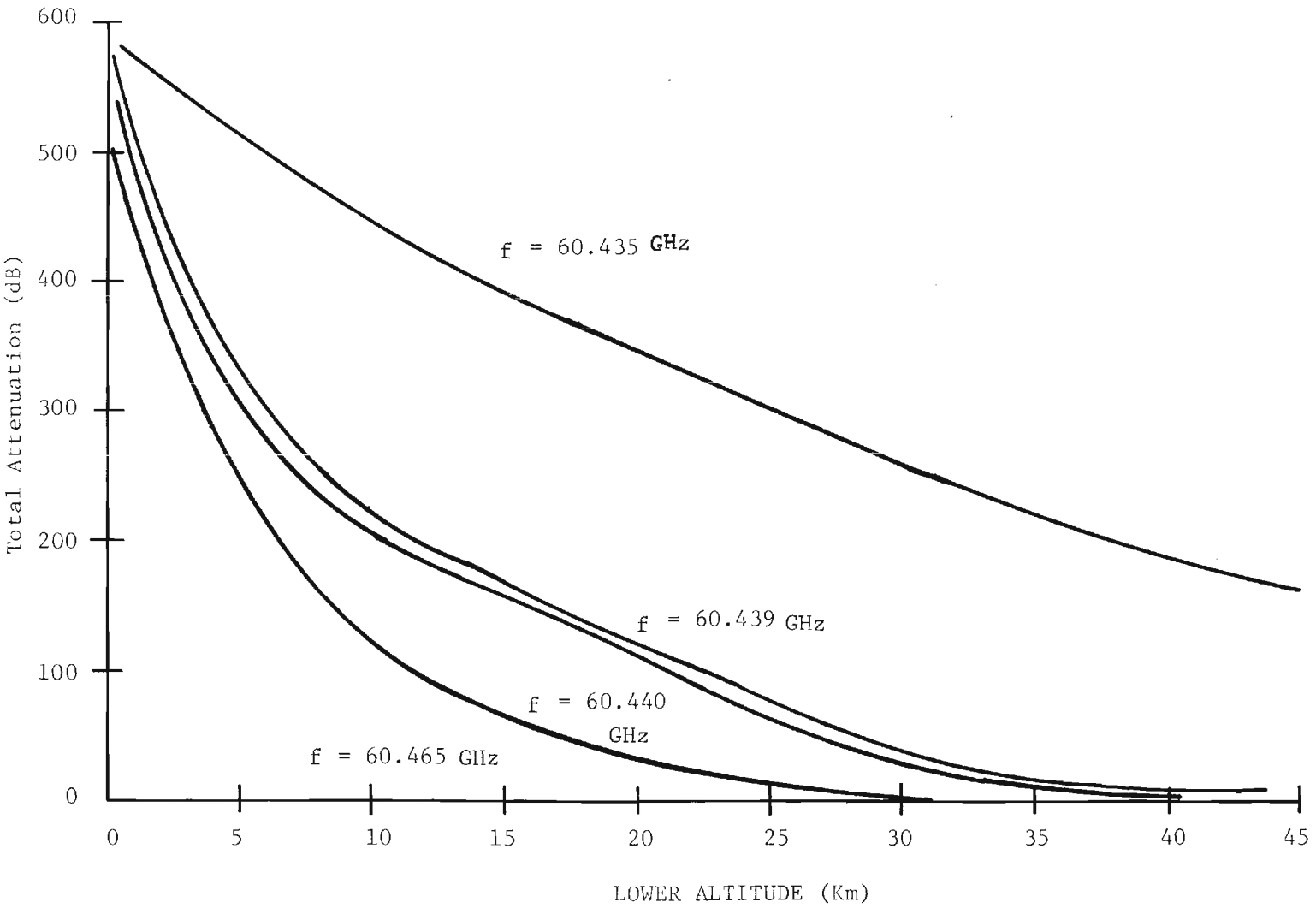

Figure IV-4. Atmospheric Attenuation Due to O_2 Lines From a Lower Altitude Through The Higher Atmosphere at 0° Zenith Angle

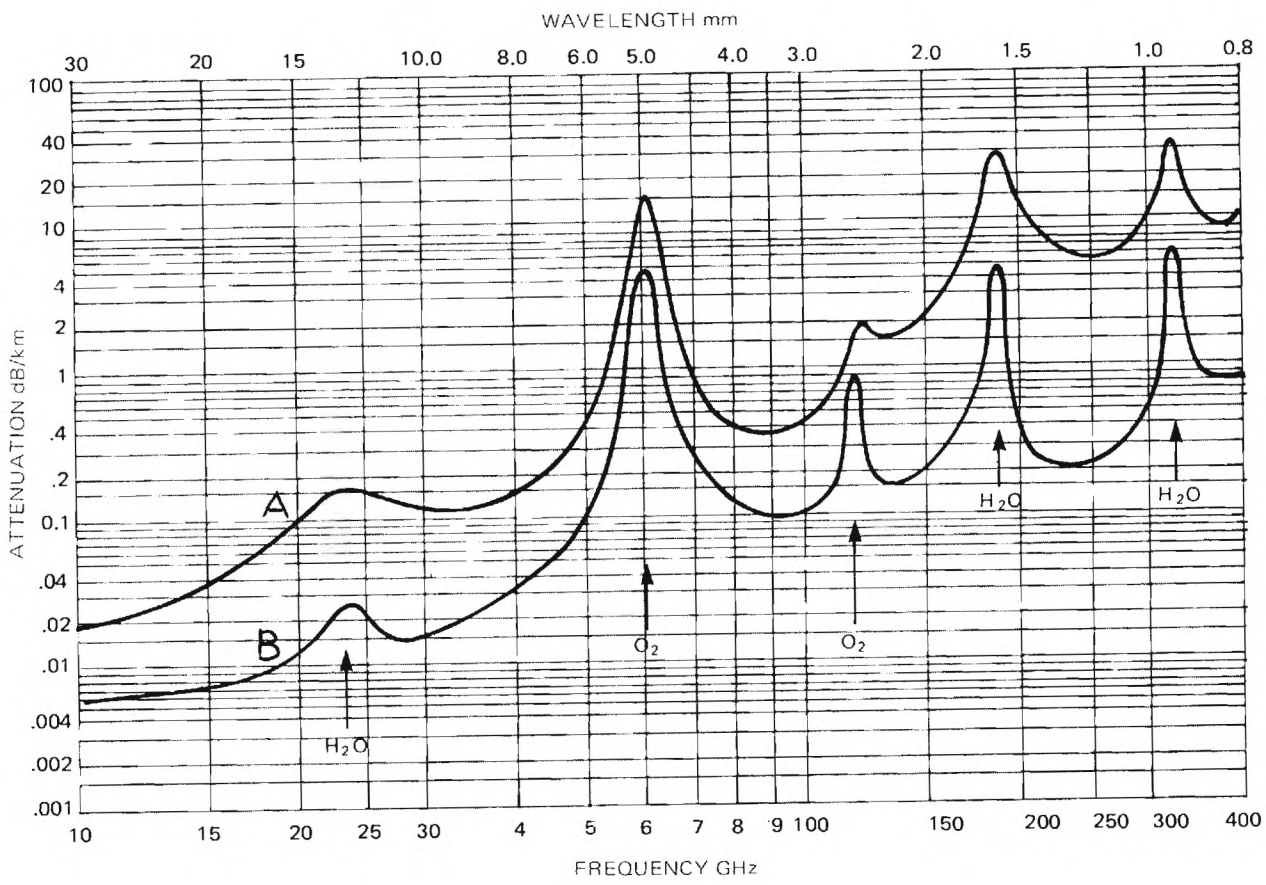

Figure IV-5. Average Atmospheric Absorption of Millimeter Waves. [4]

A: Sea Level
T = 20°C
P = 760 mm
P_{H_2O} = 7.5 gr/m^3

B: 4 km
T = 0°C
P_{H_2O} = 1 gr/m^3

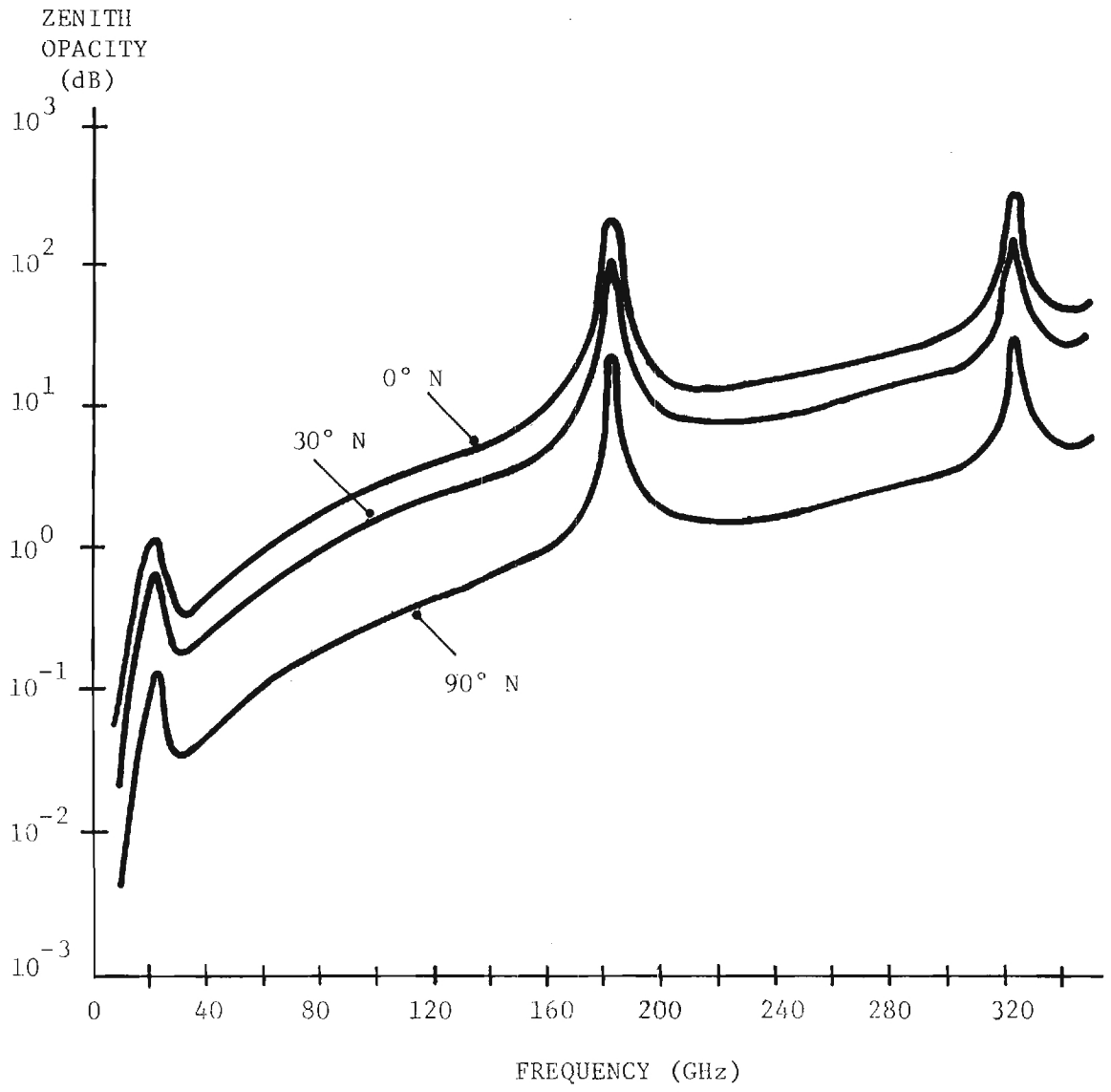

Figure IV-6. The opacity due to atmospheric water vapor between 10 and 350 GHz for 0.5, 2.5 and 4.5 gm/cm^2, corresponding approximately to mean zonal value at 0°, 30°N and 90°N. [5]

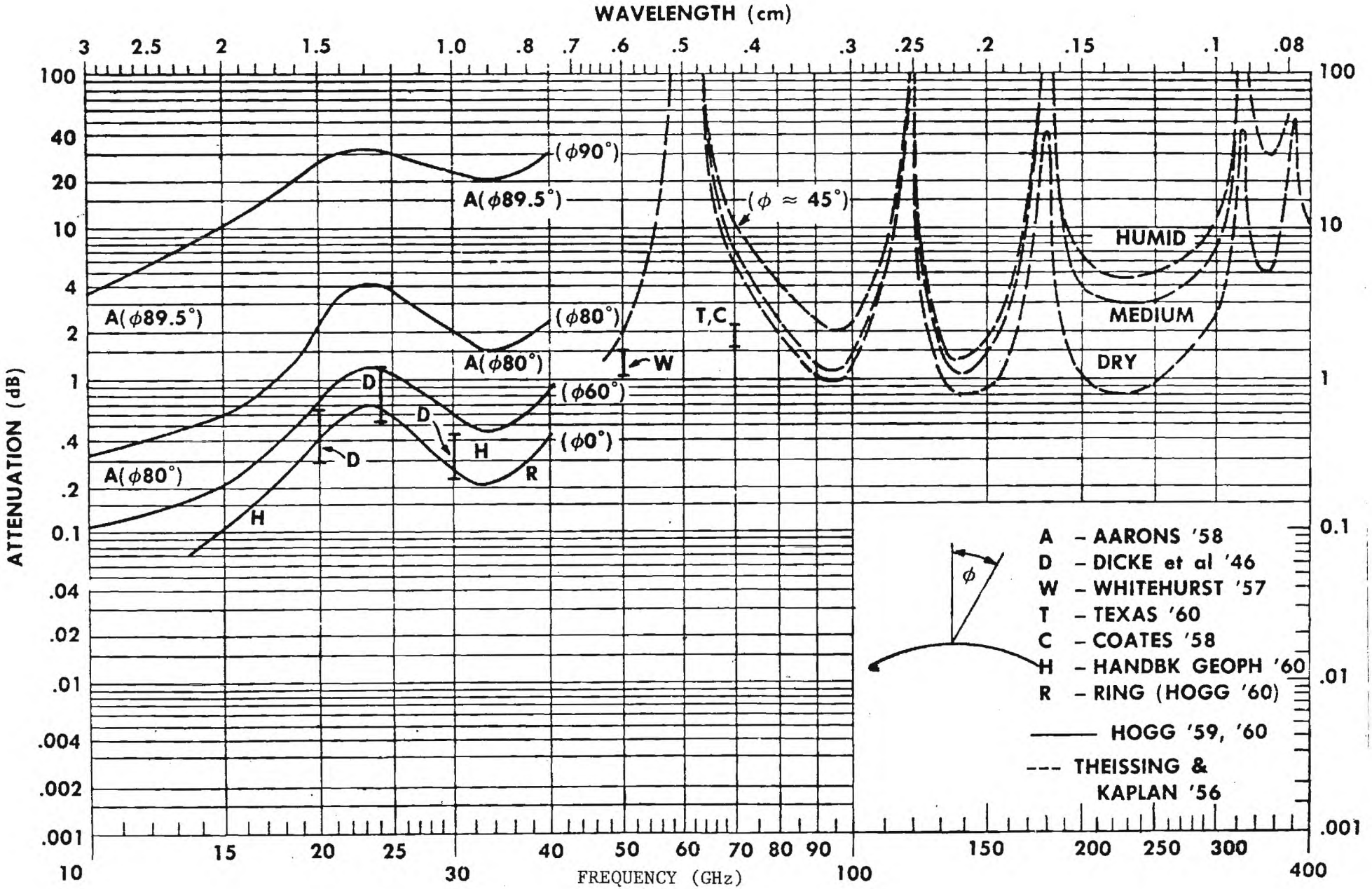

Figure IV-7. Total Attenuation For One-Way Transmission Through The Atmosphere [4]

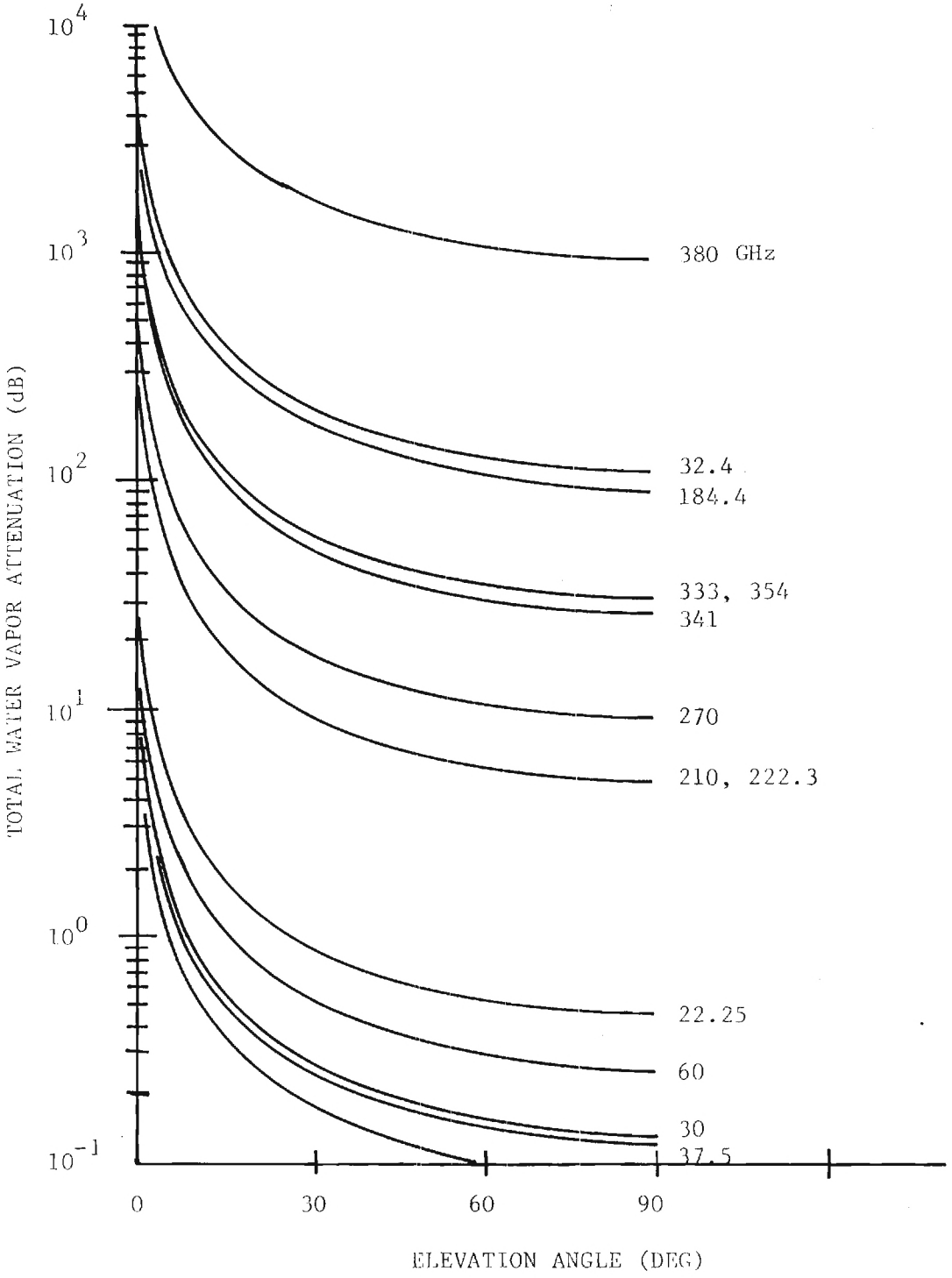

Figure IV-8. Total Water Vapor Attenuation Through Atmosphere as a Function of Elevation Angle

(ρ_{H_2O} = 7.5 g/m^3)

TABLE IV-1

MILLIMETER AND SUBMILLIMETER WAVE
ATMOSPHERIC TRANSPARENCY WINDOWS
($T = 300°K$, $P = 1$ atm, H_2O density = 7.5 $gm \cdot m^{-3}$)

Wavelength of Minimum Absorption (μm)	Absorption Coefficient (dB/km)
350	45
450	38
620	37
645	35
735	13
880	6
1350	5.5
2141	1.6
3190	0.37

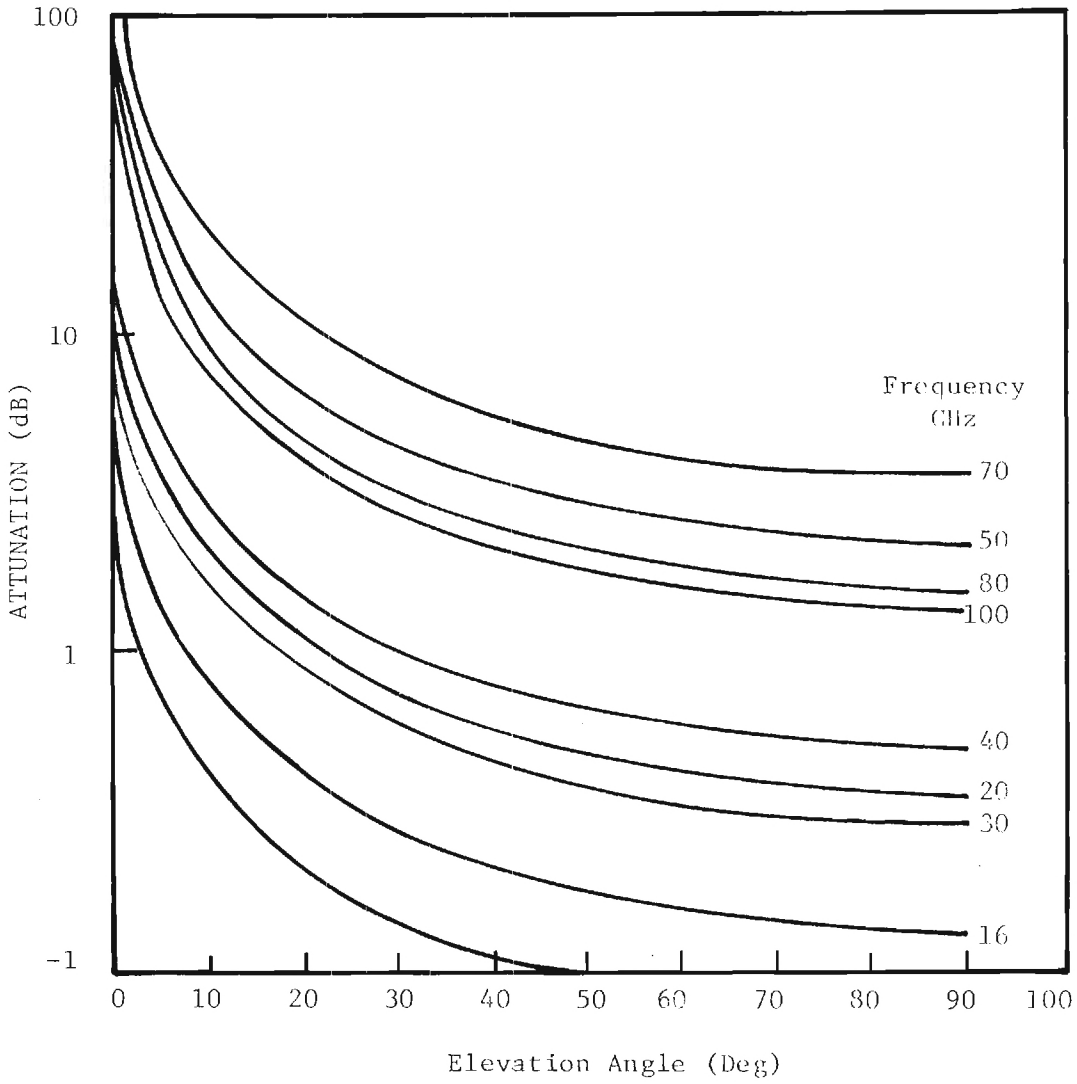

Figure IV-9. Total Absorption versus Antenna Angle for Paths Through The Atmosphere at Various Frequencies (P_o = 7.5 g/m^3).

transmission windows can be identified as possible regions for operation of a GW source. These windows, in addition to the millimeter wavelength windows at 1.35 mm, 2.14 mm and 3.2 mm constitute the major spectral operational points for applications, except in the case of covert uses in which high absorption wavelengths are employed. The submillimeter and millimeter wave transparency windows are given in Table IV-1, which lists the values as shown in References 1 and 4. Considerable differences exist in the results, both experimental and theoretical, which appear in the literature for submillimeter attenuation. The parameters at atmospheric pressure are considered standard for water density of 7.5 g/m^3 and I = 300°. In addition to the discrepancies which exist for these standard conditions, large variations in attenuation occur as a function of the humidity. This is shown in Figures IV-6 and IV-7, and, in addition, the zenith opacity at several millimeter frequencies is given in Figure IV-10. Several very useful curves are given by Webster [6] for temperature dependence of the absorption coefficient in the submillimeter wavelength region, for absorption in the windows at various altitudes as a function of humidity and temperature, and of the total zenith attenuation as a function of altitude and humidity. To show the variations which exist in the literature, Table IV-2 shows the attenuation, as given by various investigators, for the window regions of the millimeter and submillimeter wavelength regions (assumed ρH_2O = 7.5 g/m^3 and T = 300°K at P = 760 torr). It is interesting that the calculations of Webster [6] which is based on a simple model of 16 water lines is probably as reliable as most existing data on attenuation in the windows of the submillimeter region.

A number of studies have been made in the short millimeter and long submillimeter wavelength region on the atmospheric absorption. Despite these studies, further investigations are necessary under a variety of climatic conditions. Considerable submillimeter effort is currently under way in the Soviet Union with carcinotrons (see Appendix I) as the radiation source. The effects of water vapor absorption in the submillimeter wavelength region are indicated by the following comments.

The absorption is determined by the overlap of the large number of absorption lines which exist for the H_2O molecule. Figure IV-11 shows this

TABLE IV-2

Millimeter and Submillimeter Window Regions as Given by Various Investigators

Wavelength (μm)	Absorption Coefficients (dB/km) [1]	[6]	[4]	[7]	Miscellaneous Values
350	45	53		50	
450	38	47		50	
620	37	42		39	
645	35	35		40	
735	13	16		10	16
880	6	9	9	6	10
1350	1.4	-	5.5	1.0	2
2141	-	-	1.5		1
3190	-	-	0.37		

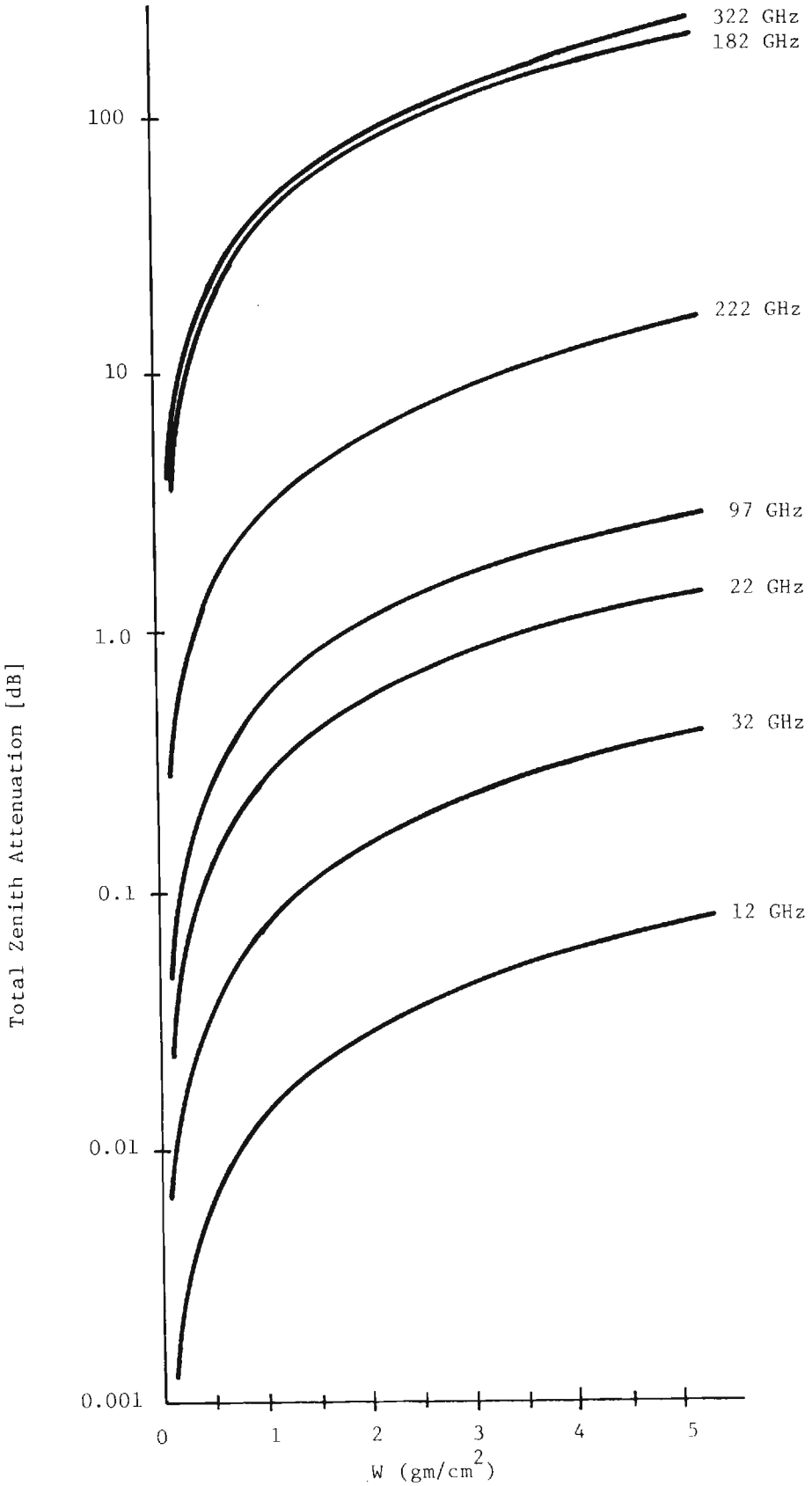

Figure IV-10. Atmospheric Opacity Due to Water Vapor Alone Versus Precipitable Water in Vapor Form For 12, 22, 32, 97, 182, 222 and 322 GHz. [5]

summation of lines. The importance of the $1_{-1} \rightarrow 1_1$, transition at approximately 0.52 mm can be seen from this summation of lines. The inclusion of mm O_2 transitions changes the absorption coefficient for $\lambda \simeq 2$ mm. Oxygen transitions exist in the submillimeter wavelength region, but these are too weak to change the submillimeter absorption significantly. Actually there is some evidence [7] that a slight contribution to the absorption on the short wavelength wing of the 0.73 mm window is made by the O_2 rotational line at 15.17 cm^{-1} (0.659 mm). Water isotopes D_2O and HDO are also weak absorbers throughout the long wavelength regions.

Detailed studies of individual lines and the spectral regions in their wings have been made. The investigations show the nature of absorption in the so called "windows". Figure IV-12 gives an indication of the absorption due to the 183 GHz line and in the important 1.35 mm window [8]. The more narrow line solid curve shows the absorption for the water vapor monomer line, the dashed line for the predicted water vapor dimer line and the third trace, the summation of the monomer and dimer absorptions. Experimental points on the figure show that investigations have been in agreement with both the monomer alone and the case of the monomer and dimer being present. It is important in making measurements in this spectral region that the conditions of the vapor (temperature, humidity, pressure, etc.) be accurately recorded; it is possible that lack of knowledge of all parameters involved is the source of the wide variety of values that exist in the literature. Fluctuations in intensity of signals have been measured at 110 GHz [9], and these results indicate a much stronger frequency dependence of the fluctuation level than can be attributed to refractive scintillation effects alone. Variations in the absorption over the path and the existence of dimers are considered as causes of the large observed fluctuations [9]. The same window at 1.35 mm is shown in Figure IV-13 with the absorption lines at 183 GHz and 321 GHz as calculated by various theoretical line shapes [10]. Experimental measurements fit the 183 GHz line well but yield high values in the other regions of the curve. Figures IV-14 through IV-16 show curves of other investigators for this wavelength region. All curves show a consistently higher absorption experimentally for the window regions than predicted by the theoretical

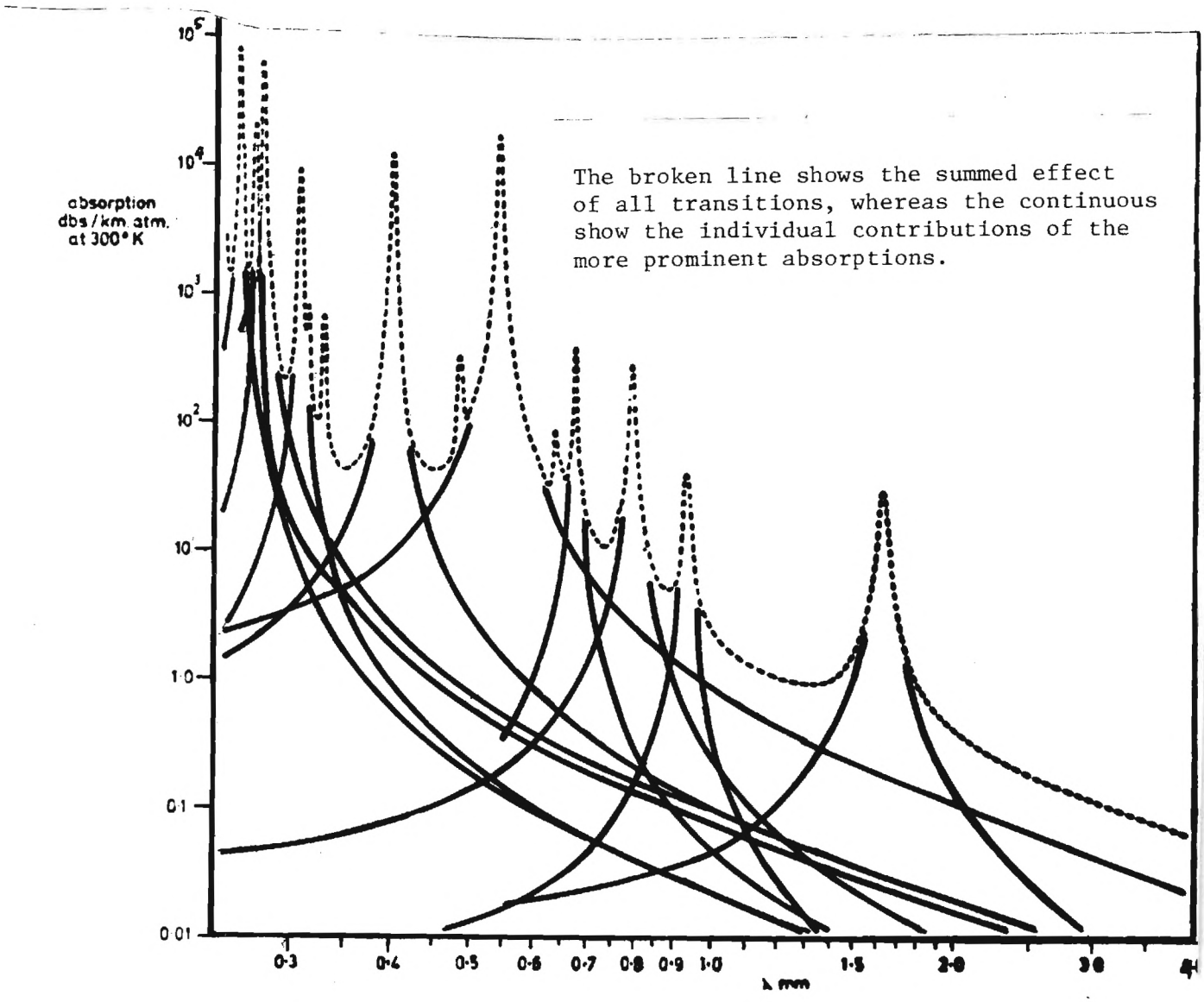

Figure IV-11. Absorption in dB/km for an atomsphere containing 7.5g of water vapor/m^3 at 300°K and normal atmospheric pressure. [7]

Heavy narrow line for water vapor monomers, dashed for dimer, broad line for monomers and dimers.

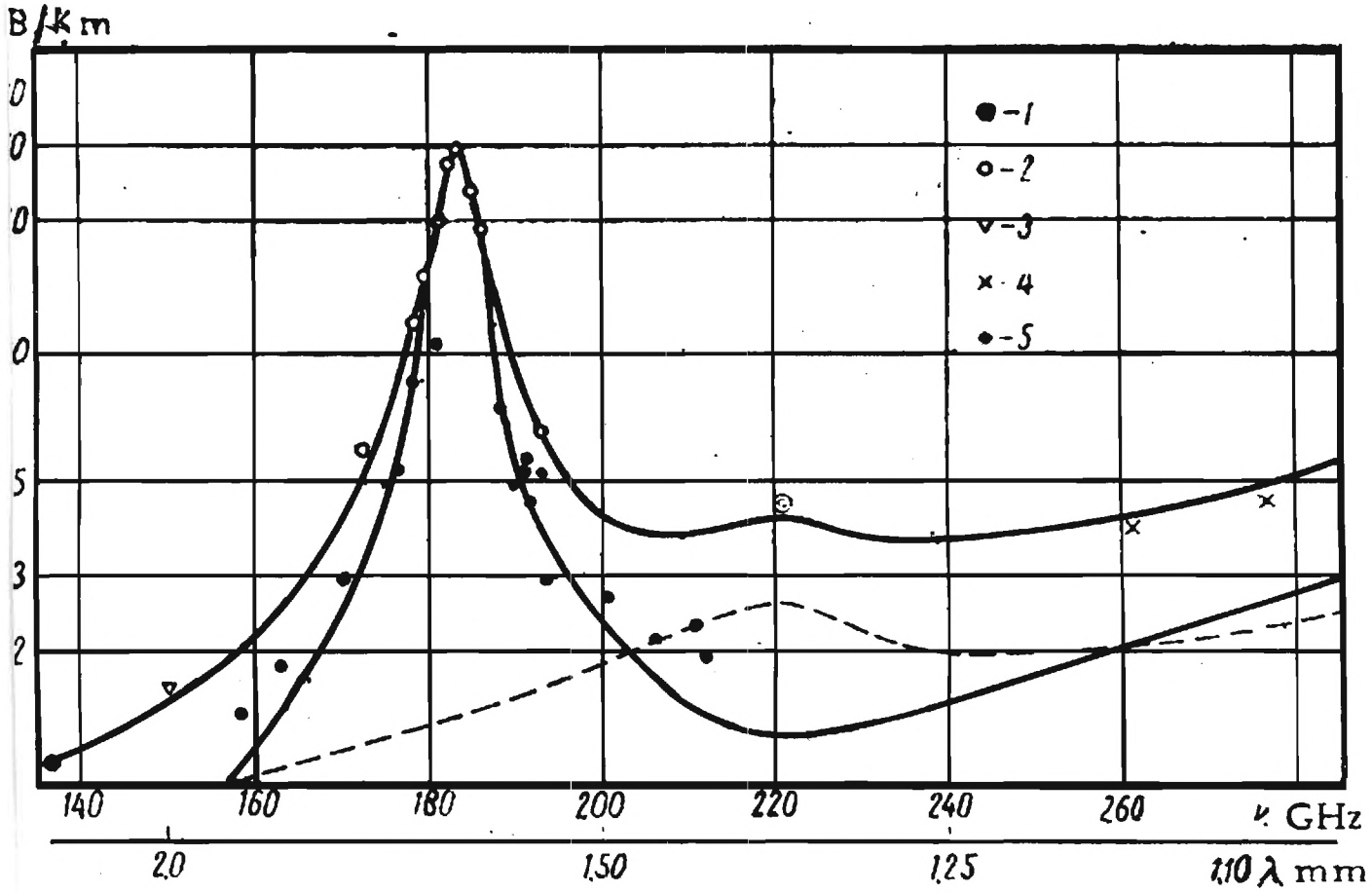

Figure IV-12. Computed and experimental data for absorption coefficients of 1-2 mm wavelength in water vapor at sea level (P - 7.5 gm/m^3). [8]

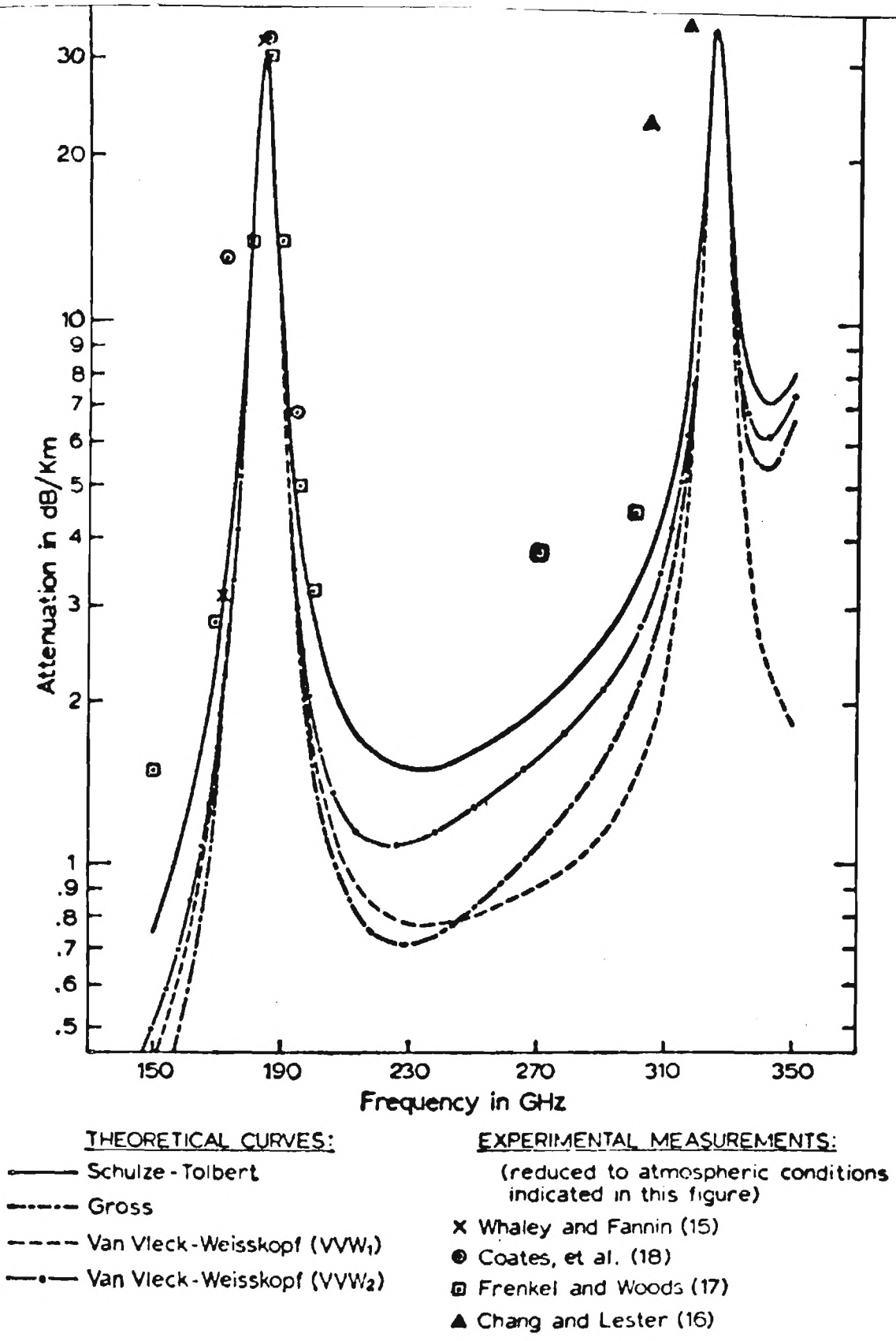

Figure IV-13. Atmospheric Attenuation at P = 760 torr, T = 300°K and ρ = 7.5 g/m^3. [10]

The continuous curve is the result of theoretical calculations.

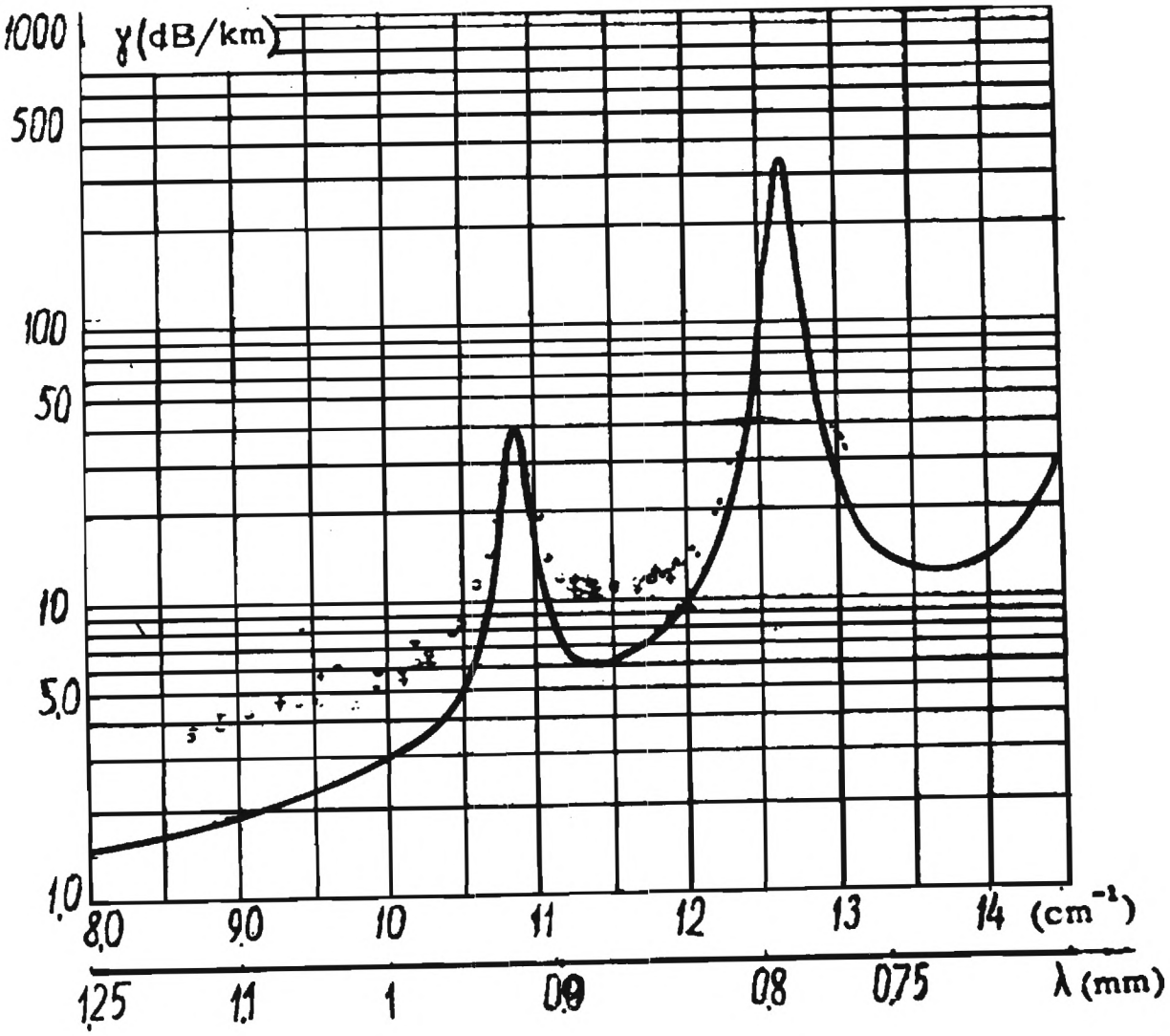

Figure IV-14. The absorption coefficient of atmospheric water vapor reduced to a standard humidity of $\rho = 7.5$ g/m^3 (P = 760 torr, T = 300°K). [11]

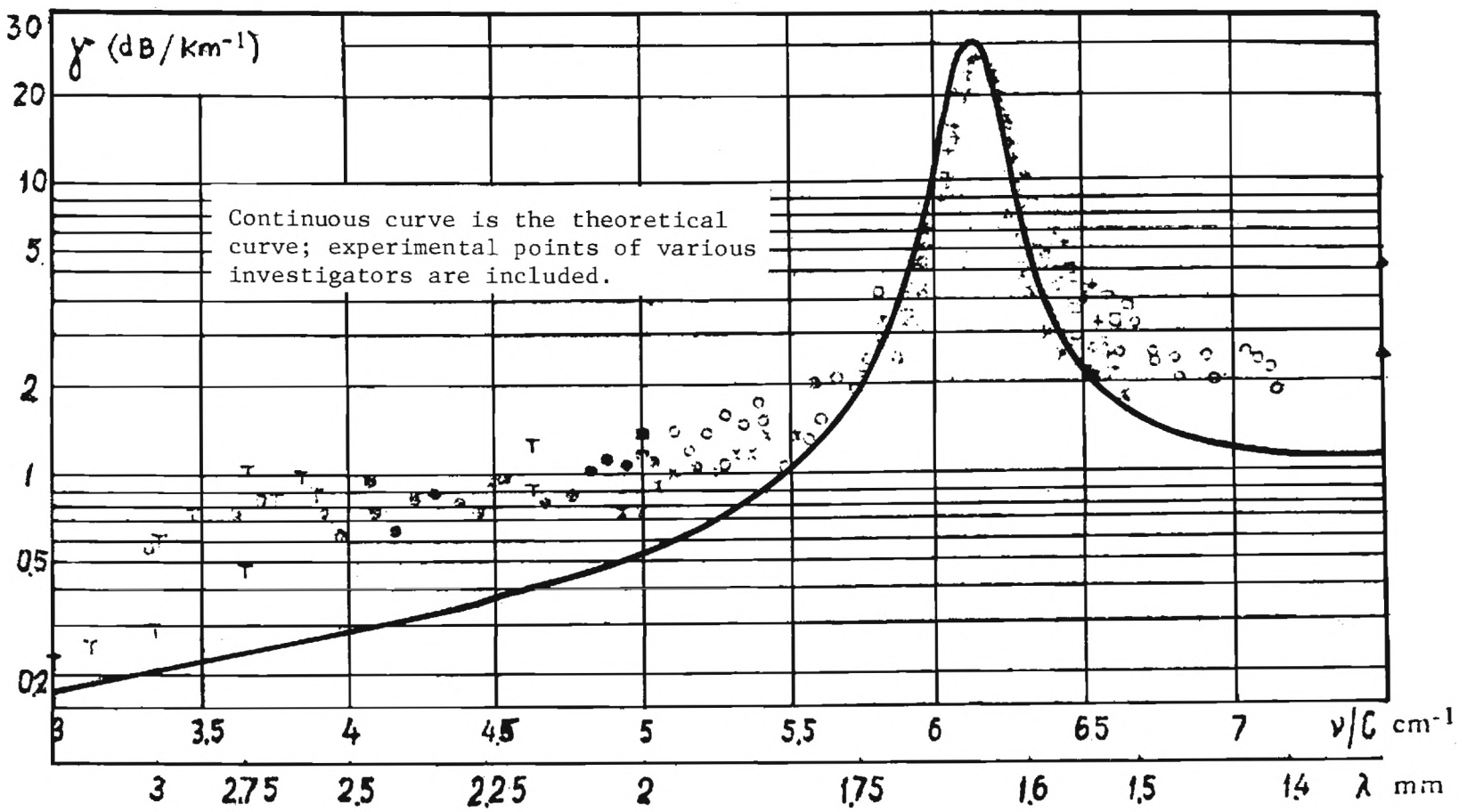

Figure IV-15. Absorption in atmospheric water vapor for wavelengths of 1.3 - 3.3 mm (T = 300°K, P = 760 torr, absolute humidity ρ = 7.5 g/m^4). [12]

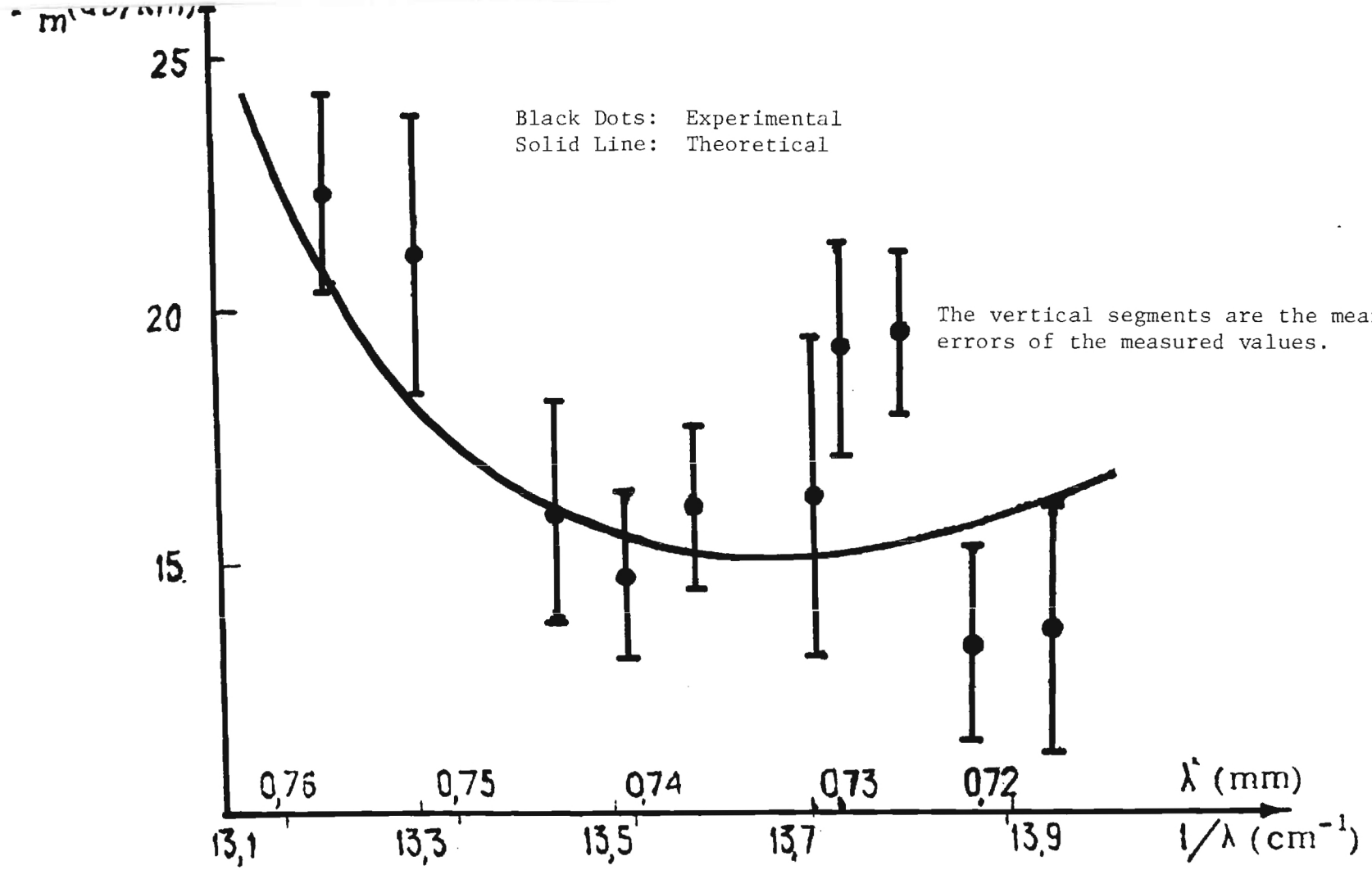

Figure IV-16. Experimental and theoretical values of the absorption co-efficient of H_2O monomers for $\rho = 7.5\ g/m^3$, $T_{AV} = 282°K$, $P = 750$ torr. [13]

calculations. In addition, the measured values shown in Figure IV-16 show far greater error bars than is acceptable for calculations associated with applications considered in the text of this report. An important molecular parameter, for which data are significantly lacking in the millimeter/submillimeter wavelength region, is the pressure broadened line width of the molecular transitions. The lack of these data is one of the sources of error in proving the correct theoretical line shape curve. It has been pointed out [7] that the least satisfactory agreement in submillimeter wave atmospheric investigations is in the atmospheric windows where the absorption is made up from the wings of adjacent absorption lines. In order to account for the remaining excess absorption measured in the windows near 1 mm, a number of mechanisms have been suggested. Among these is absorption due to dimeric water vapor [14]. Evidence continues to build up [15] in support of the dimer, but further work is necessary to identify completely the sources of excess absorption.

IV-2 Propagation Effects

The questions considered in this section are atmospheric breakdown, thermal blooming, and turbulence effects. Calculations will indicate that the three effects will not be serious problems for wavelengths near one millimeter. The breakdown field strength will be above expected field strengths for a radiated power of 10^9 Watts and antenna diameter of 1 meter or larger. For wavelengths near 1 centimeter and longer, the possibility of air breakdown must be considered carefully for sources radiating power greater than 10^9 Watt.

The effects of turbulence and thermal blooming are potential problems for high power lasers operating in the atmosphere. We show that at millimeter wavelengths the time for significant reductions in power due to atmospheric effects is of the order of 1 millisecond. This should not present a problem for pulsed systems. Turbulence effects are also greatly reduced at these wavelengths. The effects of thermal blooming and turbulence diminish as the wavelength increases.

IV-2a Atmospheric Breakdown

For situations where high peak powers will be radiated, the possibility of atmospheric breakdown due to the high electric fields must be considered. The treatment of the problem in this section was developed for analysis of nanosecond pulse radars. The breakdown condition was defined as a situation where scattering of the beam energy became significant. Scattering of the beam energy is a relatively early event in the growth process by which the initial ion-electron pairs multiply and visible arcing occurs. This definition leads to a frequency dependence for the breakdown field.

Experimental data for the effective breakdown field strength as a function of pressure and pulse length [16] was combined with pressure-altitude data to calculate the breakdown field strength versus altitude and pulse length. The rms field strength at breakdown for frequencies of interest is then determined by applying a frequency correction term. This term includes a pressure and field dependent collision frequency.

The resulting curves for the breakdown field versus altitude for various pulse lengths at 366 GHz (820 μm wavelengths) are shown in Figure IV-17. The variation in breakdown field with pulse length covers pulse lengths from one nanosecond to 100 nanoseconds.

The breakdown field strength can be compared with the radiated field strength from a source of 10^9 watts radiating from a vertically pointing antenna. The antenna diameter was taken to be 60 cm giving a beamwidth 0.1°. The peak rms field at the antenna is 1.2×10^4 V/cm which is below atmospheric breakdown. The peak field increases as the square root of the radiated power and decreases with increasing antenna diameter.

We conclude that for pulse lengths and peak powers of interest, breakdown in the near and far fields of the antenna will not occur. Furthermore, previous work [16] indicates that this conclusion is valid for microwave frequencies also.

At 3 GHz for power levels of 10^{11} Watts, regions will appear where the radiated field surpasses breakdown field strengths for 10 nanosecond pulses at beamwidths of 0.1°. This radiated power level is above values considered in this study.

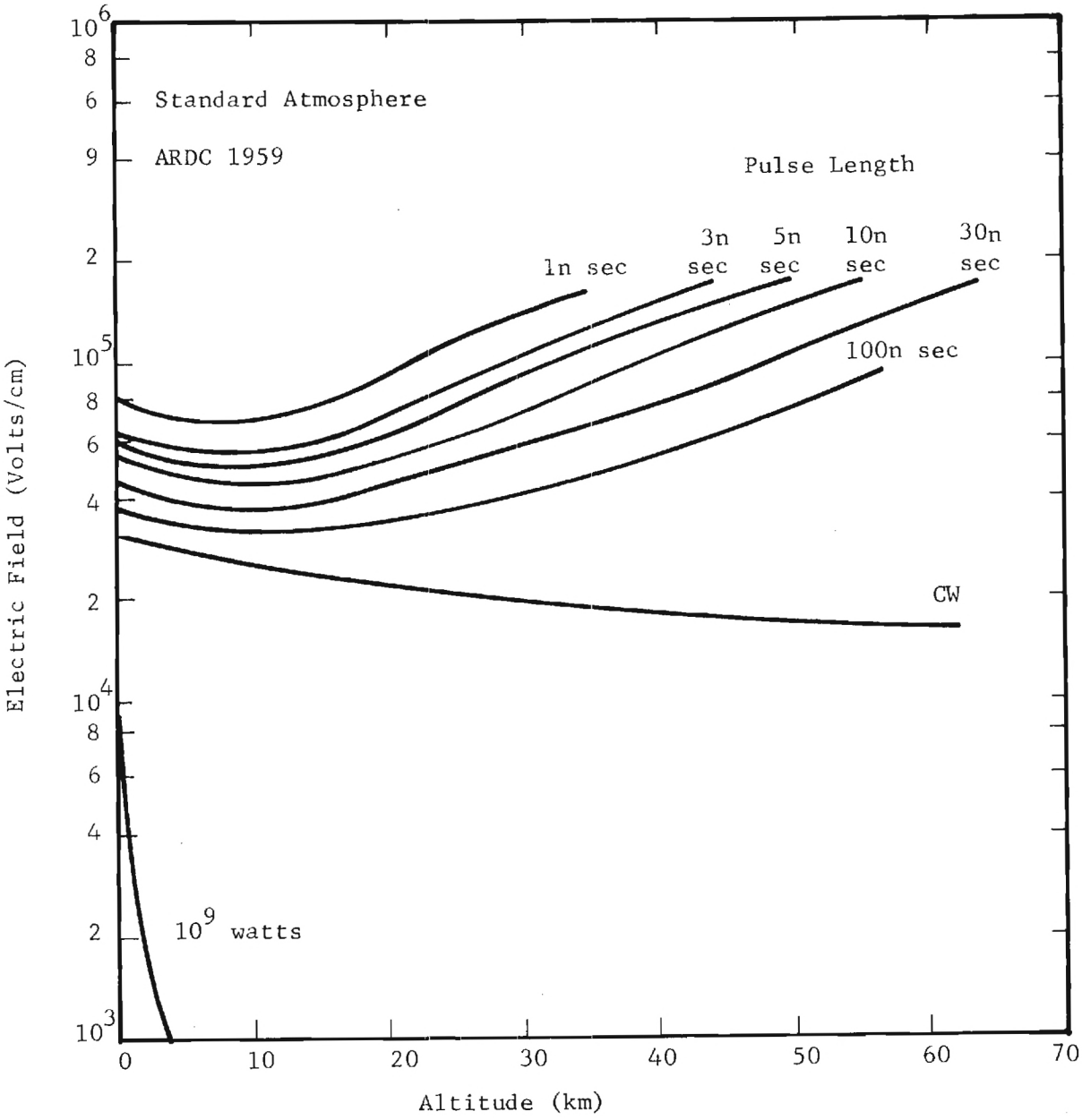

Figure IV-17. Electric field strength at breakdown vs. altitude for various pulse lengths at 366 GHz. (The electric field produced by a 60 cm antenna radiating 10^9 W vertically is shown for comparison.)

IV-2b Thermal Blooming

An intense beam of radiation passing through an absorbing medium will experience a distortion of the irradiance profiles arising from the changing index of refraction of the medium. This effect is referred to as thermal blooming of the beam. The details of the process depend strongly on beam geometry, and the energy transfer within the medium. The problem has been treated theoretically for specific conditions using various simplifying assumptions in order to obtain a manageable theoretical model.

For an atmosphere that is homogeneous, with no convection, the problem can be expressed in terms of linearized hydrodynamic equations. For any beam profile, there are two limiting cases for which tractable expressions for the change in intensity may be calculated. For times short compared to the sound transit time (the time required for a sound wave to traverse the beam radius) the ratio of the on-axis intensity of the distorted beam to the on-axis intensity of the undistorted beam in the focal plane can be written as [17]

$$I/I_o = 1 - \delta_o(E/E_f)(t^3/t_p t_f^2) \tag{1}$$

where δ_o is a numerical parameter with a value approximately 0.30.

For times long compared to the sound transit time, the on-axis intensity for a parabolic beam profile can be written in the form [18]

$$I/I_o = 2/(\cosh\ \mu z\sqrt{t}\ )^2 \tag{2}$$

In these expressions, I represents the beam intensity at the point considered and I_o the initial intensity before blooming occurs. E is the beam energy, t_p is the pulse length, and t is the time. The time t_f is related to the sound transit time across the focal radius of the beam and is given by

$$t_f = f/kac \tag{3}$$

where f is the focal length, k is the propagation constant equal to $2\pi/\lambda$, a is

the beam radius, and c is the speed of sound in the medium.

In equation (1),

$$E_f = \pi c^2/[(3N/2)(\gamma-1)\alpha k^2], \tag{4}$$

where N is the refractivity and γ is the ratio of specific heats.

In equation 2,

$$\mu = \left[\frac{2}{3} \frac{(n^2-1)(n^2+2)}{n^2} \quad \frac{3\beta c^2}{2C_p} \quad \frac{1}{a^2 t_c} \right] 1/2 \tag{5}$$

where n is the index of refraction, β is the volume expansivity, C_p is the specific heat at constant pressure, and t_c is a characteristic time required for the laser beam to cause a density change of a monatomic perfect gas equal to the original density. This time is given by the following expression:

$$t_c = 3\pi a^2 \rho_o c^2/2\alpha P \tag{6}$$

In this expression, ρ_o is the initial density of the medium, α is the absorption and P is the beam power equal to E/t_p.

Numerical values for the atmospheric constants and the beam properties assumed for these calculations are given in Table IV-3, along with values for several characteristic times and parameters. The sound transit time for the assumed conditions is 1.5 milliseconds. We are interested in calculating the time required for a significant reduction in beam intensity using the short and long time approximations. In both cases, the calculated times are close to the sound transit time, but significantly greater than the value assumed for the pulse length.

In the short time approximation, the time required for the on-axis intensity to drop by 50% is obtained from Eq. (1)

$$T_{1/2}(s) = (t_p t_f^2 E_f/2 \delta_o E)^{1/3} = 0.7 \times 10^{-3} \text{ sec.}$$

TABLE IV-3

ATMOSPHERIC AND BEAM PROPERTIES FOR
THERMAL BLOOMING CALCULATIONS

$n = 1 + 2.9 \times 10^{-4}$	$C_p = 994\ J\ kg^{-1}\ °C^{-1}$
$\alpha = 2.1 \times 10^{-3}\ m^{-1}$	$\rho_o = 1.29 \times 10^{-3}\ g/cm^3$
$\beta = 36.7 \times 10^{-4}\ °C^{-1}$	$\mu = 6.6 \times 10^{-2}\ m^{-1}\ sec^{-1/2}$
$c = 331\ m/sec$	$t_c = 0.65\ sec$
$P_o = 10^9\ W$	$f = 1\ km$
$a = 50\ cm$	$\lambda = 870\ \mu m$
$E_o = 50\ J$	$t_p = 50 \times 10^{-9}\ sec$
$k = 72.2\ cm^{-1}$	$t_f = 8.37 \times 10^{-4}\ sec$

A value near 1 millisecond is obtained for a pulse of 10^9 watts at a distance of 1 km. In the long time regime, the time required for the on-axis intensity to drop by 50% is found from Eq. (2). Again, for a range of 1 km, we obtain

$$T_{1/2}(1) = 0.4 \times 10^{-3} \text{ sec.}$$

These values for the short and long time approximations are near the sound transit time of 1.5×10^{-3} seconds, a reasonable result considering the approximations required.

We conclude that thermal blooming of intense beams of radiation at millimeter wavelengths is characterized by times in the millisecond range ϕ for the parameters considered here. For pulses significantly shorter than 1 millisecond, the effects of thermal blooming should be minimal.

Atmospheric absorption is significant in the extreme infrared-submillimeter wave region. For both shorter and longer wavelengths, regions of reduced absorption occur where the heating effect of the radiation will be diminished, with a corresponding reduction in distortion caused by thermal blooming.

IV-2c Turbulence Effects

The effects of atmospheric turbulence on laser beam transmission have been treated experimentally and theoretically by several authors. The turbulent atmosphere is considered to be an inhomogeneous medium in which the refractive index is a function of time and position. As such, it is considered as consisting of a large number of regions over which the refractive index deviates from the average. These deviations result from fluctuating masses of air at different temperatures. The dimension of these regions, called eddies, are bounded by a microscale ℓ_o and a macroscale L_o characterized by refractive-index variance

$$\langle \delta n^2(\ell) \rangle \simeq C_n^2 \ell^{2/3}$$

The parameter C_n^2 is the refractive index structure constant. It can vary with location, altitude, and time, and is a measure of the intensity of the atmospheric turbulence.

The presence of turbulent air in the transmission path of a laser signal causes random variations in the amplitude and phase of the signal. Davis [19] lists six effects which tend to degrade the performance of a laser system. The effects are beam steering, image dancing, beam spreading, image blurring, scintillation, and phase fluctuations. Quantitative treatments of turbulence are based on the work of V. I. Tatarski [20]. Tatarski, using a perturbation theory approach, has predicted an amplitude correlation function characterized by a correlation length given by $(L/K)^{1/2}$ with no appreciable correlation beyond this value. Here L is the propagation distance through the turbulence region and k is the optical wave number. Tatarski's results suggest that fluctuations in amplitude and phase may increase without bound. Experimentally, it has been found that there is an upper bound to these fluctuations.

With the assumption that the amplitude variations obey a log-normal distribution, Tatarski derives the following relationship for the fluctuation

in the logarithmic level of the amplitude

$$X_A^2 = \langle(\log A/A_o)^2\rangle = 0.31/C_n^2\ k^{7/6}\ L^{11/16} \qquad (1)$$

The fluctuation in the logarithmic level of intensity is related to that in amplitude by $X_I^2 = 4X_A^2$. Equation (1) holds for $L_o >> (\lambda L)^{1/2} >> \ell_o$.

An idealized quantitative treatment of the effects of a turbulent atmosphere as reflected in the amplitude and phase fluctuations of the transmitted wave would require a solution of the wave equation with appropriate boundary conditions. This problem has not been solved.

For calculations, we take a value of C_n appropriate to strong turbulence, $C_n = 5 \cdot 10^{-7} m^{-1/3}$. The resulting values for turbulence caused fluctuations will correspond to worst case conditions.

For wavelengths in the millimeter range, we find that turbulence related effects are minor. As an example, we calculate the lateral phase coherence length for the case of strong turbulence.

Under turbulent conditions, a variation in phase will exist between points separated a distance ρ in the receiver plane. We define the lateral phase difference over points separated a distance ρ_o to be π. When ρ_o is small compared to the beam diameter, the source no longer appears to be coherent. We determine ρ_o from the relation [20].

$$\rho_o^{5/3} = \lambda^2/2.92\ C_n^2\ R \qquad (2)$$

with λ being the wavelength and R the turbulent path length. For radiation of 870 μm wavelength and a turbulent region of length 5 km, we obtain

$$\rho_o = 25 \text{ m}$$

This value is sufficiently large for a severe worst case situation to indicate that turbulence will not be a problem. For longer wavelengths, the degradation in phase coherence as a result of atmospheric turbulence decreases. The lateral coherence length increases with wavelength as shown in equation (2).

IV-3 Hydrometeorological Effects

Precipitation, haze and fog have deleterious effects on propagation in the millimeter and submillimeter wavelength regions. Rain attenuation presents one of the most perplexing problems encountered in the design and operation of millimeter wave propagation systems. Recent interest in millimeter and submillimeter applications has resulted in both experimental and theoretical investigations. Radiometry and satellite propagation studies have yielded direct measurement of attenuation for $\lambda > 1$ cm [21]. Observations are being made to acquire long term statistics at a number of frequencies in the millimeter region and at different locations.

The attenuation due to a distribution of spherical raindrops is

$$A(\mathrm{dB/km}) = 4.343 \iint N(a)\ Q(a,\lambda)\,da$$

where $N(a)da$ is the number of drops per cubic meter with radii between a and a + da(cm), and $Q(a,\lambda)$ is the attenuation cross section (m^2) of a single spherical drop of radius a(cm) at wavelength λ(cm).

The relationship between raindrop size and rainfall rate was investigated empirically by Laws and Parsons [22] and later distributions were developed by Marshall and Palmer [23]. They showed that drop size distribution measurements can be represented by the relation

$$N(a) = N(o)e^{-\Lambda a}$$

where N(o) = value at zero radius and $\Lambda = 82\ R^{-0.21}$ where R is the rainfall rate, in mm/hr.

Medhurst applied measured drop terminal velocities and measured Laws and Parsons drop size distribution to calculate the attenuation coefficient for 2 to 100 GHz.

Gunn and East [24] have proposed an exponential expression relating attenuation and rainfall rate,

$$A(\mathrm{dB/km}) = \alpha R^{B}$$

where α and B are frequency dependent constants, and R as above is the rainfall rate (mm/hr). This expression has shown reasonably good agreement with measured values over short terrestrial paths.

The probability of occurrence of a given attenuation level, or more precisely, the probability that the attenuation has equaled or exceeded a given level, is extremely important for the design of systems where rain attenuation plays a significant part. A knowledge of this factor provides the basis for the power margin requirements for the link or conversely will indicate the expected outage time for a given link margin.

An important aspect of satellite communications is the need for spatial diversity. Only a limited amount of diversity gain data exists for millimeter wavelength earth-space propagation paths [21]. The diversity gain is defined as the difference between the path attenuations associated with the single terminal and diversity modes of operation for a given percentage time. The diversity gain is a function of the single terminal fade depth as well as the terminal separation distance.

In the case of attenuation due to absorption and scattering by hydrometeors, several extensive calculations have been carried out. Figure IV-18 shows the variation of attenuation in dB/km with frequency for various rainfall rates, as determined by Setzer [25]. The only significant difference among the results of the various authors occurs in the calculation of attenuation for low rainfall rates, on the order of 0.25 mm/hr. At frequencies approaching, or greater than, 100 GHz, depending on the rain intensity, the rate of increase of specific attenuation with frequency levels off and, at even higher frequencies, the attenuation declines. Measurements made at 110 and 890 GHz [26] show general agreement with these predictions, but, probably owing to inadequate particle size distribution measurements, the attenuation at 890 GHz was found to exceed that at 100 GHz by a factor of 1.25.

Detailed calculations of attenuation due to fog have been made by Ryde and Ryde [27], and some of these results appear in Strom's report [28]. In particular, Figure B-7 of Strom's report is important for fog of various visibilities and cloud attenuation. The Appendices of Reference 28 treat

several propagation parameters and show the need which must be filled at shorter millimeter and submillimeter wavelengths. Luke [29] has given a detailed discussion of the submillimeter region propagation problems. In Section 6.1, comparison of imaging systems at several wavelengths in a fog has been discussed. This has been based upon the results of Kruse. The importance of submillimeter attenuation measurements in fog, rain, and snow is evident from the extensive Russian literature that continues to expand.

The transmission through clouds, similar to fog, has been discussed in the above references. In addition, the effects of cloud formation on airborne radiometric measurements have also been investigated [5]. Figure IV-19 shows the absorption by ice clouds from a Rayleigh approximation. The effects of ice clouds are relatively small until wavelengths of approximately 300 μm are reached. Water clouds, on the other hand, show considerably more absorption, as indicated in Figure IV-20 but, at millimeter wavelengths, transmission is far greater than it is in the infrared [30]. The scattering and extinction coefficients for low lying stratus clouds have been calculated and compared with Staelin's empirical formula. This is shown in Figure IV-21. The advantages of millimeter and submillimeter transmission over infrared transmission through clouds are evident in these curves.

In order to utilize the REB devices properly, detailed atmospheric propagation experiments are extremely important. Extimates from existing data can be made, but more investigations are necessary when actual applications of the devices are initiated. Backscattering of millimeter wave signals has been experimentally investigated [31], but the level of effort did not permit detailed analysis. Because of the high intensity of the REB sources, further backscatter and forward scatter measurements are necessary at several wavelengths. The role played by propagation parameters in the design and performance of a military system dictates that more complete information on transmission of electromagnetic waves be available for both clear and inclement weather.

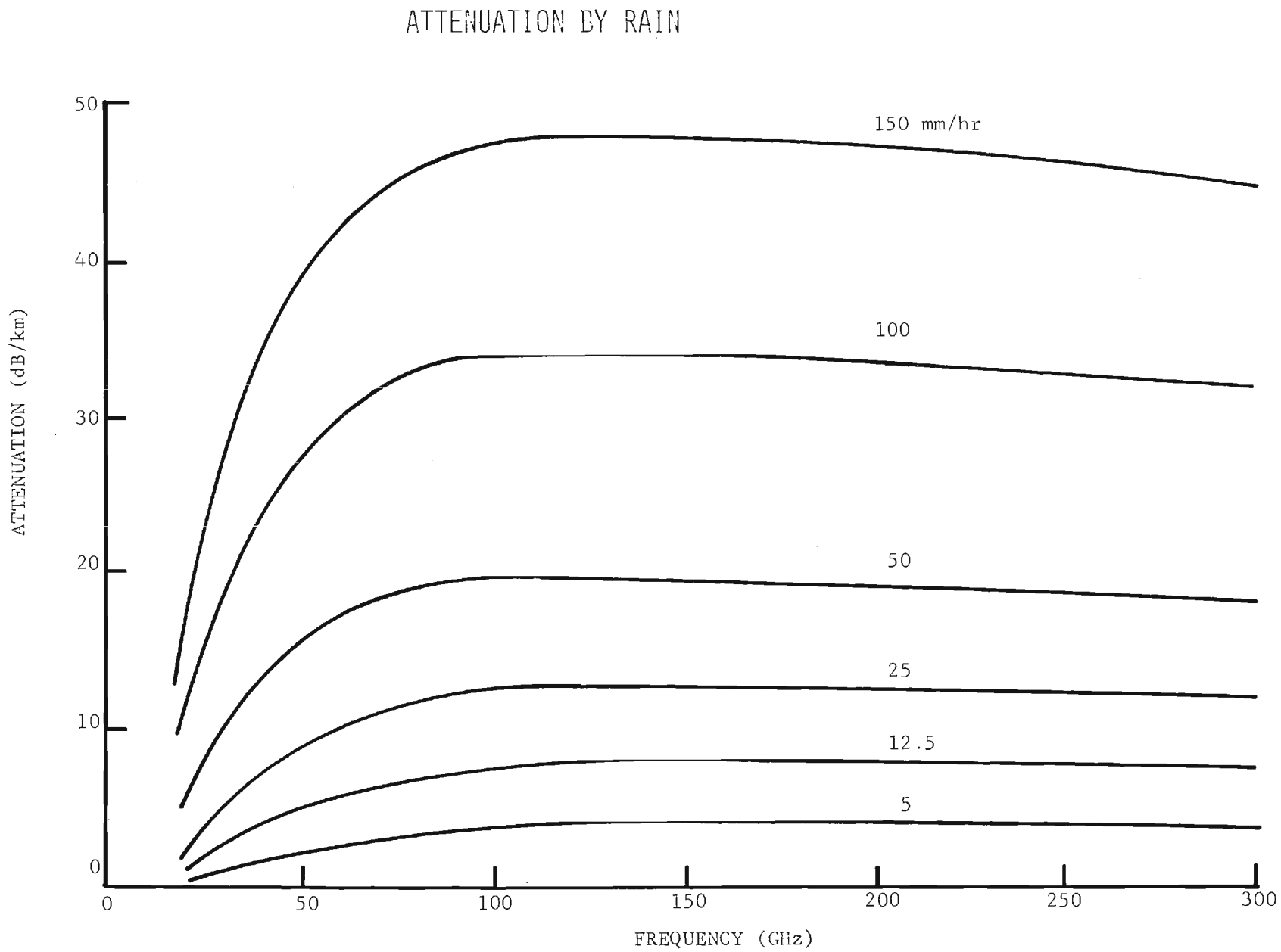

Figure IV-18. Variation of attenuation in dB/km with frequency for various rainfall rates.

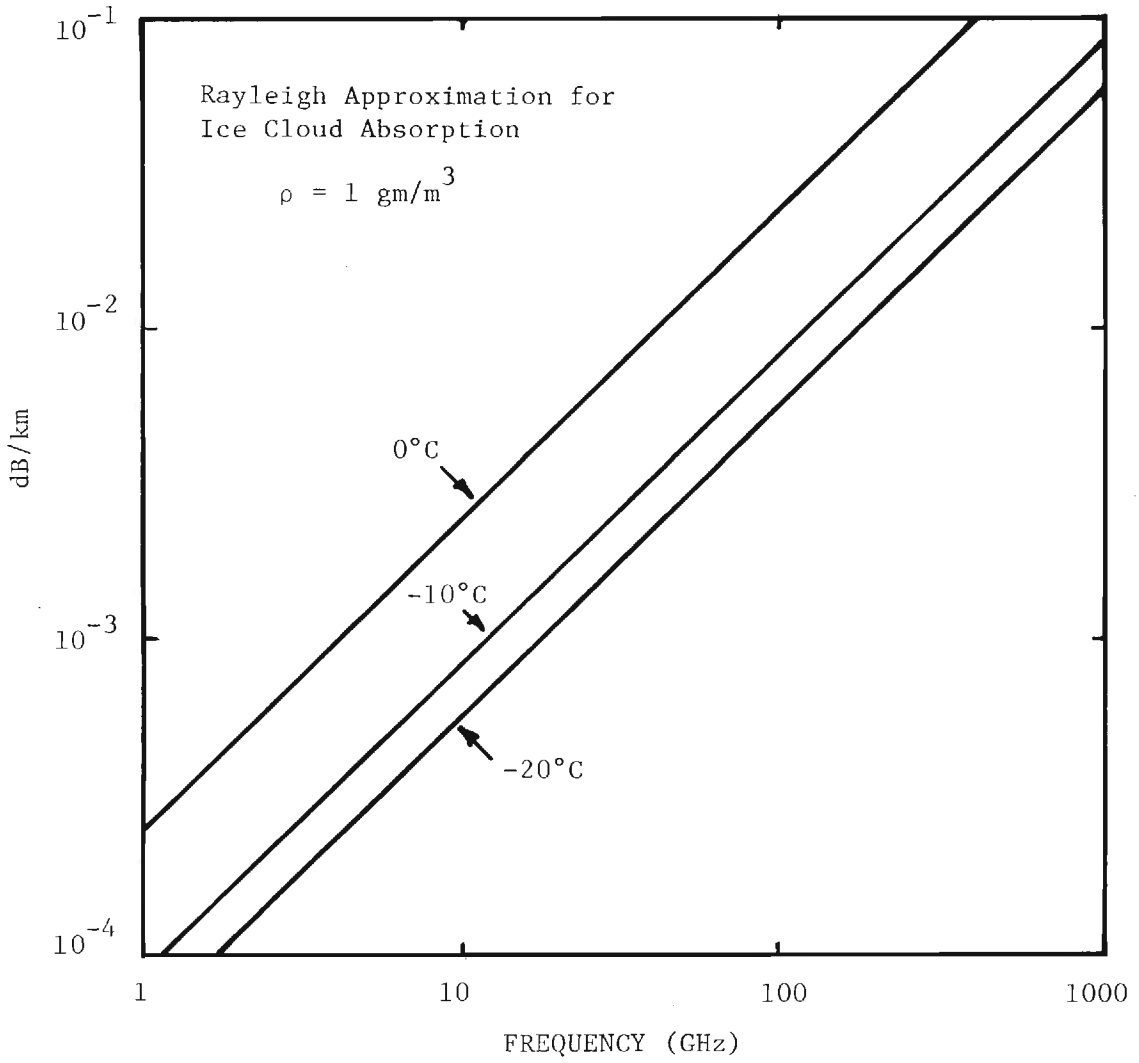

Figure IV-19. Microwave Absorption by Ice Clouds from 1 to 1000 GHz as Given by Tabulated Data of Atlas et al.

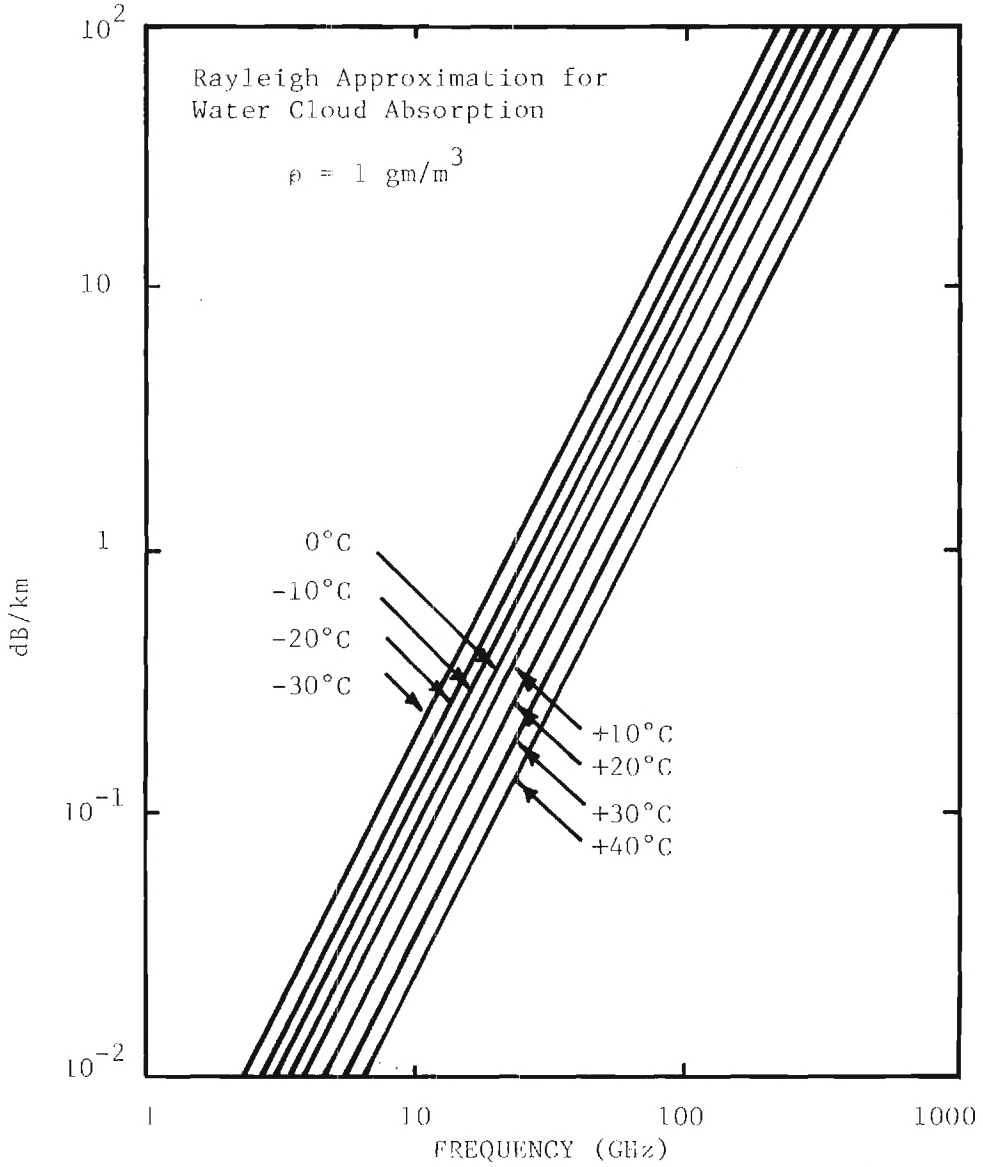

Figure IV-20. Microwave Absorption by Water Clouds from 1 to 1000 GHz as Given by the Rayleigh Approximation Formula of Staelin (1966).

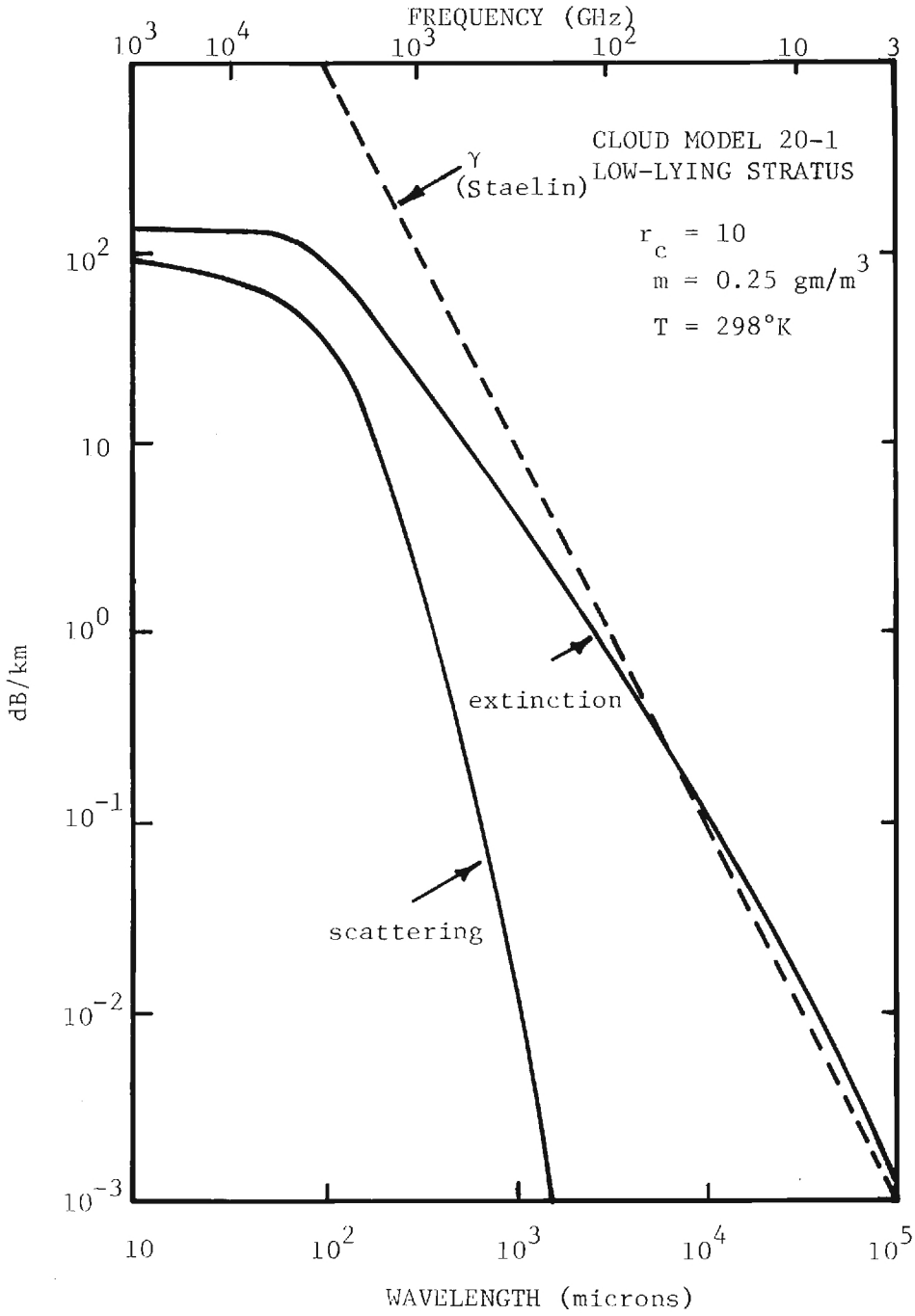

Figure IV-21. Scattering and Extinction Coefficients Computed for Lowlying Stratus as a Function of Wavelength with the Empirical Formula of Staelin (1966) Shown for Comparison.

APPENIDX IV

REFERENCES

1. S. A. Zhevakin and A. P. Naumov, "Coefficient of Absorption of Electromagnetic Waves by Water Vapor in the Range 10μm - 2cm," Radiophysics and Quantum Electronics, 6, 674 (1963).

2. S. A. Clough, private communications.

3. H. J. Liebe, "Study of Oxygen and Water Vapor Microwave Spectra Under Simulated Atmospheric Conditions," Office of Telecommunication Report 75-65, June 1975.

4. E. S. Rosenblum, "Atmospheric Absorption of 10-400 GHz Radiation," Microwave Journal 1, 91 (1961).

5. N. E. Gaut and E. C. Reifenstein, "Interaction Model of Microwave Energy and Atmospheric Variables," Final Report, Contract NAS-8-26275, February 1971, Environmental Research and Technology, Inc., Waltham, Massachusetts.

6. D. W. Webster, "Military Potential of the Extreme Infrared: Technology and Applications," NWC TP5565, Naval Weapons Center, China Lake, California, November, 1973.

7. J. A. Bastin, "Extreme Infrared Atmospheric Absorption," Infrared Physics, 6, 209 (1966).

8. Y. I. Malyshenko, "Measurement of Absorption Coefficient of Water Vapor in the Transparency Window at 1.3 mm," Radio Engineering and Electronic Physics, 14, 447 (1969).

9. P. Moffitt, "Fluctuations in Atmospheric Transmission at about 3 mm Wavelength," Inter-Union Commission on Radio Astronomy, Colloquium on Probing of Atmospheric Constituents, Bournemouth, England, May, 1975.

10. F. T. Ulaby and A. W. Straiton, "Atmospheric Absorption of Radio Waves Between 150 and 350 GHz," IEEE Transactions Antennas and Properties, AP-18, 479 (1970).

11. V. Y. Ryadov and N. I. Furashov, "Investigation of the Spectrum of Radiowave Absorption by Atmospheric Water Vapor in the 1.15 - 1.5 mm Range," Radio Physics and Quantum Electronics, 15, 1124 (1974).

12. Y. A. Dryagin, A. G. Kislyakov, L. M. Kukin, A. I., Naumov and L. I. Fredoseev, "Measurement of the Atmospheric Absorption of Radio Waves in the Range 1.36 - 3.0 mm," Radio Physics and Quantum Electronics, 9, 1078 (1966).

13. V. Y. Ryadov and N. I. Furashov, "Investigation of the Absorption of Radiowaves in the Atmospheric Transparency Window λ = 0.73 mm," Radio Physics and Quantrum Electronics, 15, 1475 (1972).

14. H. A. Gebbie, R. A. Bohlander and G. W. Pardoe, "Submillimeter Wave Absorption Anomalie's in the Lower Atmosphere and the Existence of Dimers," Wature, 230, 521 (1971).

15. H. A. Gebbie, "Molecular Complexity of Water Vapour," Inter-Union Commission on Radio Meteorology, Colloquium on Probing of Atmospheric Constituents, Bournemouth, England, May, 1975.

16. W. C. Quinn, F. E. Welker and R. C. Blackall, RADC Report, AD392823, Sept., 1968 (Confidential).

17. A. H. Aitken, J. N. Hayes, and P. B. Ulrich, Applied Optics 12, 193 (1973).

18. J. N. Hayes, Applied Optics 11, 455 (1972).

19. J. I. Davis, Applied Optics 5, 139 (1966).

20. V. I. Tatarski, "Wave Propagation in a Turbulent Medium," McGraw Hill, New York (1961).

21. L. J. Ippolito, "20 and 30 GHz Millimeter Wave Experiments with the ATS-6 Satellite", Report X-951-75-211, Goddard Space Flight Center, Greenbelt, Maryland, August, 1975

22. J. O. Laws and D. A. Parsons, "The Relation of Raindrop-size to Intensity", Trans. Amer. Geophys. Union 24, 432 (1943)

23. J. S. Marshall and W. M. Palmer, "The Distribution of Raindrops with Size", Journ. Meteorol. 5, 165 (1968)

24. K. L. S. Gunn and T. W. R. East, "The Microwave Properties of Precipitation Particles", Quart. Journ. Roy. Met. Soc. 13, 550 (1965)

25. D. E. Setzer, "Computed Transmission Through Rain at Microwave and Visible Frequencies", Bell System Technical Journal 49, 1873 (1970)

26. D. T. Llewellyn-Jones and A. M. Zavody, "Rainfall Attenuation at 100 and 890 GHz", Electronics Lett 7, 321 (1971)

27. J. W. Ryde and D. Ryde, "Attenuation of Centimeter Waves by Rain, Hail and Clouds", General Electric Co. Research Lab, Wembley, England, Report 8516, August, 1944.

28. L. Strom, "Applications for Millimeter Radars", Systems Planning Corp., Report 108, Contract DNA 001-73-C-0098, ARPA Order No. 2353, 31 Dec. 1973.

29. G. D. Luke, "Penetrability of Haze, Fog, Clouds and Precipitation by Radiant Energy Over the Spectral Range 0.1 Microns to 10 Centimeters", NAVWAG Study 61, May 1968

30. D. H. Staelin, "Measurement and Interpretation of the Microwave Spectrum of the Terrestrial Atmosphere Near 1-centimeter Wavelength", Journ. Geophys. Research 71, 2875 (1966).

31. N. C. Currie, F. D. Dyer and R. H. Hayes, "Analysis of Radar Rain Return at Frequencies of 9.375, 35, 70 and 95 GHz", Engineering Experiment Station, Georgia Institute of Technology, Technical Report No. 2, Contract DAAA-25-73-C-0256, 1 February, 1975

APPENDIX V

SUBMILLIMETER OPTICALLY PUMPED LASERS

Recent interest in optically pumped lasers has resulted in a large number of submillimeter sources covering the spectral region from 37 μm to 1.8 mm wavelength. The technique of optical pumping employs a visible or infrared laser as an excitation source for producing submillimeter radiation. Most lines are generated by pumping with a CO_2 laser. The resultant emission has been in the form of CW, pulsed or super-radiant output power. A tabulation of lines which are known to result from optical pumping is given in Table V-1. Approximately 450 transitions have yielded submillimeter radiation under optical pumping. The transitions are listed in the Table for CW mode, pulsed operation and super-radiant emission. Output wavelength, pump line and output power (where known) are given in the Table. The last part of the Table which gives pulse output power under pumping by CO_2 lasers was received [21] after the initial tabulation was made.

In order to show the spectral position of some of the optically pumped transitions, Figure V-1 shows the absorption spectrum of H_2O [22], which constitutes the submillimeter atmospheric absorption with the exception of minor contributions from O_2. The spectrum extends from the microwave region to approximately 9.8 μm. The stronger transitions are indicated at the bottom of the figure, where it can be seen that the majority of the transitions occur at the long wavelength end of the spectrum. While no lines are listed on the figure for $\lambda < 33$ μm, the remainder of the spectrum is shown to demonstrate the improvement in transmission at shorter wavelengths. The curves were computed for sea level conditions of $P = 760$ torr, $\rho = 7.5$ g/cm^3 and $T = 290°K$. The two curves shown are for (1) the Gross line shape [23] and (2) the VanVleck-Weisskopf line shape [24]. It is seen that, at the short and long wavelength extremes of the spectrum, the VanVleck-Weisskopf line shape does not fit the experimental data in the wings of the absorption lines. Similar curves are available for conditions of altitudes of 10 and 20 km [25], so that absorption for airborne applications throughout the submillimeter region can be determined. It should be pointed out that the absorption spectrum which is shown was calculated for rotational transitions to $J = 12$. Currently available data yields transitions for J

as high as 40, so that a far more accurate representation of submillimeter absorption should now be possible.

From Table V-1, it is seen that no source can compete in power output or efficiency with the relativistic beam devices. In addition, the optically pumped sources produce single lines with extremely small tunability around each output. The most powerful outputs have been from super-radiant sources with 10^5W for D_2O at 66 μm and for CH_3F at 496 μm. Both of these lines occur, however, at wavelengths where the attenuation is approximately 700 dB/km. The efficiency of the optically pumped lasers is limited by the Manley-Rowe relations, so that, for a CO_2 pump source of ∿10%, a submillimeter source with an output near 1 mm wavelength has an efficiency of 0.1%. The pump source for a super-radiant output must, in turn, be a CO_2 TEA laser. Recently, the CH_3F line at 496 μm has been operated as a pulsed single mode laser [26] with an improvement of the power conversion efficiency (submm power out/CO_2 pump power in) to 1.5×10^{-3} over the previous value of 10^{-3}-10^{-4}. The conversion efficiency of 1.5×10^{-3} approaches the Manley-Rowe limit for $\lambda = 496$ μm of 2×10^{-3}.

While the optically pumped lasers do not approach the REB devices for the high power applications of interest, they are important and useful sources for several low power applications. In particular, the tabulation of these transitions is important for picking local oscillators for superheterodyne receiver applications of the REB sources.

In addition to the optically pumped laser sources, several other sources have been investigated for the generation of submillimeter radiation. None of these techniques appear capable of generating output powers comparable with the electron beam devices. Several nonlinear optical pumping schemes have been investigated with the most recent of these being the noncollinear mixing of two CO_2 lasers in a nonlinear crystal (e.g. GaAs or CdTe) [27]. While this technique shows promise of some interesting physical investigations, it is not evident that the use of two TEA lasers with an easily damaged nonlinear crystal which must be critically aligned can result in a submillimeter generator of high power. The quasi-tunability of the output is also not competitive with the REB units.

A technique which warrants some considerations has been proposed by Corcoran [28] and utilizes an array of submillimeter lasers, either optically pumped or direct electrically excited, phased to produce the sum of the lasers. The technique could result in high power output which could be readily steered for phased array applications. The difficulty of the scheme lies in the complexity of phase locking a large array of lasers, the lack of frequency tunability and the fact that the array will have an efficiency no greater than the individual lasers.

A final note should be made on the direct discharge excited submillimeter laser. The interest which has been generated by the optically pumped laser has resulted in less interest in the directly excited lasers, such as HCN. The optical pumping scheme has produced more laser outputs than can ever be achieved by the discharge technique and, in turn, has the potential for low noise local oscillators and amplifiers. However, only in the case of the super-radiant source does the power exceed that which has been achieved for HCN. A recent compact HCN laser [29] has shown the possibility of good sources for applications. Very little attention has been given to new molecules, improved configurations, transverse pumping schemes, etc., which could improve the output power and efficiency of the discharge lasers.

TABLE V-1(a)

OPTICALLY PUMPED SUBMILLIMETER LASERS
CW MODE

Molecule	Output λ(μm)	Output Power (mW)	Pump Line	Reference
CH_3OH	37.5	0.5	CO_2 P(32) 9.657 μm	15
CH_3OH	40.2	1	CO_2 P(34) 9.676 μm	15
CH_3OH	41.7	4	CO_2 P(32) 9.657 μm	15
CH_3OH	43.4	0.1	CO_2 P(34) 9.676 μm	15
CH_3OH	65.6	0.5	CO_2 P(34) 9.676 μm	15
CH_3OH	70.6	1	CO_2 P(34) 9.6 μm	12
CH_3OH	80.3	0.2	CO_2 P(34) 9.676 μm	15
NH_3	81.5	0.1	N_2O P(13) 10.78 μm	8
CH_3OH	118.8	1	CO_2 P(36) 9.6 μm	12
CH_3NH_2	148.5	10	CO_2 9.585 μm	17
CH_3OH	162	0.6	CO_2 R(38) 10.136 μm	20
CH_3OH	614.3	1	CO_2 P(16) 9.6 μm	12
CH_3OH	170.6	1	CO_2 P(36) 9.6 μm	12
CH_3NH_2	180	1×10^{-4}	CO_2 P(46) 9.794 μm	20
CH_3F	192.8	4.7	CO_2 10.17 μm	13
CH_3OH	193.2	0.1	CO_2 P(38) 9.714 μm	15
CH_3NH_2	198	1	CO_2 9.585 μm	17
CH_3OH	198.8	1	CO_2 P(38) 9.6 μm	12
CH_3F	199.1	1	CO_2 10.17 μm	13
CH_3OH	202.4	1	CO_2 P(36) 9.6 μm	12
CH_3NH_2	218.0	1	CO_2 9.585 μm	17
CH_3OH	223.5	1	CO_2 P(16) 9.6 μm	12
CH_3OH	232	0.03	CO_2 R(10) 9.329 μm	20
CH_3OH	237.6	1	CO_2 P(34) 9.6 μm	12
CH_3OH	249	0.2	CO_2 R(34) 10.159 μm	20

Molecule	Output λ(μm)	Output Power (mW)	Pump Line	Reference
CH_3NH_2	251.3	0.3	CO_2 9.585 μm	17
CH_3F	251.9	0.2	CO_2 10.159 μm	13
CH_3OH	253.6	1	CO_2 P(34) 9.6 μm	12
CH_3OH	254	0.6	CO_2 R(38) 10.136 μm	20
CH_3OH	254.1	1	CO_2 P(34) 9.6 μm	12
NH_3	263.4	0.1	N_2O P(13) 10.78 μm	8
CH_3OH	263.7	1	CO_2 P(34) 9.6 μm	12
CH_3CH_2F	264	0.015	CO_2 P(18) 9.536 μm	20
CH_3OH	264.6	1	CO_2 P(34) 9.6 μm	12
CH_2CHCN	270.6	0.06	CO_2 10.653 μm	17
CH_3NH_2	288	0.015	CO_2 R(4) 9.367 μm	20
$C_2H_2F_2$	288.5	0.3	CO_2 10.513 μm	17
CH_3OH	292	0.03	CO_2 R(10) 10.318	20
CH_3CN	303.5	3×10^{-3}	CO_2 10.494 μm	13
CH_3NH_2	314	0.03	CO_2 R(4) 9.367 μm	20
CH_3CH_2F	336	0.003	CO_2 R(16) 9.29 μm	20
CH_3OH	369.1	1	CO_2 P(16) 9.6 μm	12
CH_3F	372.7	5.8	CO_2 9.836 μm	13
CH_3CN	372.9	3.5	CO_2 10.59 μm	13
$C_2H_2F_2$	375	1.6	CO_2 10.513 μm	17
CH_3CN	380.7	0.007	CO_2 10.55 μm	13
$H_2C{:}CHCl$	386	1	CO_2 P(22) 10.6 μm	12
CH_3CN	392	5×10^{-4}	CO_2 R(12) 9.317 μm	20
CH_3OH	392.3	1	CO_2 P(36) 9.6 μm	12
CH_3F	397.5	1	CO_2 9.836 μm	13
CH_3CH_2F	404	0.01	CO_2 R(30) 9.22 μm	20

Molecule	Output λ(μm)	Output Power (mW)	Pump Line	Reference
CH_3CH_2F	405	3×10^{-4}	CO_2 P(34) 9.676 μm	20
$C_2H_2F_2$	415	1	CO_2 P(14) 10.532 μm	15
CH_3OH	417.8	1	CO_2 P(36) 9.6 μm	12
CH_3CN	422.1	0.017	CO_2 10.63 μm	13
CH_2CHCl	424	0.003	CO_2 R(28) 10.195 μm	20
CH_3CCH	427.89	0.003	CO_2 10.494 μm	13
CH_3CN	430.6	0.19	CO_2 10.57 μm	13
CH_2CHCl	445	0.001	CO_2 R(18) 10.260 μm	20
CH_3CN	456	0.004	CO_2 R(16) 9.294 μm	20
$C_2H_4F_2$	458	1	CO_2 P(20) 10.591 μm	15
$C_2H_2F_2$	458	0.2	CO_2 10.695	17
$C_2H_2F_2$	464.3	0.3	CO_2 10.245 μm	17
CH_3OH	471	0.2	CO_2 R(38) 10.136 μm	20
CH_3CH_2F	486	0.005	CO_2 R(24) 9.25 μm	20
CH_2CHCl	487	6×10^{-5}	CO_2 P(10) 9.473 μm	20
CH_3CCH	488.88	0.06	CO_2 10.513 μm	13
CH_2CHCN	489	6×10^{-5}	CO_2 P(8) 10.476 μm	20
CH_3CN	496	0.006	CO_2 P(6) 9.443 μm	20
CH_3F	496	1	CO_2 P(20) 9.6 μm	12
CH_2CHCN	503	4×10^{-5}	CO_2 R(12) 9.317 μm	20
CH_3CH_2F	504	0.015	CO_2 R(24) 9.25 μm	20
H_2C: CHCl	507.7	1	CO_2 P(22) 10.6 μm	12
CH_2CHCl	519	4×10^{-4}	CO_2 P(34) 10.741 μm	20
CH_3CH_2F	519	0.001	CO_2 R(4) 9.367 μm	20
$C_2H_2F_2$	523	0.001	CO_2 P(16) 10.551 μm	20

Molecule	Output λ(μm)	Output Power (mW)	Pump Line	Reference
CH_2CHCl	532	0.001	CO_2 P(16) 9.520 μm	20
$C_2H_4F_2$	533	1	CO_2 P(20) 10.591 μm	15
CH_2CHCl	538	1×10^{-4}	CO_2 R(4) 10.365 μm	20
CH_2CHCN	550.0	0.6	CO_2 10.532 μm	17
$C_2H_2F_2$	554	1	CO_2 P(14) 10.532	5
CH_3CCH	563.13	0.009	CO_2 10.632 μm	13
$C_2H_2F_2$	568	1	CO_2 P(24) 10.632 μm	15
CH_3OH	570.5	1	CO_2 P(16) 9.6 μm	12
CH_2CHCl	574	0.015	CO_2 P(16) 10.551 μm	20
CH_2CHCl	574.4	0.3	CO_2 10.274 μm	17
CH_2CHCN	578	0.001	CO_2 R(14) 10.289 μm	20
CH_2CHCN	584.0	0.06	CO_2 10.513 μm	17
CH_2CHCN	586.6	0.32	CO_2 10.591 μm	17
CH_3CH_2F	595	0.002	CO_2 P(36) 9.695 μm	20
CH_2CHCl	603	0.025	CO_2 P(38) 10.787 μm	20
CH_3CH_2F	620	0.002	CO_2 P(22) 9.639 μm	20
CH_2CHCN	623	1×10^{-4}	CO_2 R(12) 10.303 μm	20
CH_2CHCN	631	1×10^{-4}	CO_2 R(6) 10.349 μm	20
$H_2C{:}CHCl$	634.4	1	CO_2 P(20) 9.6 μm	12
CH_2CHCl	638	0.003	CO_2 P(6) 10.458 μm	20
CH_3CCH	647.89	3.3	CO_2 10.532 μm	13
CH_3CCH	649.59	0.001	CO_2 10.741 μm	13
CH_3CN	653	5×10^{-4}	CO_2 P(30) 9.639 μm	20
$C_2H_2F_2$	663	0.1	CO_2 P(24) 10.632	15
CH_2CHCl	699	6×10^{-4}	CO_2 P(22) 9.569 μm	20
CH_3OH	699.5	0.5	CO_2 P(34) 9.676 μm	15
CH_2CHCl	707	0.01	CO_2 P(18) 9.536 μm	20

Molecule	Output λ(μm)	Output Power (mW)	Pump Line	Reference
CH_3CN	713.7	0.68	CO_2 10.718 μm	13
CH_2CHCN	722	5×10^{-5}	CO_2 P(42) 10.835 μm	20
CH_2CHCN	738	6×10^{-5}	CO_2 P(16) 10.551 μm	20
CH_3CCH	757.4	0.003	CO_2 10.494 μm	13
HCOOH	761	5×10^{-4}	CO_2 R(24) 9.25 μm	20
CH_2CHCN	775	1×10^{-4}	CO_2 R(42) 10.115 μm	20
HCOOH	785	0.01	CO_2 R(40) 9.174 μm	20
CH_2CHCN	793	1×10^{-4}	CO_2 R(40) 10.125 μm	20
CH_3CCH	798.55	0.013	CO_2 10.591 μm	13
CH_2CHCN	828	1×10^{-4}	CO_2 R(18) 10.260 μm	20
CH_2CHCl	828	0.002	CO_2 P(24) 9.586 μm	20
CH_3CH_2F	853	0.002	CO_2 P(30) 9.639 μm	20
$C_2H_2F_2$	884	1	CO_2 P(12) 10.513 μm	15
$C_2H_2F_2$	890	0.1	CO_2 P(22) 10.6114 μm	15
$C_2H_2F_2$	890.1	0.2	CO_2 10.611 μm	17
CH_2CHCN	910	1×10^{-4}	CO_2 R(12) 10.303 μm	20
CH_2CHCl	935	5×10^{-4}	CO_2 P(46) 10.885 μm	20
CH_2CHCN	940	1×10^{-4}	CO_2 P(28) 10.675 μm	20
$C_2H_2F_2$	990	0.2	CO_2 10.611 μm	17
CH_2CHCl	995	0.002	CO_2 R(26) 10.207 μm	20
CH_3CH_2F	1013	1×10^{-4}	CO_2 P(28) 9.621 μm	20
$C_2H_2F_2$	1020	0.05	CO_2 P(14) 10.532 μm	15
CH_2CHCl	1041	0.002	CO_2 R(36) 10.147 μm	20
CH_3CH_2F	1069	0.003	CO_2 R(10) 9.329 μm	20
CH_2CHCN	1156	6×10^{-5}	CO_2 P(26) 10.653 μm	20
CH_3CCH	1174.87	2.7	CO_2 10.859 μm	13
CH_2CHCN	1184	6×10^{-4}	CO_2 R(38) 10.136 μm	20

Molecule	Output λ(μm)	Output Power (mW)	Pump Line	Reference
CH_3OH	1217	0.1	CO_2 P(16) 9.52 μm	16
$C^{13}H_3F$	1221.8	2.4	CO_2 9.657 μm	13
CH_3CH_2F	1546	3×10^{-4}	CO_2 P(10) 9.473 μm	20
CH_3CN	1814.4	0.34	CO_2 10.88 μm	13

TABLE V-1(b)

OPTICALLY PUMPED SUBMILLIMETER LASERS

Super-Radiant Mode

Molecule	Output λ(μm)	Pump Output (W)	Pump Line	Comment	Reference
D_2O	50.5	67	CO_2 P(32) 9.6 μm	High Power, 0.3 μJ	2
D_2O	66	100×10^3	CO_2 P(32) 9.6 μm	High Power, 4.2 mJ	2
D_2O	83	330	CO_2 P(32) 9.6 μm	High Power, 2 μJ	2
D_2O	94	10×10^3	CO_2 R(12) 9.6 μm	High Power, 60 μJ	2
D_2O	114	3×10^3	CO_2 R(12) 9.6 μm	High Power, 18 μJ	2
NH_3	151	10×10^3	CO_2 P(32) 10.6 μm	High Power, 60 μJ	2
NH_3	290	20×10^3	CO_2 P(32) 10.6 μm	High Power, 0.12 nJ	2
NH_3	291	2×10^3	CO_2 R(6) 10.6 μm	Short Pulse Giving High Power, 12 μJ	2
CH_3Cl	333	20	CO_2 P(42) 9.6 μm	0.1 μJ	2
CH_3CN	373	2×10^3	CO_2 P(20) 10.6 μm	High Power 12 μJ	2
D_2O	385	9×10^3	CO_2 R(22) 9.6 μm	High Power, 54 μJ	2
CH_3F	496	100×10^3	CO_2 P(20) 9.6 μm	0.6 mJ	2

TABLE V-1(c)

OPTICALLY PUMPED SUBMILLIMETER LASERS

Pulse Mode

Molecule	Output λ(μm)	Pump Output (W)	Pump Line	Comment	Reference
NH_3	34.26		CO_2 P(12) 10 μm	0.1 W Output	10
NH_3	35.1		CO_2 P(14) 10 μm	0.1 W Output	10
NH_3	36.15		CO_2 P(24) 9 μm	0.1 W Output	10
HF	36.5		HF Laser, 2.782 μm	1mW Output	18
HF	42.4		HF Laser, 2.744 μm	1mW Output	18
HF	50.8		HF Laser, 2.707 μm	1mW Output	18
NH_3	58.0		CO_2 P(32) 10.72 μm R(4) 10.6 μm	10 W Output	14
CH_3OH	58.1		CO_2 P(14) 9.6 μm	1.2 W Output	5
$C_2H_4(OH)_2$	62.5	100	CO_2 R(16) 10.6 μm	4 W Output	19
HF	63.4		HF Laser, 2.672 μm	1 mW Output	18
NH_3	64.7		CO_2, P(24) 9 μm	1 W Output	10
CH_3OH	65.1		CO_2 R(18) 9.6 μm	3 W Output	5
NH_3	67.25		CO_2 R(30) 9 μm	1 W Output, Dry Spectrometer	10
$C_2H_4(OH)_2$	69.1	100	CO_2 R(16) 10.6 μm	4 W Output	19
$C_2H_2(OH)_2$	70.1	100	CO_2 P(34) 9.6 μm	10 mW Output	19
NH_3	72.6		CO_2 R(6) 10.35 μm	10 W Output	14
$C_2H_4(OH)_2$	75.2	100	CO_2 P(32) 9.6 μm	1 W Output	19
$C_2H_4(OH_2)$	77.4	100	CO_2 R(16) 10.6 μm	1 mW Output	19
HF	84.4		HF laser, 2.639 μm	1 mW Output	18
NH_3	88.2		CO_2 R(6)		11
NH_3	88.9		CO_2 R(30) 9 μm	1 W Output	10
NH_3	90.55		CO_2 R(16) 9 μm	1 W Output	10
$C_2H_4(OH)_2$	90.8	100	CO_2 P(32) 9.6 μm	1 mW Output	19

Molecule	Output λ(μm)	Pump Output (W)	Pump Line	Comment	Reference
$C_2H_4(OH)_2$	95.8	100	CO_2 R(10) 9.6 μm	8 mW Output	19
CH_3OH	96.5		CO_2 R(10) 9.6 μm	∿mW Output	7
CH_3NH_2	99.5	100	CO_2 R(14) 9.6 μm	1 mW Output	19
CH_3NH_2	104	100	CO_2 P(28) 9.6 μm	1 mW Output	19
$C_2H_4(OH)_2$	109.1	100	CO_2 R(16) 9.6 μm	1 mW Output	19
NH_3	114		CO_2 P(12)		11
CH_3NH_2	115.5	100	CO_2 P(44) 9.6 μm	4 mW Output	19
$C_2H_4(OH)_2$	117.1	100	CO_2 P(14) 9.6 μm	8 mW Output	19
CH_3NH_2	118	100	CO_2 P(8) 9.6 μm	1 mW Output	19
$C_2H_4(OH)_2$	118	100	CO_2 P(36) 9.6 μm CO_2 P(30) 10.6 μm	4 mW Output	19
$C_2H_4(OH)_2$	118.9	100	CO_2 P(34) 9.6 μm	8 mW Output	19
O_3	121		CO_2 P(14) 9.6 μm	Small Pulse ∿mW Output	7
$C_2H_4(OH)_2$	125.8	100	CO_2 P(34) 9.6 μm	4 mW Output	19
CH_3NH_2	126	100	CO_2 R(6) 10.6 μm	4 mW Output	19
HF	126.5		HF laser, 2.608 μm	1 mW Output	18
$C_2H_4(OH)_2$	132	100	CO_2 P(36), P(24), 9.6 μm	4 mW Output	19
CH_3NH_2	134	100	CO_2 R(14), R(18), 9.6 μm	1 mW Output	19
$C_2H_4(OH)_2$	135	100	CO_2 P(36) 9.6 μm	1 mW Output	19
CH_3NH_2	139	100	CO_2 R(14) 9.6 μm	1 mW Output	19
CH_3NH_2	141	100	CO_2 R(22) 10.6 μm	1 mW Output	19
CH_3NH_2	143	100	CO_2 R(14) 9.6 μm	1 mW Output	19
CH_3NH_2	147	100	CO_2 P(24) 9.6 μm	8 mW Output	19
NH_3	147		CO_2 R(30) 9.6 μm	Small Pulse ∿mW Output	7
CH_3OH	151.4		CO_2 R(26) 9.6 μm	Small Pulse ∿mW Output	7

Molecule	Output λ(μm)	Pump Output (W)	Pump Line	Comment	Reference
NH_3	151.5		CO_2P(32)		11
NH_3	151.8		CO_2 P932) 10 μm	1 W Output	10
CH_3NH_2	153	100	CO_2 P(8) 9.6 μm	4 mW Output	19
CH_3NH_2	159	100	CO_2 P(24) 9.6 μm	4 mW Output	19
CH_3OH	163		CO_2 R(34) 10.6 μm	Small pulse ∿mW Output	7
O_3	163.61		CO_2 P(40) 9.733 μm	∿mW Output	7
CH_3OH	163.9		CO_2 P(12) 9.488 μm	10 W Output	4
CH_3NH_2	164	100	CO_2 R(18) 9.6 μm	4 mW Output	19
$C_2H_4(OH)_2$	164	100	CO_2 P(14), P(16), R(10) 9.6 μm	4 mW Output	19
CH_3NH_2	166	100	CO_2 P(32) 9.6 μm	4 mW Output	19
CH_3NH_2	168	100	CO_2 R(22) 9.6 μm	1 mW Output	19
$C_2H_4(OH)_2$	169	100	CO_2 P(36) 9.6 μm	1 mW Output	19
$C_2H_4(OH)_2$	171	100	CO_2 R(8) 9.6 μm	1 mW Output	19
O_3	171.5	10^{-3}	CO_2 P(30) 9.6 μm	Small Pulse ∿mW Output	7
CH_3NH_2	175	100	CO_2 R(6) 10.6 μm	1 mW Output	19
CH_3NH_2	176	100	CO_2 R(32) 10.6 μm	4 mW Output	19
CH_3NH_2	177	100	CO_2 R(12) 9.6 μm	4 mW Output	19
CH_3NH_2	183	100	CO_2 R(14) 9.6 μm	4 mW Output	19
$C_2H_4(OH)_2$	185	100	CO_2 P(34) 9.6 μm	4 mW Output	19
CH_3OH	186.0		CO_2 R(18) 9.6 μm	Small Pulse ∿mW Output	7
$C_2H_4(OH)_2$	189	100	CO_2 P(34), P(36) 9.6 μm	4 mW Output	19
CH_3F	190.3		CO_2 P(30) 9.64 μm	10 W Output	14
CH_3OH	191.2		CO_2 R(4) 10.6 μm	Small Pulse ∿mW Output	7
CH_3OH	191.67		CO_2 R(10) 10.6 μm	Small Pulse ∿mW Output	7

Molecule	Output λ(μm)	Pump Output (W)	Pump Line	Comment	Reference
CH_3OH	191.63		CO_2 R(16) 9.6 μm	Small Pulse ∿mW Output	7
$C_2H_4(OH)_2$	192	100	CO_2 P(38) 9.6 μm	1 mW Output	19
CH_3NH_2	194	100	CO_2 R(8) 9.6 μm	1 mW Output	19
CH_3F	195		CO_2 R(42) 9.166 μm	10 W Output	4
$C_2H_4(OH)_2$	197	100	CO_2 P(38) 9.6 μm	10 mW Output	19
$C_2H_4(OH)_2$	200	100	CO_2 P(36) 9.6 μm	1 mW Output	19
CH_3F	200.3		CO_2 R(40) 9.174 μm	10 W Output	4
CH_3NH_2	201	100	CO_2 R(12) 9.6 μm	1 mW Output	19
CH_3OH	205.3		CO_2 P(18) 9.536 μm	10 W Output	14
CH_3CH_2F	206.6		CO_2 P(36) 10.6 μm	Small Pulse ∿mW Output	7
CH_3NH_2	208	100	CO_2 R(12) 9.6 μm	4 mW Output	19
CH_3F	215.3		CO_2 R(36) 9.192 μm	10 W Output	14
NH_3	216.38		CO_2 P(6) 10 μm	0.1 W Output	10
CH_3CH_2F	217.1		CO_2 R(14) 9.6 μm	Small Pulse ∿mW Output	7
CH_3NH_2	219	100	CO_2 P(32) 9.6 μm	4 mW Output	19
NH_3	225.33		CO_2 P(4) 10 μm	0.1 W Output	10
CH_3CH_2F	226.9		CO_2 P(40) 10.6 μm	Small Pulse ∿mW Output	7
HCOOH	229.4		CO_2 R(32) 9.6 μm	Small Pulse ∿mW Output	7
$C_2H_4(OH)_2$	231	100	CO_2 R(10) 9.6 μm	4 mW Output	19
CH_3OH	232.9		CO_2 R(8) 9.6 μm	Small Pulse ∿mW Output	7
$C_2H_4(OH)_2$	240	100	CO_2 R(10) 9.6 μm	4 mW Output	19
CH_3OH	242.8		CO_2 R(32) 10.6 μm	Small Pulse ∿mW Output	7
CH_3NH_2	243	100	CO_2 P(24) 9.6 μm	4 mW Output	19

Molecule	Output λ(μm)	Pump Output (W)	Pump Line	Comment	Reference
CH_3Cl	250.4		CO_2 P(30) 9.6 μm	10 W Output	14
$C_2H_4(OH)_2$	252	100	CO_2 P(34) 9.6 μm	1 mW Output	19
HCOOH	254.8		CO_2 P(20) 9.6 μm	Small Pulse ∿mW Output	7
NH_3	256.67		CO_2 R(14) 10 μm	1 W Output	10
$C_2H_4(OH)_2$	262	100	CO_2 P(34) 9.6 μm	4 mW Output	19
CH_3CH_2F	264.7		CO_2 P(18) 9.6 μm	Small Pulse ∿mW Output	7
CH_3NH_2	267	100	CO_2 P(40) 9.6 μm	4 mW Output	19
CH_3NH_2	268	100	CO_2 R(12) 9.6 μm	4 mW Output	19
CH_3Cl	273.7		CO_2 P(12) 9.48 μm	10 W Output	14
$C_2H_4(OH)_2$	277	100	CO_2 P(38) 9.6 μm	8 mW Output	19
HCOOH	278.6		CO_2 P(30) 9.6 μm	Small Pulse ∿mW Output	7
NH_3	280.5		CO_2 R(8) 10.33 μm	10 W Output	14
NH_3	281.27		CO_2 R(14) 10 μm	0.1 W Output	10
NH_3	281.4		CO_2 R(8) 10 μm	1 W Output	10
CH_3CH_2F	282.3		CO_2 R(12) 9.6 μm	Small Pulse ∿mW Output	7
$C_2H_4(OH)_2$	288	100	CO_2 P(12) 9.6 μm	1 mW Output	19
$C_2H_4(OH)_2$	290	100	CO_2 P(38) 9.6 μm	4 mW Output	19
NH_3	291.2		CO_2 R(6) 10.35 μm	10 W Output	14
NH_3	291.27		CO_2 P(32) 10 μm	0.1 W Output	10
$C_2H_4(OH)_2$	299	100	CO_2 P(34) 9.6 μm	4 mW Output	19
HCOOH	302.1		CO_2 P(8) 9.6 μm	Small Pulse ∿mW Output	7
HCOOH	309.2		CO_2 R(4) 9.6 μm	Small Pulse ∿mW Output	7
HCOOH	311.5		CO_2 R(22) 10.6 μm	∿mW Output	7
NH_3	311.7		CO_2 R(4) 10 μm bard	1 W Output	10

Molecule	Output λ(μm)	Pump Output (W)	Pump Line	Comment	Reference
HCOOH	319.5		CO_2 R(22) 10.6 μm	Small Pulse ∿mW Output	7
CH_3CH_2F	330.2		CO_2 R(22) 9.6 μm	Small Pulse ∿mW Output	7
HCOOH	334.8		CO_2 P(18) 9.6 μm	Small Pulse ∿mW Output	7
HCOOH	334.9		CO_2 R(14) 9.6 μm	Small Pulse ∿mW Output	7
CH_3CH_2F	336.7		CO_2 R(16) 9.6 μm	Small Pulse ∿mW Output	7
HCOOH	342.7		CO_2 R(14) 9.6 μm	Small Pulse ∿mW Output	7
$C_2H_4(OH)_2$	344	100	CO_2 P(22) 9.6 μm	1 mW Output	19
CH_3NH_2	347	100	CO_2 R(20) 10.6 μm	4 mW Output	19
$C_2H_4(OH)_2$	358	100	CO_2 P(34) 9.6 μm	1 mW Output	19
HCOOH	359.8		CO_2 R(34) 9.6 μm	Small Pulse ∿mW Output	7
CH_3CH_2F	362.1		CO_2 R(18) 9.6 μm	Small Pulse ∿mW Output	7
CH_3Cl	364.5		CO_2 R(16) 9.29 μm	10 W Output	14
HCOOH	368	100	CO_2 R(18) 9.6 μm	4 mW Output	19
CH_3OCH_3	375	100	CO_2 P(20) 10.6 μm	4 mW Output	19
CH_3CH_2F	376.0		CO_2 R(14) 9.6 μm	Small Pulse ∿mW Output	7
CH_3CH_2F	378		CO_2 R(32) 9.6 μm	Small Pulse ∿mW Output	7
CH_3CF_3	379		CO_2 P(32) 10.72 μm	10 W Output	4
HCOOH	388	100	CO_2 R(16) 9.6 μm	10 mW Output	19
$C_2H_4(OH)_2$	388	100	CO_2 P(36) 9.6 μm	1 mW Output	19
HCOOH	392	100	CO_2 R(18) 9.6 μm	4 mW Output	19
HCOOH	393.6		CO_2 R(18) 9.6 μm	Small Pulse ∿mW Output	7

Molecule	Output λ(μm)	Pump Output (W)	Pump Line	Comment	Reference
CH_3Cl	397.6		CO_2 R(24) 10.22 μm	10 W Output	14
HCOOH	401	100	CO_2 R(16) 9.6 μm	4 mW Output	19
HCOOH	403	100	CO_2 R(18) 9.6 μm	4 mW Output	19
CH_3CH_2F	404		CO_2 P(34) 9.6 μm	Small Pulse ∿mW Output	7
HCOOH	404.1		CO_2 R(42) 10.6 μm	Small Pulse ∿mW Output	7
CH_3CH_2F	405.5		CO_2 R(30) 9.6 μm	Small Pulse ∿mW Output	7
HCOOH	405.6		CO_2 R(18) 9.6 μm	Small Pulse ∿mW Output	7
HCOOH	405.8		CO_2 P(26) 9.6 μm	Small Pulse ∿mW Output	7
HCOOH	413	100	CO_2 R(16) 9.6 μm	1 mW Output	19
HCOOH	414	100	CO_2 R(22), R(20) 9.6 μm	10 mW Output	19
$C_2H_4(OH)_2$	415	100	CO_2 P(14) 9.6 μm	4 mW Output	19
HCOOH	418.5		CO_2 R(24) 9.6 μm	∿mW Output	7
HCOOH	419.6		CO_2 R(22) 9.6 μm	Small Pulse ∿mW Output	7
HCOOH	420.3		CO_2 R(8) 9.6 μm	Small Pulse ∿mW Output	7
HCOOH	421		CO_2 R(18) 9.6 μm	Small Pulse ∿mW Output	7
HCOOH	428	100	CO_2 R(20) 9.6 μm	10 mW Output	19
HCOOH	432.5		CO_2 R(20) 9.6 μm	Small Pulse ∿mW Output	7
HCOOH	433.1		CO_2 R(22) 9.6 μm	Small Pulse ∿mW Output	7
HCOOH	435	100	CO_2 P(16) 9.6 μm	1 mW Output	19
HCOOH	437.7		CO_2 P(16) 9.6 μm	Small Pulse ∿mW Output	7
HCOOH	441	100	CO_2 R(18) 9.6 μm	1 mW Output	19

Molecule	Output λ(μm)	Pump Output (W)	Pump Line	Comment	Reference
HCOOH	445.2		CO_2 P(14) 10.6 μm	Small Pulse ∿mW Output	7
HCOOH	445.8		CO_2 R(20) 9.6 μm	Small Pulse ∿mW Output	7
HCOOH	446.8		CO_2 R(16) 9.6 μm	Small Pulse ∿mW Output	7
HCOOH	447.6		CO_2 R(22) 9.6 μm	Small Pulse ∿mW Output	7
CH_3OH	451.9		CO_2 P(12) 9.6 μm	0.4 W Output	5
CH_3F	451.9		CO_2 P(20) 9.6 μm	∿mW Output	12
HCOOH	458.4		CO_2 R(36) 9.6 μm	∿mW Output	7
HCOOH	460.5		CO_2 R(10) 9.6 μm	Small Pulse ∿mW Output	7
CH_3OCH_3	461	100	CO_2 P(34) 10.6 μm	1 mW Output	19
CH_3CH_2F	462.9		CO_2 P(32) 9.6 μm	Small Pulse ∿mW Output	7
CH_3CHF_2	464		CO_2 P(20) 10.59 μm	10 W Output	14
CH_3OCH_3	480	100	CO_2 P(34) 10.6 μm	1 mW Output	19
CH_3OCH_3	492	100	CO_2 P(34) 10.6 μm	10 mW Output	19
HCOOH	492		CO_2 P(42) 9.6 μm	Small Pulse ∿mW Output	7
HCOOH	493.3		CO_2 P(14) 9.6 μm	Small Pulse ∿mW Output	7
CH_3OCH_3	495	100	CO_2 P(12) 10.6 μm	1 mW Output	19
CH_3F	496		CO_2 P(20) 9.6 μm	10 W Output	4
CH_3CH_2F	502.2		CO_2 R(24) 9.6 μm	Small Pulse ∿mW Output	7
HCOOH	512.9		CO_2 R(28) 9.6 μm	Small Pulse ∿mW Output	7
HCOOH	518.8		CO_2 P(16) 9.6 μm	Small Pulse ∿mW Output	7
CH_3OCH_3	520	100	CO_3 P(12) 10.6 μm	10 mW Output	19

Molecule	Output λ (μm)	Pump Output (W)	Pump Line	Comment	Reference
HCOOH	530	100	CO_2 R(28) 9.6 μm	1 mW Output	9
CH_3CH_2F	540.9		CO_2 P(38) 9.714 μm	∿mW Output	7
CH_3F	541.1		CO_2 P(20) 9.6 μm	∿mW Output	12
CH_3OH	570		CO_2 P(16) 9.6 μm	20 mW Output	4
HCOOH	577	100	CO_2 P(38) 9.6 μm	4 mW Output	19
HCOOH	580.5		CO_2 P(38) 9.6 μm	Small Pulse ∿mW Output	7
CH_3CH_2F	593.3		CO_2 P(36) 9.6 μm	Small Pulse ∿mW Output	7
CH_3CH_2F	620.4		CO_2 P(22) 9.6 μm	Small Pulse ∿mW Output	7
CH_3OH	627.3		CO_2 P(16) 9.6 μm	Small Pulse ∿mW Output	7
$C_2H_4(OH)_2$	696	100	CO_2 P(34) 9.6 μm	4 mW Output	19
CH_3CHF_2	755		CO_2 P(14) 10.53 μm	10 W Output	14
CH_3CH_2F	851.9		CO_2 P(30) 9.6 μm	Small Pulse ∿mW Output	7

TABLE V-1(d)

PULSE MODE

[Reference 21]

Molecule	Output λ (μm)	Pump Output (W)	CO_2 pump Line (μm)	Output Power (mW)
CH_3Cl	227.15	26	P(48), 9.8	0.072
CH_3Cl	236.25	13	R(2), 9.4	0.10
CH_3Cl	240.98	90	P(10), 10.5	1.3
CH_3Br	245.04	57	P(28), 9.6	0.89
CH_3Cl	261.03	106	P(34), 10.7	0.069
CH_3Br	264.05	73	R(10), 10.3	5.3
CH_3Cl	271.29	86	P(20), 10.6	0.33
CH_3Cl	275.00	44	R(14), 9.3	1.7
CH_3Cl	275.09	60	R(36), 9.2	0.05
CH_3Br	279.81	51	R(52), 10.1	0.012
CH_3CN	281.18	44	P(34), 9.7	0.018
CH_3Cl	281.67	-	- -	-
CH_3CN	281.98	38	P(50), 9.8	0.67
CH_3Cl	286.79	69	R(34), 10.2	0.31
CH_3CN	286.88	38	- -	0.29
CH_3Br	294.28	117	R(28), 10.2	1.1
CH_3Cl	307.65	23	P(19), 11.0	0.57
CH_3Br	311.07	69	R(12), 10.3	0.019
CH_3Br	311.10	52	P(20), 10.6	1.0
CH_3Br	311.20	21	P(40), 10.8	1.5
CH_3Br	311.21	15	R(50), 10.1	0.33
CH_3Br	332.86	64	R(6), 10.3	0.35
CH_3Br	333.15	83	P(8), 10.5	0.009
CH_3Cl	333.96	47	P(42), 9.8	44
CH_3CN	346.32	70	P(16), 9.5	0.45
CH_3Cl	349.34	89	R(18), 10.3	7.4
CH_3Br	352.75	66	P(18), 9.5	2.3
CH_3I	377.45	47	R(16), 9.3	5.1

PULSE MODE (Cont.)

Molecule	Output λ (μm)	Pump Output (W)	CO_2 pump Line (mμ)	Output Power (mW)
CH_3Cl	378.57	29	R(16), 9.3	0.18
CH_3Br	380.02	83	R(18), 10.3	7.0
CH_3CN	386.41	42	P(46), 9.8	0.003
CH_3CN	387.31	44	R(12), 9.3	0.38
CH_3CN	388.39	69	P(22), 9.6	0.005
CH_3I	390.53	57	P(42), 10.8	1.8
CH_3I	392.48	40	R(14), 9.3	0.017
CH_3Br	407.72	57	P(28), 9.6	0.013
CH_3Br	414.98	46	R(2), 10.4	17
CH_3Br	418.31	101	P(26), 10.7	0.49
CH_3Br	422.78	117	R(26), 10.2	0.009
CH_3CN	427.04	61	P(26), 9.6	0.024
CH_3CCH	428.87	20	R(38), 9.2	0.012
CH_3CN	441.15	43	- -	0.18
CH_3I	447.17	103	P(18), 10.6	23
CH_3CN	453.41	43	R(16), 9.3	0.75
CH_3I	457.25	-	- -	-
CH_3I	459.18	69	P(8), 10.5	0.16
CH_3Cl	461.20	11	R(42), 9.2	0.027
CH_3CN	466.25	43	- -	9.56
CH_3I	477.87	82	P(26), 9.6	0.021
CH_3CN	480.01	43	- -	0.20
CH_3CN	494.74	51	P(6), 9.4	4.0
CH_3I	508.37	66	P(34), 9.7	13
CH_3Br	508.48	47	R(42), 10.1	2.1
CH_3CN	510.16	51	- -	0.19
CH_3Cl	511.90	17	R(52), 10.1	0.065

PULSE MODE (Cont.)

Molecule	Output λ(μm)	Pump Output (W)	CO_2 pump Line(mμ)	Output Power (mW)
CH_3CCH	516.77	47	R(12), 9.3	0.006
CH_3I	517.33	81	P(14), 10.5	0.38
CH_3I	525.32	26	P(4), 9.4	0.093
CH_3I	529.28	60	P(36), 10.8	3.2
CH_3Br	531.06	108	P(24), 10.6	5.5
CH_3CCH	531.08	45	P(6), 9.4	0.004
CH_3I	542.99	99	P(26), 10.7	0.002
CH_3Br	545.21	39	P(38), 10.8	8.8
CH_3Br	545.39	63	R(32), 10.2	10
CH_3CN	561.41	42	R(8), 9.3	0.18
CH_3Br	564.68	-	- -	-
CH_3CCH	566.44	63	P(18), 9.5	0.58
CH3Cl	568.81	97	R(26), 10.2	0.022
CH_3I	576.17	58	P(16), 10.6	1.6
CH_3I	578.90	68	R(34), 10.2	0.98
CH_3CCH	583.77	50	P(20), 9.6	0.004
CH_3I	583.87	32	P(4), 9.4	0.12
CH_3Br	585.72	49	P(40), 9.7	3.3
CH_3Br	631.93	78	P(16), 10.6	0.0021
CH_3Br	632.00	88	P(22), 10.6	0.025
CH_3I	639.73	35	P(6), 9.4	0.17
CH_3CN	652.68	77	P(30), 9.6	0.32
CH_3Br	658.53	52	P(56), 9.9	5.2
CH_3Br	660.70	68	R(20), 10.2	15
CH_3I	670.99	91	P(28), 10.7	0.93
CH_3CCH	675.29	55	P(40), 9.7	0.33
CH_3CN	704.53	41	R(34), 9.2	0.12
CH_3Br	715.40	63	R(14), 10.3	1.6

PULSE MODE (Cont.)

Molecule	Output λ(μm)	Pump Output (W)	CO_2 pump Line(mμ)	Output Power (mW)
CH_3I	719.30	52	P(22), 10.6	0.33
CH_3CN	741.62	48	R(8), 9.3	0.23
CH_3Br	749.29	73	P(14), 10.5	2.8
CH_3Br	749.36	-	- -	-
CH_3Br	831.13	105	P(28), 10.7	5.4
CH_3CN	854.41	70	P(16), 9.5	0.13
CH_3Cl	870.80	16	P(52), 9.9	1.3
CH_3Br	925.52	33	R(46), 10.1	14
CH_3Cl	943.97	45	R(12), 9.3	13
CH_3Cl	958.25	40	P(38), 9.7	0.52
CH_3Br	990.51	95	P(10), 10.5	1.3
CH_3CN	1014.89	43	R(14), 9.3	0.018
CH_3CN	1016.33	33	P(8), 9.5	0.045
CH_3I	1063.29	71	P(38), 10.8	6.5
CH_3CN	1086.89	46	P(40), 9.7	0.15
CH_3CCH	1097.11	50	P(8), 9.5	0.32
CH_3CN	1164.83	45	P(10), 9.5	0.050
CH_3I	1253.67	98	P(32), 10.7	13
CH_3Br	1310.38	90	R(4), 10.4	5.3
CH_3CN	1351.78	49	R(20), 9.3	0.02
CH_3Br	1572.64	58	P(4), 10.4	2.2
CH_3Cl	1886.87	57	P(26), 9.6	1.6
CH_3Br	1965.34	105	P(28), 10.7	1.3

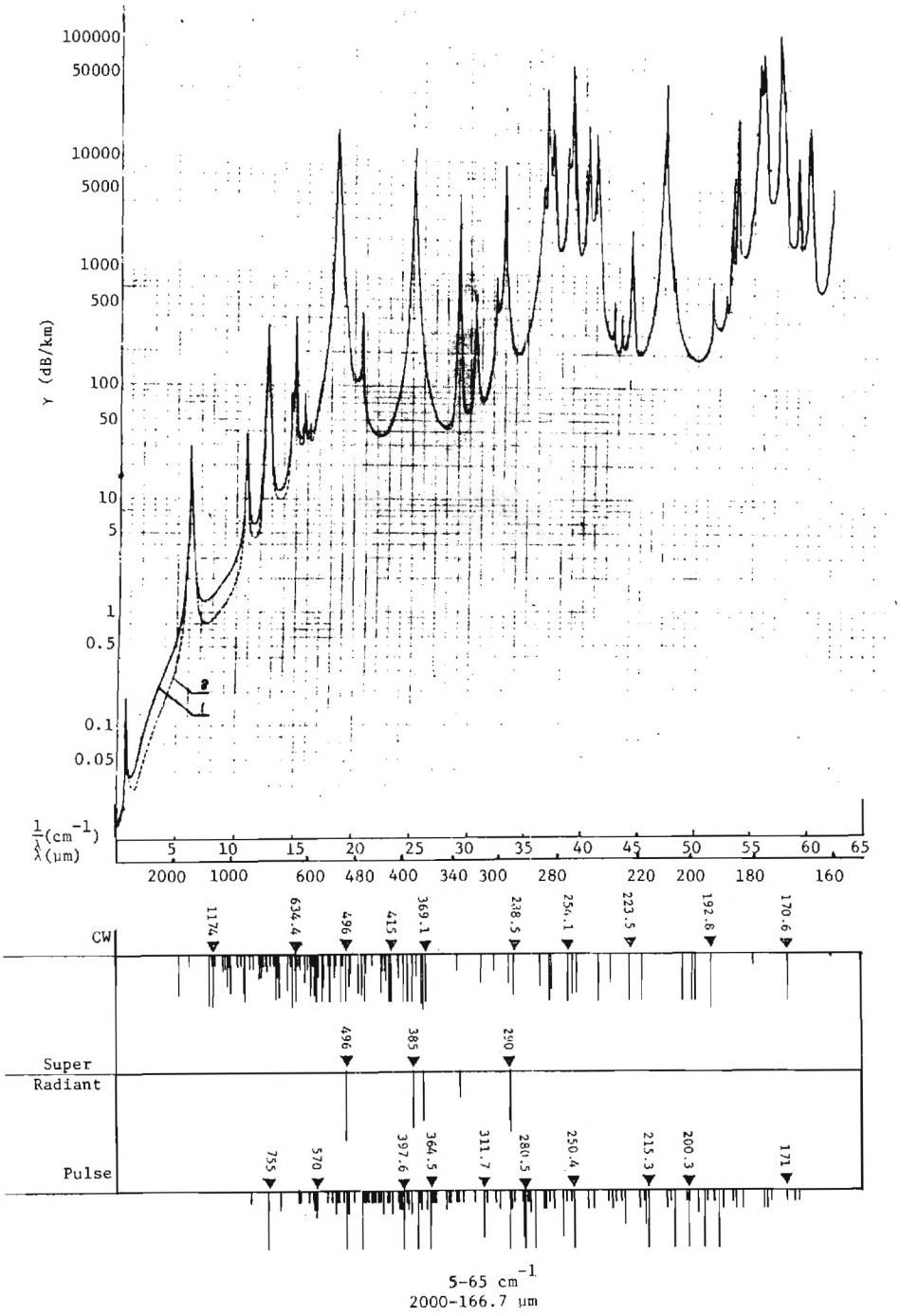

Figure V-1. Submillimeter Atmospheric Absorption with Optically Pumped Laser Frequencies Indicated.

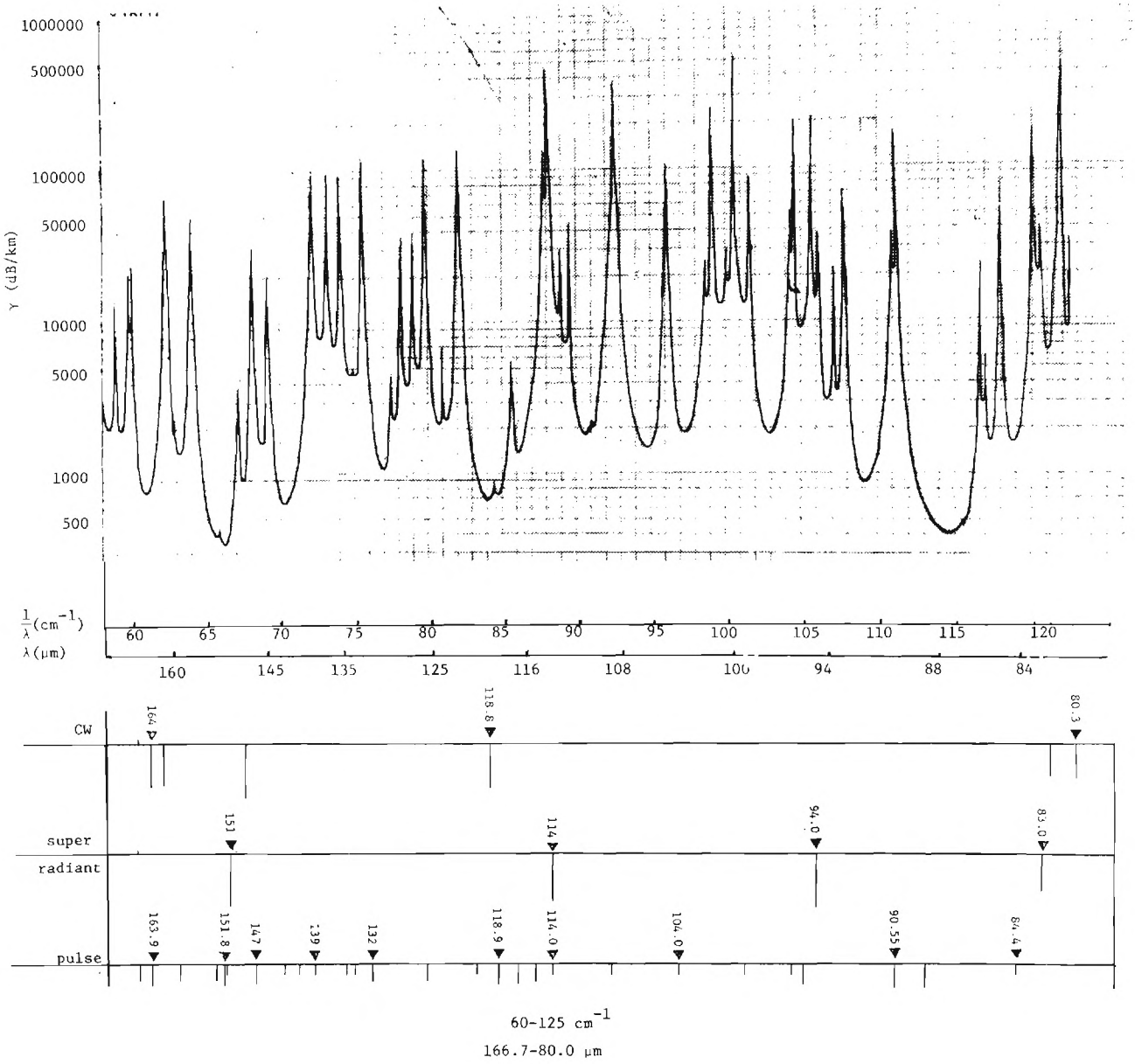

Figure V-1 (Continued). Submillimeter Atmospheric Absorption with Optically Pumped Laser Frequencies Indicated.

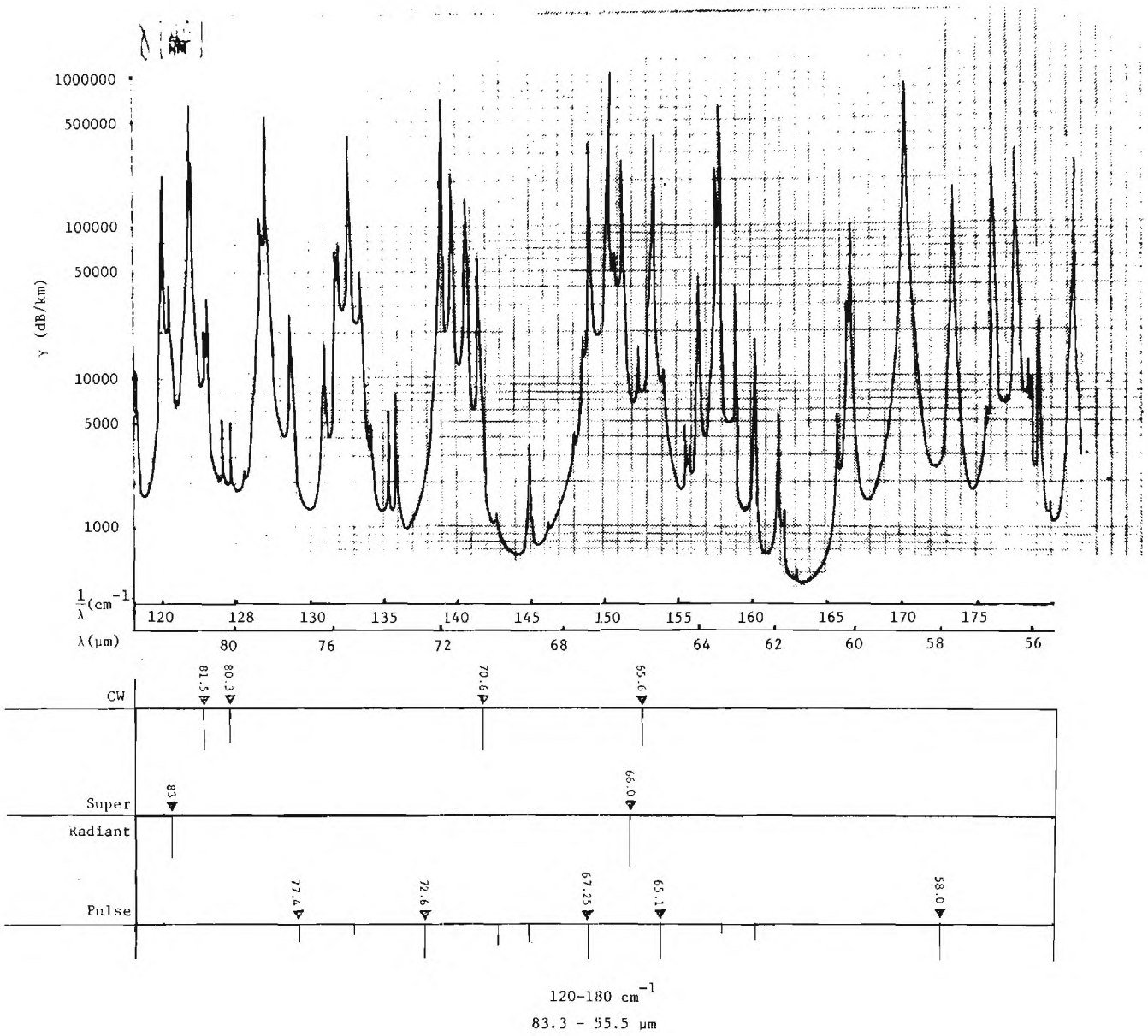

Figure V-1 (Continued). Submillimeter Atmospheric Absorption with Optically Pumped Laser Frequencies Indicated.

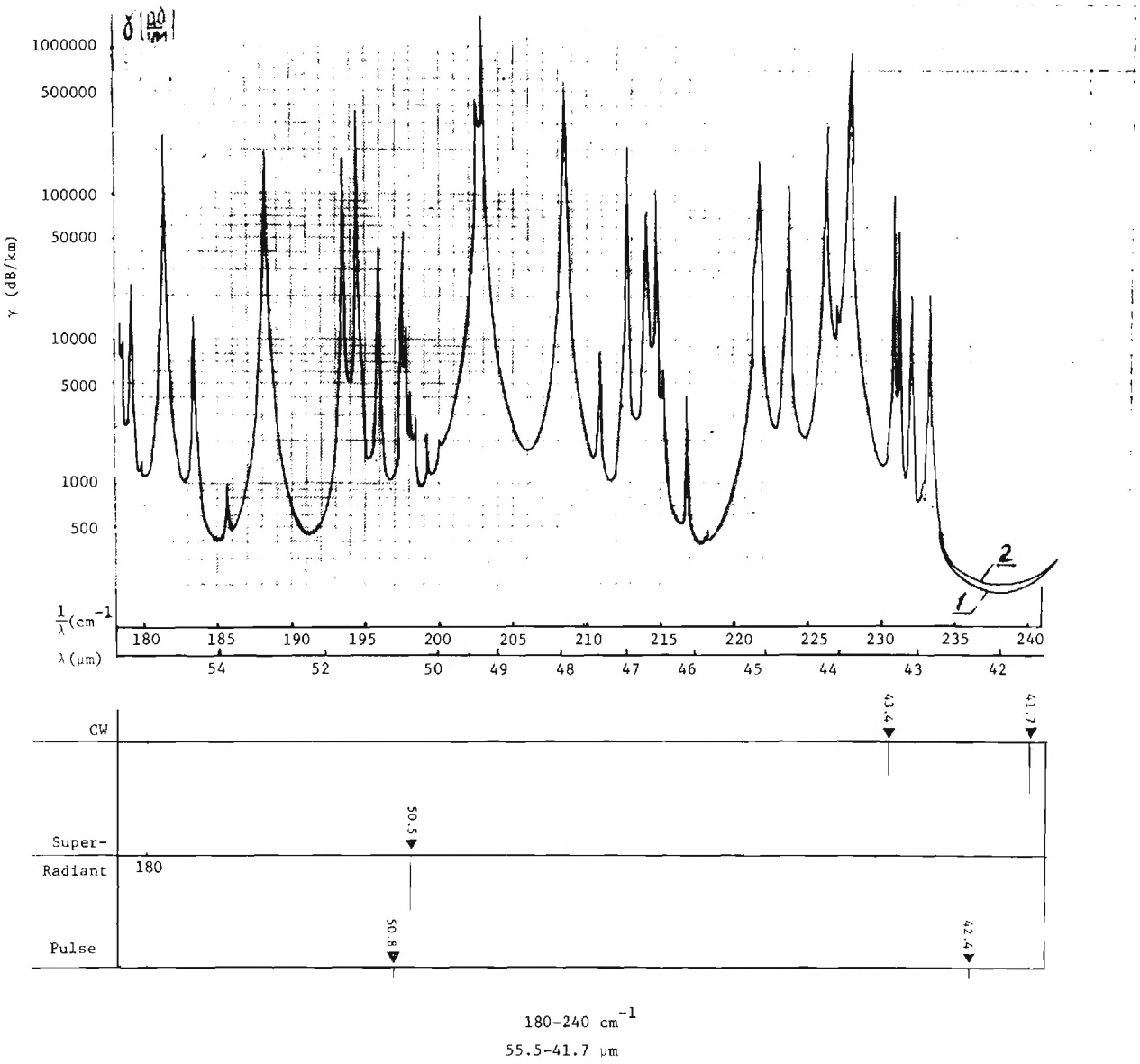

Figure V-1 (Continued). Submillimeter Atmospheric Absorption with Optically Pumped Laser Frequencies Indicated.

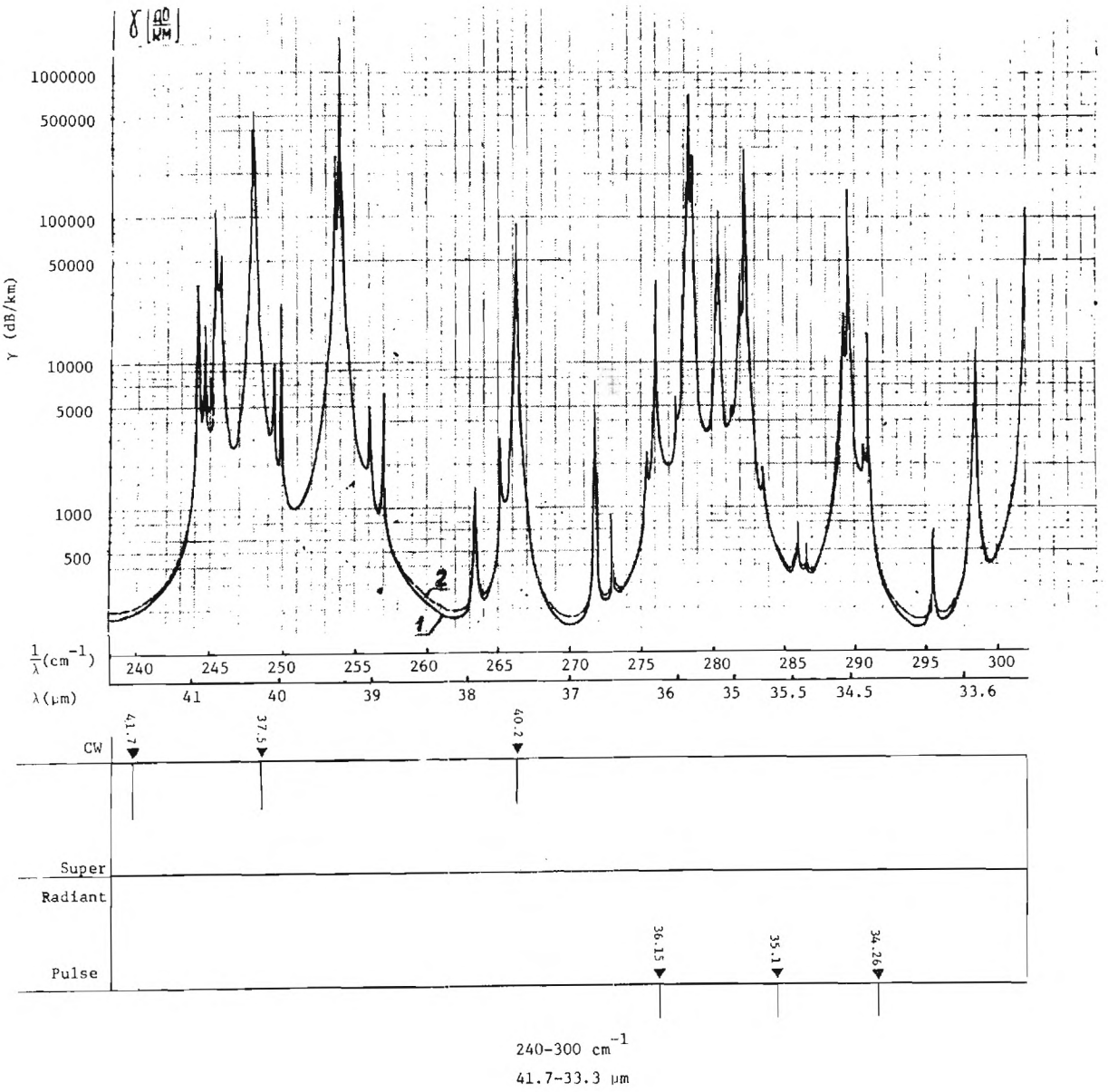

Figure V-1 (Continued). Submillimeter Atmospheric Absorption with Optically Pumped Laser Frequencies Indicated.

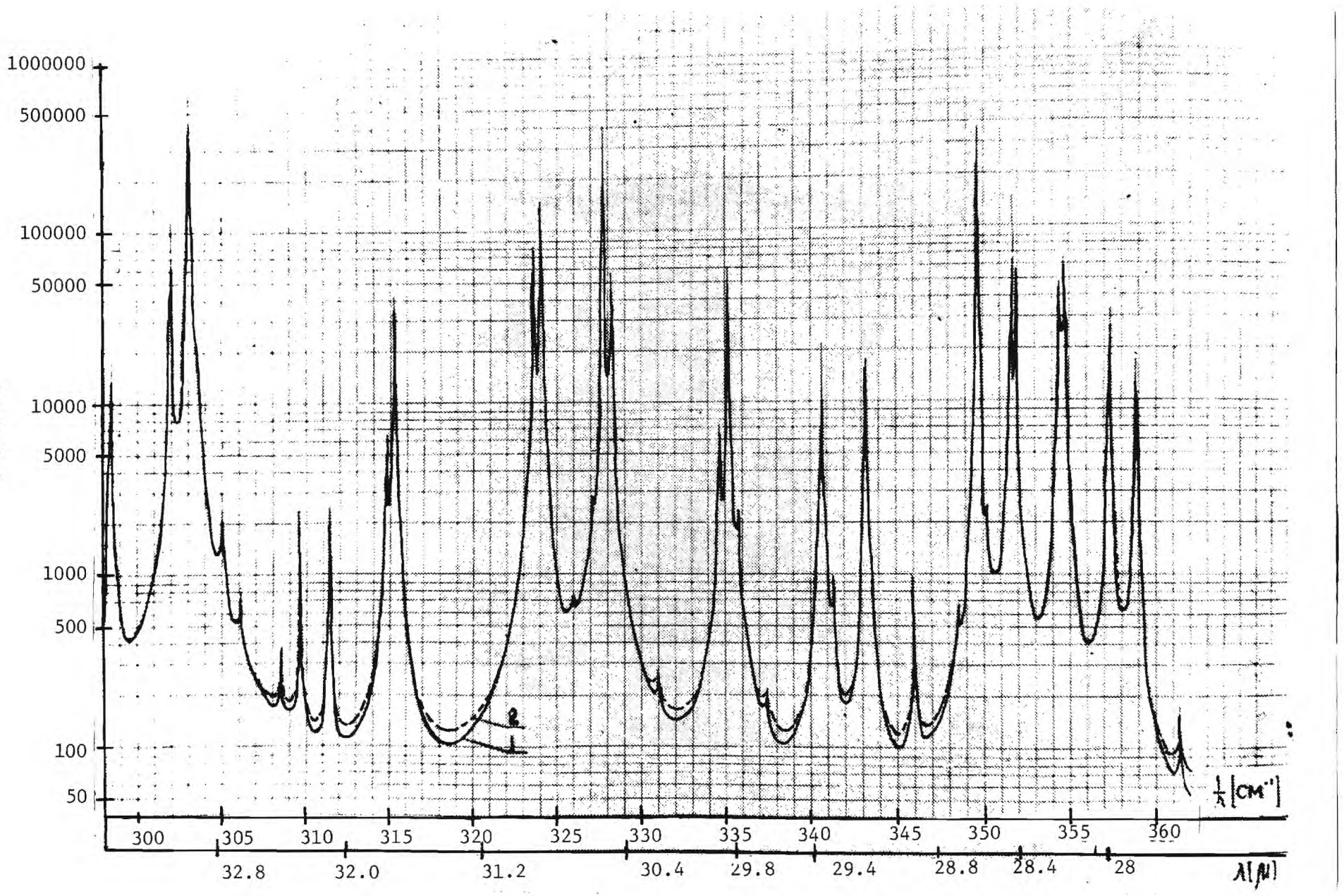

Figure V-1. Submillimeter Atmospheric Absorption with Optically

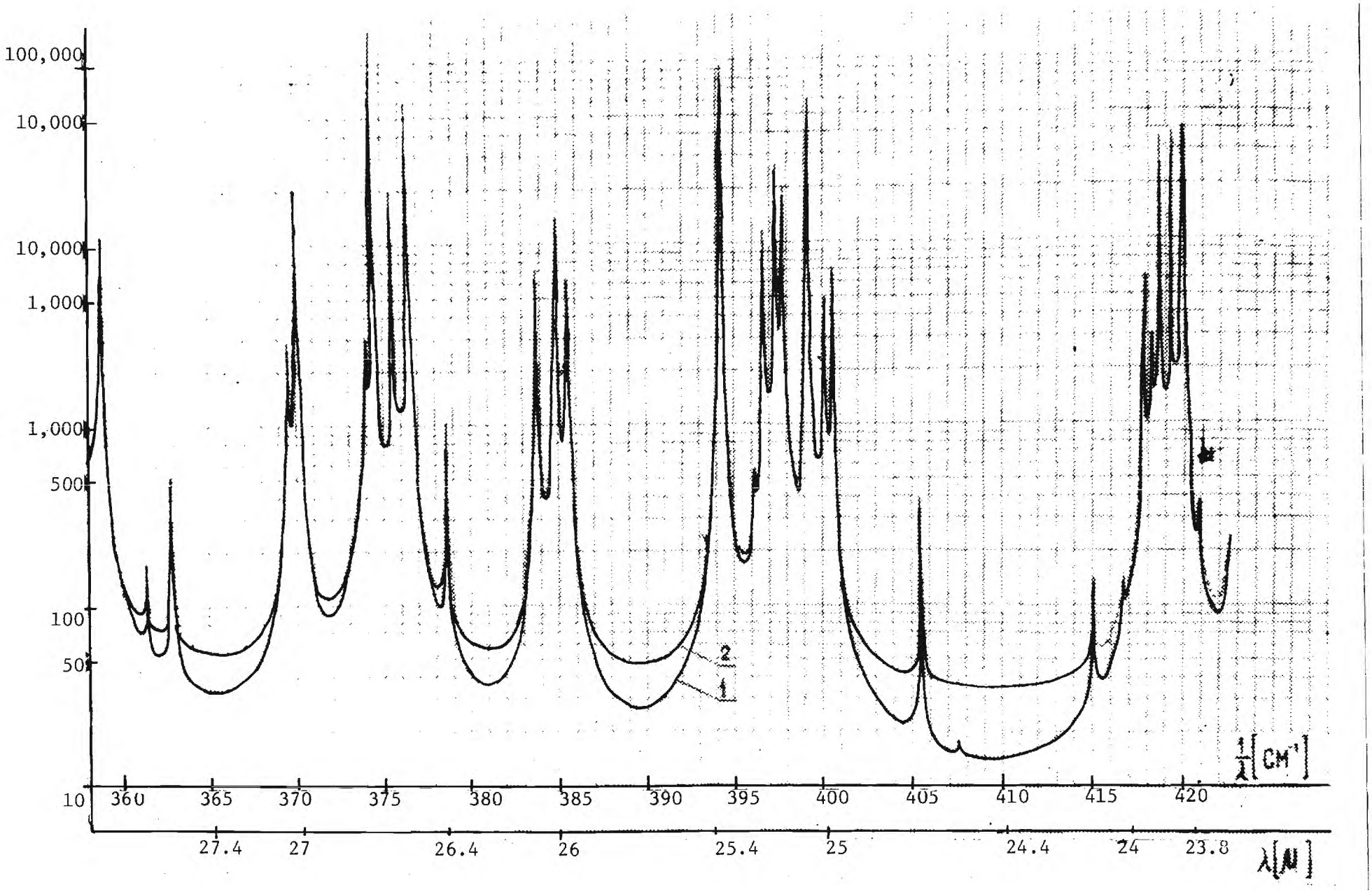

Figure V-1. (Continued)

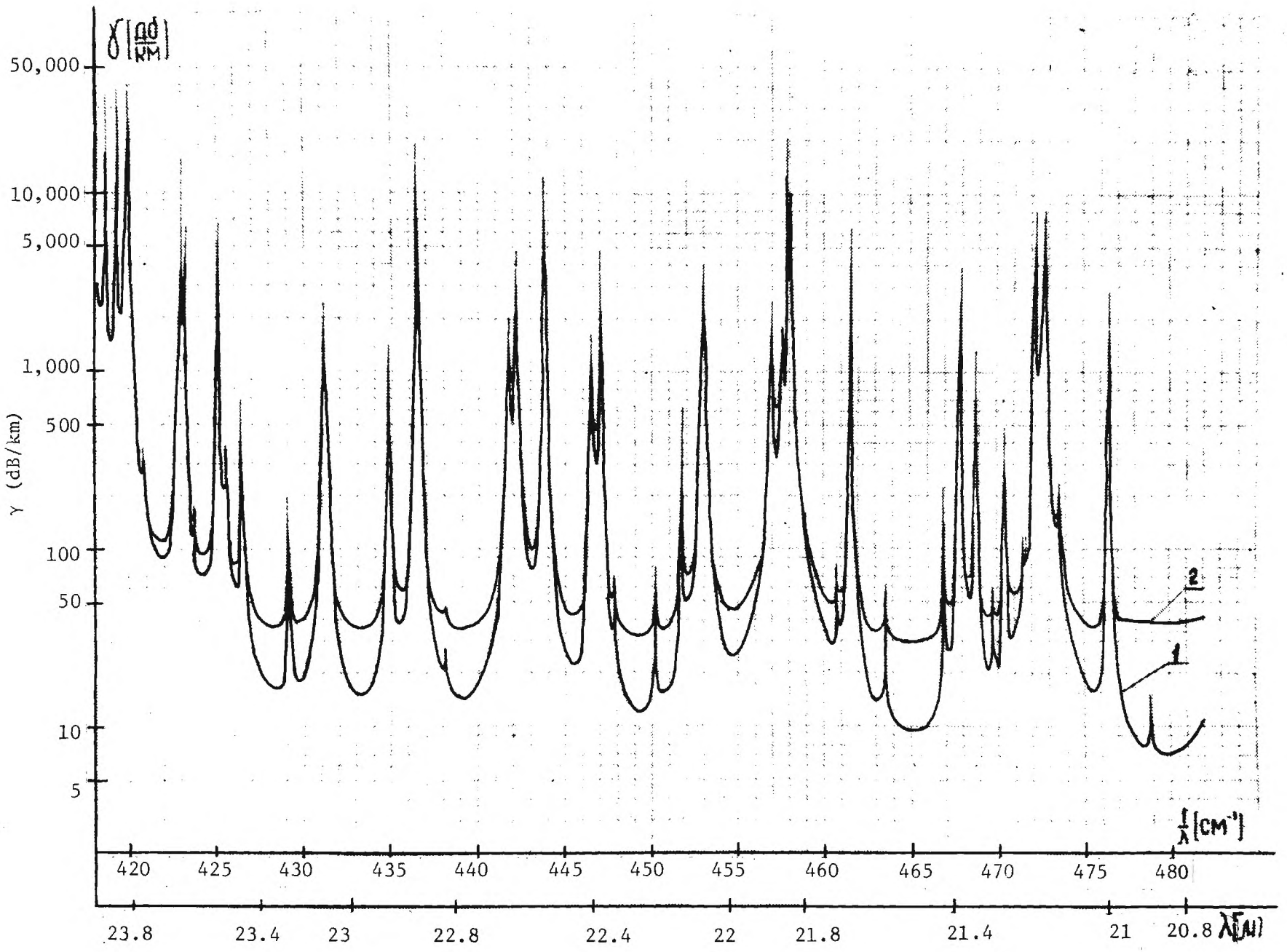
γ [dB/km]
50,000
10,000
5,000
1,000
500
100
50
10
5
γ (dB/km)
2
1
1/λ [cm⁻¹]
420
425
430
435
440
445
450
455
460
465
470
475
480
23.8
23.4
23
22.8
22.4
22
21.8
21.4
21
20.8
λ [μm]

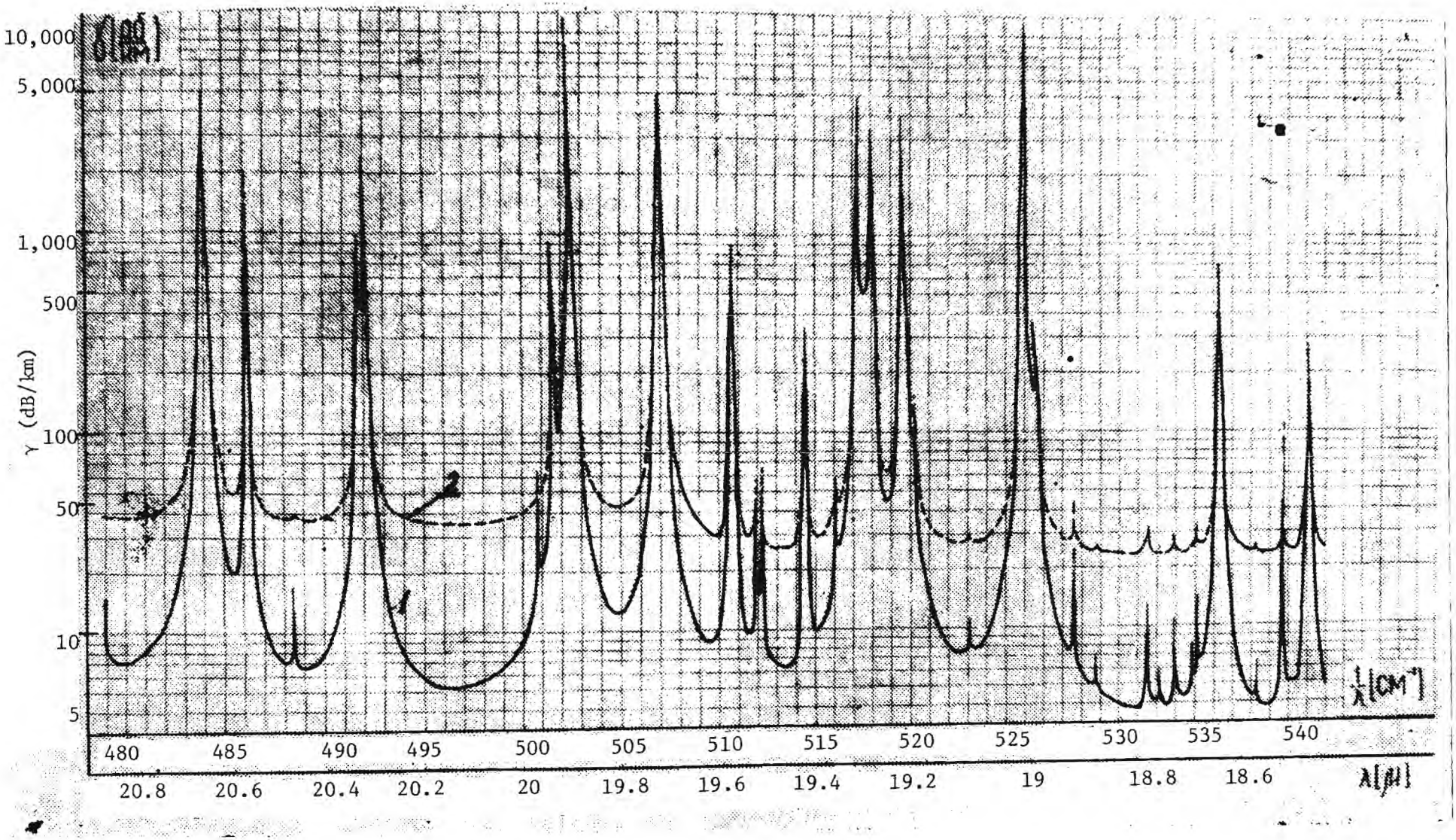

Figure V-1. (Continued)

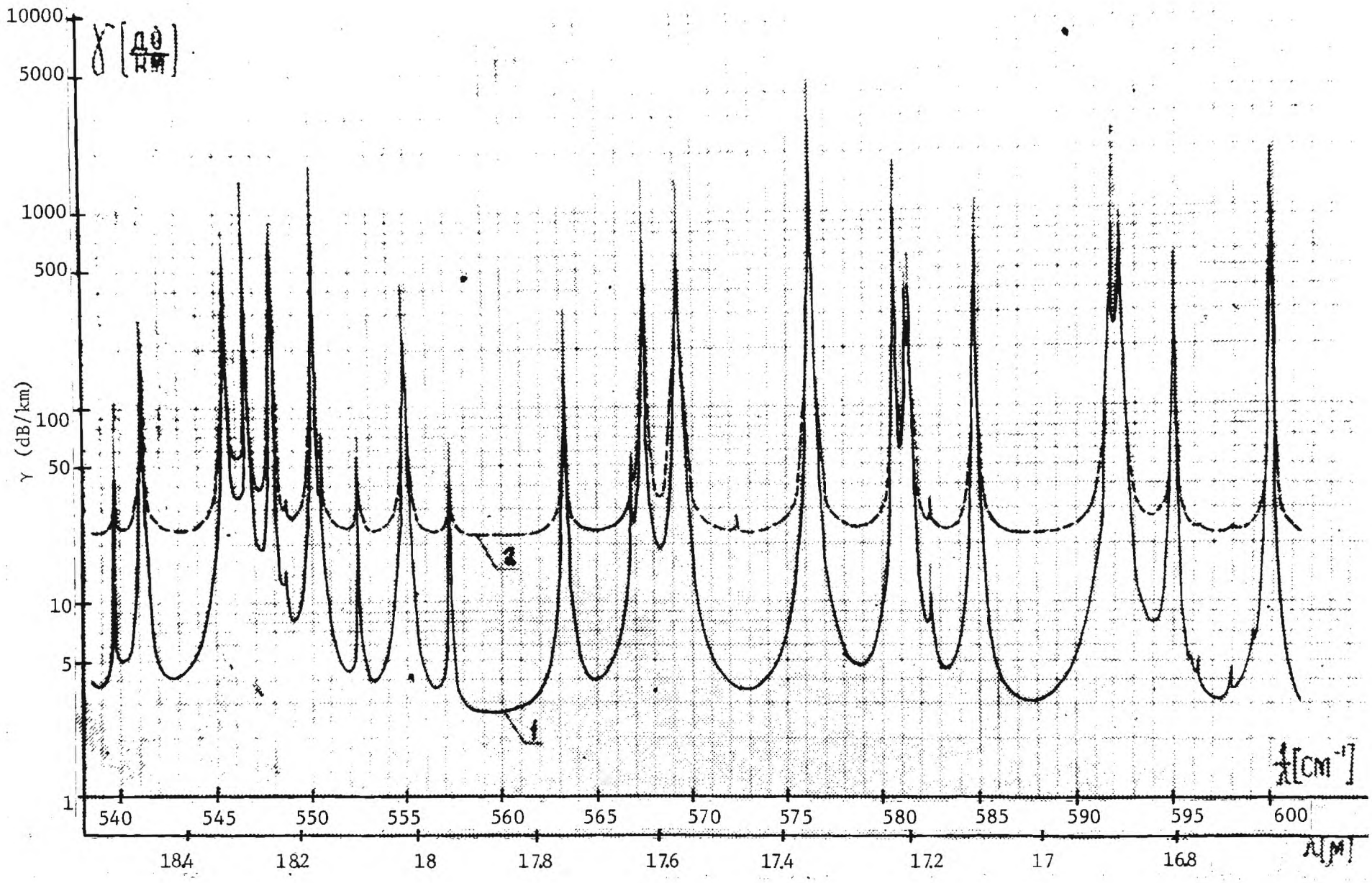

Figure V-1. (Continued)

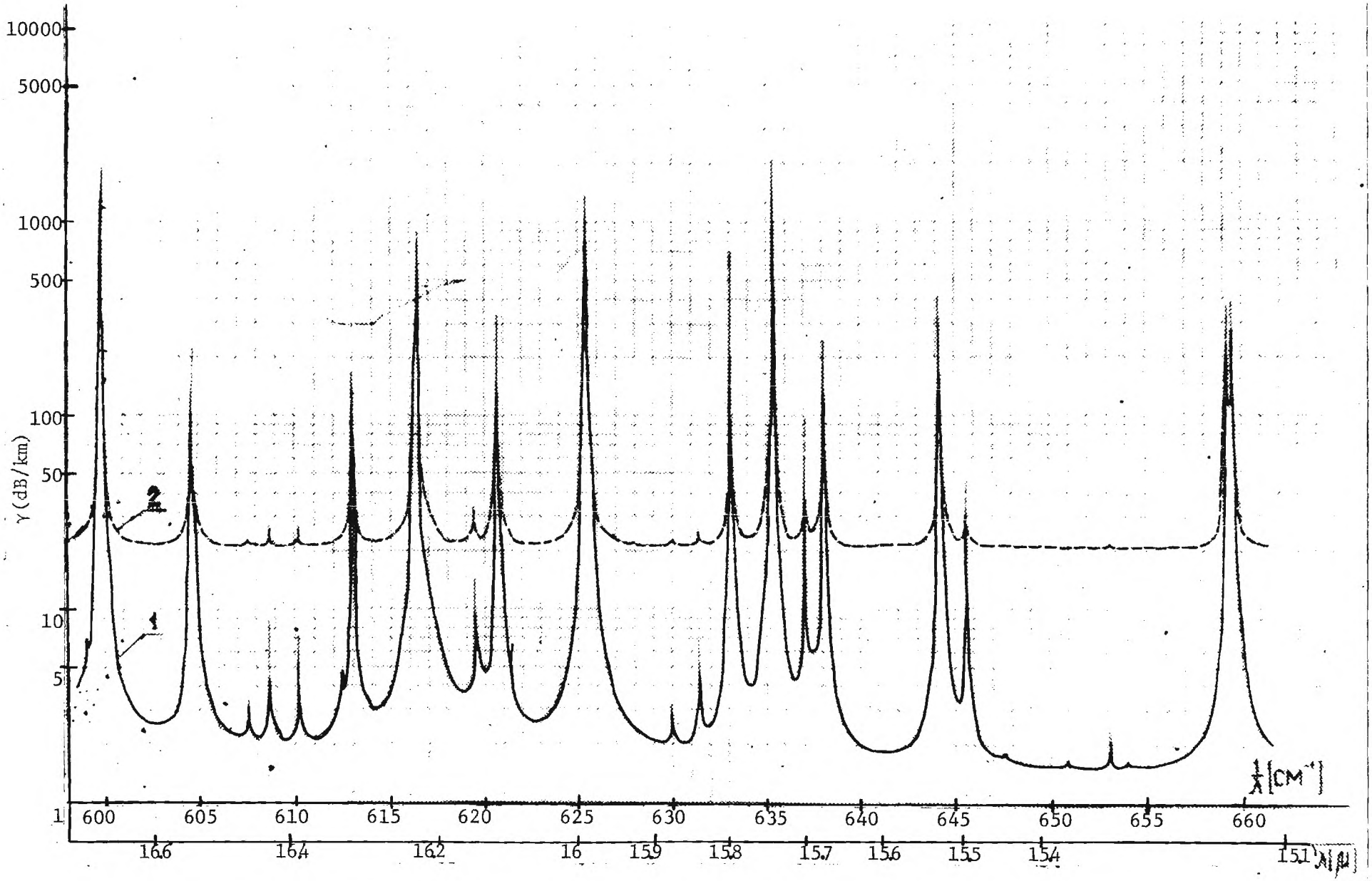

Figure V-1. (Continued)

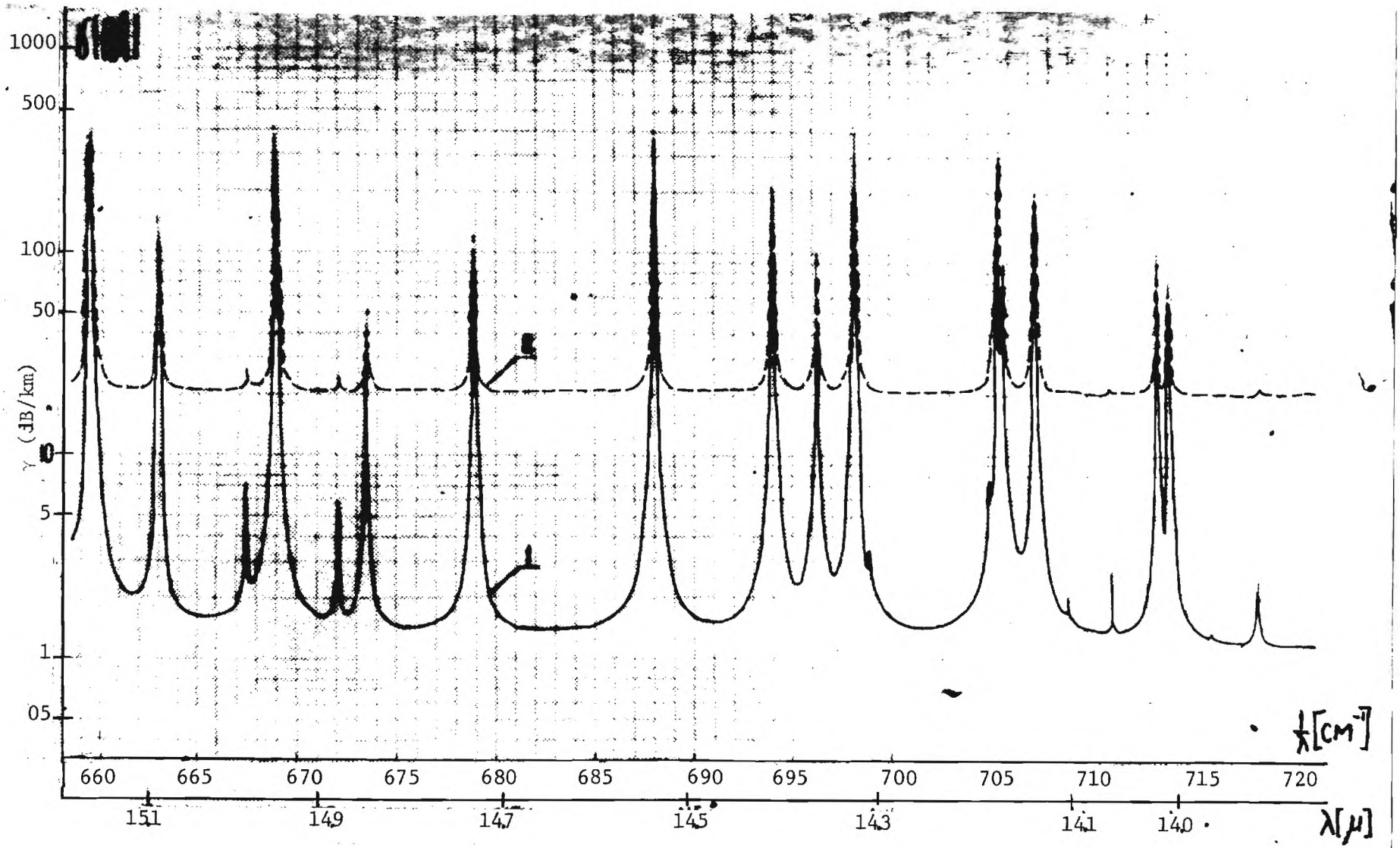

Figure V-1. (Continued)

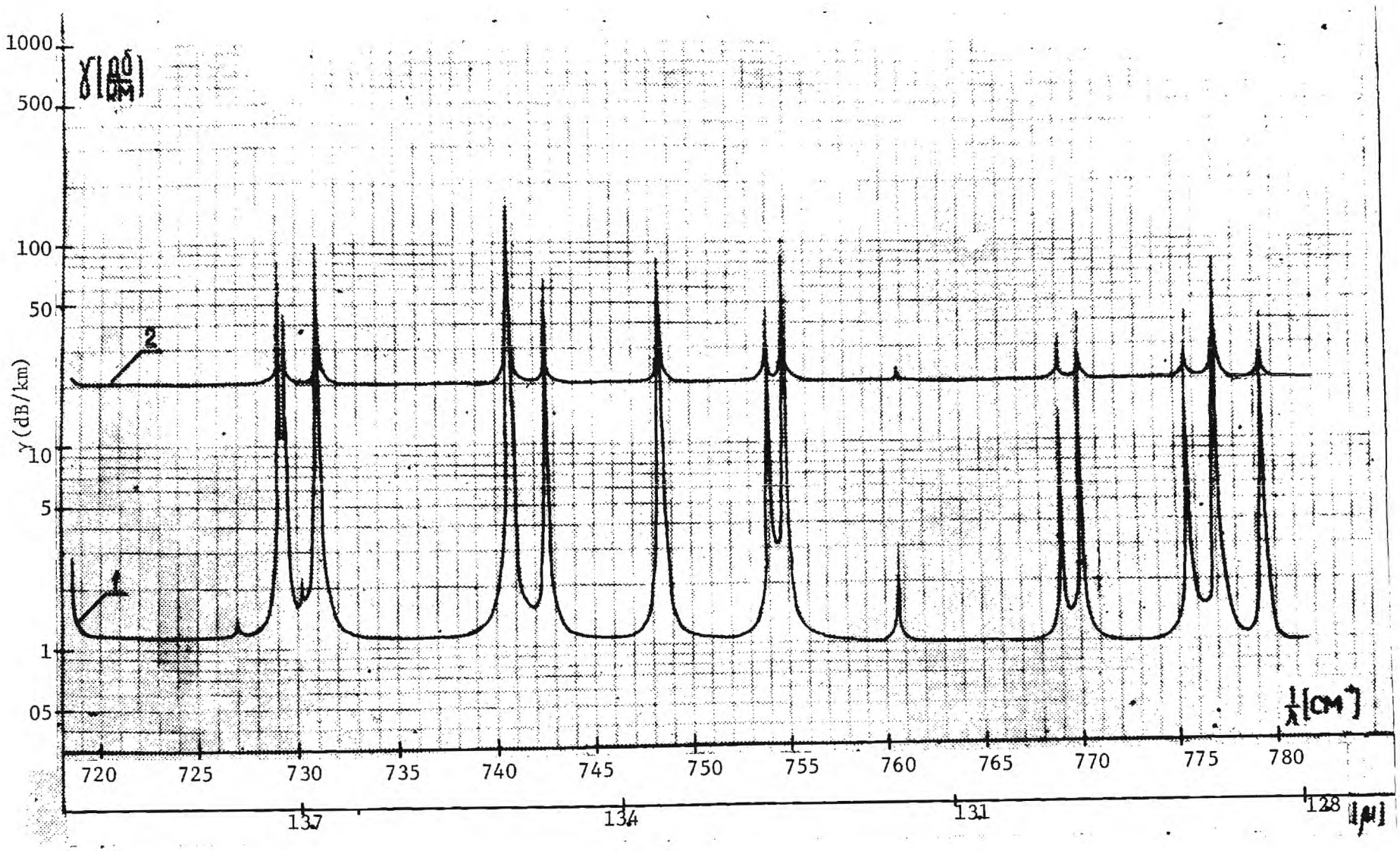

Figure V-1.(Continued)

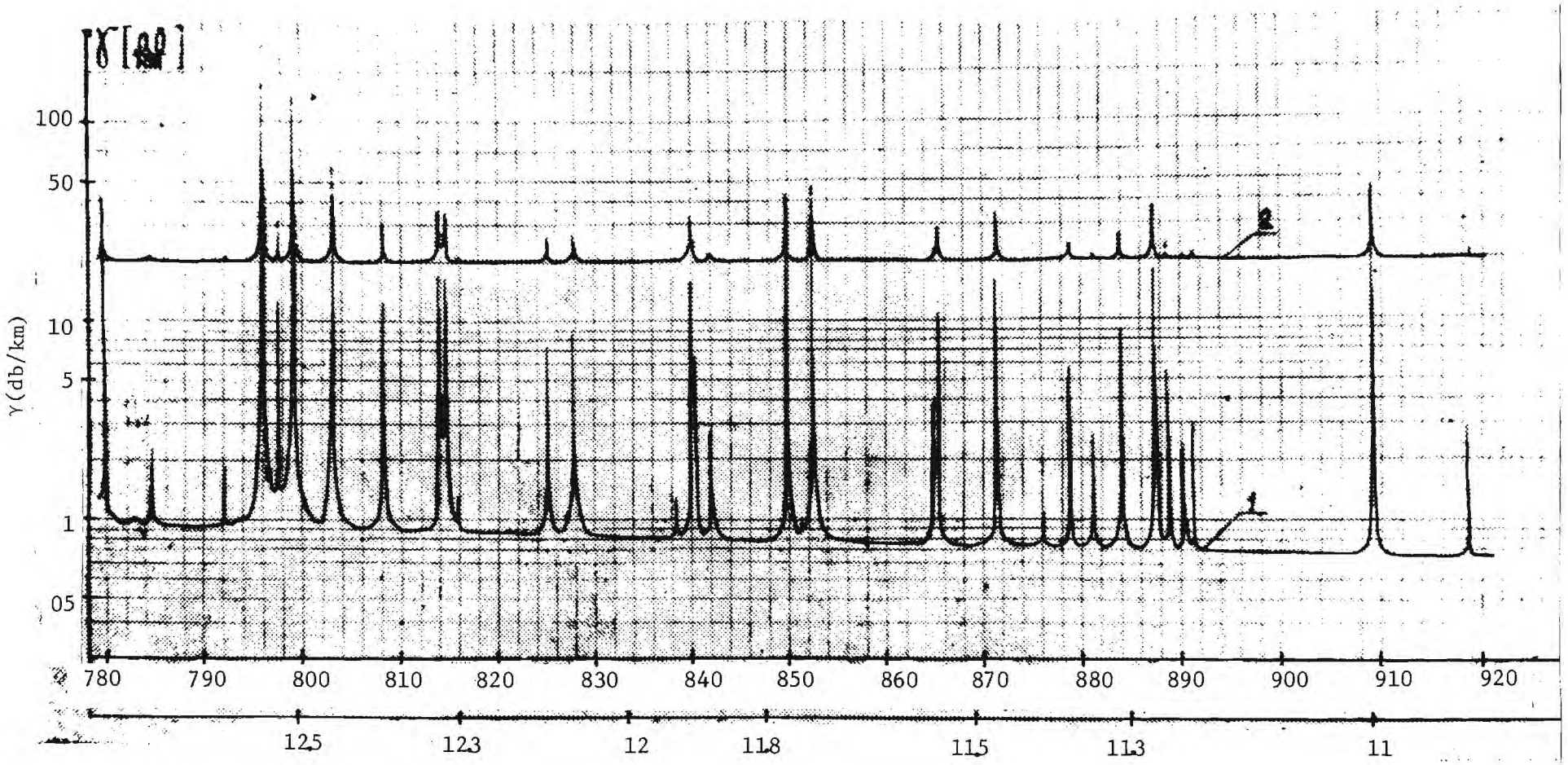

Figure V-1. (Continued)

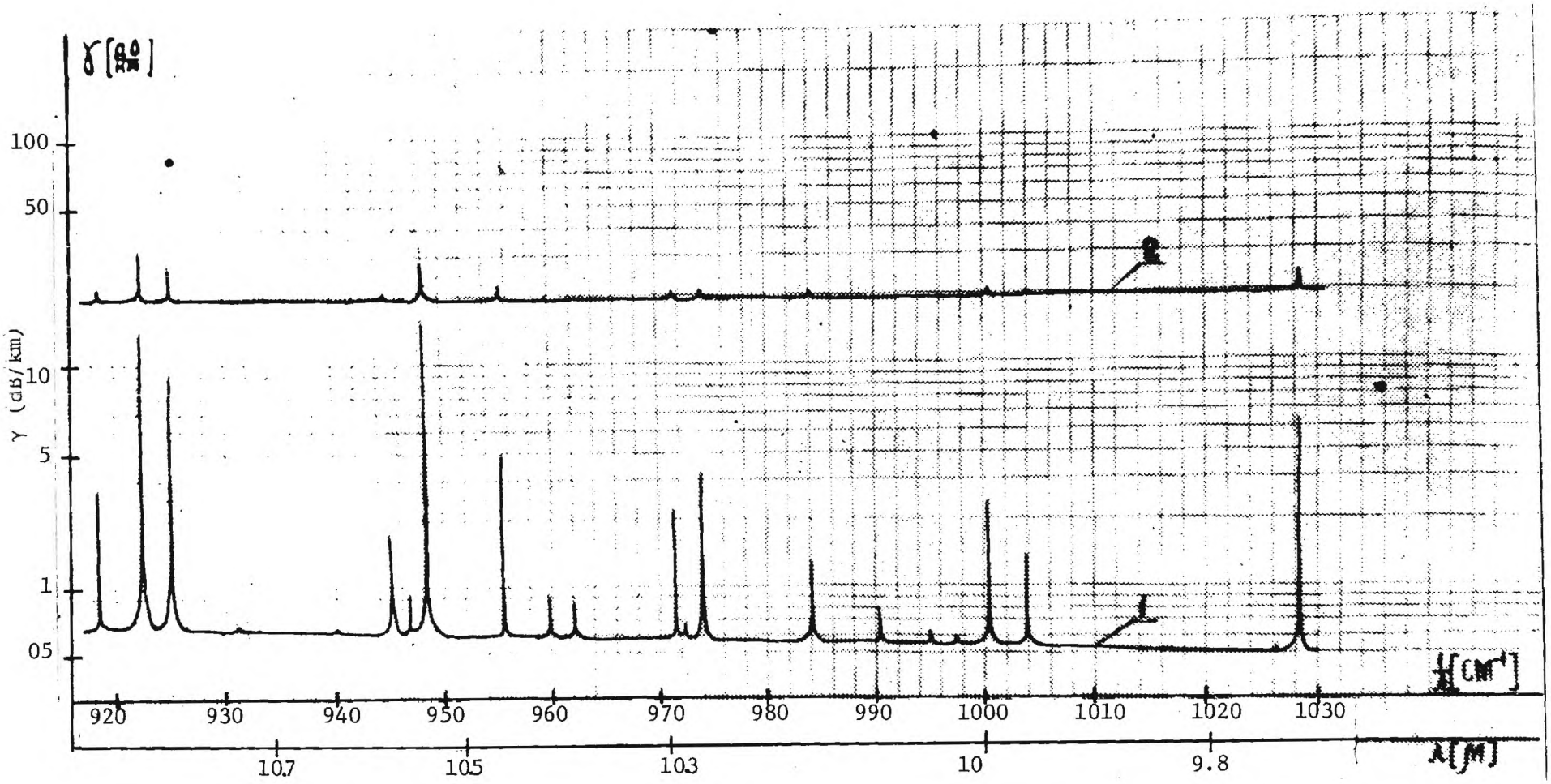

Figure V-1. (Continued)

APPENDIX V

REFERENCES

1. T. Y. Chang, "Optically Pumped Submillimeter Wave Sources," IEEE Trans. Microwave Theory and Techniques, MTT-22 983(1974).

2. T. K. Plant, L. A. Newman, E. J. Danielewicz, T. A. DeTemple and P. D. Coleman, "High Power Optically Pumped Far Infrared Lasers," IEEE Trans. Microwave Theory and Techniques MTT-22, 988 (1974).

3. M. Yamanaka and H. Yoshinaga, "Compact Waveguide Lasers in the Submillimeter and Millimeter Wave Regions," Digest of International Conference on Submillimeter Waves and their Applications, pp. 26-27, Atlanta, Ga., June 1974.

4. F. Brown, E. Silver, C. E. Chase, K. J. Button and B. Lax, "10 W Methyl Fluoride Laser at 496 μm," IEEE J. Quantum Electron. QE-8 499 (1972).

5. J. Izatt, B. Bean and J. Caudle, unpublished - private communication.

6. F. Brown, Kronheim and E. Silver, "Tunable Far Infrared Methyl Fluoride Laser Using Transverse Optical Pumping," Digest of International Conference on Submillimeter Waves and Their Applications, pp. 48-49, Atlanta, Georgia, June 1974.

7. R. J. Wagner, A. J. Zelano, and L. H. Ngai, "New Submillimeter Laser Lines in Optically Pumped Gas Molecules," Opt. Commun. 8, 46 (1973).

8. T. Y. Chang, T. J. Bridges and E. G. Burkhardt, "CW Laser Action at 81.5 and 263.4 μm in Optically Pumped Ammonia Gas," Appl. Phys. Lett 17, 357 (1970).

9. T. A. DeTemple, T. K. Plant and P. D. Coleman; "Intense Super-radiant Emission at 496 μm from Optically Pumped Methyl Fluoride," Appl. Phys. Lett. 22, 644 (1973).

10. K. Gullberg, B. Hartman and B. Kleman, "Submillimeter Emission from Optically Pumped Gas Molecules," Opt. Commun. 8, 177 (1973).

11. H. R. Fetterman and H. R. Schlossberg, "Submillimeter Wave Optically Pumped Molecular Lasers," Microwave Journal, October, 1974.

12. T. Y. Chang, T. J. Bridges and E. G. Burkhardt, "CW Submillimeter Wave Laser Action in Optically Pumped Methyl Fluoride, Methyl Alcohol and Vinyl Chloride Gases," Appl. Phys. Lett. 17, 249 (1970)

13. T. Y. Chang and J. D. McGee, "Millimeter and Submillimeter Wave Laser Action in Symmetric Top Molecules Optically Pumped via Parallel Absorption Bands," Appl. Phys. Lett. 19, 103 (1971).

14. H. R. Fetterman, H. R. Schlossberg and J. Waldman, "Submillimeter Lasers Optically Pumped Off Resonance," Opt. Commun. 6, 156 (1972).

15. D. T. Hodges, R. D. Reel and D. H. Barker, "Low-Threshold CW Submillimeter-and Millimeter-Wave Laser Action in CO_2-laser-pumped $C_2H_4F_2$, $C_2H_2F_2$, and CH_3OH," IEEE Journ. Quant. Electron. QE-9, 1159 (1973).

16. A. Tanaka, A. Tanimoto, N. Murata, M. Yamanaka and H. Yoshinga, "Optically Pumped Far-infrared and Millimeter Wave Waveguide Lasers," Japan. Journ. Appl. Physics 13, 1491 (1974)

17. S. F. Dyubko, V. A. Svich and L. D. Fresenko, "Submillimeter-band Gas Laser Pumped by a CO_2 Laser," METP Lett 16, 418 (1972).

18. N. Skrinbanowitz, I. P. Herman, R. M. Osgood, Jr., M.S. Feld and A. Javan," Anisotropic Ultrahigh Gain Emission Observed in Rotational Transitions in Optically Pumped HF Gas," Appl. Phys. Lett. 20, 428 (1972).

19. T. K. Plant, P. D. Coleman and T. A. DeTemple, "New Optically Pumped Far-Infrared Lasers," IEEE Journ. Quant. Electron., QE-9, 962 (1973).

20. H. E. Radford, "New CW Lines from a Submillimeter Waveguide Laser," IEEE Journ. Quant. Electron., QE-11, 213 (1975).

21. T. Y. Chang and J. D. McGee, "Millimeter and Submillimeter Wave Laser action in Symmetric Top Molecules Optically Pumped Via Perpendicular Absorption Bands," submitted to IEEE Journ. Quant. Electron.

22. S. A. Zhevakin and A. P. Naumov, "The Absorption Coefficient of Water Vapor for Electromagnetic Waves in the Range 2 cm-10 μm", Radiophysics and Quantum Electronics 6, 675 (1963).

23. E. P. Gross, "Shape of Collision - Broadened Spectral Lines," Phys. Rev. 97, 395 (1955).

24. J. H. Van Vleck and V. F. Weisskopf, "On The Shape of Collision - Broadened Lines," Rev. Mod. Phys. 17, 227 (1945).

25. S. A. Zhevakin and A. P. Naumov, "Absorption of Electromagnetic Radiation By Water Vapor on 10 μm - 2 cm Waves in The Upper Atmosphere," Geomagnetism and Aeronomy 4, 537 (1963).

26. D. R. Cohn, T. Fuse, K. J. Button, B. Lax and Z. Drozdowicz, "Development of an Efficient 9-kW 496 μm CH_3F Laser Oscillator," Appl. Phys. Lett. 27, 281 (1975).

27. B. Lax and R. L. Aggrival, "Tunable Radiation Sources in the Submillimeter Region," Microwave Journal, p. 31, November, 1974.

28. V. J. Corcoran, IEEE Trans. Microwave Theory and Techniques, MTT-22, 1103 (1974).

29. P. Belland, A. I. Ciura, D. Véron and L. B. Whitbourn, "CW 377 μm HCN Laser Gain Saturation, Emission Line-Shape and Power," Digest of International Conference on Submillimeter Waves and Their Applications, Atlanta, Georgia, June 1974.